Molecular Regulation of $CD8^+$ T cell stemness and function

Elisa Clark

A dissertation

submitted in partial fulfillment of the

requirements for the degree of

Doctor of Philosophy

University of Washington

2024

Reading Committee:

Hao Yuan Kueh, Chair

Dustin Maly

Shivani Srivastava

Program Authorized to Offer Degree:

Bioengineering

University of Washington

Abstract

Molecular regulation of $CD8^+$ T cell stemness and function

Elisa Clark

Chair of the Supervisory Committee:
Hao Yuan Kueh
Bioengineering

To robustly defend the body against disease, the immune system needs to rapidly generate large, heterogeneous populations of specialized cells in response to stimuli. In this dissertation, I will focus on a subtype of adaptive immune cells, cytotoxic $CD8^+$ T cells. Upon recognition of foreign proteins from infected and malignant cells, these cells migrate to the required tissue location to perform their effector functions, and importantly, the majority of these cells need to terminally differentiate and die after the threat is cleared to prevent immunopathology. However, a remarkable ability of the adaptive immune system is the memory recall response to past threats, whereby a small population of the responding cells with pathogen specificity are set aside and remain quiescent and stem-like so that they can be long-lived. These memory cells can then mount faster and stronger responses if the same threat reemerges. In this dissertation, I will focus on how

$CD8^+$ T cells exert this population level control. In Chapter 1, I will briefly review the literature on $CD8^+$ T cell differentiation and introduce the scope of this work. In Chapter 2 and Chapter 3, I will focus on cell-intrinsic regulation of a key gene necessary for T cell stemness, *Tcf7*. In Chapter 4, I will focus on the extrinsic signals that control $CD8^+$ T cell differentiation: antigen stimulation, co-stimulation, and cytokine signaling, and building tools to probe these stimuli in multiplexed experiments. And finally, in Chapter 5, I will briefly discuss how these insights and tools can be used to develop improved immunotherapies.

TABLE OF CONTENTS

LIST OF FIGURES

LIST OF TABLES

ACKNOWLEDGEMENTS

Pursuing this degree has been both one of the greatest challenges and rewarding experiences of my life. I would like to acknowledge first my scientific collaborators and mentors throughout this PhD journey, without whom none of this work would have been possible. To my committee members, Philip Greenberg, Dustin Maly, Shivani Srivastava, and Kim Woodrow: thank you for your helpful discussions and feedback over the years. I am especially grateful to Shivani for her help with tumor experiment design and collaboration with CAR-T cell projects and to my collaborators in her lab, Sarah Garrison, and Mitchell Kluesner.

To my advisor, Kueh, thank you for taking a chance and letting me join your lab a few years into my PhD journey, for giving me countless hours of your time, always having optimism when I did not, and guiding me through the uncertainty of this process. To Kathleen Abadie, who has been my partner on most of this work: thank you for your mentorship, collaboration, and friendship. To my primary co-authors, Sriram Pendyala, Matthew Wither, Arjun Kumar: thank you for your collaboration in the lab, for making the long days feel less long, and for opening my mind on new analysis strategies. To Raj Valanparambil and Rafi Ahmed: thank you for your collaboration on the *in vivo* portion of our memory story. I am excited for it to come out right as I am wrapping up my PhD. I would also like to thank the many animals that gave their lives for this work to be possible, and the husbandry staff in the UW animal facilities. To the other Kueh lab members past and present: Nick Pease, Sam Nguyen, Kenny Ng, Marcus Woodworth, Morgan Bean, Katie Denecke, Will White, Maddie Wong, Rebecca Wu, Selena Yeung, Michael Yirdaw, Allan

Wang, and Jumana Fathima, thank you for your company in the lab, and dedication to making our lab a fun place to work. A special thank you to Paul Leanza and Lihua Chen for managing the lab and keeping us all organized and safe. I would also like to thank those who guided me at the beginning of my PhD journey, Jason Miklas, Julie Mathieu, Shiri Levy, Hannele Ruohola-Baker, Alec Smith, and Deok-Ho Kim: thank you for your mentorship and time spent on my development as a scientist. There were many others who mentored me early on in my career and inspired me to pursue graduate studies, including David Kaplan, Antonios Mikos, Glenn Gaudette, Johnny Lam, and Rosalyn Abbot. Thank you for inspiring my love of research, and putting up with me in the lab when I really did not know what I was doing. I'd also like to thank my industry mentors at ImmunoGen, Seth Kitchener and Sven Loebrich for supporting my development as a scientist beyond academia and inspiring my love for process development.

Lastly, I would like to thank the family and friends who supported me during this process. To my friends that I made here in Seattle, including my Bioengineering cohort mates, thank you for your companionship and commiseration during tougher times. To my parents: thank you for inspiring me from a young age to be curious about the world and showing me what a career in science could look like. To my mom especially: you are my greatest inspiration. Thank you for paving the path for me and countless women in biosciences/engineering, I will be forever grateful. To my brother Calvin, and my sister-in-law Liz, thank you for visiting me all the way in Seattle, and encouraging me to have some fun every once in a while. And lastly, thank you so much to Chris Maynor for being my partner throughout this process. Thank you for the daily reminders that I am good enough, and for the countless meals you made while I was at the lab late or working on a deadline. I am so excited for the next step in our lives together.

Chapter 1. INTRODUCTION

1.1 $CD8^+$ T CELL RESPONSES IN ACUTE INFECTION, CHRONIC INFECTION, AND CANCER

$CD8^+$ T cells are a critical component of the adaptive immune system due to their high specificity for non-self-antigens, cytotoxic capabilities, and generation of memory[1]. These functions enable rapid clearance of acute viral and bacterial infections, control over tumor growth, and enhanced protection to secondary exposure to antigen. To perform these functions, single naive T cell clones expand and differentiate to a broad range of cell states[2]. These heterogeneous cell states differ in their cytotoxic effector function, self-renewal and persistence capabilities, and circulation or tissue localization[2,3]. Here, we briefly describe the cytotoxic T cell response in acute infections, chronic infections, and cancer, with a focus on the stem-like, self-renewing subsets that form in each type of challenge.

1.1.1 *Acute infection*

Naive $CD8^+$ T cells typically first encounter antigen through display by an antigen presenting cell (APC) such as a dendritic cell, in the lymph nodes or spleen[1,4]. This interaction allows the T cell exposure to three signals necessary for a functional differentiation response, signal 1: stimulation through the T cell receptor (TCR), signal 2: co-stimulation, through ligation of surface molecules such as CD28 on the T cell, and signal 3: instructive inflammatory cytokines such as type I interferon (IFN-I) or interleukin (IL)-12[5–8] (Reviewed in **1.1.4**). This initial activation leads to a large, up to 1000-fold clonal expansion within the first week of infection[9]. This expanded pool consists of heterogeneous cell populations, notably cytotoxic effector T cells (T_{EFF}) which are the main actuators of pathogen clearance and have potent secretory abilities for

inflammatory cytokines such as Interferon-gamma (IFN-γ) and Tumor Necrosis Factor-alpha (TNF-α), and cytotoxic molecules such as Perforin and Granzyme B (GZMB)[1]. Effector cells also uniquely express the surface receptor Killer cell lectin-like receptor subfamily G member 1 (KLRG1) which aids in their identification at various stages of the immune response[10] and have high expression of the transcription factor T-bet (*Tbx21* gene)[10,11]. Effector cells are short-lived, and upon pathogen clearance there is a rapid decline of the effector population known as contraction. However, a small population, typically 5-10% of the peak total effector population, of quiescent antigen specific T cells remains after contraction[12,13]. This fraction of cells has been termed memory cells due to their capability to mount a faster response to secondary antigen challenge and persistence over years to decades after initial challenge in the absence of re-stimulation[2]. Memory cells have been characterized by expression of the surface receptors CD127 (IL-7 receptor alpha, *Il7r* gene)[14], and CD62L (L-selectin, *Sell* gene)[12,15], and the transcription factor T cell factor 1 (TCF1[16,17], *Tcf7* gene) among others.

How this small subset of memory cells arises from naive cells over the course of acute infection is still unresolved, despite numerous conflicting studies (**Fig. 1.1A**). There is experimental evidence that these cells differentiate early and separately from effector cells through asymmetric cell division, whereby one daughter cell retains memory potential while the other daughter cell becomes an effector cell[18–20]. A second possibility is that memory cells arise later, during the contraction phase, through dedifferentiation of a select subset of effector cells[21,22]. However, recent studies have demonstrated that once cells silence TCF1 and thereby lose memory potential they are irreversibly committed to the effector fate and cannot dedifferentiate[23–25], which would exclude the late-stage dedifferentiation pathway to memory. Such differences in results across

many studies may be a product of differences in experimental model selection, which necessitates the use of reductionist experimental methods that provide precise control of stimulation and tracking of individual cells at the clonal level (reviewed in **1.4**). Furthermore, it may be advantageous for memory cells to be able to form through more than one pathway to allow for diversification and generate the large degree of heterogeneous memory subsets required for long-term immunity[3].

1.1.2 *Chronic infection*

While acute threats are eliminated by effector cells, more virulent threats can lead to host-pathogen coexistence for extended periods without clearance, due to a loss of function of effector-like cells[2,26]. This failure to clear the pathogen also leads to failure to form true memory responses, even when the pathogen is cleared through pharmaceutical intervention[27,28]. Instead of expansion followed by contraction, T cells responding to chronic infections display initial expansion and effector function, followed by persistence of a smaller pool of dysfunctional T cells[2] (**Fig. 1.1A**). Hepatitis B and C, and Human Immunodeficiency Virus (HIV) become chronic infections in humans, and certain strains of lymphocytic choriomeningitis virus (LCMV) in mice, such as LCMV clone 13, develop into chronic infections while others, such as the Armstrong strain, remain acute[26]. These dysfunctional yet persistent T cells were first identified in chronic LCMV infection in mice and have been termed "exhausted" T cells (T_{EX})[29]. Despite their persistence, the self-renewal and memory recall responses of T_{EX} are poor, and T_{EX} are transcriptionally and epigenetically distinct from effector and memory cells generated during acute infection[30]. Additionally, T_{EX} are characterized by upregulation of inhibitory receptors such as PD-1[31,32], CTLA4[33], TIM3[34–36], LAG3[37], TIGIT[38] and CD39[39,40], each of which have been explored as therapeutic targets[26]. Strategies to block the interactions between these

inhibitory receptors and their ligands, known as immune checkpoint blockade (ICB), have demonstrated reinvigoration of the immune response in chronic infection[41], and have been used to treat even late-stage cancers with remarkable efficacy, leading to awarding of the Nobel prize in medicine in 2018 to Honjo and Allison for PD-1 and CTLA4 blockade, respectively[42].

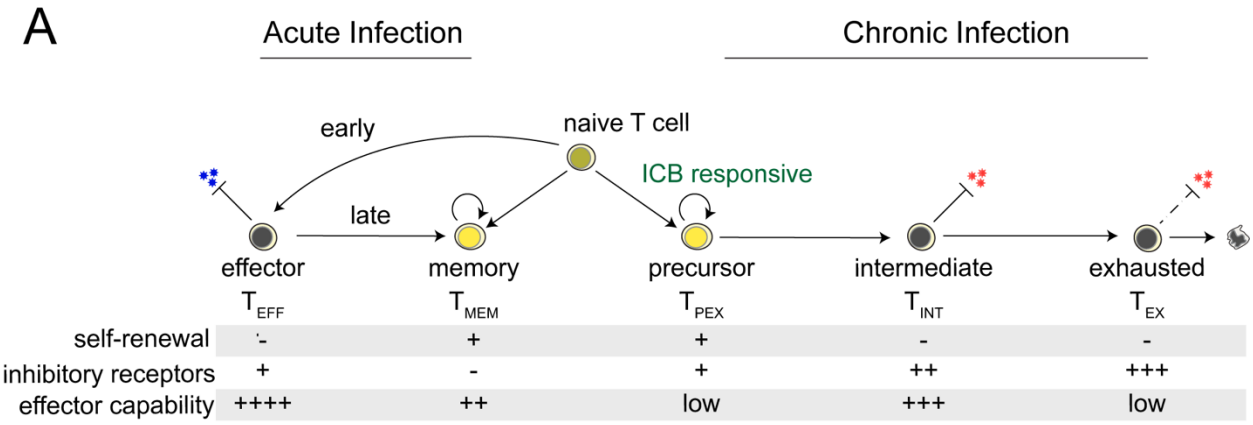

Figure 1.1 CD8$^+$ T cell differentiation in acute and chronic infection.
(A) Upon acute immune challenge (left), naive T cells differentiate into effector and memory cells. Memory cells may form either through early divergence to effector and memory states, or by later differentiation from effector cells. Memory cells have self-renewal potential, lack inhibitory receptors, and have moderate effector capability. Effector cells lack self-renewal, have moderate inhibitory receptor expression, and have high effector capability. (Right) With chronic challenge, naive cells first differentiate into precursors (T_{PEX}), which are self-renewing but have low to moderate inhibitory receptor expression. These cells have low effector capability but give rise to functional intermediate cells with effector capability but increased inhibitory receptor expression and no self-renewal. These intermediate cells transition to exhausted cells (T_{EX}) which have no self-renewal capability, high inhibitory receptor expression, and low effector capability. While these exhausted cells have adapted to persist in chronic stimulation, they eventually die and are replenished by the precursor pool.

Recent studies have implicated the transcription factor TOX (thymocyte selection-associated HMG BOX) as the driver of the expression of such inhibitory receptor genes and necessary for development of the exhausted phenotype[43,44]. TOX itself is upregulated by chronic TCR stimulation, through a nuclear factor of activated T cells (NFAT) dependent mechanism[43,45], however, the role of TOX in loss of effector function is less clear[44], suggesting that these hallmark features of exhausted cells may be decoupled. The factors that lead to each of these hallmarks of exhaustion are difficult to disentangle in an ongoing infection, leaving many

unanswered questions about which individual or combinatorial stimuli drive specific aspects of the exhausted phenotype.

The differentiation trajectory of exhausted cells has also been characterized recently and is thought to occur progressively over time on stimulation (**Fig. 1.1A**). The cells that give rise to exhausted cells have been termed precursors of exhausted cells (T_{PEX}) and share some characteristics with memory cells in their persistence and ability to self-renew, however these cells are a transcriptionally and epigenetically distinct subset from effector and memory cells[46]. T_{PEX} are characterized by high levels of TCF1, which is required for their self-renewal, as well as TOX and low levels of inhibitory receptors[47]. Typically, high TCF1 but lack of the inhibitory receptor TIM3 is utilized to identify precursor cells, while the presence of TIM3 with loss of TCF1 marks more terminally differentiated cells[35,36,47,48]. T_{PEX} have recently gained clinical interest, as recent studies have determined that these cells are responsible for the reinvigoration of the immune response to chronic infection after ICB[36,46]. As a result of ICB, these cells rapidly proliferate and differentiate to functional effector-like cells. While ICB is unable to change the epigenetic state of any of the subsets along the differentiation trajectory[49], it drives an increase in the effector fraction from the precursor pool, thus providing a functional pathogen clearance response. How, when, and where these $TCF1^+$ T_{PEX} are formed and maintained over the course of a chronic infection, and whether the epigenetically fixed T_{EX} state can be reverted to the T_{PEX} state remain outstanding questions in the field.

1.1.3 *Cancer*

$CD8^+$ T cells are also capable of eradicating cancer cells, and the presence of tumor infiltrating lymphocytes (TIL) has been characterized in many tumor types. The continued growth of cancer

cells despite the presence of cytotoxic T cells within the tumor suggests a loss of function in these cells. Many studies have identified dysfunctional TIL that share characteristics of the exhausted phenotype from chronic infection[50,51]. These dysfunctional/exhausted TIL have been a major target of recent therapeutic strategies. Clinical efforts have involved targeting the patient's own tumor responsive cells to increase proliferation and function, using interventions such as ICB. Similarly to chronic infection, ICB acts on the $TCF1^+$, T_{PEX} cells, driving proliferation and differentiation[52]. However, the presence of these $TCF1^+$ cells within tumors is heterogeneous between patients and between tumor types, and their location of residence in secondary lymphoid organs or in the tumor environment has not been resolved[50,53–55].

Additionally, engineered T cells, such as Chimeric Antigen Receptor (CAR)-T cells have been used successfully to treat hematologic malignancies[56]. However, in solid tumors, these treatments have been less successful due in part to acquisition of the exhausted phenotype[57]. Whether CAR-T cells differentiate along a similar trajectory, through a $TCF1^+$ precursor state, has yet to be determined. Strategies to enhance CAR-T cell function by maintaining the $TCF1^+$ state during *ex vivo* expansion have been proposed, and more memory-like CAR-T cells display enhanced antitumor efficacy[58], suggesting that CAR-T cells likely follow a similar differentiation paradigm.

1.2 Epigenetic control of T cell differentiation

Differentiation of naive T cells into heterogeneous states, described in **1.1.1** occurs due to changes in gene expression downstream of initial activation of the T cell. All cells, including T cells, are able to regulate gene expression in the absence of signals, and across generations of cell divisions through epigenetic mechanisms[59,60]. Epigenetic gene regulation can be broken down

into 2 categories: cis– regulation, which is defined as a mechanism that occurs directly at the chromatin level, or trans– regulation, in which the expression of a gene is controlled by a network of transcription factors (TF), upregulated by the initial stimulus[59,60]. Cis– mechanisms can be further categorized into modifications occurring directly to DNA, such as DNA methylation, and post-translational modifications on histones, the proteins that organize chromatin structure[61]. In this section, we review briefly the known cis– and trans– mechanisms required for $CD8^+$ T cell differentiation.

1.2.1 *Cis– regulation of T cell differentiation*

Repressed genes are found in areas of chromatin that are less accessible, or closed, known as heterochromatin, and active genes are found in open, euchromatin[59,60]. One mechanism for DNA compaction, and thereby inaccessibility and transcriptional repression, is methylation at cytosine residues (5-methylcytosine (5mC))[62,63]. DNA methylation is mediated by enzymes called DNA methyltransferases (DNMT), of which there are DNMT1, and DNMT3a/DNMT3b. DNMT3a and DNMT3b are able to methylate DNA *de novo*, while DNMT1 is proposed to maintain methylation across cell divisions. DNA can be demethylated by the TET methylcytosine dioxygenases, TET1/TET2/TET3[62,63]. DNA methylation has been proposed as a mechanism for differentiation of naive $CD8^+$ T cells into terminal effector cells during acute infection by repressing memory differentiation, with DNMT3a knockout enhancing memory differentiation[22]. Blocking DNA methylation by DNMT3a has also been demonstrated to reduce T cell exhaustion and enhance responsiveness of checkpoint blockade[64]. However, DNA demethylation by TET2 has also been shown to repress memory formation, with TET2 knockouts leading to enhanced memory cells and memory like cells after acute infection[65] and in CAR-T cells[66]. These opposing

results by global knockouts of DNA methylation and demethylation enzymes suggest complexity to the network of genes being methylated at various activation stages and highlight the necessity for screening epigenetic control of T cell differentiation across signaling contexts.

Chromatin compaction and thereby gene repression can also occur as a result of post-translational histone modifications. Known repressive histone modifications are methylation of histone 3, lysines 9 and 27 (H3K9me2/3 and H3K27me3), as well as monoubiquitination of histone 2A at lysine 119 (H2AK119Ub1)[61]. Such repressive histone modifications are written by histone methyltransferase (HMT) enzymes, which in the case of H3K9me2/3 are the suppressor of variegation (SUV) family enzymes SUV39H1 and SUV39H2[61,67]. In this dissertation, I will focus primarily on the other class of HMTs, the polycomb repressive complexes (PRC) 1 and 2, which write H2AK119Ub1 and H3K27me3 histone modifications respectively[61].

Both PRC1 and PRC2 are formed through cooperation of multiple enzymatic subunits. For PRC1, the canonical form of the complex consists of the catalytic subunit, ring finger protein (RING1A/RING1B), a chromobox (CBX2/4/6/7/8) domain, that can read histone modifications such as H3K27me3 deposited by PRC2, a polycomb group protein (PCGF2/4), and a polyhomeotic homolog family protein (PHC1/2/3)[68–70]. There are various non-canonical PRC1 complexes that can form but will not be reviewed in this dissertation. In $CD8^+$ T cells, PRC1 activity has been demonstrated to promote effector differentiation by repressing memory genes, with knockout of *Cbx4* leading to enhanced memory differentiation in acute infection[71]. Similarly to PRC1, PRC2 is formed as a complex of 4 major classes of enzymes consisting of the catalytic subunit is enhancer of zeste (EZH1/2), the DNA binding domain embryonic ectoderm

development (EED), suppressor of zeste 12 (SUZ12), and RB binding protein (RBBP4/7)[72]. There are other proteins that can associate and cooperate with PRC2, but these are the minimum required for H3K23me3 deposition[72]. Similarly to PRC1, PRC2 has been implicated in terminal effector differentiation through suppression of memory genes in acute infection[73].

The role of PRC1/2 in maintaining the exhausted phenotype is less well characterized. Exhausted cells differ transcriptomically and epigenetically from naive, memory, and effector T cells, and are thought to be irreversibly epigenetically locked-down, such that they cannot be dedifferentiated to progenitor cells or their chromatin state rewired by ICB[49]. A recent study in a B16 melanoma model probed the repressed chromatin state of exhausted cells using CUT&RUN (Cleavage Under Targets & Release Using Nuclease) for H3K27me3 residues[74,75]. They found that terminally exhausted cells had increased H3K27me3 deposition at key precursor genes, including *Tcf7*, suggesting that PRC2 in part mediates the loss of stemness in exhaustion differentiation[75]. A recent study also demonstrated that stimulation withdrawal can reverse differentiation and restore function in exhausted CAR-T cells and is dependent on EZH2[76]. However, the role of PRC1 in exhaustion differentiation is unknown, and how PRC1 and 2 may work together, in conjunction with other epigenetic mechanisms to drive the irreversibly exhausted state remains unexplored.

1.2.2 *Transcription factors governing T cell differentiation*

There are numerous transcription factors that have been identified to control $CD8^+$ T cell differentiation to memory, effector, and exhausted states. Here, I briefly highlight the effects of some of these key transcription factors on $CD8^+$ T cell differentiation to memory, effector, and exhausted states, however there are many TFs that control important state transition genes in

$CD8^+$ T cells that I have not highlighted here. There are other transcription factors downstream of cytokine signaling that exert control of T cell differentiation, which will be reviewed in the next section (**1.1.3**).

There are 3 major TF pathways that are directly downstream of the TCR and become activated as a result of antigen engagement and coordinate the early stages of the T cell response: NFAT, MAPK, and NF-κB[77]. Each of these pathways has TFs directly downstream, and these TFs can also cooperatively bind to certain motifs or act alone. Downstream of the MAPK pathway are the TFs: FOS, JUN, and AP-1, all of which can cooperatively bind with NFAT. NF-κB itself is a TF and can also cooperatively bind with the TF REL to regulate transcription of target genes[77]. There is a network of TFs that govern memory $CD8^+$ T cell differentiation, including TCF1[16,78–80], which will be described more in **Chapters 2 and 3**, LEF1[78], c-MYB[81], and FOXO1[82]. Conversely, the TFs that drive effector differentiation, T-bet[10,11], ZEB2[11], and BLIMP1[17,83] have been specifically demonstrated to suppress memory potential.

As mentioned in **1.1.2** the transcription factor TOX is a key driver of exhaustion differentiation[43–45,84]. A recent study demonstrated that TOX directly suppresses T-bet to promote exhaustion differentiation and dampen effector differentiation[85]. TOX is upregulated due to chronic NFAT signaling[43,45], and chronic NFAT in the absence of AP-1 binding partners is thought to be a key driver of the exhausted state[86]. Other transcription factors that coordinate with NFAT to drive exhaustion differentiation are IRF4, and BATF[87]. In addition to its role in effector differentiation, BLIMP1 has also been implicated in exhaustion differentiation[88,89].

Another class of transcription factors downstream of NFAT that have been demonstrated to drive exhaustion differentiation are the nuclear receptor subfamily 4A proteins (NR4A1/2/3)[45,89].

What can be appreciated from this brief review of transcription factors is that there is a large network of transcription factors that can drive T cell differentiation in response to or in the absence of stimuli, and there is a need to uncover how these transcription factors coordinate T cell differentiation in a stage and stimulus specific manner. Recent developments in CRISPR-Cas9 screening tools[90] will allow for such studies. In this dissertation work, we sought to uncover the role of both cis– and trans– regulatory mechanisms specifically on the regulation of *Tcf7*/TCF1 in acute and chronic stimulation environments (**Chapter 3**), however the field could benefit from such screening efforts on other functional phenotypes in $CD8^+$ T cells.

1.3 CYTOKINE CONTROL OF $CD8^+$ T CELL DIFFERENTIATION

Cytokines are proteins utilized by the immune system for cell-cell communication and exert potent effects on cell differentiation by modulating gene expression through downstream transcription factor signaling pathways. There are approximately 30 cytokines that can be sensed by $CD8^+$ T cells, and they can be grouped into the following superfamilies based on their receptors: common γ-chain cytokines (γc), interferons (IFN), tumor necrosis factor (TNF), interleukin (IL)-1, IL-6/IL-12/glycoprotein 130 (gp130), IL-10, and transforming growth factor (TGF)-β[91,92]. There have been numerous studies of cytokine effects on $CD8^+$ T cells. Here, I briefly review the structure and function of cytokine receptors, and the major effects of a subset of cytokines from each superfamily on $CD8^+$ T cell differentiation and function.

Cytokine receptors are cell surface proteins that bind cytokines with high specificity and mediate downstream signaling through phosphorylation of secondary messengers, which then lead to activation and nuclear localization of transcription factors, and thereby changes in gene expression. Many cytokine receptors form from dimers or trimers of heterogeneous subunits[93] which can phosphorylate the immediate downstream effectors, janus kinases (JAK) that then phosphorylate the downstream transcription factors in the signal transducer and activator of transcription (STAT) family[91,94]. The individual JAK and STAT proteins downstream of cytokines have been identified and are reviewed extensively by Salas *et al.*[91] and others[94,95]. I will therefore focus the remainder of this section on the effects of cytokines as a result of downstream STATs on $CD8^+$ T cell differentiation.

The γc cytokines, IL-2, IL-4, IL-7, IL-9, IL-15, and IL-21, are some of the most well characterized in $CD8^+$ T cells[96]. IL-2 is produced by $CD8^+$ T cells upon activation, primarily signals through STAT5 and to a lesser extent STAT1 and STAT3 and is necessary for $CD8^+$ T cell proliferation upon TCR engagement[97]. Differential IL-2 signaling has been demonstrated to promote effector differentiation (higher IL-2) over memory T cell differentiation (lower IL-2)[98,99]. Similarly, high levels of IL-2 are thought to promote exhaustion in conjunction with chronic antigen stimulation[100]. IL-7 is required for the homeostatic proliferation of naive T cells[101], while IL-15 supports the proliferation of memory T cells[102] and exhausted T cells[51,103]. Both IL-7 and IL-15, similarly to IL-2, signal primarily through STAT5 and to a lesser extent through STAT1/3[96]. IL-21 on the other hand, is produced by $CD4^+$ and $CD8^+$ T cells and signals primarily through STAT1 and STAT3 and has been demonstrated to promote both effector[104] and memory T cell differentiation in acute infections[96,105]. The functional effects of IL-4 on

$CD8^+$ T cells are less well defined. IL-4 is produced by many immune cells, and signals primarily through STAT6 in $CD4^+$ T cells, though it has been demonstrated to also signal through STAT1/3/5 in $CD8^+$ T cells[106,107].

Although they have different receptor subunits, many other cytokines signal through the same downstream STAT molecules as the γc cytokines but have differential functions in $CD8^+$ T cells. For example, like IL-21, IL-10, IFN (α/β/γ), and IL-6 family members also phosphorylate STAT3 but have different effects on $CD8^+$ T cells[91]. IFN-α/β (type I IFN) are produced by many cell types in the body in response to viral infection, and modulate CD8 T cell effector differentiation[6] and exhaustion[108,109], in part through direct suppression of *Tcf7*/TCF1[79,109]. It has been recently demonstrated that type I IFN can also signal in naive T cells and aid in their homeostatic proliferation in the absence of antigen in a similar manner to IL-7[110]. IL-6 also signals through STAT3 but is known to repress $CD8^+$ T cell cytotoxicity *in vitro*[111]. This is similar to the known role of IL-21 in promoting effector differentiation, but that these effectors have limited IFN-γ secretion[104]. IL-10 is thought to also have immunosuppressive function in $CD8^+$ T cells by inhibiting their sensitivity to antigen[112], but has also been potentially shown to protect precursor cells from becoming exhausted[113], and to metabolically reprogram exhausted cells and thereby increase their function[114].

Despite signaling through the same receptor subunit as IL-6, gp130, IL-12 and its family members signal primarily through STAT4[91]. IL-12 is known to promote effector differentiation[115], high cytotoxic function[116], and silencing of *Tcf7*[79]. Lastly, cytokines in the TGF-β family do not signal through STATs but instead through a different class of transcription

factors, the Smad family[117]. TGF-β is known to exert unique effects on $CD8^+$ T cells. It can act in an immunosuppressive manner to decrease secretion of IFN-γ[118], and is thought to both exclude T cells from solid tumors[119], but also potentially promote their infiltration of solid tumors through reprogramming T cells to a resident memory (RM)-like phenotype[120,121]. Lastly, TGF-β has been shown to both slow and exacerbate exhaustion differentiation in chronic infection, depending on the differentiation state of the cells on which it acts[122,123].

A consistent theme amongst the cytokines reviewed here is seemingly opposing behaviors depending on signaling context. This underscores the importance of studying cytokine effects on $CD8^+$ T cells across a wide range of signaling contexts. We still lack a comprehensive understanding of the gene networks downstream of cytokine signaling in various stimulation contexts that $CD8^+$ T cells may face. A recent study characterized the transcriptomic effects of cytokines *in vivo* on many immune cell types, including $CD8^+$ T cells, however this study was exclusively performed on naive cells in lymph nodes and not responding to antigen simuli[92]. Large datasets like this, and the one we demonstrate in **Chapter 4** of this dissertation are crucial for understanding how $CD8^+$ T cells respond to cytokines and could potentially be applied to transcriptomic and epigenetic datasets from the literature in the hopes of mapping cell state back to the signaling environment the cells may have experienced *in vivo*.

1.4 EX VIVO T CELL DIFFERENTIATION AND SCOPE OF THIS WORK

Most of our knowledge of $CD8^+$ T cell differentiation comes from mouse models of infection and tumors, and human blood or tissue biopsy samples. While these can provide an excellent opportunity for cell phenotyping, it is difficult to track single cells over time, and difficult to precisely control the type and duration of stimulation that cells receive. In all the studies in this

dissertation work, we therefore sought to differentiate $CD8^+$ T cells *ex vivo* to allow for precise control over each stage of the differentiation process. *Ex vivo* activation of $CD8^+$ T cells with cognate antigen, TCR stimulating antibodies, and small molecules such as Phorbol myristate acetate (PMA) and ionomycin to assess proliferation and function, has been performed routinely for decades[124]. The role of various instructive cytokines on T cell phenotypes has also been explored *in vitro* due to the ability to precisely control dose and timing of stimulation[125]. Additionally, there have been studies of *in vitro* differentiation of $CD4^+$ T cells[126] and $CD8^+$ T cells[25,127,128] that have yielded surface and transcriptomic phenotypes similar to their *in vivo* counterparts. While it has been demonstrated that T cells *in vitro* have distinct metabolic characteristics compared to those *in vivo*[129], we and others have generated evidence to support that *ex vivo* differentiated cells maintain their phenotypes and function after adoptive transfer[130,131]. Recently there have been numerous studies that have also demonstrated the ability to generate exhausted T cells *in vitro* via chronic antigen stimulation, through cognate antigen stimulation or polyclonal stimulation via the CD3 domain of the TCR[90,131–135]. Another recent study demonstrated that prolonged tonic CAR signaling leads to exhaustion differentiation in CAR-T cells *in vitro*[76]. We therefore believe that there is ample precedent for the success of these *ex vivo* differentiation models, and that there is a need to use such precise, tunable differentiation systems to study unanswered questions in the field of T cell differentiation.

1.5 REFERENCES

1. Zhang, N. & Bevan, M. J. CD8+ T Cells: Foot Soldiers of the Immune System. *Immunity* **35**, 161–168 (2011).
2. Chung, H. K., McDonald, B. & Kaech, S. M. The architectural design of CD8+ T cell responses in acute and chronic infection: Parallel structures with divergent fates. *J. Exp. Med.* **218**, e20201730 (2021).
3. Jameson, S. C. & Masopust, D. Understanding Subset Diversity in T Cell Memory. *Immunity* **48**, 214–226 (2018).

4. Charles A Janeway, J., Travers, P., Walport, M. & Shlomchik, M. J. The production of armed effector T cells. *Immunobiol. Immune Syst. Health Dis. 5th Ed.* (2001).
5. Curtsinger, J. M. *et al.* Inflammatory Cytokines Provide a Third Signal for Activation of Naive CD4+ and CD8+ T Cells. *J. Immunol.* **162**, 3256–3262 (1999).
6. Curtsinger, J. M., Valenzuela, J. O., Agarwal, P., Lins, D. & Mescher, M. F. Cutting Edge: Type I IFNs Provide a Third Signal to CD8 T Cells to Stimulate Clonal Expansion and Differentiation. *J. Immunol.* **174**, 4465–4469 (2005).
7. Curtsinger, J. M. & Mescher, M. F. Inflammatory cytokines as a third signal for T cell activation. *Curr. Opin. Immunol.* **22**, 333–340 (2010).
8. Tai, Y., Wang, Q., Korner, H., Zhang, L. & Wei, W. Molecular Mechanisms of T Cells Activation by Dendritic Cells in Autoimmune Diseases. *Front. Pharmacol.* **9**, (2018).
9. Butz, E. A. & Bevan, M. J. Massive Expansion of Antigen-Specific CD8+ T Cells during an Acute Virus Infection. *Immunity* **8**, 167–175 (1998).
10. Joshi, N. S. *et al.* Inflammation Directs Memory Precursor and Short-Lived Effector CD8+ T Cell Fates via the Graded Expression of T-bet Transcription Factor. *Immunity* **27**, 281–295 (2007).
11. Dominguez, C. X. *et al.* The transcription factors ZEB2 and T-bet cooperate to program cytotoxic T cell terminal differentiation in response to LCMV viral infection. *J. Exp. Med.* **212**, 2041–2056 (2015).
12. Kaech, S. M., Hemby, S., Kersh, E. & Ahmed, R. Molecular and Functional Profiling of Memory CD8 T Cell Differentiation. *Cell* **111**, 837–851 (2002).
13. Murali-Krishna, K. *et al.* Counting Antigen-Specific CD8 T Cells: A Reevaluation of Bystander Activation during Viral Infection. *Immunity* **8**, 177–187 (1998).
14. Huster, K. M. *et al.* Selective expression of IL-7 receptor on memory T cells identifies early CD40L-dependent generation of distinct CD8+ memory T cell subsets. *Proc. Natl. Acad. Sci. U. S. A.* **101**, 5610–5615 (2004).
15. Kaech, S. M. & Ahmed, R. Memory CD8+ T cell differentiation: initial antigen encounter triggers a developmental program in naïve cells. *Nat. Immunol.* **2**, 415–422 (2001).
16. Escobar, G., Mangani, D. & Anderson, A. C. T cell factor 1 (Tcf1): a master regulator of the T cell response in disease. *Sci. Immunol.* **5**, eabb9726 (2020).
17. Kaech, S. M. & Cui, W. Transcriptional control of effector and memory CD8+ T cell differentiation. *Nat. Rev. Immunol.* **12**, 749–761 (2012).
18. Arsenio, J. *et al.* Early specification of CD8+ T lymphocyte fates during adaptive immunity revealed by single-cell gene-expression analyses. *Nat. Immunol.* **15**, 365–372 (2014).
19. Borsa, M. *et al.* Modulation of asymmetric cell division as a mechanism to boost CD8+ T cell memory. *Sci. Immunol.* **4**, eaav1730 (2019).
20. Chang, J. T. *et al.* Asymmetric Proteasome Segregation as a Mechanism for Unequal Partitioning of the Transcription Factor T-bet during T Lymphocyte Division. *Immunity* **34**, 492–504 (2011).
21. Herndler-Brandstetter, D. *et al.* KLRG1+ Effector CD8+ T Cells Lose KLRG1, Differentiate into All Memory T Cell Lineages, and Convey Enhanced Protective Immunity. *Immunity* **48**, 716-729.e8 (2018).
22. Youngblood, B. *et al.* Effector CD8 T cells dedifferentiate into long-lived memory cells. *Nature* **552**, 404–409 (2017).
23. Pais Ferreira, D. *et al.* Central memory CD8+ T cells derive from stem-like Tcf7hi effector cells in the absence of cytotoxic differentiation. *Immunity* **53**, 985-1000.e11 (2020).

24. Silva, J. G. *et al.* Emergence and fate of stem cell–like Tcf7+ CD8+ T cells during a primary immune response to viral infection. *Sci. Immunol.* **8**, eadh3113 (2023).
25. Lin, W.-H. W. *et al.* CD8+ T Lymphocyte Self-Renewal during Effector Cell Determination. *Cell Rep.* **17**, 1773–1782 (2016).
26. McLane, L. M., Abdel-Hakeem, M. S. & Wherry, E. J. CD8 T Cell Exhaustion During Chronic Viral Infection and Cancer. *Annu. Rev. Immunol.* **37**, 457–495 (2019).
27. Abdel-Hakeem, M. S. *et al.* Epigenetic scarring of exhausted T cells hinders memory differentiation upon eliminating chronic antigenic stimulation. *Nat. Immunol.* **22**, 1008–1019 (2021).
28. Yates, K. B. *et al.* Epigenetic scars of CD8+ T cell exhaustion persist after cure of chronic infection in humans. *Nat. Immunol.* **22**, 1020–1029 (2021).
29. Zajac, A. J. *et al.* Viral Immune Evasion Due to Persistence of Activated T Cells Without Effector Function. *J. Exp. Med.* **188**, 2205–2213 (1998).
30. Sen, D. R. *et al.* The epigenetic landscape of T cell exhaustion. *Science* **354**, 1165–1169 (2016).
31. Blackburn, S. D. *et al.* Coregulation of CD8+ T cell exhaustion by multiple inhibitory receptors during chronic viral infection. *Nat. Immunol.* **10**, 29–37 (2009).
32. Jubel, J. M., Barbati, Z. R., Burger, C., Wirtz, D. C. & Schildberg, F. A. The Role of PD-1 in Acute and Chronic Infection. *Front. Immunol.* **11**, (2020).
33. CD28 and CTLA-4 have opposing effects on the response of T cells to stimulation. *J. Exp. Med.* **182**, 459–465 (1995).
34. Wolf, Y., Anderson, A. C. & Kuchroo, V. K. TIM3 comes of age as an inhibitory receptor. *Nat. Rev. Immunol.* **20**, 173–185 (2020).
35. Miller, B. C. *et al.* Subsets of exhausted CD8+ T cells differentially mediate tumor control and respond to checkpoint blockade. *Nat. Immunol.* **20**, 326–336 (2019).
36. Im, S. J. *et al.* Defining CD8+ T cells that provide the proliferative burst after PD-1 therapy. *Nature* **537**, 417–421 (2016).
37. Aggarwal, V., Workman, C. J. & Vignali, D. A. A. LAG-3 as the third checkpoint inhibitor. *Nat. Immunol.* **24**, 1415–1422 (2023).
38. Guillerey, C. *et al.* TIGIT immune checkpoint blockade restores CD8+ T-cell immunity against multiple myeloma. *Blood* **132**, 1689–1694 (2018).
39. Duhen, T. *et al.* Co-expression of CD39 and CD103 identifies tumor-reactive CD8 T cells in human solid tumors. *Nat. Commun.* **9**, 2724 (2018).
40. Gupta, P. K. *et al.* CD39 Expression Identifies Terminally Exhausted CD8+ T Cells. *PLOS Pathog.* **11**, e1005177 (2015).
41. Barber, D. L. *et al.* Restoring function in exhausted CD8 T cells during chronic viral infection. *Nature* **439**, 682–687 (2006).
42. Ledford, H., Else, H. & Warren, M. Cancer immunologists scoop medicine Nobel prize. *Nature* **562**, 20–21 (2018).
43. Khan, O. *et al.* TOX transcriptionally and epigenetically programs CD8 + T cell exhaustion. *Nature* **571**, 211–218 (2019).
44. Scott, A. C. *et al.* TOX is a critical regulator of tumour-specific T cell differentiation. *Nature* **571**, 270–274 (2019).
45. Seo, H. *et al.* TOX and TOX2 transcription factors cooperate with NR4A transcription factors to impose CD8+ T cell exhaustion. *Proc. Natl. Acad. Sci.* **116**, 12410–12415 (2019).

46. Utzschneider, D. T. *et al.* Early precursor T cells establish and propagate T cell exhaustion in chronic infection. *Nat. Immunol.* (2020) doi:10.1038/s41590-020-0760-z.
47. Zehn, D., Thimme, R., Lugli, E., de Almeida, G. P. & Oxenius, A. 'Stem-like' precursors are the fount to sustain persistent CD8+ T cell responses. *Nat. Immunol.* 1–12 (2022) doi:10.1038/s41590-022-01219-w.
48. Franco, F., Jaccard, A., Romero, P., Yu, Y.-R. & Ho, P.-C. Metabolic and epigenetic regulation of T-cell exhaustion. *Nat. Metab.* **2**, 1001–1012 (2020).
49. Pauken, K. E. *et al.* Epigenetic stability of exhausted T cells limits durability of reinvigoration by PD-1 blockade. *Science* **354**, 1160–1165 (2016).
50. Philip, M. & Schietinger, A. CD8+ T cell differentiation and dysfunction in cancer. *Nat. Rev. Immunol.* **22**, 209–223 (2022).
51. Philip, M. *et al.* Chromatin states define tumor-specific T cell dysfunction and reprogramming. *Nature* **545**, 452–456 (2017).
52. Sade-Feldman, M. *et al.* Defining T Cell States Associated with Response to Checkpoint Immunotherapy in Melanoma. *Cell* **175**, 998-1013.e20 (2018).
53. Connolly, K. A. *et al.* A reservoir of stem-like CD8+ T cells in the tumor-draining lymph node preserves the ongoing antitumor immune response. *Sci. Immunol.* **6**, eabg7836 (2021).
54. Jansen, C. S. *et al.* An intra-tumoral niche maintains and differentiates stem-like CD8 T cells. *Nature* **576**, 465–470 (2019).
55. Li, H. *et al.* Dysfunctional CD8 T Cells Form a Proliferative, Dynamically Regulated Compartment within Human Melanoma. *Cell* **176**, 775-789.e18 (2019).
56. Maude, S. L. *et al.* Chimeric Antigen Receptor T Cells for Sustained Remissions in Leukemia. *N. Engl. J. Med.* **371**, 1507–1517 (2014).
57. Hou, A. J., Chen, L. C. & Chen, Y. Y. Navigating CAR-T cells through the solid-tumour microenvironment. *Nat. Rev. Drug Discov.* **20**, 531–550 (2021).
58. Alizadeh, D. *et al.* IL15 Enhances CAR-T Cell Antitumor Activity by Reducing mTORC1 Activity and Preserving Their Stem Cell Memory Phenotype. *Cancer Immunol. Res.* **7**, 759–772 (2019).
59. Allis, C. D. & Jenuwein, T. The molecular hallmarks of epigenetic control. *Nat. Rev. Genet.* **17**, 487–500 (2016).
60. Bonasio, R., Tu, S. & Reinberg, D. Molecular Signals of Epigenetic States. *Science* **330**, 612–616 (2010).
61. Millán-Zambrano, G., Burton, A., Bannister, A. J. & Schneider, R. Histone post-translational modifications — cause and consequence of genome function. *Nat. Rev. Genet.* **23**, 563–580 (2022).
62. Greenberg, M. V. C. & Bourc'his, D. The diverse roles of DNA methylation in mammalian development and disease. *Nat. Rev. Mol. Cell Biol.* **20**, 590–607 (2019).
63. Correa, L. O., Jordan, M. S. & Carty, S. A. DNA Methylation in T-Cell Development and Differentiation. *Crit. Rev. Immunol.* **40**, 135–156 (2020).
64. Ghoneim, H. E. *et al.* DE NOVO EPIGENETIC PROGRAMS INHIBIT PD-1 BLOCKADE-MEDIATED T-CELL REJUVENATION. *Cell* **170**, 142-157.e19 (2017).
65. Carty, S. A. *et al.* The loss of TET2 promotes CD8+ T cell memory differentiation. *J. Immunol. Baltim. Md 1950* **200**, 82–91 (2018).
66. Fraietta, J. A. *et al.* Disruption of TET2 Promotes the Therapeutic Efficacy of CD19-targeted T-cells. *Nature* **558**, 307–312 (2018).

67. Padeken, J., Methot, S. P. & Gasser, S. M. Establishment of H3K9-methylated heterochromatin and its functions in tissue differentiation and maintenance. *Nat. Rev. Mol. Cell Biol.* **23**, 623–640 (2022).
68. Vidal, M. & Starowicz, K. Polycomb complexes PRC1 and their function in hematopoiesis. *Exp. Hematol.* **48**, 12–31 (2017).
69. Turner, S. A. & Bracken, A. P. A "Complex" Issue: Deciphering the Role of Variant PRC1 in ESCs. *Cell Stem Cell* **12**, 145–146 (2013).
70. Blackledge, N. P. & Klose, R. J. The molecular principles of gene regulation by Polycomb repressive complexes. *Nat. Rev. Mol. Cell Biol.* **22**, 815–833 (2021).
71. Melo, G. A. *et al.* Cutting Edge: Polycomb Repressive Complex 1 Subunit Cbx4 Positively Regulates Effector Responses in CD8 T Cells. *J. Immunol.* ji2200757 (2023) doi:10.4049/jimmunol.2200757.
72. Piunti, A. & Shilatifard, A. The roles of Polycomb repressive complexes in mammalian development and cancer. *Nat. Rev. Mol. Cell Biol.* **22**, 326–345 (2021).
73. Gray, S. M., Amezquita, R. A., Guan, T., Kleinstein, S. H. & Kaech, S. M. Polycomb Repressive Complex 2-Mediated Chromatin Repression Guides Effector CD8+ T Cell Terminal Differentiation and Loss of Multipotency. *Immunity* **46**, 596–608 (2017).
74. Skene, P. J. & Henikoff, S. An efficient targeted nuclease strategy for high-resolution mapping of DNA binding sites. *eLife* **6**, e21856 (2017).
75. Ford, B. R. *et al.* Tumor microenvironmental signals reshape chromatin landscapes to limit the functional potential of exhausted T cells. *Sci. Immunol.* **7**, eabj9123 (2022).
76. Weber, E. W. *et al.* Transient rest restores functionality in exhausted CAR-T cells through epigenetic remodeling. *Science* **372**, (2021).
77. Gaud, G., Lesourne, R. & Love, P. E. Regulatory mechanisms in T cell receptor signalling. *Nat. Rev. Immunol.* **18**, 485–497 (2018).
78. Zhou, X. & Xue, H.-H. Generation of memory precursors and functional memory CD8+ T cells depends on TCF-1 and LEF-1. *J. Immunol. Baltim. Md 1950* **189**, 2722–2726 (2012).
79. Danilo, M., Chennupati, V., Silva, J. G., Siegert, S. & Held, W. Suppression of Tcf1 by Inflammatory Cytokines Facilitates Effector CD8 T Cell Differentiation. *Cell Rep.* **22**, 2107–2117 (2018).
80. Kratchmarov, R., Magun, A. M. & Reiner, S. L. TCF1 expression marks self-renewing human CD8+ T cells. *Blood Adv.* **2**, 1685–1690 (2018).
81. Gautam, S. *et al.* The transcription factor c-Myb regulates CD8+ T cell stemness and antitumor immunity. *Nat. Immunol.* **20**, 337–349 (2019).
82. Hess Michelini, R., Doedens, A. L., Goldrath, A. W. & Hedrick, S. M. Differentiation of CD8 memory T cells depends on Foxo1. *J. Exp. Med.* **210**, 1189–1200 (2013).
83. Rutishauser, R. L. *et al.* Transcriptional Repressor Blimp-1 Promotes CD8+ T Cell Terminal Differentiation and Represses the Acquisition of Central Memory T Cell Properties. *Immunity* **31**, 296–308 (2009).
84. Yao, C. *et al.* Single-cell RNA-seq reveals TOX as a key regulator of CD8+ T cell persistence in chronic infection. *Nat. Immunol.* **20**, 890–901 (2019).
85. Beltra, J.-C. *et al.* Stat5 opposes the transcription factor Tox and rewires exhausted CD8+ T cells toward durable effector-like states during chronic antigen exposure. *Immunity* **56**, 2699-2718.e11 (2023).
86. Martinez, G. J. *et al.* The Transcription Factor NFAT Promotes Exhaustion of Activated CD8+ T Cells. *Immunity* **42**, 265–278 (2015).

87. Man, K. *et al.* Transcription Factor IRF4 Promotes CD8+ T Cell Exhaustion and Limits the Development of Memory-like T Cells during Chronic Infection. *Immunity* **47**, 1129-1141.e5 (2017).
88. Guo, H. *et al.* PRDM1 Drives Human Primary T Cell Hyporesponsiveness by Altering the T Cell Transcriptome and Epigenome. *Front. Immunol.* **13**, 879501 (2022).
89. Jung, I.-Y. *et al.* BLIMP1 and NR4A3 transcription factors reciprocally regulate antitumor CAR T cell stemness and exhaustion. *Sci. Transl. Med.* **14**, eabn7336 (2022).
90. Belk, J. A. *et al.* Genome-wide CRISPR screens of T cell exhaustion identify chromatin remodeling factors that limit T cell persistence. *Cancer Cell* **40**, 768-786.e7 (2022).
91. Salas, A. *et al.* JAK–STAT pathway targeting for the treatment of inflammatory bowel disease. *Nat. Rev. Gastroenterol. Hepatol.* **17**, 323–337 (2020).
92. Cui, A. *et al.* Dictionary of immune responses to cytokines at single-cell resolution. *Nature* 1–8 (2023) doi:10.1038/s41586-023-06816-9.
93. Wang, X., Lupardus, P., LaPorte, S. L. & Garcia, K. C. Structural Biology of Shared Cytokine Receptors. *Annu. Rev. Immunol.* **27**, 29–60 (2009).
94. JAKs and STATs in Immunity, Immunodeficiency, and Cancer | NEJM. https://www.nejm.org/doi/10.1056/NEJMra1202117.
95. Hu, X., Li, J., Fu, M., Zhao, X. & Wang, W. The JAK/STAT signaling pathway: from bench to clinic. *Signal Transduct. Target. Ther.* **6**, 1–33 (2021).
96. Shourian, M., Beltra, J.-C., Bourdin, B. & Decaluwe, H. Common gamma chain cytokines and CD8 T cells in cancer. *Semin. Immunol.* **42**, 101307 (2019).
97. Cornish, G. H., Sinclair, L. V. & Cantrell, D. A. Differential regulation of T-cell growth by IL-2 and IL-15. *Blood* **108**, 600–608 (2006).
98. Kalia, V. *et al.* Prolonged Interleukin-2Rα Expression on Virus-Specific CD8+ T Cells Favors Terminal-Effector Differentiation In Vivo. *Immunity* **32**, 91–103 (2010).
99. Kalia, V. & Sarkar, S. Regulation of Effector and Memory CD8 T Cell Differentiation by IL-2—A Balancing Act. *Front. Immunol.* **9**, (2018).
100. Beltra, J.-C. *et al.* IL2Rβ-dependent signals drive terminal exhaustion and suppress memory development during chronic viral infection. *Proc. Natl. Acad. Sci.* **113**, E5444–E5453 (2016).
101. Tan, J. T. *et al.* IL-7 is critical for homeostatic proliferation and survival of naive T cells. *Proc. Natl. Acad. Sci. U. S. A.* **98**, 8732–8737 (2001).
102. Richer, M. J. *et al.* Inflammatory IL-15 is required for optimal memory T cell responses. *J. Clin. Invest.* **125**, 3477–3490 (2015).
103. Teague, R. M. *et al.* Interleukin-15 rescues tolerant CD8+ T cells for use in adoptive immunotherapy of established tumors. *Nat. Med.* **12**, 335–341 (2006).
104. Casey, K. A. & Mescher, M. F. IL-21 Promotes Differentiation of Naive CD8 T Cells to a Unique Effector Phenotype1. *J. Immunol.* **178**, 7640–7648 (2007).
105. Barker, B. R., Gladstone, M. N., Gillard, G. O., Panas, M. W. & Letvin, N. L. Critical role for IL-21 in both primary and memory anti-viral CD8+ T-cell responses. *Eur. J. Immunol.* **40**, 3085–3096 (2010).
106. Acacia de Sa Pinheiro, A. *et al.* IL-4 induces a wide-spectrum intracellular signaling cascade in CD8+ T cells. *J. Leukoc. Biol.* **81**, 1102–1110 (2007).
107. Silva-Filho, J. L., Caruso-Neves, C. & Pinheiro, A. A. S. IL-4: an important cytokine in determining the fate of T cells. *Biophys. Rev.* **6**, 111–118 (2014).

108. Sumida, T. S. *et al.* Type I interferon transcriptional network regulates expression of coinhibitory receptors in human T cells. *Nat. Immunol.* **23**, 632–642 (2022).
109. Wu, T. *et al.* The TCF1-Bcl6 axis counteracts type I interferon to repress exhaustion and maintain T cell stemness. *Sci. Immunol.* **1**, eaai8593 (2016).
110. Jergović, M. *et al.* Infection-induced type I interferons critically modulate the homeostasis and function of CD8+ naïve T cells. *Nat. Commun.* **12**, 5303 (2021).
111. Huseni, M. A. *et al.* CD8+ T cell-intrinsic IL-6 signaling promotes resistance to anti-PD-L1 immunotherapy. *Cell Rep. Med.* **4**, 100878 (2023).
112. Smith, L. K. *et al.* Interleukin-10 Directly Inhibits CD8+ T Cell Function by Enhancing N-Glycan Branching to Decrease Antigen Sensitivity. *Immunity* **48**, 299-312.e5 (2018).
113. Hanna, B. S. *et al.* Interleukin-10 receptor signaling promotes the maintenance of a PD-1int TCF-1+ CD8+ T cell population that sustains anti-tumor immunity. *Immunity* **54**, 2825-2841.e10 (2021).
114. Guo, Y. *et al.* Metabolic reprogramming of terminally exhausted CD8+ T cells by IL-10 enhances anti-tumor immunity. *Nat. Immunol.* **22**, 746–756 (2021).
115. Curtsinger, J. M., Johnson, C. M. & Mescher, M. F. CD8 T Cell Clonal Expansion and Development of Effector Function Require Prolonged Exposure to Antigen, Costimulation, and Signal 3 Cytokine. *J. Immunol.* **171**, 5165–5171 (2003).
116. Zebley, C. C. *et al.* Proinflammatory cytokines promote TET2-mediated DNA demethylation during CD8 T cell effector differentiation. *Cell Rep.* **37**, 109796 (2021).
117. Oh, S. A. & Li, M. O. TGF-β: Guardian of T Cell Function. *J. Immunol. Baltim. Md 1950* **191**, 3973–3979 (2013).
118. Thomas, D. A. & Massagué, J. TGF-β directly targets cytotoxic T cell functions during tumor evasion of immune surveillance. *Cancer Cell* **8**, 369–380 (2005).
119. Bald, T. & Smyth, M. J. TGFβ shuts the door on T cells. *Br. J. Cancer* **119**, 1–3 (2018).
120. Mani, V. *et al.* Migratory DCs activate TGF-β to precondition naïve CD8+ T cells for tissue-resident memory fate. *Science* **366**, eaav5728 (2019).
121. Jung, I.-Y. *et al.* Tissue-resident memory CAR T cells with stem-like characteristics display enhanced efficacy against solid and liquid tumors. *Cell Rep. Med.* **4**, 101053 (2023).
122. Gabriel, S. S. *et al.* Transforming growth factor-β-regulated mTOR activity preserves cellular metabolism to maintain long-term T cell responses in chronic infection. *Immunity* **0**, (2021).
123. Hu, Y. *et al.* TGF-β regulates the stem-like state of PD-1+ TCF-1+ virus-specific CD8 T cells during chronic infection. *J. Exp. Med.* **219**, e20211574 (2022).
124. Weiss, A. & Imboden, J. B. Cell Surface Molecules and Early Events Involved in Human T Lymphocyte Activation. in *Advances in Immunology* (eds. Dixon, F. J., Austen, K. F., Hood, L. E. & Uhr, J. W.) vol. 41 1–38 (Academic Press, 1987).
125. Freeman, B. E., Hammarlund, E., Raué, H.-P. & Slifka, M. K. Regulation of innate CD8+ T-cell activation mediated by cytokines. *Proc. Natl. Acad. Sci. U. S. A.* **109**, 9971–9976 (2012).
126. Proserpio, V. *et al.* Single-cell analysis of CD4+ T-cell differentiation reveals three major cell states and progressive acceleration of proliferation. *Genome Biol.* **17**, 103 (2016).
127. Lin, W.-H. W. *et al.* Asymmetric PI3K Signaling Driving Developmental and Regenerative Cell Fate Bifurcation. *Cell Rep.* **13**, 2203–2218 (2015).

128. Neitzke-Montinelli, V. *et al.* Differentiation of Memory CD8 T Cells Unravel Gene Expression Pattern Common to Effector and Memory Precursors. *Front. Immunol.* **13**, (2022).
129. Ma, E. H. *et al.* Metabolic Profiling Using Stable Isotope Tracing Reveals Distinct Patterns of Glucose Utilization by Physiologically Activated CD8+ T Cells. *Immunity* **51**, 856-870.e5 (2019).
130. Pipkin, M. E. *et al.* Interleukin-2 and Inflammation Induce Distinct Transcriptional Programs that Promote the Differentiation of Effector Cytolytic T Cells. *Immunity* **32**, 79–90 (2010).
131. Vardhana, S. A. *et al.* Impaired mitochondrial oxidative phosphorylation limits the self-renewal of T cells exposed to persistent antigen. *Nat. Immunol.* **21**, 1022–1033 (2020).
132. Corselli, M. *et al.* Single cell multiomic analysis of T cell exhaustion in vitro. *Cytometry A* **101**, 27–44 (2022).
133. Dunsford, L. S., Thoirs, R. H., Rathbone, E. & Patakas, A. A Human In Vitro T Cell Exhaustion Model for Assessing Immuno-Oncology Therapies. in *Immuno-Oncology: Cellular and Translational Approaches* (ed. Tan, S.-L.) 89–101 (Springer US, 2020). doi:10.1007/978-1-0716-0171-6_6.
134. Scharping, N. E. *et al.* Mitochondrial stress induced by continuous stimulation under hypoxia rapidly drives T cell exhaustion. *Nat. Immunol.* **22**, 205–215 (2021).
135. Zhao, M. *et al.* Rapid in vitro generation of bona fide exhausted CD8+ T cells is accompanied by Tcf7 promotor methylation. *PLOS Pathog.* **16**, e1008555 (2020).

Chapter 2. MULTIPLE PATHS TO CD8$^+$ T CELL MEMORY VIA REVERSIBLE EPIGENETIC SILENCING OF TCF1

This chapter and corresponding Mathematical Appendix were minimally modified from a published manuscript in *Immunity*, Vol 57, Issue 2, Abadie*, **Clark***, Valanparambil* et al., **Reversible, tunable epigenetic silencing of TCF1 generates flexibility in the T cell memory decision**, Pages 271-286.e13, Copyright Elsevier (2024):

*co-first authors

Supplemental Tables 1-4 and **Supplemental Movies 1-3** are available with the original article in *Immunity* at this link: https://doi.org/10.1016/j.immuni.2023.12.006

2.1 ABSTRACT

The immune system encodes information about the severity of a pathogenic threat in the quantity and type of memory cells it forms. This encoding emerges from lymphocyte decisions to maintain or lose self-renewal and memory potential during a challenge. By tracking responding CD8$^+$ T cells at the single-cell and clonal lineage level using time-resolved transcriptomics, quantitative live imaging, and an acute infection model, we find that T cells may initially maintain or lose memory potential early after antigen recognition, but following pathogen clearance, may regain memory potential if initially lost. Mechanistically, this flexibility in memory decision making is implemented by a stochastic cis-epigenetic switch that reversibly silences the memory regulator TCF1 in response to stimulation. Mathematical modeling shows how this flexibility allows memory T cell numbers to scale robustly with pathogen virulence and immune response magnitudes. We propose that flexibility and stochasticity in cellular decision making ensures optimal immune responses against diverse threats.

2.2 INTRODUCTION

The immune system stores information about the nature and severity of prior infections through the generation of long-lived pathogen-specific memory lymphocytes during an immune response. This memory is encoded by the numbers and types of memory lymphocytes generated upon challenge. The quantity of memory T cells, in particular, scales with the magnitude of a prior infection, such that the memory population is a fixed fraction of the T cell number at the infection peak, across a range of pathogenic challenges[1–3]. This scaling in memory production is robust across T cell clones with different epitope specificities and allows the body to generate memory proportional to the severity of the pathogenic challenge. The regulatory mechanisms that enable this critical feature of adaptive immunity are not well understood.

The size and characteristics of the memory compartment are determined by the lineage decisions of T cells responding to an acute infection[4]. As naive $CD8^+$ T cells respond to antigens, some maintain long-term viability and self-renewal potential, and thereby persist to form memory cells as the infection is cleared, while the majority terminally differentiate to form cytotoxic effectors. One class of models posits that memory cells form directly from naive cells without passing through an effector phase, through an early lineage bifurcation that concurrently gives rise to either memory-precursor or terminal effector cells[5–7]. A second class of models posits that this decision to progress toward memory or become short-lived effectors occurs later, only after cells have undergone effector differentiation and upon resolution of an infection[8–10]. However, in contrast with both models, it is also possible that this process is inherently flexible[11], such that T cells have multiple opportunities to commit to the memory state. In a number of stem cell systems, cell differentiation decisions are sometimes reversible[12,13], and this plasticity may

enable organisms to robustly maintain cell population sizes amid different settings. During an immune response, flexibility could optimize T cell memory formation for threats whose properties may only manifest as they unfold over time. It is unclear whether there exists such flexibility in T cell memory formation and, if so, what the underlying mechanisms and functional roles are.

T cell effector and memory differentiation is controlled by a circuit of transcription factors and chromatin regulators that enable transitions between different states in response to external signals. A central node in this regulatory circuit is TCF1 (encoded by *Tcf7*), a transcription factor essential for memory cell generation and self-renewal[14]. *Tcf7* is expressed in naive and memory cells, where it is crucial for maintaining self-renewal, and is silenced during effector differentiation, resulting in loss of memory potential and entry into a short-lived state[5,15].

To follow *Tcf7* regulation and memory decision-making in a controlled environment where cells can be continuously observed and signaling inputs carefully manipulated, we developed an *ex vivo* system to study T cell differentiation in response to stimulatory signals present during an acute infection. Using this system and complementary testing in an *in vivo* acute infection model, we uncovered a flexible decision-making strategy: T cells can gain or lose memory potential at multiple junctures after antigen encounter, and do so in a stochastic and reversible manner. Mathematical modeling revealed that this flexible decision-making strategy allows for the number of memory cells to scale linearly with total numbers of expanded T cells at the peak of infection, thereby encoding information about the severity of the prior threat. These findings unify two major models for memory lineage specification that are often regarded as mutually

opposed, and provide a quantitative framework for understanding immunological memory encoding.

2.3 RESULTS

2.3.1 *A minimal* ex vivo *system for effector and memory differentiation of CD8$^+$ T cells*

To disentangle candidate models for memory T cell formation (**Fig. 2.1A**), we developed a minimal system (**Fig. 2.1B**) in which naive (CD44$^-$CD62L$^+$) CD8$^+$ T cells with a YFP reporter for *Tcf7*[16] were activated with plate-immobilized anti-CD3 and anti-CD28 antibodies and IL-2, together with additional cytokines present during acute infection (IL-12, IL-7, and IL-15[17–19]). These conditions minimized variability in the exposure of individual cells to stimulatory signals, enabling cell-intrinsic lineage control mechanisms to be studied apart from environmental heterogeneity.

In this system, all cells began dividing rapidly after 24 hours and upregulated the transmembrane glycoprotein CD44, indicating uniform activation (**Fig. 2.1C**). Activated cells downregulated *Tcf7* and the lymph node-homing adhesion molecule CD62L, consistent with effector differentiation. The inflammatory cytokines IL-12 and IFN-β1 enhanced *Tcf7*-YFP silencing (**Fig. 2.1D; Fig. 2.2C-D**), consistent with their roles in driving effector differentiation[20,21]. When TCR stimulation (anti-CD3/CD28) and inflammation (IL-12) were removed to mimic pathogen clearance, the cells demonstrated a population-level increase in CD62L and *Tcf7*-YFP while continuing to divide, as previously observed[4]. *Tcf7* and CD62L protein levels were heterogeneous both during stimulation and after removal, suggestive of an early memory and

effector differentiation decision. YFP expression closely matched TCF1 protein levels throughout activation, validating use of the reporter in this system (**Fig. 2.2A-B**).

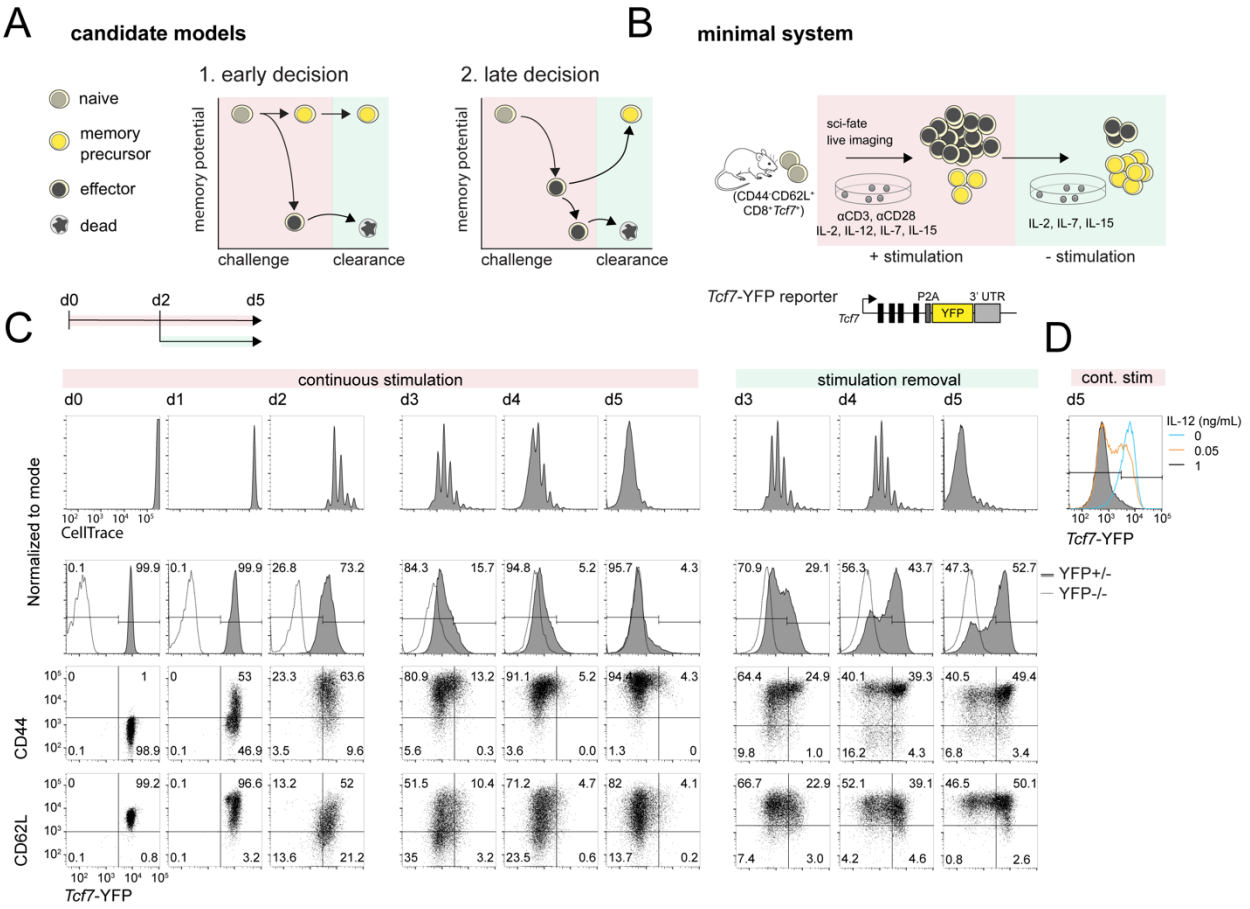

Figure 2.1. A minimal *ex vivo* system to track CD8$^+$ T cell effector and memory decision making dynamics. (**A**) Candidate decision-making strategies for CD8$^+$ T cell memory generation (**B**) a minimal *ex vivo* system for tracking memory decision-making dynamics at the single-cell level. (**C-D**) Naive CD8$^+$ T cells were isolated from *Tcf*7-YFP reporter mice, then cultured using this *ex vivo* system. (**C**) Flow cytometry plots show analysis of cultured cells during initial stimulation for 2 days (left) and continued stimulation to day 5 (middle), or after stimulation withdrawal (removal of αCD3/αCD28 after day 2 and IL-12 after day 3) (right). From top to bottom: CellTrace Violet (CTV) dilution; *Tcf*7-YFP histograms (shaded histograms are from *Tcf*7-YFP$^{+/-}$ mice and open histograms are from wild type mice); Flow plots of CD44 against *Tcf*7-YFP; and of CD62L against *Tcf*7-YFP. (**D**) *Tcf*7-YFP silencing is tunable by IL-12 concentration. [C-D] Data are from a single experiment representative of at least 3 independent experiments.

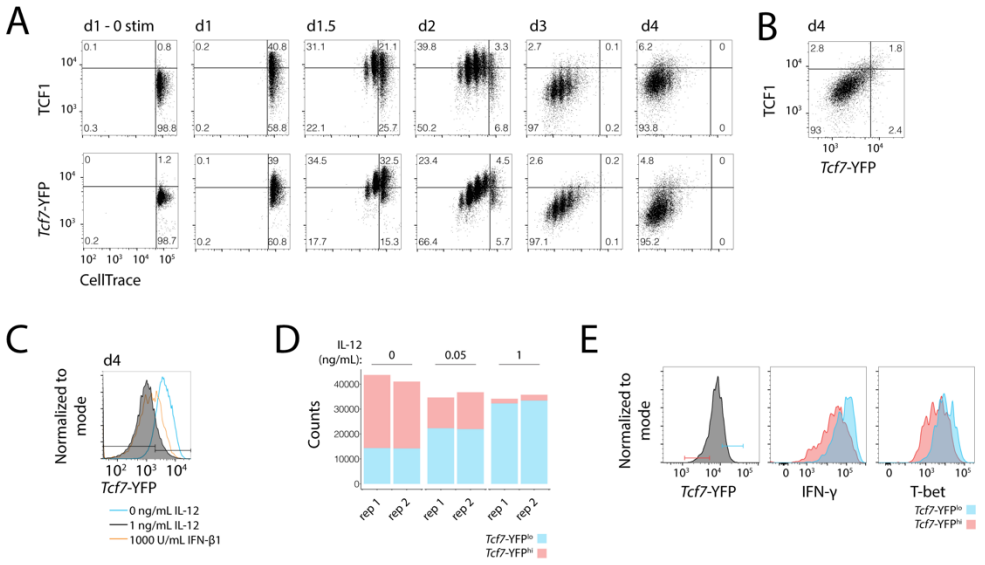

Figure 2.2. Characterization of the *Tcf7*-YFP reporter during *ex vivo* CD8$^+$ T cell activation.
Related to Figure 2.1. (**A-B**) TCF1 and *Tcf7*-YFP correlation in cells activated with 1 ng/ml IL-12. Note, *Tcf7*-YFP dynamic range is reduced in fixed and permeabilized samples due to leakage of fluorescent protein out of permeabilized cells. (**C**) *Tcf7* silencing in cells stimulated with IFN-β1 or IL-12. (**D**) Total *Tcf7*-YFP^{hi} and *Tcf7*-YFP^{lo} cell counts for samples activated for 4 days with different IL-12 levels. (**E**) IFN-ɣ and T-bet levels in cells stimulated for 2 days with IL-12. Data are from a single experiment representative of [A-B] 2 independent experiments, [C] 1 experiment for IFN-β1 and at least 3 for others, [D] at least 3 independent experiments, [E] 1 experiment.

2.3.2 *Naive CD8$^+$ T cells bifurcate early into effectors and memory precursors*

To determine whether the heterogeneity in *Tcf7* and CD62L regulation reflects early memory and effector programming (**Fig. 2.1**), we analyzed *ex vivo* activated cells using the temporally-resolved single-cell transcriptome sequencing method, *sci-fate*[22]. Here, metabolic labeling of newly-synthesized transcripts reveals a cell's current activity state apart from its history[22,23] (**Fig. 2.3A**). We subjected cells at days 1, 2, and 4 to 4-thiouridine (4sU) pulse-labeling for 2 hrs, followed by sequencing and analysis as previously described[22]. We obtained old and new transcriptomes for ~17,000 single cells, with a median of 17,574 total and 2,529 new transcripts detected per cell (**Fig. 2.4A**). To disentangle effector and memory gene programs from other activation-induced programs, we performed an integrative analysis of our temporally-resolved

transcriptome data and existing transcription factor (TF) binding data[24] to identify TF modules, consisting of co-regulated groups of TFs and their cognate target genes (see **2.6 Methods**). This analysis revealed two main TF modules: a cell cycle module and a T cell differentiation module, the latter further separable into submodules that included known regulators of effector and memory differentiation (**Fig. 2.3B; Fig. 2.4C**).

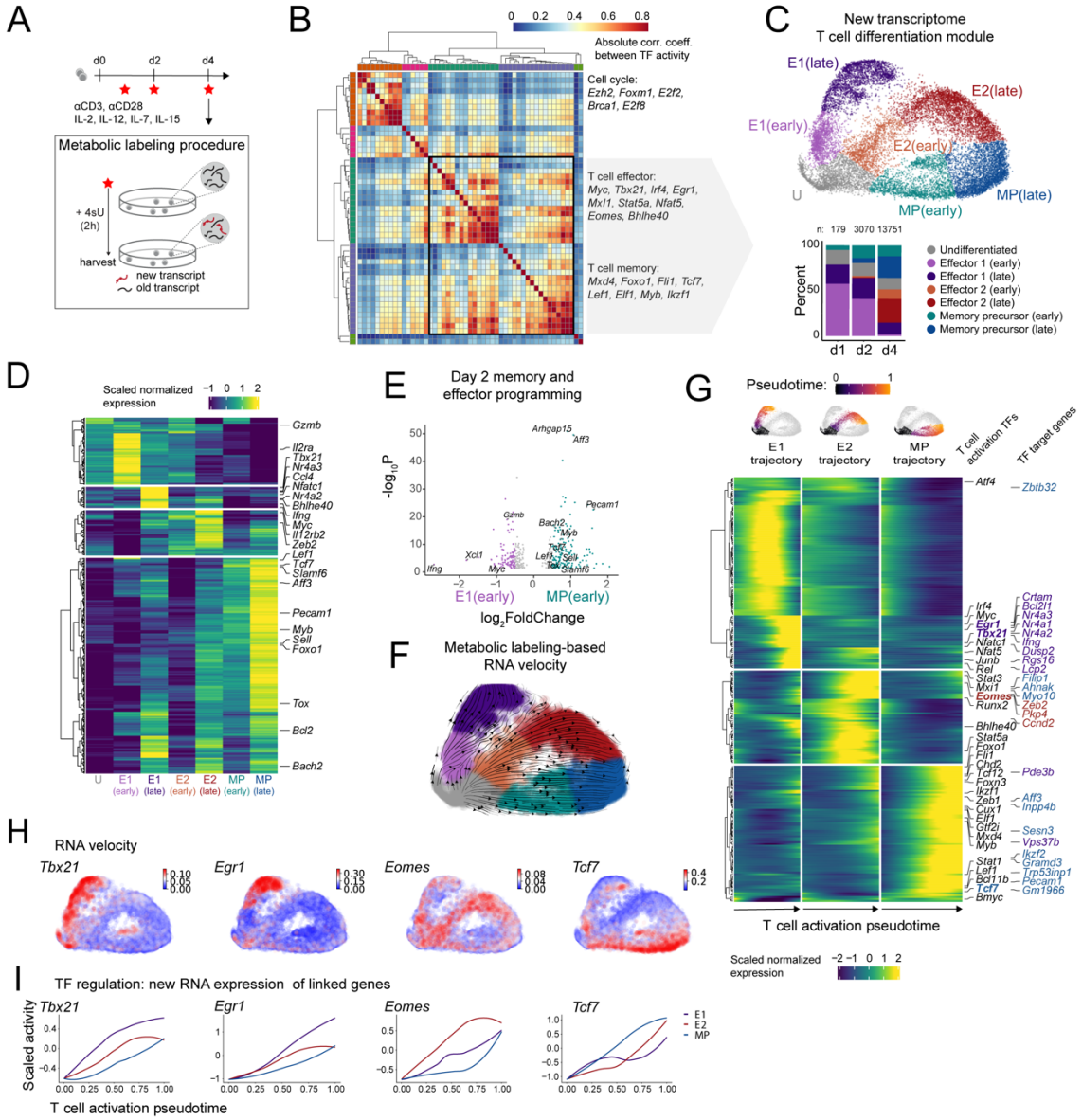

Figure 2.3. Naive cells diverge into effector and memory states early after activation.
(**A**) Naive $CD8^+$ T cells were activated with αCD3 and αCD28 and 0.05 ng/mL IL-12, as well as IL-2, IL-7 and IL-15. After 1, 2, and 4 days, cells were treated with 4sU for 2 hours to label new transcripts, then harvested for time-resolved transcriptomics using *sci-fate*. (**B**) Heatmap showing the absolute Pearson's correlation coefficient between the activities of pairs of TFs. Key TFs in each module are labeled at right. T cell differentiation module used for subsequent analysis is boxed. (**C**) UMAP visualization of cells based on the activity of T cell differentiation-related TF module, using newly synthesized mRNA, colored by cluster ID (top). Percentage of cells in each T cell differentiation state cluster after indicated days (bottom). (**D**) Aggregated expression (scaled, $\log_{10}$ normalized) of top 400 differentially expressed (DE) genes between clusters ($q < 3 \times 10^{-45}$ for all genes except for *Ifng*, $q = 7.3 \times 10^{-29}$). (**E**) DE genes between E1(early) and MP(early) at day 2 only; log2FC > 0.5 and adj. $p < 0.05$. (**F**) UMAP visualization as in (C), characterized by labeling-based RNA velocity analysis. Streamlines indicate the integration paths that connect local projections from the observed state to the extrapolated future state[26]. (**G**) Pseudotemporal ordering of top 200 DE genes and additional genes of interest ($q < 1.4 \times 10^{-17}$) between trajectories. Gene labels correspond to all DE TFs in the T cell differentiation TF module (left text) and DE target genes linked to *Tbx21*, *Egr1*, *Eomes*, and *Tcf7* (right text). (**H**) RNA velocity magnitude and (**I**) Loess smoothed TF activity over pseudotime for four of the most DE genes between trajectories. TF activity is calculated as the normalized aggregation of newly synthesized mRNA for all TF target genes, scaled across all cells. Cells in the undifferentiated (U) cluster are set to pseudotime = 0 for each trajectory.

By visualizing cell states using genes in the T cell differentiation module for Uniform Manifold Approximation and Projection (UMAP) dimensionality reduction, we resolved distinct effector and memory states with coherence between timepoints (**Fig. 2.3C; Fig. 2.4B, D**). Unsupervised clustering and differential gene expression analysis revealed early and late effector (E1 and E2) and memory precursor (MP) states. E1 and E2 cells exhibited higher expression of the effector-associated genes *Gzmb, Ifng, Tbx21, Zeb2,* and *IL12rb2,* while MP cells had higher expression of the stem- and memory-associated factors *Bach2, Lef1, Tcf7, Sell*, and *Slamf6*, and lower expression of effector-associated genes (**Fig. 2.3D-E; Fig. 2.4E-F; Supplemental Table 1**)[25]. These differential gene expression patterns were present at day 2 and amplified at day 4.

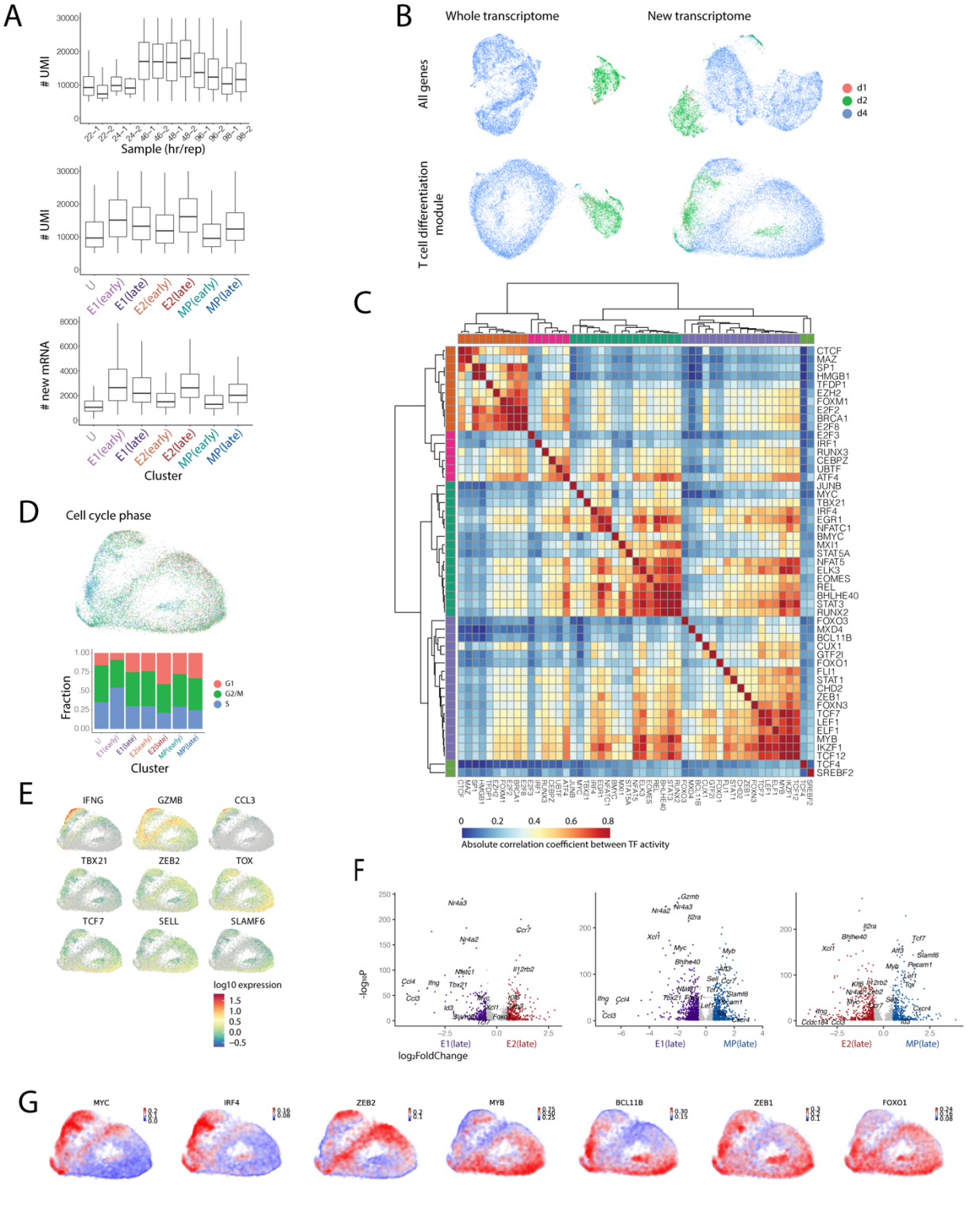
A
UMI
Sample (hr/rep)
new mRNA
U
E1(early)
E1(late)
E2(early)
E2(late)
MP(early)
MP(late)
Cluster
B
Whole transcriptome
New transcriptome
All genes
T cell differentiation module
d1
d2
d4
C
Absolute correlation coefficient between TF activity
D
Cell cycle phase
Fraction
G1
G2/M
S
E
IFNG
GZMB
CCL3
TBX21
ZEB2
TOX
TCF7
SELL
SLAMF6
log10 expression
F
-log10P
log2FoldChange
G
MYC
IRF4
ZEB2
MYB
BCL11B
ZEB1
FOXO1

Figure 2.4. *Sci-fate* metrics and TF module analysis.
Related to Figure 2.3. (**A**) Number of UMI per cell for each time point and replicate sample (top); number of UMI (middle) and newly synthesized reads (bottom) per cell for each cluster. (**B**) UMAP projections of cells using whole or new transcriptome and all genes or only T cell differentiation module genes. (**C**) Transcription factor module analysis as in Fig. 2B, enlarged to show direct TF correlations. (**D**) UMAP projection with cells colored by cell cycle phase [1] and fraction of cells in each phase for all clusters. (**E**) Expression of representative genes in UMAP space. **(F)** Differentially expressed genes between indicated clusters, using cells from all timepoints; log2FC > 0.5 and adj. $p < 0.05$. (**G**) RNA velocity magnitude for additional effector and memory genes, similar to Fig. 2H.

Consistent with an early fate bifurcation, RNA velocity vectors calculated using reads from newly synthesized transcripts originate from the undifferentiated state (U), and flow along separate effector and memory branches[26,27] (**Fig. 2.3F**). To gain insight into the dynamics of genes differentially regulated between divergent trajectories, we visualized their expression over pseudotime along each trajectory (**Fig. 2.3G; Supplemental Table 1**). This analysis, together with RNA velocity and TF activity analysis (**Fig. 2.3H-I; Fig. 2.4G**), identified effector and memory regulators with greatest differential regulation along their respective trajectories. *Tbx21, Egr1,* and *Irf4*, among other effector regulatory genes, were specifically active along the E1 trajectory, while a distinct set of effector regulators, including *Eomes, Bhlhe40*, *Stat5a* and *Stat3*, characterize the E2 trajectory. This effector heterogeneity and its potential influence on downstream differentiation will be interesting to investigate in future studies but is not further pursued here. Finally, regulators of T cell stemness and survival, including *Tcf7, Myb, Mxd4,* and *Fli1*, were active in the MP trajectory. *Tcf7* was the most significantly differentially expressed gene between trajectories, upregulated early along the MP trajectory and absent in both E1 and E2 trajectories. Its expression furthermore coincided with that of target genes identified through TF linkage that promote self-renewal, such as *Ikzf2*, *Sesn3*, *Aff3*, and *Pecam1* (CD31). Thus, *Tcf7* is a critical driver of this early divergent memory trajectory in our system.

2.3.3 *The early effector and memory decision occurs heterogeneously within CD8$^+$ T cell clones*

The divergence of cells into effector and memory lineages, occurring even under the strong, uniform stimulatory conditions of our *ex vivo* system, is suggestive of a cell-intrinsic regulatory mechanism involving *Tcf7* that generates heterogeneity in fate outcomes. To elucidate the degree to which this decision is heterogeneous within cell lineages amid constant environmental signals, we acquired multi-day time-lapse movies of clonal CD8$^+$ T cell lineages during activation with continuous measurement of *Tcf7*-YFP expression (**Fig 2.5**). As T cells are difficult to track with live imaging due to their high mobility, tendency to adhere to one another, and rapid proliferation, we optimized adhesion conditions and computational analyses that allow continuous tracking of a fate regulating TF across clonal CD8$^+$ T cell lineages (**Fig. 2.5; Fig. 2.6;** see **2.6 Methods**)[28]. We note that adhering T cells to plate-bound stimulatory molecules is expected to create differences compared to stimulation by antigen presenting cells. However, we chose this minimal system to ensure that all cells received a uniform signaling environment, to disentangle cell-extrinsic versus intrinsic sources of heterogeneity. Using this method, we tracked 104 lineages over 4 days and an average of 4.4 cell generations, where each lineage is a family of imaged cells derived from a single naive precursor.

Naive cells in these time-lapse movies started small, adhered to the antibody-bound plate, acquired CD69 expression, increased dramatically in size, and divided rapidly after 1-2 days (**Fig. 2.6G; Supplemental Movie 1**). Individual activating T cell clones often gave rise to *Tcf7*-YFP^{hi} and *Tcf7*-YFP^{lo} subpopulations (**Fig. 2.5A; Fig. 2.6J; Supplemental Movie 1**), indicating that the effector and memory decision is made heterogeneously within clones. *Tcf7*-YFP^{hi} and

Tcf7-YFP^{lo} cells showed similar degrees of attachment to the surface, indicating that these intra-clonal differences were not due to differences in TCR stimulation, but more likely due to cell-intrinsic mechanisms generating heterogeneity in *Tcf7* silencing.

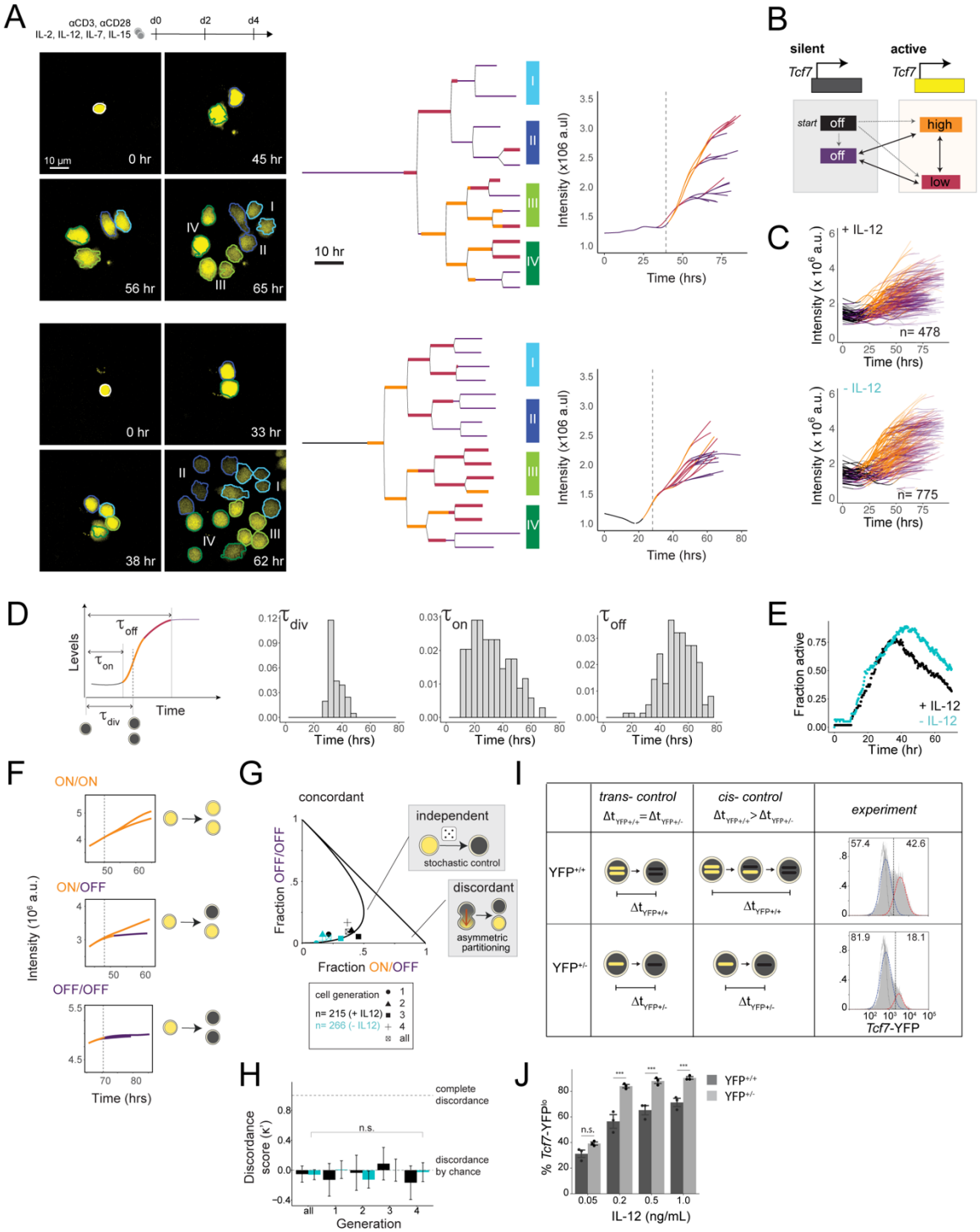

Figure 2.5. Heterogeneous *Tcf7* silencing within clones is controlled by a stochastic epigenetic switch.
(**A**) top: Naive $CD8^+$ T cells were activated with αCD3, αCD28, and IL-12, as well as IL-2, IL-7 and IL-15. Cells are cultured with 1 ng/ml IL-12 unless otherwise indicated. (**A**) bottom: Representative lineages demonstrating clonal heterogeneity in *Tcf7*-YFP silencing: image snap shots (left), lineage trees (middle), and reporter intensity (area x median YFP fluorescence) over time for each track (right), with the first cell division marked by a vertical dashed line. Cell borders in snapshots are colored and labeled to match their corresponding leaves in the lineage trees. Lineage trees and tracks are colored by HMM-derived promoter state, outlined in (**B**). (**C**) Reporter intensity for all overlaid cell tracks, colored by promoter state, where n is equivalent to the number of progeny across all lineages in the dataset at the end of observation. (**D**) For each track, from left to right: time of first division, time of first transition to a stable active state, time of first transition to a stable silent state (stable state ≥ 10 hrs). (**E**) For all lineages combined, fraction of cells in an active promoter state over time. (**F-H**) Each division of a parent cell with the *Tcf7* promoter ON was categorized as giving rise to zero, one, or two daughters that transition to an OFF state. (**F**) Examples of each division category. (**G**) The OFF/OFF fraction by ON/OFF fraction is plotted separately for each generation to distinguish concordant, independent, and asymmetric silencing mechanisms. (**H**) Modified Cohen's kappa test for division events in (G). (**I**) Comparison of $YFP^{+/+}$ and $YFP^{+/-}$ reporters to distinguish *cis* and *trans* regulation of *Tcf7* silencing (left). YFP distributions for $YFP^{+/+}$and $YFP^{+/-}$ reporters cultured for 5 days with 0.2 ng/ml IL-12 (right). *Tcf7*-YFP^{lo} fractions are calculated from gaussian fits to distributions. (**J**) *Tcf7*-YFP^{lo} percentages as in (I), over a range of IL-12 concentrations. Mean ± s.d. Statistical significance was calculated with an unpaired two-tailed t test; n.s. p=0.05, ***p<0.005. Individual data points are from a single experiment representative of 2 independent experiments (I-J).

Differences in *Tcf7*-YFP expression after multiple cell divisions likely stemmed from earlier *Tcf7* silencing events propagated through dilution of the stable fluorescent protein by cell division. To pinpoint the timing of early regulatory events that gave rise to these differences in *Tcf7*-YFP expression, we calculated the *Tcf7* promoter activity over time in single cells, defined as the rate at which total *Tcf7*-YFP abundance increased over time, using a Hidden Markov Model (HMM) to assign *Tcf7* promoter activity states to each cell at each timepoint and identify switching points between those states (**Fig. 2.5A-C; Fig. 2.6A-F;** see **2.6 Methods**). This analysis revealed that cells silenced *Tcf7* expression at variable times after the onset of stimulation, and could do so as early as the first cell division, as well as at later generations. Cells activated the *Tcf7* promoter prior to the first cell division, reflecting exit from quiescence, and then proceeded to switch the *Tcf7* promoter to a silent state.

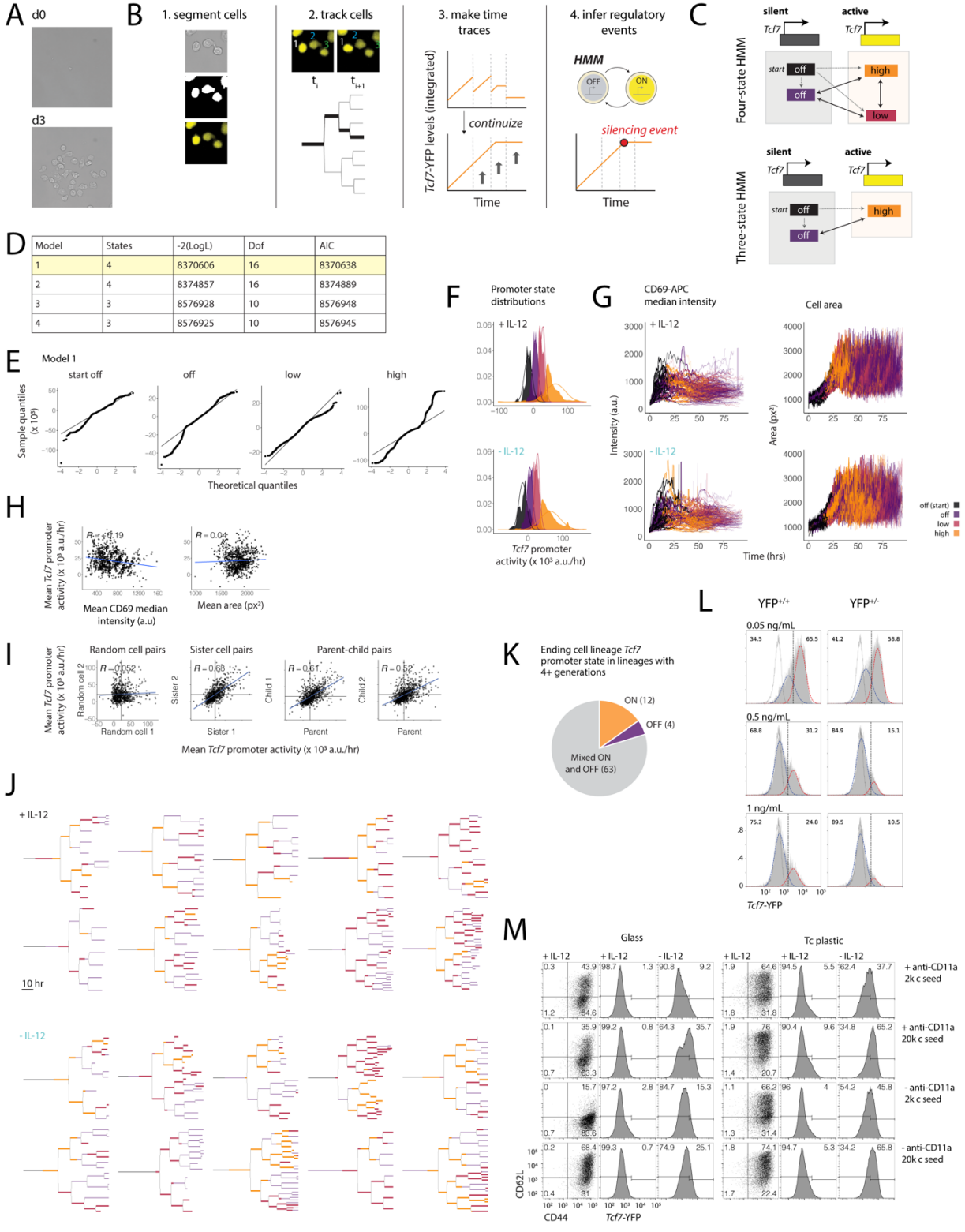
A
d0
d3
B
1. segment cells
2. track cells
3. make time traces
4. infer regulatory events
Tcf7-YFP levels (integrated)
continuize
Time
HMM
OFF
ON
silencing event
Time
C
silent
active
Tcf7
Four-state HMM
start
off
high
low
Three-state HMM
D
Model
States
-2(LogL)
Dof
AIC
1 4 8370606 16 8370638
2 4 8374857 16 8374889
3 3 8576928 10 8576948
4 3 8576925 10 8576945
E
Model 1
start off
off
low
high
Sample quantiles (x 10³)
Theoretical quantiles
F
Promoter state distributions
+ IL-12
- IL-12
Tcf7 promoter activity (x 10³ a.u./hr)
G
CD69-APC median intensity
Cell area
Intensity (a.u.)
Area (px²)
Time (hrs)
off (start)
off
low
high
H
Mean Tcf7 promoter activity (x 10³ a.u./hr)
R = 0.19
R = 0.04
Mean CD69 median intensity (a.u)
Mean area (px²)
I
Random cell pairs
Sister cell pairs
Parent-child pairs
R = 0.052
R = 0.68
R = 0.61
R = 0.52
Random cell 1
Random cell 2
Sister 1
Sister 2
Parent
Child 1
Child 2
Mean Tcf7 promoter activity (x 10³ a.u./hr)
J
+ IL-12
10 hr
- IL-12
K
Ending cell lineage Tcf7 promoter state in lineages with 4+ generations
ON (12)
OFF (4)
Mixed ON and OFF (63)
L
YFP+/+
YFP+/-
0.05 ng/mL
0.5 ng/mL
1 ng/mL
Tcf7-YFP
M
Glass
Tc plastic
+ IL-12
- IL-12
+ anti-CD11a 2k c seed
+ anti-CD11a 20k c seed
- anti-CD11a 2k c seed
- anti-CD11a 20k c seed
CD62L
CD44
Tcf7-YFP

Figure 2.6. Quantitative live imaging reveals dynamics of epigenetic *Tcf7* silencing in clonal lineages.
Related to Figure 2.5. (**A**) Representative images of a single clone adhered to the imaging plate at day 0 and day 3. (**B**) Quantitative image analysis procedure. (**C**) Four and three-state HMMs were compared and (**D**) evaluated by log-likelihood and AIC. Models 2 and 3 compared to models 1 and 4 have tighter constraints on the promoter activity range of the off states. (**E**) For each state in the selected HMM (model 1), quantiles of the theoretical gaussian distribution versus the quantiles of the observed residuals. The observed residuals would fall on the straight line in a perfect fit [2]. (**F**) *Tcf7*-YFP derivative, or promoter activity, of cells assigned to each HMM-derived promoter state. Theoretical distributions for each are overlaid as lines. (**G**) Median CD69 intensity and cell mask area for all overlaid tracks, colored by promoter state. (**H**) Average *Tcf7* promoter activity versus average CD69 median intensity and area for each cell trace, where a cell trace is an ending cell tracked from its naive progenitor. (**I**) Promoter activity averaged over the entire cell cycle for related cells. (**J**) Additional lineage trees, as in Fig. 3A. (**K**) Classification of lineages with cells tracked to at least 4 generations as having either all ON, all OFF, or mixed promoter states of terminal progeny. (**L**) YFP distributions for homozygous ($YFP^{+/+}$) and heterozygous ($YFP^{+/-}$) reporters cultured for 5 days. (**M**) CD62L x CD44 and *Tcf7*-YFP distributions for varied activation conditions after 4 days of stimulation. [L] Data are from a single experiment representative of 2 independent experiments. [M] Data are representative of one experiment.

The timing at which the *Tcf7* promoter transitioned to the silent state varied between cell tracks both within and between cell lineages, consistent with observed heterogeneity in *Tcf7*-YFP expression within clones (**Fig. 2.5A-D**). Lineages with variability in *Tcf7* promoter states in their terminal progeny were more prevalent than those having a uniform ON or OFF promoter state (80%, N = 79), indicating that intraclonal heterogeneity in *Tcf7* regulation is the norm (**Fig. 2.6J-K**). Removing IL-12 increased the fraction of cells in an active promoter state (**Fig. 2.5C,E**). Silent *Tcf7* promoter states persisted across multiple cell divisions (**Fig.2.5A; Fig. 2.6I-J**) and thus represent heritable regulatory changes as opposed to more transient dynamics such as transcriptional bursting. These results provide evidence that a cell-intrinsic *Tcf7* silencing event, occurring heterogeneously within clones, underlies the early divergence in effector and memory states.

2.3.4 *A stochastic epigenetic switch controlling* Tcf7 *silencing underlies the early $CD8^+$ T cell effector and memory decision*

Heterogeneity in *Tcf7* silencing, as observed in our imaging assay, could derive from asymmetric cell division[6,29], whereby cell fate determinants partition unequally, giving rise to discordant

behavior between two sister cells. Alternatively, this heterogeneity could result from other molecular mechanisms that operate in an inherently stochastic manner[30–33], and would thus cause two sisters to make *Tcf7* silencing decisions independently. While two sister cells could still silence *Tcf7* discordantly, they would do so no more frequently than expected by chance. To test these predictions, we analyzed the fractions of daughter cell pairs that silenced *Tcf7* either discordantly (ON/OFF) or concordantly (OFF/OFF), doing so for cell pairs across all cell generations, with or without IL-12 (**Fig. 2.5F**). By plotting concordant (OFF/OFF) versus discordant (ON/OFF) sister pair fractions, we found that all data points adhered to a theoretical curve representing the expected relationship between sister pair fractions for independent regulation (**Fig. 2.5G**). Consistently, by statistical analysis using a modified Cohen's kappa coefficient (κ'), we found that daughter cells were no more likely to make discordant decisions than expected by chance (**Fig. 2.5H; Supplemental Table 2**). These findings support the view that *Tcf7* silences in a stochastic manner to drive divergent decisions within clones. These results do not rule out an asymmetric division as a mechanism for memory and effector heterogeneity, whereby dendritic cell proximity and thus antigen exposure drives divergent fate decisions; however, they argue that differences in external signals are not necessary for the emergence of clonal heterogeneity in lineage decisions.

Epigenetic switching mechanisms, involving changes in chromatin modifications or conformation at gene loci, can introduce stochastic rate-limiting steps to gene activation or silencing[34–36]. While epigenetic switching mechanisms are initiated by upstream transcription factors (TFs), they occur in an inherently stochastic manner, such that these upstream TFs do not directly modulate the levels of transcription, but control the probabilities of all-or-none gene

activation or silencing. As *Tcf7* silencing involves repressive DNA or histone methylation[14,20,37,38], it could be gated by such a mechanism. Epigenetic mechanisms act in cis- at individual gene loci and therefore would silence each *Tcf7* locus independently. To test for this mechanism, we compared *Tcf7*-YFP silencing kinetics in cells from mice homozygous (*Tcf7*-YFP$^{+/+}$) and heterozygous (*Tcf7*-YFP$^{+/-}$) for the reporter, with the prediction that *Tcf7*-YFP$^{+/+}$ reporter cells would yield a smaller population of *Tcf7*-YFP^{lo} cells, since both loci need to silence for loss of reporter expression (**Fig. 2.5I-J; Fig. 2.6L**). Indeed, the *Tcf7*-YFP^{lo} population was smaller in *Tcf7*-YFP$^{+/+}$ reporter cells and increased with IL-12, consistent with a cis-epigenetic silencing mechanism modulated by inflammation. Together, these results indicate that a stochastic cis-epigenetic switch, tunable by external stimuli, enables clonally related cells to make divergent effector and memory decisions, even when they are subject to uniform external signals.

2.3.5 *Reversibility of* Tcf7 *silencing enables a late CD8$^+$ T cell memory decision*

Tcf7 silencing has been proposed to be an irreversible event that marks a 'point of no return' for effector differentiation and loss of memory potential[5,39,40]. Conversely, various studies show that cells that undergo effector differentiation are able to populate memory compartments after an infection is resolved[8,9,41], suggesting that *Tcf7*-silenced effectors may still be able to reactivate *Tcf7* and reacquire memory potential. Our data thus far provide evidence for an early T cell decision to lose or maintain memory potential, driven by stochasticity in antigen-driven *Tcf7* silencing, but do not exclude the possibility that effector cells can regain memory potential later after withdrawal of stimulation.

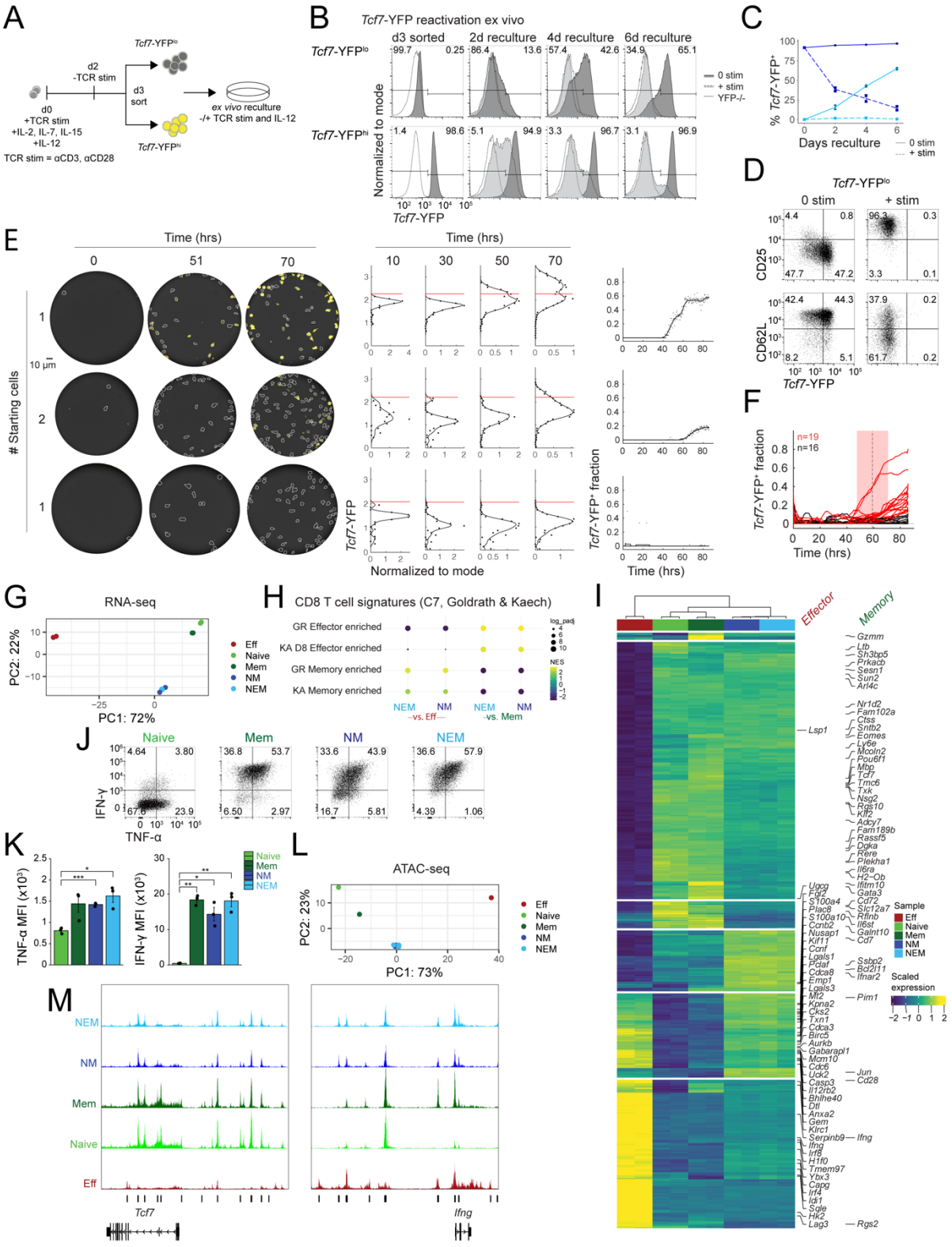
A
Tcf7-YFPlo
d2
-TCR stim
d3
sort
d0
+TCR stim
+IL-2, IL-7, IL-15
+IL-12
ex vivo reculture
-/+ TCR stim and IL-12
Tcf7-YFPhi
TCR stim = αCD3, αCD28
B
Tcf7-YFP reactivation ex vivo
d3 sorted
2d reculture
4d reculture
6d reculture
Tcf7-YFPlo
Tcf7-YFPhi
Normalized to mode
Tcf7-YFP
0 stim
+ stim
YFP-/-
C
% Tcf7-YFP+
Days reculture
0 stim
+ stim
D
Tcf7-YFPlo
0 stim
+ stim
CD25
CD62L
Tcf7-YFP
E
Time (hrs)
Starting cells
10 μm
Normalized to mode
Tcf7-YFP fraction
Time (hrs)
F
Tcf7-YFP+ fraction
n=19
n=16
Time (hrs)
G
RNA-seq
PC2: 22%
PC1: 72%
Eff
Naive
Mem
NM
NEM
H
CD8 T cell signatures (C7, Goldrath & Kaech)
GR Effector enriched
KA D8 Effector enriched
GR Memory enriched
KA Memory enriched
log_padj
NES
NEM
NM
NEM
NM
vs. Eff
vs. Mem
I
Effector
Memory
Gzmm
Ltb
Sh3bp5
Prkacb
Sesn1
Sun2
Arl4c
Nr1d2
Fam102a
Ctss
Sntb2
Eomes
Ly6e
Mcoln2
Pou6f1
Mbp
Tcf7
Tmc6
Txk
Nsg2
Rgs10
Klf2
Adcy7
Fam189b
Rassf5
Dgka
Rere
Plekha1
Il6ra
H2-Ob
Ifitm10
Gata3
Cd72
Slc12a7
Rflnb
Il6st
Galnt10
Cd7
Ssbp2
Bcl2l11
Ifnar2
Pim1
Jun
Cd28
Ifng
Rgs2
Lsp1
Ugcg
Fgl2
S100a4
Plac8
S100a10
Ccnb2
Nusap1
Klf11
Ccnf
Lgals1
Pclaf
Cdca8
Emp1
Lgals3
Mlf2
Kpna2
Cks2
Txn1
Cdca3
Birc5
Aurkb
Gabarapl1
Mcm10
Cdk6
Uck2
Casp3
Il12rb2
Bhlhe40
Dtl
Anxa2
Gem
Klrc1
Serpinb9
Ifng
Irf8
H1f0
Tmem97
Ybx3
Capg
Irf4
Id1
Sqle
Hk2
Lag3
Sample
Eff
Naive
Mem
NM
NEM
Scaled expression
J
Naive
Mem
NM
NEM
IFN-γ
TNF-α
K
TNF-α MFI (x10³)
IFN-γ MFI (x10³)
Naive
Mem
NM
NEM
L
ATAC-seq
PC2: 23%
PC1: 73%
Eff
Naive
Mem
NM
NEM
M
NEM
NM
Mem
Naive
Eff
Tcf7
Ifng

Figure 2.7. Effector cells reverse *Tcf7* silencing and regain memory potential upon stimulation withdrawal. (**A**) Naive cells from *Tcf7*-YFP mice were stimulated with αCD3 and αCD28 (TCR stim) for 2 days with IL-2, IL-7, IL-15, and IL-12. At day 2, TCR stimulation was removed but the same cytokine cocktail was used. At day 3, cells were sorted for *Tcf7*-YFP^{lo} and *Tcf7*-YFP^{hi} populations and recultured *ex vivo* with and without continued TCR stimulation and IL-12 in the presence of IL-2, IL-7, and IL-15. Light and dark blue coloring throughout correspond to sorted *Tcf7*-YFP^{lo} and *Tcf7*-YFP^{hi} populations, respectively. (**B-C**) *Tcf7*-YFP expression during reculture. **(D)** CD25, CD62L, and *Tcf7*-YFP expression in *Tcf7*-YFP^{lo} cells recultured for 6 days. (**E**) Representative microwells of *Tcf7*-YFP^{lo} cells recultured without stimulation: snap shots (left), top and bottom wells represent single clones; corresponding histograms (middle) with binned cell data for each time point, with YFP +/- gate drawn at 2 standard deviations above the mean YFP intensity from the first 25 hrs; corresponding YFP^{+} fractions over time (right). (**F**) YFP^{+} fraction for all wells overlaid. Mean activation time = 59.1 hr. [C] Mean ± s.d. [B-D] Data are from a single experiment representative of 1 and 3 independent experiments for +stim and 0 stim, respectively. (**G**) PCA of RNA-seq profiles (top 500 DE genes) for recultured cells compared to day 3 *ex vivo* activated effector (Eff) and day 0 (isolated from a naive mouse spleen) naive (CD44^{-}CD62L^{+}) and memory (CD44^{+}CD62L^{+}, Mem) controls. NM and NEM cells were sorted as *Tcf7*-YFP^{hi} and *Tcf7*-YFP^{lo} on day 3, respectively. (**H**) GSEA of gene signatures from MSigDB (C7, collections deposited by Goldrath (GR) and Kaech (KA) comparing recultured populations to Eff and Mem controls. (**I**) Heatmap displaying top 500 DE genes (lfc ≥ 2, Bonferroni-adjusted p value <0.05) between recultured populations and Eff, N, and Mem controls. Scale bar indicates row z-scores of regularized log transformed count data. Memory and effector associated genes from MSigDB Goldrath and Kaech collections are highlighted. (**J-K**) Cytokine secretion of recultured cells compared to N and Mem controls after PMA/Ionomcyin restimulation. (**L**) PCA of ATAC-seq counts of top 500 differentially accessible peaks between recultured cells and controls. (**M**) ATAC-seq read coverage tracks; vertical bars annotate differentially accessible peaks between recultured cells and controls. [G-I] n = 2 biological replicates for each sample. [K] Mean ± s.e.m.. Statistical significance was calculated with an unpaired two-tailed t test performed between groups. *p<0.5, **p<0.01, ***p<0.001. Data are n=3 biological replicates from a single experiment. [L-M] n=1 biological replicate for Eff, N, Mem, n=2 for NM, n=3 for NEM.

To test this possibility, we sorted *Tcf7*-YFP^{lo} and *Tcf7*-YFP^{hi} cells after initial culture and subjected them to reculture with variable stimulation conditions *ex vivo* (**Fig. 2.7A**). As expected, sorted *Tcf7*-YFP^{hi} cells maintained *Tcf7*-YFP expression without stimulation but underwent heterogeneous silencing under continuing stimulation (**Fig. 2.7B-C; Fig. 2.8A**). Furthermore, *Tcf7*-YFP^{lo} cells maintained a silent state upon continued stimulation, as observed. However, upon stimulation withdrawal, *Tcf7*-YFP^{lo} cells reactivated *Tcf7*, with the fraction of *Tcf7* expressing cells increasing over 6 days. *Tcf7* reactivation upon stimulation withdrawal coincided with CD25 downregulation and CD62L upregulation, suggesting re-entry into a memory state (**Fig. 2.7D**). We next used clonal live imaging of sorted *Tcf7*-YFP^{lo}cells confined in microwells to test if *Tcf7* reactivation was heterogeneous within individual effector clones, as would be expected if reactivation occurs via reversal of stochastic *cis*-epigenetic silencing (**Fig. 2.5**). Consistent with reactivation observed from bulk starting populations, we found that a sub-

population of starting cells could reactivate *Tcf7* to give rise to *Tcf7*-YFP^{hi} cells (**Fig. 2.7E-F; Supplemental Movies 2 and 3; Supplemental Table 3**). Similar to the initial *Tcf7* silencing event, reactivation was heterogeneous within clones. Overall, these results indicate that cells that have silenced *Tcf7* and lost memory potential can reverse this decision later, after resolution of an immune challenge.

A subpopulation of starting cells in these clonal imaging experiments did not reactivate *Tcf7* during imaging observation, suggesting that they may have irreversibly entered a *Tcf7* silenced state and lost their memory potential (**Fig. 2.7E-F**). T cells differentiate into a terminal effector state upon continued stimulation with inflammation[21]; as such, we asked whether the ability to reactivate *Tcf7* was dependent on the duration of antigen stimulation. We stimulated cells *ex vivo* for 2, 4, and 6 days, respectively, and analyzed *Tcf7* reactivation after 7 days of stimulation withdrawal. We observed that longer stimulation reduced the fraction of *Tcf7* reactivated cells (**Fig. 2.8B**). We then asked whether this loss in plasticity was associated with inaccessibility at the *Tcf7* locus due to polycomb repressive complex 2 (PRC2) mediated cis-epigenetic changes, as previously described[42]. We observed increased *Tcf7* reactivation in cells recultured in the presence of Tazemetostat or GSK126, Ezh2/PRC2 inhibitors, suggesting that polycomb-mediated repression indeed plays a role in this loss of reactivation potential (**Fig. 2.8C**). Taken together, these observations suggest that *Tcf7* repression is initially reversible, enabling effector cells to regain memory potential, but that this flexibility diminishes with continued stimulation in a polycomb-dependent manner.

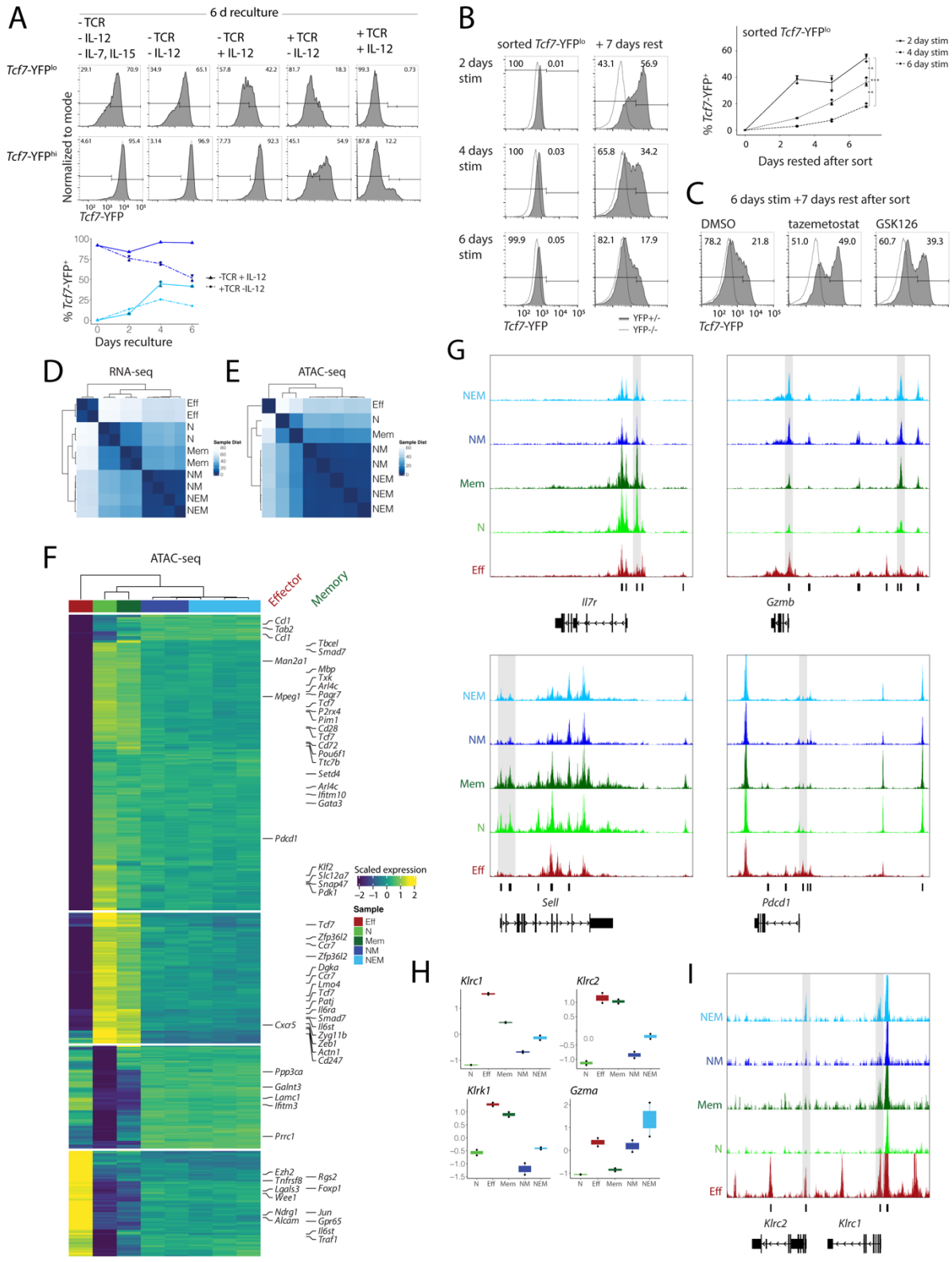
A
6 d reculture
- TCR
- IL-12
- IL-7, IL-15
- TCR
- IL-12
- TCR
+ IL-12
+ TCR
- IL-12
+ TCR
+ IL-12
Tcf7-YFPlo
Tcf7-YFPhi
Normalized to mode
Tcf7-YFP
% Tcf7-YFP+
-TCR + IL-12
+TCR -IL-12
Days reculture
B
sorted Tcf7-YFPlo
+ 7 days rest
2 days stim
4 days stim
6 days stim
Tcf7-YFP
YFP+/-
YFP-/-
2 day stim
4 day stim
6 day stim
Days rested after sort
C
6 days stim +7 days rest after sort
DMSO
tazemetostat
GSK126
D
RNA-seq
E
ATAC-seq
F
ATAC-seq
Effector
Memory
Scaled expression
Sample
Eff
N
Mem
NM
NEM
Ccl1
Tab2
Cd1
Tbcel
Smad7
Man2a1
Mbp
Txk
Arl4c
Poqr7
Tcf7
P2rx4
Pim1
Cd28
Tcf7
Cd72
Pou6f1
Ttc7b
Setd4
Arl4c
Ifitm10
Gata3
Pdcd1
Klf2
Slc12a7
Snap47
Pdk1
Tcf7
Zfp36l2
Ccr7
Zfp36l2
Dgka
Ccr7
Lmo4
Tcf7
Patj
Il6ra
Smad7
Il6st
Zyg11b
Zeb1
Actn1
Cd247
Cxcr5
Ppp3ca
Galnt3
Lamc1
Ifitm3
Prrc1
Ezh2
Tnfrsf8
Lgals3
Wee1
Rgs2
Foxp1
Ndrg1
Alcam
Jun
Gpr65
Il6st
Traf1
G
NEM
NM
Mem
N
Eff
Il7r
Gzmb
Sell
Pdcd1
H
Klrc1
Klrc2
Klrk1
Gzma
I
Klrc2
Klrc1

Figure 2.8. *Tcf7* reactivation upon signal withdrawal is accompanied by memory reprogramming.
Related to Figure 2.7. (**A**) Naive *Tcf7*-YFP^{lo} and *Tcf7*-YFP^{hi} cells were sorted after 2 days of TCR stimulation with IL-12 and one day with removal of TCR stimulation. Sorted populations were recultured *ex vivo* under different conditions, with or without TCR stimulation and IL-12. All conditions are with continued IL-7 and IL-15 except where indicated. Blue and light blue represent naive-to-memory (NM) and naive-to-effector-to-memory (NEM) cells, respectively. (**B**) Bulk CD8$^+$ cells from *Tcf7*-YFP x P14 mice were stimulated *ex vivo* for 2, 4, or 6 days with IL-12, sorted as *Tcf7*-YFP^{lo} after 1 day of rest (removal of TCR stimulation and IL-12), and rested for 7 additional days. Representative histograms of *Tcf7* reactivation in sorted *Tcf7*-YFP^{lo} cells after 2, 4, and 6 days of stimulation. Quantification of percentage of *Tcf7*-YFP$^+$ cells over time in rested sorted *Tcf7*-YFP^{lo} cells. (**C**) Representative histograms of sorted *Tcf7*-YFP^{lo} cells after 6 days of stimulation as in (B), followed by 7 days of rest post-sort in the presence of 3 μM Tazemetostat or 5 μM GSK126. (**D**) Alternative representation to Fig. 4G: correlation matrix of RNA-seq profiles (top 500 DEG) for recultured cells compared to effector (Eff) and day 0 naive (N) and memory (Mem) controls. (**E**) Alternative representation to Fig. 4L: PCA of ATAC-seq counts of top 500 differential peaks between recultured cells and controls. (**F**) Heatmap displaying top 500 differentially accessible peaks (lfc ≥ 2, Bonferroni-adjusted p value < 0.05) between recultured populations and Eff, N, and Mem controls. Color legend indicates row z-scores of regularized log transformed count data. Memory and effector associated genes from MSigDB Goldrath and Kaech collections are highlighted in green and red, respectively. (**G**) ATAC-seq read coverage tracks. Vertical bars annotate differentially accessible peaks between recultured cells and controls, and grey shading highlights peaks of interest. (**H**) Scaled gene expression from bulk RNA-seq for DE genes (lfc ≥ 2, Bonferroni-adjusted p value < 0.05 except for *Gzma*: non-adjusted p = 0.0175) between day 9 recultured NM and NEM cells (see Fig. 5). (**I**) ATAC-seq read coverage tracks. Vertical bars annotate differentially accessible peaks between recultured cells and controls, and grey shading highlights peaks of interest. [A-C] Mean +/- SD, data are from a single experiment representative of n = 2 or more experiments. [D, H] n=2 biological replicates for each sample. [E-F, I] n=1 biological replicate for Eff, N, Mem, n=2 for NM, n=3 for NEM.

2.3.6 Tcf7-*YFP^{hi} CD8$^+$ T cells formed through early and late decisions acquire a common memory program*

From the above experiments, we find that naive cells in our *ex vivo* system can form memory through two pathways: a "naive to memory" (NM) pathway, whereby some cells maintain *Tcf7* expression during initial antigen stimulation, and a "naive to effector to memory" (NEM) pathway, by which cells that have silenced *Tcf7* and entered an effector state can turn expression back on after stimulation removal. To determine whether *Tcf7*-YFP^{hi} cells emerging through these two pathways both have genomic and functional memory programs, we subjected them to transcriptomic, epigenomic, and cytokine secretion analysis, alongside control *in vivo* naive (CD44$^-$CD62L$^+$), memory (Mem, CD44$^+$CD62L$^+$), and *ex vivo* generated effector (Eff) cells (**Fig. 2.7G-M**).

Despite their different *Tcf7* regulatory history, NM and NEM cells showed similar memory characteristics. They were both more similar to naive and memory *in vivo* controls compared to *ex vivo* generated effector cells in their shared expression of memory-defining genes, though they also maintained some effector characteristics, in line with their recent stimulation (**Fig. 2.7G-I; Fig. 2.8D; Supplemental Table 4**). Similar to memory controls, NM and NEM cells demonstrated greater TNF-α and IFN-ɣ secretion upon re-stimulation compared to naive cells (**Fig. 2.7J-K**). NM and NEM cells were most similar in global chromatin accessibility to memory controls (**Fig. 2.7L; Fig. 2.8E-F**). NEM cells recovered similar *Tcf7* accessibility to NM cells (**Fig. 2.7M**). At the *Ifng* locus, intermediate accessibility of NM and NEM cells between naive and effector controls suggests that both were poised for rapid recall response, and accessibility at other memory- and effector- associated loci support this conclusion (**Fig. 2.8G**).

While NM and NEM cells were largely similar, differences in gene expression suggest they may exhibit different functional properties. NEM cells had higher expression and accessibility of some effector-associated genes compared to NM, possibly indicative of enhanced effector capabilities or an effector memory state[39,41] (**Fig. 2.8H-I**). Overall, both NM and NEM decision strategies gave rise to cells with genomic and functional characteristics of memory, suggesting that memory formation may proceed through a flexible decision-making strategy, allowing both for memory and effector divergence during the initial immune challenge and for effector reacquisition of memory potential after the challenge is resolved.

2.3.7 *Memory CD8$^+$ T cells form through early and late decisions during acute infection*

To determine if the flexible decision-making strategy we characterized in our *ex vivo* system plays a role in memory formation *in vivo*, we monitored memory and effector differentiation in the lymphocytic choriomeningitis virus (LCMV) acute infection mouse model. First, to determine if the early decision of naive T cells to silence *Tcf7* expression and enter an effector state also occurs heterogeneously *in vivo*, we transferred CellTrace Violet-labeled *Tcf7*-YFP x P14 CD8$^+$ T cells to recipient mice that were then infected with LCMV Armstrong (LCMV-Arm) (**Fig. 2.9A**), using a high viral dose (2x10^6 p.f.u.) to ensure that the large starting population is completely activated (1x10^6 cells). After 3 days of infection, transferred CD8$^+$ T cells divided and bifurcated into distinct populations with high and low *Tcf7*-YFP and TCF1 protein levels (**Fig. 2.9B**), consistent with *ex vivo* observations (**Fig. 2.1**). PD-1 expression, an indicator of antigen exposure, was uniform across the entire population (**Fig. 2.9B**), consistent with this early decision to silence *Tcf7* being controlled by stochastic epigenetic mechanisms (**Fig. 2.5**).

Figure 2.9. (Below) T cells show reversible *Tcf7* silencing and flexible memory pathway choice in acute LCMV infection.
(**A**) Congenically marked *Tcf7*-YFPxP14 cells (1x10^6) were CellTrace Violet (CTV) labeled and transferred into naive mice and infected with 2x10^6 p.f.u of LCMV Armstrong. Cells were isolated from the recipient mice after 3 days. (**B**) CTV dilution and expression of *Tcf7*-YFP, TCF1, and PD-1 on the transferred P14 CD8$^+$ T cells before infection (top) and 3 days after infection (bottom). (**C**) Congenically distinct (CD45.2) naive *Tcf7*-YFP P14 cells (1x10^6) were transferred into CD45.1 naive mice that were then infected with 2x10^6 p.f.u of LCMV Armstrong. The activated and proliferating P14 cells were sorted 3 days post-infection into *Tcf7*-YFP^{hi}, *Tcf7*-YFP^{mid}, and *Tcf7*-YFP^{lo} subsets and transferred into recipient mice that had been infected with 2x10^5 p.f.u of LCMV Armstrong 5 days earlier. (**D**) Expression of *Tcf7*-YFP and TCF1 on the transferred *Tcf7*-YFP^{hi}, *Tcf7*-YFP^{mid}, and *Tcf7*-YFP^{lo} P14 CD8$^+$ T cell subsets isolated from the spleens of recipient mice at 15 hrs and 15 days post-transfer. (**E**) Mean frequencies of the transferred P14 CD8$^+$ T cell populations expressing *Tcf7*-YFP (top) and TCF1 (bottom) prior to transfer and at 15 hrs and 15 days post-transfer. (**F**) TCF1, PD-1, CD62L, CD127, and KLRG1 expression for transferred populations 15 hrs and day 15 post-transfer. [B] Data are representative of n=2 naive mice and n=5 day 3 mice. [D-F] n=2 mice for 0 and 15 hours and n=6 mice for 15 days after transfer.

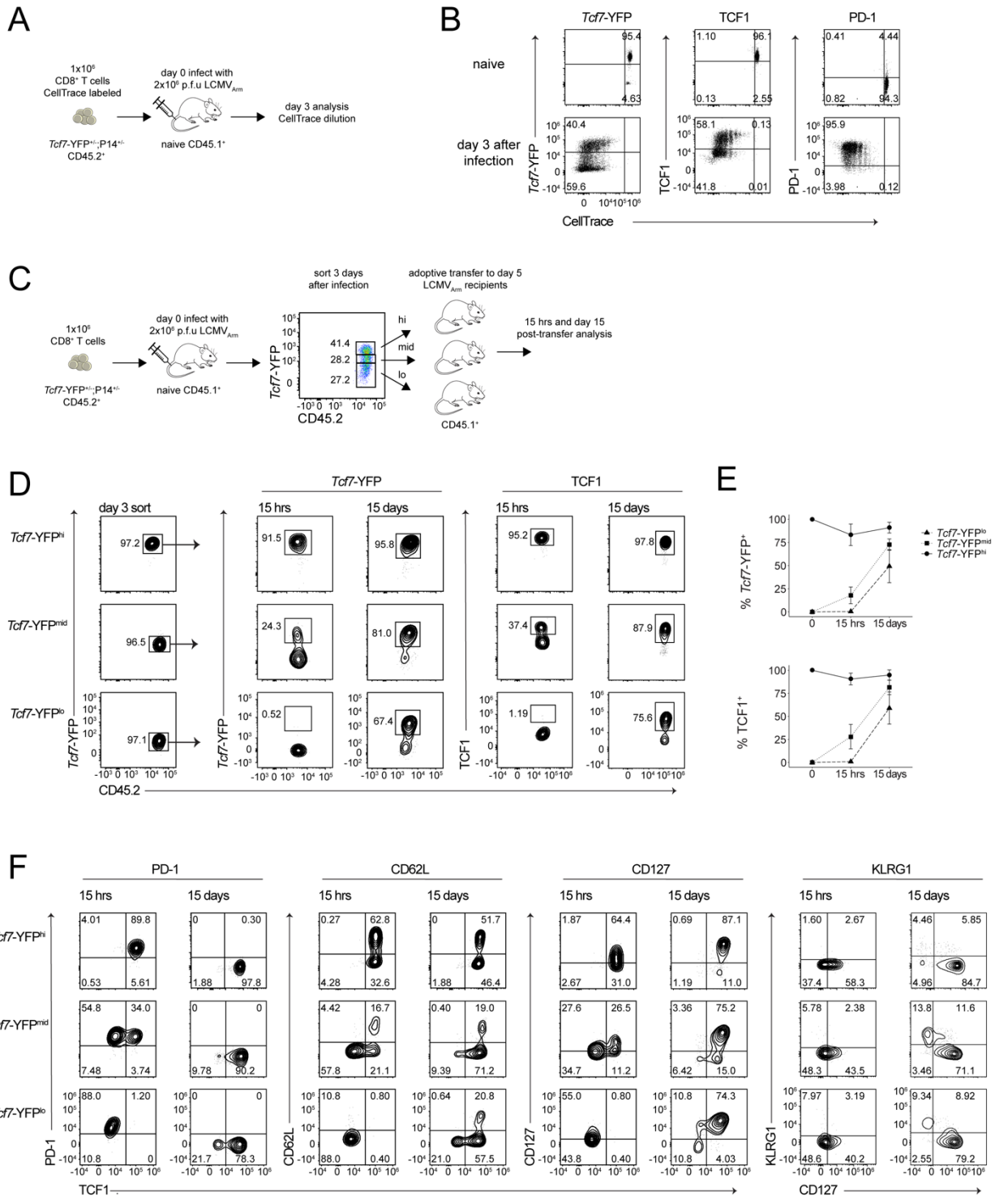

We next determined whether T cells that silenced *Tcf7* in response to LCMV-Arm challenge had the capacity to reactivate the *Tcf7* locus and re-express TCF1 protein to form memory upon

infection clearance. To do so, we sorted *Tcf7*-YFP^{lo}, *Tcf7*-YFP^{mid}, and *Tcf7*-YFP^{hi} cells at 72 hours post infection, and re-transferred them into secondary infected recipient mice to assay their memory potential (**Fig. 2.9C**). Analysis shortly after transfer (15 hrs) demonstrated purity of the *Tcf7*-YFP^{lo} and *Tcf7*-YFP^{hi} transferred populations, with each maintaining similar expression levels to the respective sorted population. The *Tcf7*-YFP^{mid} transferred population bifurcated into *Tcf7* high and low expressing cells at 15 hours, consistent with it actively transitioning between *Tcf7* high and low states at the time of transfer. Upon infection clearance (Day 15), *Tcf7*-YFP^{hi} cells maintained *Tcf7*/TCF1 expression (Day 15) (**Fig. 2.9D-E; Fig. 2.10A-C**). *Tcf7*-YFP^{mid} cells gave rise to an intermediate fraction of *Tcf7*/TCF1 high cells between that of the *Tcf7*-YFP^{hi} and *Tcf7*-YFP^{lo} cells, again consistent with their transitory nature. *Tcf7*-YFP^{lo} cells robustly reactivated *Tcf7*/TCF1 expression, and to similar levels as *Tcf7*-YFP^{hi} cells (**Fig. 2.9D-E**), in line with findings in our *ex vivo* system (**Fig. 2.7**). The majority of transferred *Tcf7*-YFP^{hi} cells maintained a central memory phenotype (KLRG1^{-}CD127^{+}CD62L^{+}) at Day 15 (**Fig. 2.9F**), as expected. *Tcf7*-YFP^{lo} cells that reactivated *Tcf7* expression also re-expressed CD127 and CD62L to acquire a central memory phenotype, indicating that these *Tcf7*-YFP^{lo} starting cells maintain the potential to form central memory cells. *Tcf7*-YFP^{lo} and *Tcf7*-YFP^{mid} sorted cells also gave rise to KLRG1^{+}CD127^{-} cells without *Tcf7*/TCF1 expression, consistent with their giving rise to terminal effector cells (**Fig. 2.9F**). In all transferred populations, PD-1 expression was initially high after transfer (at 15 hrs), indicating continuing antigen exposure, but dropped markedly at 15 days, consistent with antigen clearance and memory formation occurring over this duration. Taken together, these results show that memory decisions can be made both early and late during acute viral infection, as is the case in our *ex vivo* system.

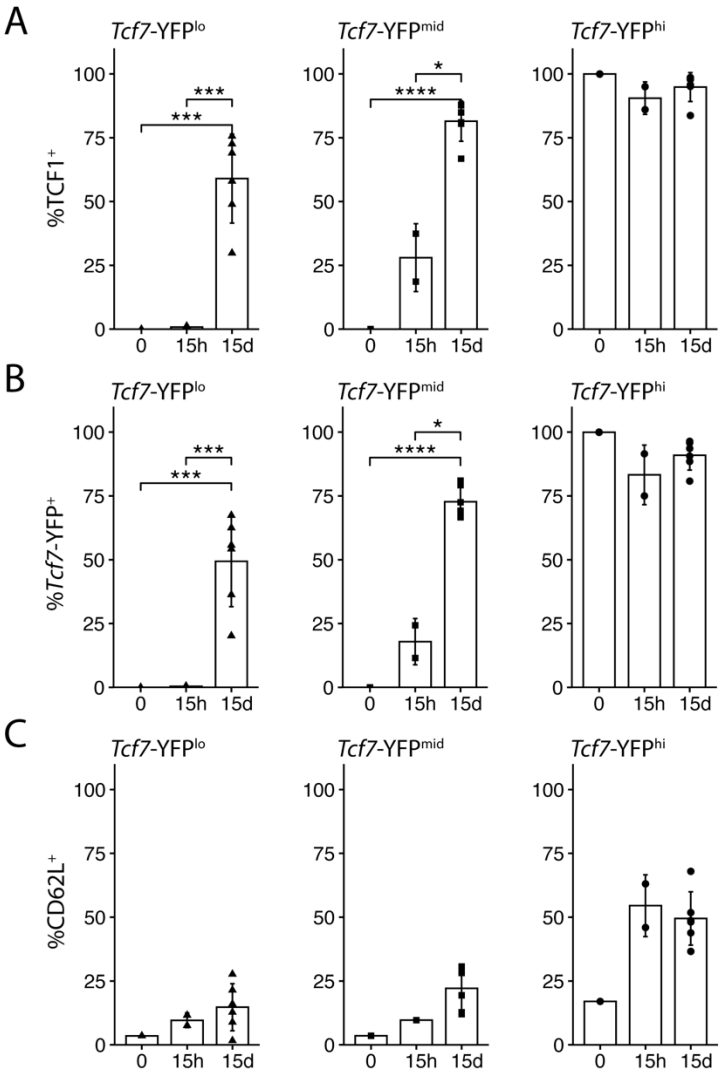

Figure 2.10. *Tcf7* silences heterogeneously to form distinct subsets that can all express *Tcf7* and CD62L after infection clearance.

Related to Figure 3.9. (**A-C**) Kinetics of *Tcf7*-YFP^{lo} (left), *Tcf7*-YFP^{mid} (middle), and *Tcf7*-YFP^{hi} (right) P14 cells from experiment outlined in Fig. 5C. Statistical significance was calculated with a one-tailed t test performed between time points for *Tcf7*-YFP and TCF1 protein. *p<0.05, **p<0.01, ***p<0.001, ****p<0.0001 (n=2 mice at day 0 and 15 hours after transfer; n=6 mice at 15 days after transfer).

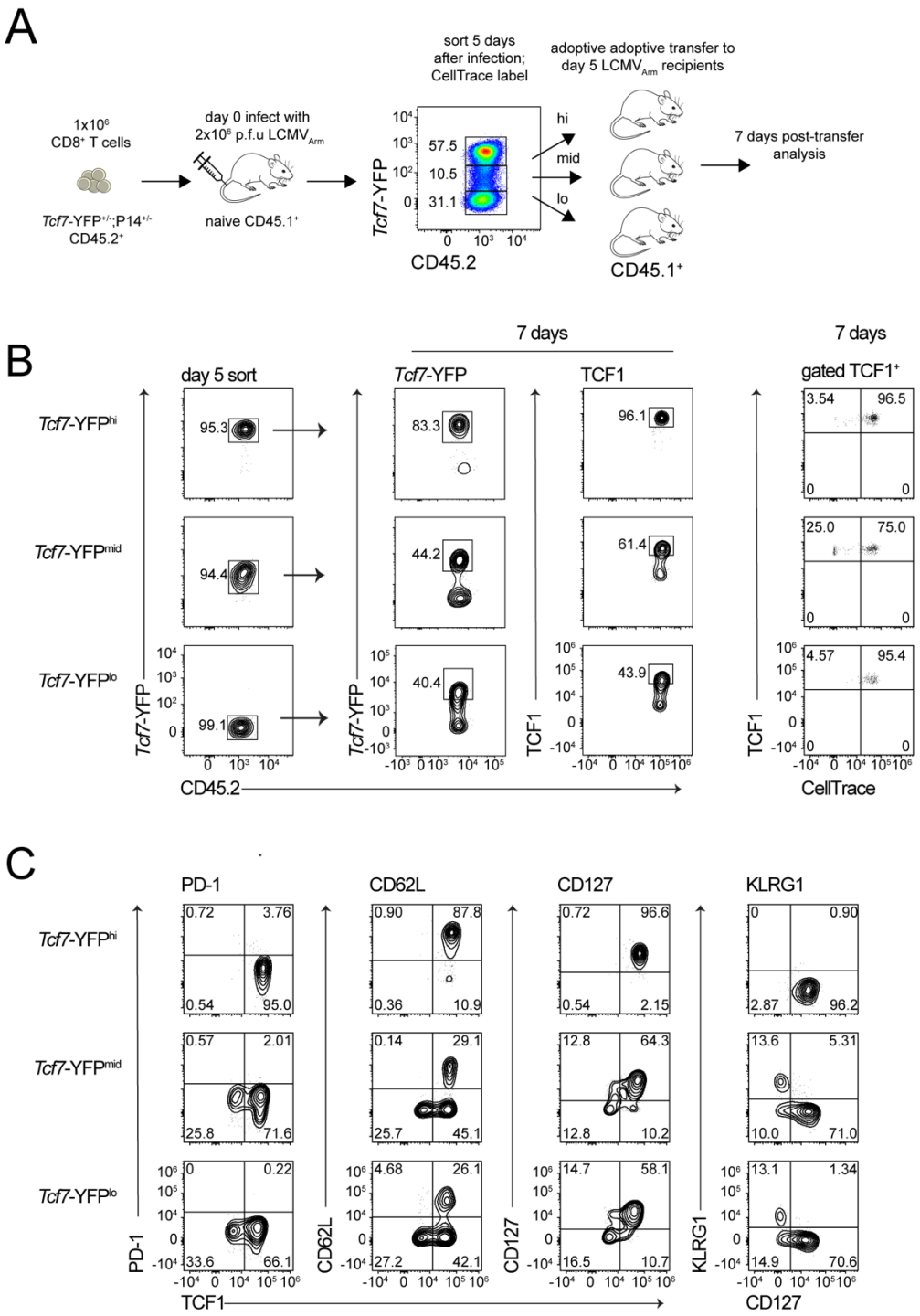

Figure 2.11. Reversal of *Tcf7* silencing occurs in the absence of division *in vivo*.
(**A**) *Tcf7*-YFP P14 cells ($1x10^6$) were transferred into naive mice and infected with $2x10^6$ p.f.u LCMV Armstrong. After 5 days of infection, P14 cells were sorted into *Tcf7*-YFP^{hi}, *Tcf7*-YFP^{mid}, and *Tcf7*-YFP^{lo} subsets. These subsets were CTV labeled and transferred into time-matched secondary infected recipient mice as in **Fig. 2.9.** (**B**) *Tcf7*-YFP and TCF1 expression on the transferred cells isolated from the spleens of the recipient mice at 7 days post-transfer (middle). CTV dilution on the transferred cells expressing TCF1 (right). (**C**) TCF1, PD-1, CD62L, CD127, and

KLRG1 expression for transferred *Tcf7*-YFP^{hi}, *Tcf7*-YFP^{mid}, and *Tcf7*-YFP^{lo} cells 7 days post-transfer. [B-C] n=3 mice per group.

Tcf7 reactivation and the late memory decision may require cell division or may occur with little or no cell division, potentially via active removal of repressive modifications at the *Tcf7* locus[8]. To distinguish between these possibilities, we repeated these transfer experiments using sorted *Tcf7*-YFP^{lo}, *Tcf7*-YFP^{mid}, and *Tcf7*-YFP^{hi} populations additionally labeled by CellTrace Violet (**Fig. 2.11A**). These populations were sorted at day 5 post infection, CellTrace-labeled, and transferred into time-matched secondary infected recipients and analyzed 7 days after transfer. As with cells sorted at 3 days post infection, cells sorted from 5 days post infection also had the ability to reactivate *Tcf7*/TCF1 and reacquire a memory phenotype (KLRG1^{-}CD127^{+}CD62L^{+}) (**Fig. 2.11B-C**), indicating that this flexibility in reactivation potential extends beyond the first few days of infection. *Tcf7* reactivation occurred selectively in a cell population that underwent minimal to no cell division during the 7 days after transfer (**Fig. 2.11B, right; Fig. 2.12**), with the fast-dividing population more strongly upholding *Tcf7* silencing and effector phenotypes (CD127^{-}KLRG1^{+}) (**Fig. 2.12**). These results rule out the possibility that this population arose from rare *Tcf7* expressing cells that expanded in number after transfer, and additionally show that *Tcf7*/TCF1 reactivation can occur with minimal cell division upon infection clearance.

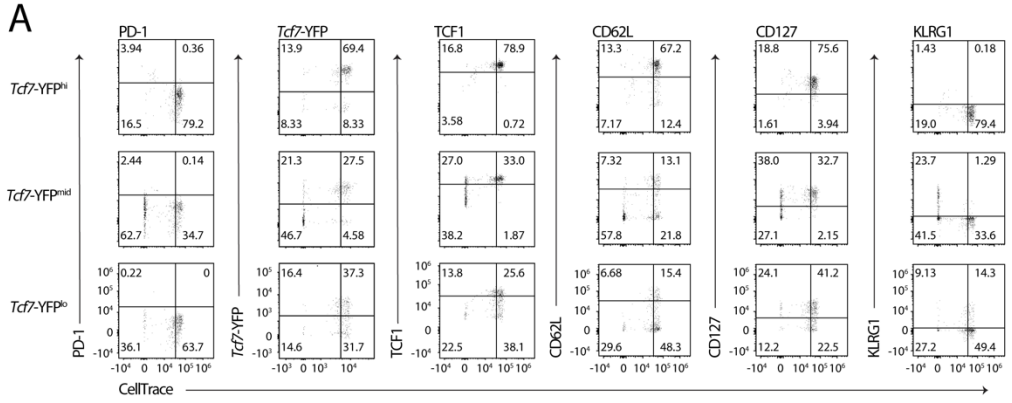

Figure 2.12. Reversal of *Tcf7* silencing and acquisition of a memory phenotype occurs with minimal cell division upon infection clearance.
Related to Figure 2.11. (**A**) For experiment described in Fig. 6A, representative flow plots showing dilution of CTV on the transferred cells and expression of PD-1, *Tcf7*-YFP, TCF1, CD62L, CD127 and KLRG1 on the cells that had undergone division and on the cells that did not divide (n=3 mice per group).

2.3.8 *Multiple paths to memory enable robust encoding of pathogen experience through memory population size*

An ability for T cells to make memory lineage decisions at multiple junctures during an infection may be important for robust protective immunity against diverse threats; in particular, it may enable the memory population sizes to scale with infection severity and immune response magnitudes, as observed[1,43]. To test this idea, we used mathematical modeling to evaluate different T cell decision-making strategies in their memory outcomes in response to pathogens of different virulence, modeled as having different rates of replication (see **Mathematical Appendix**). In our first model, we considered the flexible strategy we observed (**Fig. 2.13A**). Here, naive T cells (T_n) initially transition to a *Tcf7*-expressing memory-competent state (MC, T_m) that divides upon exposure to pathogen (v), but stops dividing and persists upon pathogen clearance. These cells can either maintain memory competence upon continuing stimulation, or transition to the *Tcf7*-silent effector state (T_e), where they control pathogen growth, but are short-lived. Effector cells can reverse *Tcf7* silencing and re-enter the memory-competent state in the absence of pathogen, as observed (**Figs. 2.7-2.12**). Based on our findings that both *Tcf7* silencing and reactivation occur with probabilities that depend on whether or not stimulatory signals are present (**Fig. 2.5 and Fig. 2.7**), we modeled transitions between effector and memory states using first order transition rates that vary with pathogen abundance, with the assumption that increasing pathogen levels result in greater antigen and inflammatory stimulation.

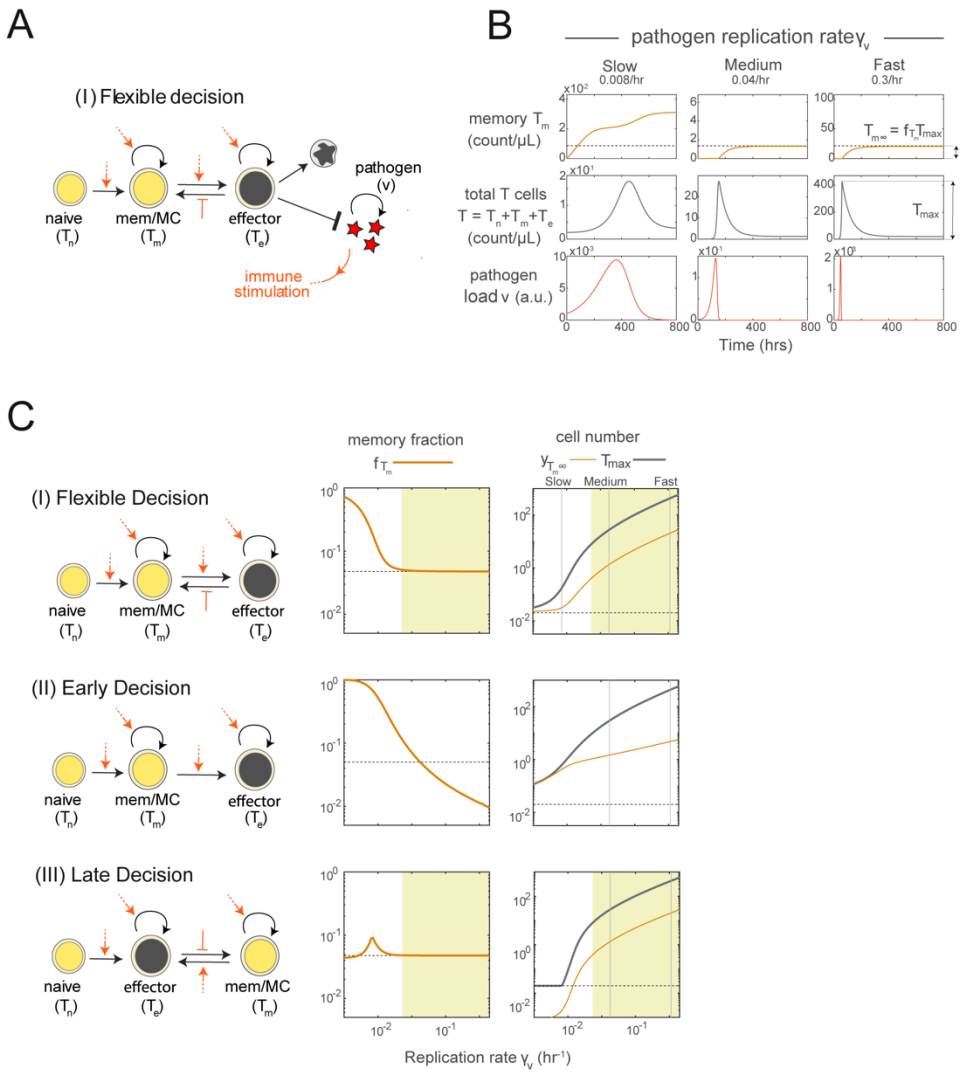

Figure 2.13. Flexible decision making enables quantitative encoding of pathogen experience during T cell memory formation.
(**A**) Model incorporates pathogen proliferation, T cell memory decision making through reversible epigenetic switching. Orange arrows indicate modulation of T cell state transitions by pathogen load. (**B**) Time traces show memory T cell concentrations (top), total T cell concentrations (middle) and pathogen load (bottom), for different rates of pathogen replication (left to right). Dotted line shows the number of memory T cells formed in the case when this number is a defined fraction of the peak total T cell number, f_{Tm}. (**C**) Distinct strategies for memory decision making: flexible (top), early (middle) or late (bottom); the fraction of T cells at the response peak that become memory cells f_{Tm}; the peak cell number (black) and memory cell number (orange), both plotted against pathogen replication rate γ_v. The dotted line indicates the number of starting naive cells, and the yellow shading marks scalable memory.

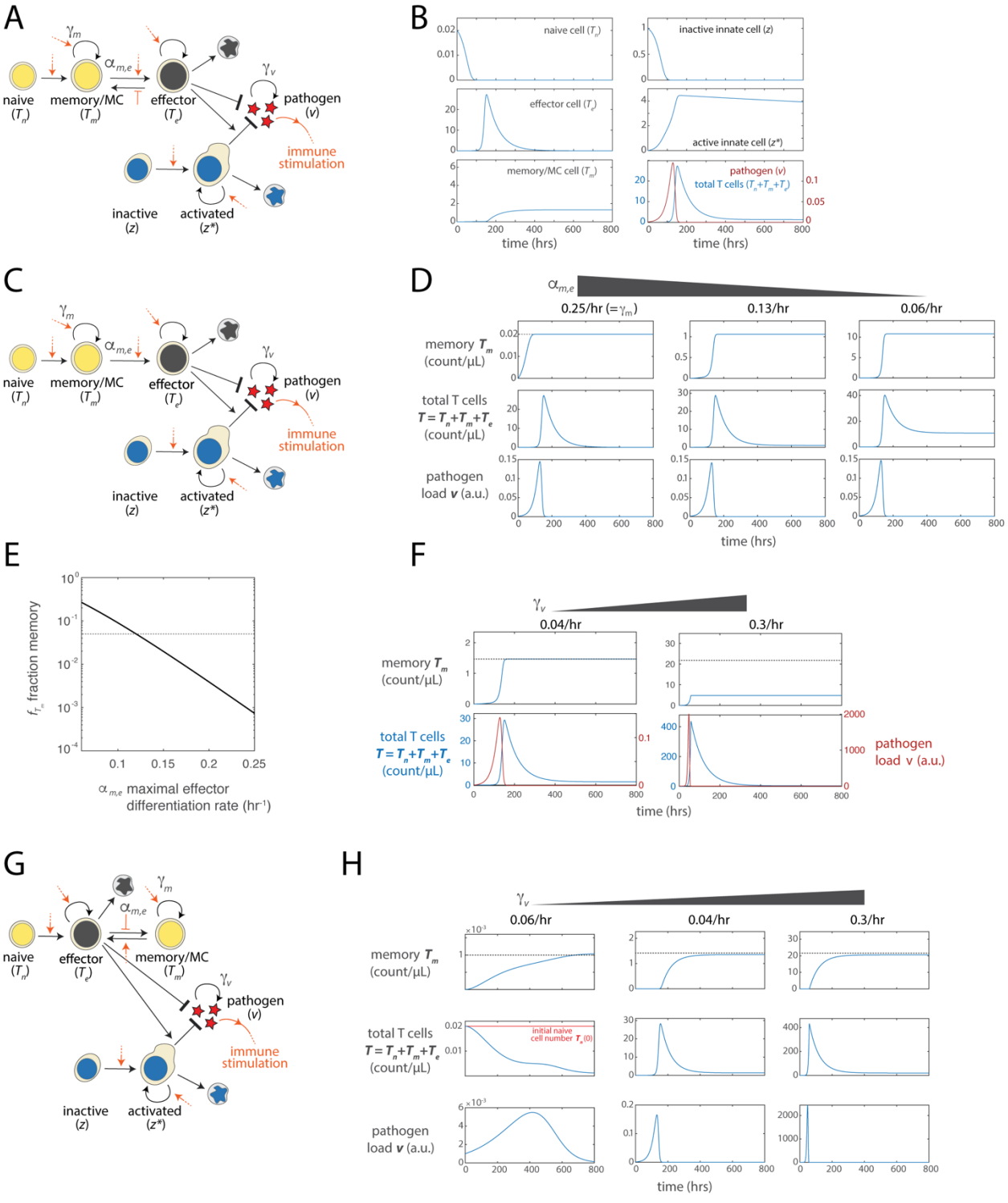

Figure 2.14. Immune response dynamics for flexible, early, and late decision models.
Related to Figure 2.13. *The flexible T cell decision making model (A-B) recapitulates the canonical immune response.* (**A**) Schematic for the flexible decision model, including the rate constants for effector differentiation ($\alpha_{m,e}$), memory precursor proliferation (γ_m), and pathogen replication (γ_v). (**B**) Time traces show the time evolution of the concentrations (counts/μL) of naive T cells (T_n), effector T cells (T_e), memory/MC T cells (T_m), inactive innate immune cells (z), active innate immune cells (z^*), as well as pathogen load (v, a.u.). Following pathogen

emergence, there is an increase in the numbers of activated innate immune cells, followed by an expansion in T cell number that occurs concomitantly with a decrease in pathogen load. Following pathogen clearance, there is a decline in T cell numbers to a stable level, reflecting a rise in the number of long-lived memory cells. *In the early (irreversible) decision model (C-F), the balance between effector differentiation and memory precursor proliferation sets the size of the memory population.* (**C**) Schematic for the early decision model, indicating the rate constants for effector differentiation ($\alpha_{m,e}$), memory precursor proliferation (γ_m), and pathogen replication (γ_v). (**D**) Simulation traces showing time evolution of memory cell concentration (top), total T cell concentration (middle), and pathogen load (bottom, *v*), obtained for different values of $\alpha_{m,e}$. Dotted line (top left) shows the initial number of naive cells in the system. Reducing the rate of effector differentiation relative to memory precursor proliferation increases the size of the resultant memory population. (**E**) Plot showing the fraction of cells at the peak of expansion that become memory cells, f_{Tm}, as a function of the effector differentiation rate $\alpha_{m,e}$. Dotted line shows a memory fraction $f_{Tm} = 0.05$, used to set the differentiation rate for comparison with the reversible switching model. (**F**) Simulation traces showing time evolution of memory cell concentration (top), total T cell concentration and pathogen load (bottom), for different pathogen replication rates. *A late (obligate reversible) decision strategy (G-H) enables scalable memory generation but fails to generate memory upon a mild challenge.* (**G**) Schematic for the late decision model, indicating the rate constants for effector differentiation ($\alpha_{m,e}$), memory precursor proliferation (γ_m), and pathogen replication (γ_v). (**H**) Simulation traces showing time evolution of memory cell concentration (top), total T cell concentration (middle), and pathogen load (bottom, *v*), obtained for different rates of pathogen replication γ_v. Dotted line (top) shows the final memory cell number in the system. Red line (middle left) indicates the initial number of naive cells in the system. At low rates of pathogen proliferation, the number of memory cells formed are only a small fraction of the initial number of naive cells; the system is unable to store substantial amounts of memory in this regime. See Mathematical Appendix Table 2 for parameter values used for simulations of all models.

Mathematical simulations of this flexible decision model recapitulated the canonical features of the T cell response to acute infection (**Fig. 2.13B; Fig. 2.14A-B**). T cells expanded rapidly in response to pathogen, reaching a peak 4-8 days after infection onset that consisted mostly of effector cells, followed by a contraction to a stable, lower level of memory-competent cells (T_m). Consistent with known studies[1,43], the quantity of memory cells was ~5% of the peak cell number. In response to pathogens with varying replication rates, this flexible decision model allowed memory cells to form robustly and scale linearly with peak cell expansion numbers. Increasing effector expansion with faster pathogen replication was accompanied by a proportional increase in memory cells, such that the memory fraction relative to the peak T cell number remained constant (**Fig. 2.13B and C**– top, yellow shading, γ_v>0.02/hr). This relation is given by:

$$f_{T_m} = \frac{\beta_{e,m}}{\beta_{e,m} + \delta_e}$$

where *e,m* is the maximum effector to memory conversion rate and *e* is the effector death rate. This scaling breaks down when pathogen replication is slow (γ_v<0.02/hr): reduced antigen encounter decreases the probability of the early effector cell decision, such that the number of memory cells generated converges to the starting naive cell number rather than increasing with pathogen replication rate. This ensures a baseline level of memory amid weak challenges that do not elicit a full effector response[3].

To ask whether flexibility is necessary for scalable memory encoding, we analyzed two alternative decision models, where memory decisions are made at only one juncture. The early decision model, where naive cells irreversibly commit to the *Tcf7*-silent effector state, generated robust memory upon challenge with slow-dividing pathogens but could not reproduce the linear scaling of the memory population to the peak population in response to faster-replicating pathogens (**Fig. 2.13C, middle; Fig. 2.14C-F;** see also **Mathematical Appendix**). Conversely, the late decision model, where naive cells transition obligatorily to the effector state and decide later whether to regain memory competence, generated constant memory fractions upon stronger challenges but attenuated memory populations in response to weaker challenges (**Fig. 2.13C,** bottom**; Fig. 2.14G-H**). These analyses underscore the importance of flexibility in memory decision making for optimal long-term immunity against variable threats.

2.4 DISCUSSION

Our finding that reversible epigenetic silencing of *Tcf7* generates inherent flexibility in the T cell memory decision reconciles two prevailing models for memory development that have often been regarded as mutually opposed. While there is evidence that memory cells can form both directly from naive cells with little or no effector differentiation and from effector cells that

dedifferentiate upon infection clearance[8,9], both in mice and in humans[44], no model has explained how both pathways can coexist. In this mechanism, stochastic control of *Tcf7* silencing enables early divergent memory and effector decision making, and its reversibility enables late effector dedifferentiation. Antigen and inflammatory signals tune the decision-making probabilities at both junctures and would thereby influence which pathway would predominate across challenges that differ in signal duration and intensity[45]. This study, together with others[35], implicates stochastic epigenetic switches as drivers of cellular diversification in the immune system. Through regulatory events that initiate over timescales spanning cell generations, these switches allow multiple cell populations to emerge in defined numbers without strict spatially organized cues[46], facilitating division of labor for optimal pathogen defense.

Our modeling results lay the groundwork for understanding how the adaptive immune system can encode information about the nature and severity of a pathogen in its memory cell population. In future work, it will be interesting to determine whether other pathogen features, such as antigenicity or latency, may also be encoded quantitatively. Our findings that memory cells emerging from different decision points may differ in their functional and phenotypic properties raise the possibility that flexible decision making could underlie qualitative encoding of pathogen information through the generation of heterogeneous memory subsets[39,41]. In future work, it will be interesting to investigate the extent to which each decision pathway is utilized under various threats *in vivo* and whether cells emerging from different pathways are functionally heterogeneous[47].

Overall, our study highlights the utility of plasticity in cell fate decision making in biological

systems. From a social and cognitive sciences perspective[48,49], flexibility allows decision making agents to adapt and mount optimal responses amid uncertain and dynamic environments. For immune cells responding to a pathogen, the flexibility to make the memory fate decision at multiple junctures, may enable greater responsiveness as an immune challenge evolves. Observed plasticity in mammalian stem cell fate decision making[50,51] may similarly allow the body to rapidly adapt its regenerative output to changing physiological needs[52]. A fuller consideration of flexibility in cellular decision making, along with its mechanisms and roles, will shed light into design principles of these systems and provide valuable insight for harnessing cells as environmentally-responsive therapeutic agents.

2.5 LIMITATIONS OF THE STUDY

Our *ex vivo* system intentionally minimizes environmental heterogeneity to enable analysis of cell-intrinsic mechanisms for generating heterogeneity. While this setup enabled us to identify stochastic epigenetic switching as a contributor to intraclonal heterogeneity, it cannot determine the relative degrees to which this cell-intrinsic mechanism and environmental factors contribute to lineage outcomes. While our LCMV experiments show that the mechanism we identified is indeed operational during acute infection, further *in vivo* studies will be needed to distinguish the contributions of myriad factors for heterogeneity in lineage decision making in different settings. Furthermore, future work is needed to elucidate the molecular mechanisms that mediate stochastic and reversible *Tcf7* silencing. These include investigation of transcription factors and *cis*-regulatory elements that control *Tcf7* silencing probabilities, as well as chromatin regulators important for maintenance of the *Tcf7* silenced state.

2.6 METHODS

Quantification and Statistical Analysis

All analyses and p or adjusted p value significance are listed with each figure caption. Statistics were performed in R using the rstatix package (v0.7.0) or Python using scipy (v1.5.2).

Mice and viruses

Tcf7-YFP mice have been described[16]. We note that a small number of experiments utilized mice harboring an additional non-perturbing *Tbx21*-CFP BAC transgene reporter allele[62], though this reporter was not further analyzed for this study. All mice used in experiments were heterozygous for the *Tcf7*-YFP reporter except where specified. WT C57BL/6 mice (Jackson Laboratory) were utilized as reporter negative controls, where applicable. Both male and female mice were used for *ex vivo* experiments, aged 8 to 12 weeks. Polyclonal T cells were used for all *ex vivo* experiments except where specified. For donors for adoptive transfer experiments, homozygous *Tcf7*-YFP mice were crossed with an LCMV specific TCR transgenic strain[63] (P14) (Jackson Laboratory), and female heterozygous offspring were used.

For LCMV adoptive transfer experiments, LCMV infections were performed as previously described[64]. C57BL/6J and CD45.1 congenic female mice were purchased from the Jackson Laboratory. For LCMV infections, 6- to 8-week-old mice were either injected intravenously with 2×10^6 plaque-forming units (p.f.u) of LCMV Armstrong or intraperitoneally with 2×10^5 p.f.u of LCMV Armstrong.

All mice were used in accordance with Institutional Animal Care and Use Committee guidelines for the University of Washington or the Emory University Institutional Animal Care and Use Committee.

Naive T cell extraction

Spleens were harvested from mice, massaged between rough glass slides to generate a single-cell suspension, and filtered through 40 µm nylon mesh into HBH (HBSS, 10 mM HEPES, 0.5% BSA, pH 7.4). Cells were spun down for 5 min at 300g, resuspended in 3 mL red blood cell (RBC) lysis buffer (150 mM NH_4Cl, 10 mM $NaHCO_3$, 1 mM EDTA) for 3-5 min, and quenched with HBH. Cells were spun down for 5 min at 300g and resuspended in HBH with 2.4G2 blocking solution and incubated for 30 min on ice. Cells were counted, spun down again, and then enriched for $CD8^+$ T cells using a $CD8a^+$ T Cell Isolation Kit, mouse (Miltenyi, #130-104-075), with the volume and amount of antibodies and microbeads used scaled down to 70% of that specified by the manufacturer. One LS column was used per spleen (Miltenyi, # 130-042-401). To obtain a pure population of naive $CD8^+$ T cells, the cell suspension was stained with anti-$CD8^+$ (PerCP/Cyanine5.5, eBioscience, # 45-0081-82 or Biolegend, #100734), anti-CD44 (APC or PE, Invitrogen, #17-0441-82, or #12-0331-82), and anti-CD62L (APC/eFluor780, Invitrogen, #47-0621-82) at 1:600 antibody to cell suspension volume ratio in $30x10^6$ cell/mL HBH with Fc block for 15-30 min on ice and then sorted with a BD FACS Aria III (BD Biosciences) with assistance from the University of Washington Pathology Flow Cytometry Core Facility. The naive population was gated as $CD8^+CD44^-CD62L^+$*Tcf7*-YFP^+. Memory cells were gated as $CD8^+CD44^+CD62L^+$*Tcf7*-YFP^+. The cells were sorted into HBH and kept on ice until plating.

Ex vivo T cell differentiation

One day prior to T cell harvest and activation (day -1), plates were prepared by coating with anti-CD3e (Tonbo, #40-0031-U100), anti-CD28 (Tonbo, #40-0281-U100), RetroNectin (Takara, #T100B), and when specified, anti-CD11a (Biolegend, #101117). Unless otherwise specified, each well of a 96-well plate received 0.2 µg anti-CD3, 0.1 µg anti-CD28, 1 µg Retronectin, and (when specified) 1 µg anti-CD11a in 50 µL of PBS. For differentiation in larger wells, these amounts were scaled up by well surface area. Plates were sealed with parafilm and incubated at 4°C overnight. On day 0, plates were allowed to come to room temperature for at least 30 min and washed 2x with PBS. Purified cells were added to wells in T cell media [85% RPMI 1640 with L-glutamine, 10% Fetal Bovine Serum, Pen-Strep-Glutamine, 20 mM HEPES, 1 mM Sodium Pyruvate, 0.1 mM NEAA, 50 µM BME] with indicated cytokine concentrations, mixed, and spun down for 1 min at 150g to ensure initial contact for all cells with the coated plate surface. Cytokines added to the media were 100 U/mL IL-2 (PeproTech, # 200-02), 0.5 ng/mL IL-7 (PeproTech, # 200-07), 50 ng/mL IL-15 (PeproTech, # 210-15), and 1 ng/mL IL-12 (PeproTech, #210-12) unless otherwise specified. Where specified, IFN-β1 (Biolegend, #581302) was added at 1000 U/mL. Where specified, Tazemetostat (3 µM, Selleckchem) or GSK126 (5 µM, Cayman Chem) were added to the culture along with 100 U/mL IL-2 in the absence of TCR stimulation. The cell seeding concentration was 0.1 - 2.5 million cells / mL unless otherwise indicated. Cells were incubated at 37°C in 5% CO_2 and split every two days by mixing, removing half of the well volume, and topping off the volume with TCM and respective cytokines. Where applicable, prior to seeding, cells were stained with 5 µM CellTrace Violet (CTV) (Invitrogen, #C34557) following the manufacturer's instructions.

Flow cytometry analysis

For timecourse analyses with cell surface protein staining, cells were spun down in round-bottom 96-well plates or 1.5 mL eppendorf tubes, resuspended in 2.4G2 blocking solution for 15-30 min on ice, stained with cell surface antibodies at 1:1200 (anti-CD8: PerCP-Cyanine5.5, eBioscience, # 45-0081-82, or Biolegend, #100734, anti-CD44: APC, Invitrogen, #17-0441-82, anti-CD62L: APC-e780, Invitrogen #47-0621-82 , anti-CD25: APC, #17-0251-82), antibody to cell suspension volume ratio for an additional 15-30 min on ice, and spun down again for a final resuspension in HBH prior to acquisition. For samples that required intracellular protein staining, cells were fixed and permeabilized using Cytofix/Cytoperm Fixation and Permeabilization kit (BD #554714) according to manufacturer instructions and incubated with antibody for 30 min on ice. The TCF1 antibody (PE, BD Biosciences, # 564217) and T-bet antibody (PE, Biolegend, #644809) were used at 1:50 and 1:200, respectively. For samples that required intracellular cytokine staining, cells were restimulated for 5 hr with PMA/Ionomycin (1x in 100 μL per sample Thermofisher, #00-4970-93) in round-bottom 96-well plates, with a protein transport inhibitor (1x ThermoFisher, #00-4980-93) added after 1 hr. For cytokine secretion after sorting (for Naive, Mem, and NM/NEM) cells were stained with Zombie Near IR at a 1:1000 dilution in PBS following the manufacturer's instructions (Biolegend, #423117). Cells were then fixed, permeabilized, and stained with antibodies for cytokine and other intracellular protein antibodies as described above. All cytokine antibodies were used at 1:100 dilution in 1x BD Perm/Wash buffer (anti-IFN-ɣ (APC/Cyanine7 or PE, Biolegend, #505849, #505808) and anti-TNF-α (BV711 Biolegend, #506349). Data were acquired using an Attune Nxt Flow Cytometer (ThermoFisher Scientific) and analyzed using FlowJo (BD) software.

Sample processing for sci-fate-seq

Naive $CD8^+$ T cells were activated *ex vivo*, as described. For this experiment, media was supplemented with 100 U/mL IL-2, 0.5 ng/mL IL-7, 50 ng/mL IL-15, and 0.05 ng/mL IL-12. The moderate level of IL-12, 0.05 ng/mL, was chosen for this experiment to produce a relatively even representation of *Tcf7* high and low cells (see **Fig. 2.1D**). At days 1, 2, and 4 of activation, two subsequent sci-fate time points were taken as follows: cells were mixed and split into two wells, which had been coated with anti-CD3 and anti-CD28 at day -1 and remained in the incubator with TCM; 4sU was added to one well for a final concentration of 200 μM, and that well was harvested 2 hr later. At that time, 4sU was similarly added to the second well, and that well was harvested 2 hr later. After each 4sU addition, cells were mixed and spun down at 150g for 1 min. Harvested cells were prepared for sci-RNA-seq as described for the sci-fate protocol [22]. Briefly, cells were fixed with ice-cold 4% PFA for 15 min, washed and flash frozen with PBSR [PBS, pH 7.4, 0.2 mg/mL bovine serum albumin (Fisher), 1% Superasein (Thermofisher) and 10 mM dithiothreitol (DTT)]. PFA-fixed cells were thawed, washed, and treated with iodoacetamide (IAA) to attach a carboxyamidomethyl group to 4sU. Following these steps, a single-cell RNA sequencing library was prepared using the sci-RNA-seq protocol[65,66]. The library was sequenced on the Illumina Novaseq system.

Computational analysis for sci-fate-seq

Read alignment, downstream processing, and TF module construction

Read alignment and downstream processing, linking of TFs to regulated genes, and construction of TF modules was performed as described in Cao et al., 2020, with minor modifications. Briefly, for each gene, across all cells, the correlation between mRNA levels of each expressed

TF and that gene was computed using LASSO (least absolute shrinkage and selection operator) regression. We sought to comprehensively define gene programs with distinct dynamics by doing this correlation separately both using only newly synthesized transcript levels for potential target genes and using overall transcript levels, expecting that target genes with more stable transcripts would be more readily identified using newly synthesized transcripts, while less abundant, more lowly detected target genes would be more readily identified in the overall transcriptome. After filtering out the resultant covariance links with a correlation coefficient less than 0.03, we identified 2,117 putative TF - target gene covariance links using newly synthesized transcriptome levels and 9,927 using overall transcriptome levels, resulting in a total of 10,405 unique links after aggregation. These were further filtered to retain only links supported by ChiP-seq binding, motif enrichment, or predicted enhancer binding[24], resulting in 1065 links between 51 TFs and 632 genes. Of these 1065 links, 147 were identified using the newly synthesized transcriptome levels, 649 were identified using the overall transcriptome levels, and 269 were identified by both. To calculate TF activity scores in each cell, newly synthesized unique molecular identifier (UMI) counts for all linked target genes were scaled by library size, log transformed, aggregated, and normalized. The absolute correlation coefficient was computed between all TF pairs with respect to their activity across all cells. Pairwise correlations were hierarchically clustered using the ward D2 method to identify TF modules, with the reasoning that co-regulatory TFs must be simultaneously active within the same cell.

Cell ordering, clustering, and differential gene expression analysis between clusters

We initially attempted to resolve T cell differentiation states by performing dimensionality reduction with Uniform Manifold Approximation and Projection (UMAP) on whole or new

transcriptomes using all detected genes. This analysis largely separated cells by the time point at which they were sampled (**Fig. 2.4B**), as previously observed[67,68], likely a consequence of the host of other temporal changes occurring during activation apart from differentiation, such as cell cycle control and metabolic programming. To characterize T cell differentiation dynamics apart from other regulatory processes, cells were represented in UMAP space using newly synthesized reads for all genes within the T cell differentiation TF module with monocle3 (v.0.2.3.0) (reduction_method = 'UMAP', umap.n_neighbors = 15L, umap.min_dist = 0.001)[53] using the function align_cds[69] to remove effects of cell cycle phase (preprocess_method = 'PCA', alignment_group = 'Phase'). The resultant UMAP was clustered using density peak clustering[70], which resulted in 5 main clusters (**Fig. 2.3C**, U and E2(early) combined, E1(early), E1(late), E2(late), and MP(early) and MP(late) combined). To further resolve observed variable T cell differentiation marker expression within two of these clusters, *k*-means clustering was used to further divide U and E2(early) into separate states and MP(early) and MP(late) into separate states (k = 2 and 2.5, respectively). Cells in different cell cycle phases were relatively evenly distributed across this UMAP, with S phase representation highest in E1(early) (**Fig. 2.4D**). Differential gene expression testing was performed between clusters using the monocle3 fit_models function.

RNA velocity analysis

RNA velocity analysis and visualization of velocity streamlines was performed using Dynamo (v.0.95.2.dev)[26,27] using expression matrices from the full and new transcriptome. The dataset was subsetted to include only the T cell differentiation module genes prior to analysis, but the resultant streamlines were similar when the analysis was performed with all genes. The

streamline results were also similar when scVelo (v.0.2.2)[54] was used for velocity analysis (data not shown), with the full and new transcriptome used as the unspliced/spliced expression matrices, indicating that the streamline results are consistent between multiple analysis methods. The scVelo results were also similar with or without subsetting to include only the T cell differentiation module genes.

Trajectory analysis

Cells in each putative trajectory (E1, E2, MP) were ordered in pseudotime based on the point position on the principal curve estimated using the princurve package[55]. To align the precursor cells between trajectories, cells in the undifferentiated (U) cluster were set to pseudotime = 0. To identify genes that distinguish the trajectories, differentially expressed genes were identified using the monocle3 fit_models function with the model formula as the trajectory and pseudotime terms. Only resulting DEG associated with the trajectory term were selected.

Time-lapse imaging

Long-term time-lapse imaging of cultured cells, both to track *Tcf7* regulation during initial activation in naive cells and to track *Tcf7* reactivation in sorted *Tcf7*-low cells, was performed as previously described with some modifications[71,72]. Images were acquired with an inverted widefield fluorescence microscope (Leica DMi8) fit with an incubator to maintain a constant humidified environment at 37°C and 5% CO2, using a 40X dry objective. For imaging of the initial 4 days of activation (**Fig. 2.5**), cells were seeded at low density (2-5k c/well) in wells of a 96-well glass bottom plate (Mattek) coated with anti-CD3, anti-CD28, anti-CD11a, and RetroNectin, as described above. For *Tcf7* reactivation imaging experiments (**Fig. 2.7**), *Tcf7*-low

cells were sorted on day 3 after 2 days of initial culture with anti-CD3 and anti-CD28 in media with IL-2, IL-7, IL-15, and IL-12 and one additional day of culture with anti-CD3 and anti-CD28 removed. These cells were seeded onto PDMS micromesh (250 μm hole diameter, Microsurfaces) mounted on top of a 24-well glass bottom plate (Mattek) to enable clonal tracking, as seeded cells show considerably enhanced motility in the absence of TCR stimulation. To prepare the micromesh for imaging, the surface was first coated with BSA while mounted on top of a 24-well plate overnight at 4°C and then transferred to a new glass well and coated with anti-CD11a and RetroNectin for improved adhesion but without anti-CD3 and anti-CD28. For reactivation experiments, cells were cultured in TCM with IL-2, IL-7, and IL-15, but without IL-12.

To determine if the experimental conditions required for imaging affect differentiation, we systematically compared expression of CD44, CD62L, and *Tcf7*-YFP in cells activated on glass or tissue culture plates, at high or low seeding density, and with or without presence of anti-CD11a (**Fig. 2.6M**). CD44 expression was comparable across all conditions, confirming that all cells activated in all conditions. In tissue culture plates, CD62L and *Tcf7*-YFP expression were also comparable, though the *Tcf7*-YFP expression was slightly reduced at lower cell density, particularly in the condition without IL-12, consistent with previous findings that memory differentiation occurs less efficiently at lower cell densities[73]. On glass plates, the fraction of CD62L low cells was increased compared to on tissue culture plates. *Tcf7* expression was similarly low for the condition with IL-12, but the combination of low seeding density and presence of anti-CD11a on the glass plate resulted in a lower *Tcf7* distribution in the no IL-12 condition than was otherwise observed. This analysis shows that the specific conditions used for

imaging do not affect overall differentiation trends but may underestimate the differences in differentiation between conditions with and without IL-12.

Computational analysis for time-lapse imaging

Image segmentation and tracking

Image pre-processing, cell segmentation, and tracking was performed in MATLAB (Mathworks, Natick, MA) using the ictrack movie analysis pipeline we described previously[72,74] (**Fig. 2.6A-B**), modified to enable segmentation of cells from brightfield movies. Importantly, to segment cells without additional fluorescent labels besides *Tcf7*-YFP, we first trained a convolutional neural network (CNN) with a U-net architecture[75] to predict fluorescence images of whole cells from brightfield images, using images of cell-trace violet labeled T cells as a training data set[28]. We trained separate CNNs for the images acquired in 96-well plates (**Fig. 2.5**) and in microwells (**Fig. 2.7**), as predictions are optimal when images for training and prediction have similar features. For each training dataset, hundreds of images of CTV-stained cells were acquired at multiple timepoints during the process of interest (e.g. initial T cell activation or culture after stimulation removal). Using the trained CNN, we then generated predicted whole-cell fluorescence images from acquired brightfield movies, which were used for cell segmentation (**Fig. 2.6B**, 1.). Briefly, in the ictrack analysis pipeline, images underwent (1) correction by subtraction of uneven background signal stemming from the bottom of the glass plate or the side of the PDMS microwells (2) Gaussian blur followed by pixel value saturation to fix uneven signal intensity within the nucleus of the cell and (3) Laplacian edge detection algorithm to identify the nucleus boundary. Non-cell objects were excluded via size and shape limit exclusions. To generate clonal lineage trees, cells were tracked automatically between adjacent

movie frames using the Munkres assignment algorithm, and the resulting cell tracks were manually checked for errors and to annotate cell divisions (**Fig. 2.6B**, 2.).

Tcf7 ***promoter state assignment and analysis***

To enable quantitative analysis of *Tcf7* promoter activity in clonal cell lineages, we assembled separate full tracks of total *Tcf7*-YFP fluorescence levels from the starting cell to each ending cell within a lineage tree, for all lineage trees analyzed (**Fig. 2.6B**, 3.). Fluorescence levels are halved at each cell division; thus, to ensure continuity in *Tcf7*-YFP fluorescence in these tracks, we calculated for each parent-daughter cell pair an offset in *Tcf7*-YFP fluorescence, that we added to the daughter cells and their progeny, as previously implemented[34]. These 'continuized' tracks were then smoothed using MATLAB medfilt1 (N=5) and smooth (span = 80 time points, equivalent to 20 hours, method = lowess), and their first derivatives with respect to time were calculated to generate single-cell tracks of *Tcf7* promoter activity for downstream HMM analysis (**Fig. 2.6B**, 4.).

Cell tracks were exported from MATLAB to R for downstream processing. *Tcf7* promoter states for each cell and time point were called from tracks of *Tcf7*-YFP level derivatives using Hidden Markov Model (HMM) modeling, implemented with the msm Package for R (v1.6.9)[56]. We initially tested four candidate HMM models with either three or four promoter states and variable constraints on the derivative ranges within each state (**Fig. 2.6C-D**). For each model, we constrained the mean and variance in *Tcf7* promoter activities of each state by fitting Gaussian distributions to the *Tcf7*-YFP derivatives at different time windows, to reflect our observations that cells are expected to be mostly in an inactive, active, or attenuated state at different times.

We then compared the performance of these four models by calculating their log-likelihood and corresponding AIC (Akaike information criterion) scores. We also checked the quality of each model's fit to the data by assessing whether residuals of the fit follow a Gaussian distribution[76] (**Fig. 2.6E**). Based on this analysis, we chose a model in which cells transition between 4 states: off (initial), low active, high active, and off (**Fig. 2.5B, Fig. 2.6F**), and all start in the off-initial state at the beginning of the track. This four-state model performed favorably compared to other models, likely because it better accounts for the distinct distributions of promoter activity of silent and active cells at initial and later time points.

Using this four-state model, we assigned promoter activity states at each time point for each cell, removing potentially spurious transient promoter states by finding all promoter states lasting less than 8 hours and replacing them with the previously assigned promoter state. From these states, we then identified promoter silencing events as those involving a switch from active (high or low) to an inactive (off) state, and activation events as those involving a switch from inactive (off-initial or off) to active (high or low) states. We did not allow transitions back to the starting inactive (off-initial) state, as this state has a distinct *Tcf7* promoter activity distribution from the later silent state (off), likely reflecting the distinct noise characteristics of *Tcf7*-YFP fluorescence at different stages after activation.

For analysis of *Tcf7* silencing between sister cells, we first assigned an ending cell state to all cells in the dataset, representing the final promoter state of the cell prior to division or the end of the cell track. Cells with a tracked duration of less than 3 hours and parents with ending cell state durations of less than 10 hours were also excluded, to ensure the analysis only includes

sufficiently tracked cells and durable promoter states. We then collected all division events for which the parent cell was in an ON promoter state prior to division and asked whether the daughter cell tracks ended in an ON or OFF promoter state. We thus calculated the number of division events that lead to no (ON/ON), unequal (ON/OFF), or concordant (OFF/OFF) daughter silencing and then calculated the fractions of each category in the entire dataset and within each generation. We statistically analyzed the degree of discordance in *Tcf7* silencing decisions between sister pairs by modifying Cohen's kappa statistical test for inter-rater reliability as follows: division events were categorized as concordant (ON/ON or OFF/OFF) or discordant (ON/OFF) between sisters. The modified Cohen's kappa coefficient, κ', was calculated as the observed percentage of discordant events minus the percentage of discordant events expected by chance, divided by 1 minus the percentage of discordant events expected by chance[77] (**Supplemental Table 2**).

Analysis of *Tcf7*-YFP negative fractions in homozygous and heterozygous reporter cells

For analysis in **Fig. 2.5I-J** and **Fig. 2.6L**, YFP distributions were exported from FlowJo as csvs, imported to Python, and represented as histograms. The positive and negative populations were fit simultaneously as two gaussian distributions using the scipy.optimize.least_squares function (scipy v1.5.2), and the gate between YFP positive and negative populations was identified as the intersection between the gaussian curves. The silent fraction was then calculated as the sum of the histogram below the gate divided by the sum of the entire histogram. Two-tailed unpaired t tests between homozygous and heterozygous YFP silent fractions were performed using scipy.stats.

Sample processing for RNA-seq

Cells were centrifuged at 500g for 5 minutes, resuspended in 350 µL of Trizol (Ambion), mixed well, and frozen at -80°C for processing, starting from step 2 of the RNeasy micro kit (Qiagen, #74004) following the manufacturer's instructions. After processing, RNA was resuspended in RNase free water, quantified using a NanoDrop 2000c (Thermo Scientific), and shipped on dry ice to Novogene Corporation Inc. (Sacramento, CA) for library preparation and sequencing.

Computational analysis for RNA-seq

Raw FASTQ files from RNA-seq paired-end sequencing were aligned to the GRCm38/mm10 reference genome using Kallisto (v0.46.1)[78], and the resultant transcript-level abundance estimates were imported to genes by cells matrices using tximport (v1.18.0) for downstream analysis. Transcripts with low counts (<10) were removed. Differentially expressed genes were identified with DESeq2 (v1.30.1)[60]. PCA plots were generated using the top 500 differentially expressed genes between NM and NEM samples and naive, memory, and effector controls. Significantly differentially expressed genes were also used for gene set enrichment analysis, performed with fgsea (v1.16.0)[61] and using gene sets from the C7 immunologic or the H Hallmark gene-sets from Molecular Signatures Database deposited by Goldrath and Kaech[79,80].

Sample processing for ATAC-seq

After sorting, cells were centrifuged at 500g for 5 minutes then supernatant was aspirated without disturbing the pellet. The pellets were resuspended in 100 µL of ATAC freezing buffer[81] (50 mM Tris at pH 8.0, 25% glycerol, 5 mM $Mg(OAc)_2$, 0.1 mM EDTA, 5 mM DTT, 1× protease inhibitor cocktail (Roche-noEDTA tablet), 1:2,500 superasin (Ambion)), flash frozen in liquid

nitrogen and stored at -80°C. On the day of processing, samples were thawed, centrifuged at 4°C 500g for 5 minutes, and washed with 100 µL of cold 1X PBS. Cells were again centrifuged and resuspended in 100 µL Omni lysis buffer[74] (RSB with 0.1% NP40, 0.1% Tween 20 and 0.01% Digitonin) and incubated on ice for 3 minutes, then quenched with 500 mL of RSB + 0.1% Tween 20. Nuclei were pelleted at 500g for 5 minutes at 4°C, resuspended in 100 µL cold PBS and counted. 50,000 nuclei were used per reaction, pelleted (500g for 5 min at 4°C), resuspended in tagmentation master mix[82] (50 µL total: 25 µL 2X TD buffer, 16.5 µL 1x DPBS, 0.5 µL 1% Digitonin, 0.5 µL 10% Tween 20, 5 µL water, 2.5 µL Tn5 enzyme), and incubated at 55°C for 30 minutes. Samples were purified using DNA Clean and Concentrate-5 (Zymo Research) and eluted in EB buffer (10 mM Tris) for amplification of tagmented DNA. PCR amplifications were performed using Illumina indexed primers and NEBNext High-Fidelity 2X PCR Master Mix. SYBR green was added to each PCR reaction to monitor amplification before it reached saturation. Samples in this study were amplified between 11-15 cycles using recommended conditions[83]. Unpurified products were run on a 6% TBE gel for quality control. PCR product/library were purified using DNA Clean and Concentrate-5 (Zymo Research) then ran on a tapestation to visualize nucleosome distribution. The libraries were normalized to 2nM then pooled equimolar for sequencing. Pooled libraries were loaded onto a NextSeq 500 High150 cycle kit at 1.5 pM loading concentration with paired ends sequencing (read 1: 74 cycles, read 2: 74 cycles, index 1: 10 cycles, index 2: 10 cycles).

Computational analysis for ATAC-seq

Raw ATAC-seq FASTQ files from paired-end sequencing were processed and aligned to the mm10 mouse genome using the PEPATAC (v0.10.3)[57] pipeline, which uses bowtie2[58] for

alignment. Unmapped, unpaired, and mitochondrial reads were removed. Following alignment, peak calling, merging across all samples, and annotation was performed using HOMER (v4.10)[59]. Differentially accessible regions were identified using DESeq2. PCA plots were generated using the top 500 differentially accessible regions between recultured samples and naive, memory, and effector controls. Coverage tracks were generated from bigwig read alignment files using karyoploteR (v1.14.1).

LCMV adoptive transfer experiments

Donor mice: 1×10^6 CD45.2$^+$ *Tcf7*-YFP P14 cells were transferred into CD45.1$^+$ mice. These mice were infected with 2×10^6 p.f.u. of LCMV Armstrong. For the transfer experiment in Figure 5, splenocytes were isolated 3 days after infection and CD8$^+$ T cells were enriched with the EasySep Mouse CD8$^+$ T Cell Isolation Kit (StemCell). For the CTV experiments in Figure 6, splenocytes were isolated 5 days after infection and subsequently labeled with CTV (ThermoFisher) according to the manufacturer's protocol. Using FACS, three populations of CD8$^+$CD45.2$^+$ T cells were isolated (*Tcf7*-YFP^{hi}, *Tcf7*-YFP^{mid} and *Tcf7*-YFP^{lo}). Cells were reconstituted in RPMI and 1x10^6 isolated cells from a single population were transferred i.v. to a single recipient CD45.1$^+$ C57BL/6J mouse which were infected with 2×10^5 p.f.u. LCMV Armstrong 5 days prior to transfer.

Flow cytometry for LCMV adoptive transfer experiments

Surface staining was performed by incubating cells with fluorochrome-conjugated antibodies against CD8$^+$ (BUV395 from BD Bioscience), CD4 (clone GK1.5; allophycocyanin (APC)–Cy7 from Biolegend), CD19 (clone 6D5; APC-Cy7 from Biolegend or BUV805 from BD), PD-1

(clone 29F.1A12; BV785 from Biolegend), CD44 (clone IM7; BUV737 from BD Bioscience), CD45.1 (clone A20; BUV563 from BD Bioscience), CD45.2 (clone 104; PE-Cy7 Biolegend), CD127 (clone AR7R34: PE from Biolegend) CD62L (clone MEL-14; BV605 Biolegend) and KLRG1 (clone 2F1; BV421 or APC from BD Bioscience). Cells were incubated on ice for 30 min in PBS + 2% FBS + 0.5 mM EDTA. TCF1 (clone C63D9; AF488 from Cell Signaling Technology) was stained intracellularly with the eBioscience Foxp3/Transcription Factor Fixation/Permeabilization Kit (ThermoFisher Scientific). Cell viability was determined with the LIVE/DEAD Fixable Aqua or near IR. Samples were analyzed with a Cytek-Aurora and data were analyzed with FlowJo software (BD). The TCF1 intracellular stain was analyzed in a separate panel from the *Tcf7*-YFP reporter, as permeabilization reduces the intensity of the reporter.

2.7 REFERENCES

2.7.1 *Text references*

1. Murali-Krishna, K., Altman, J.D., Suresh, M., Sourdive, D.J., Zajac, A.J., Miller, J.D., Slansky, J., and Ahmed, R. (1998). Counting antigen-specific CD8 T cells: a reevaluation of bystander activation during viral infection. Immunity *8*, 177–187. 10.1016/s1074-7613(00)80470-7.
2. Vijh, S., and Pamer, E.G. (1997). Immunodominant and subdominant CTL responses to Listeria monocytogenes infection. J. Immunol. *158*, 3366–3371.
3. Busch, D.H., Pilip, I.M., Vijh, S., and Pamer, E.G. (1998). Coordinate Regulation of Complex T Cell Populations Responding to Bacterial Infection. Immunity *8*, 353–362. 10.1016/S1074-7613(00)80540-3.
4. Kaech, S.M., Wherry, E.J., and Ahmed, R. (2002). Effector and memory T-cell differentiation: implications for vaccine development. Nat. Rev. Immunol. *2*, 251–262. 10.1038/nri778.
5. Lin, W.-H.W., Nish, S.A., Yen, B., Chen, Y.-H., Adams, W.C., Kratchmarov, R., Rothman, N.J., Bhandoola, A., Xue, H.-H., and Reiner, S.L. (2016). CD8 + T Lymphocyte Self-Renewal during Effector Cell Determination. Cell Rep. *17*, 1773–1782. 10.1016/j.celrep.2016.10.032.
6. Chang, J.T., Palanivel, V.R., Kinjyo, I., Schambach, F., Intlekofer, A.M., Banerjee, A., Longworth, S.A., Vinup, K.E., Mrass, P., Oliaro, J., et al. (2007). Asymmetric T Lymphocyte Division in the Initiation of Adaptive Immune Responses. Science *315*, 1687–1691. 10.1126/science.1139393.

7. Kakaradov, B., Arsenio, J., Widjaja, C.E., He, Z., Aigner, S., Metz, P.J., Yu, B., Wehrens, E.J., Lopez, J., Kim, S.H., et al. (2017). Early transcriptional and epigenetic regulation of CD8+ T cell differentiation revealed by single-cell RNA sequencing. Nat. Immunol. *18*, 422–432. 10.1038/ni.3688.
8. Youngblood, B., Hale, J.S., Kissick, H.T., Ahn, E., Xu, X., Wieland, A., Araki, K., West, E.E., Ghoneim, H.E., Fan, Y., et al. (2017). Effector CD8 T cells dedifferentiate into long-lived memory cells. Nature *552*, 404–409. 10.1038/nature25144.
9. Bannard, O., Kraman, M., and Fearon, D.T. (2009). Secondary Replicative Function of CD8+ T Cells That Had Developed an Effector Phenotype. Science *323*, 505–509. 10.1126/science.1166831.
10. Jacob, J., and Baltimore, D. (1999). Modelling T-cell memory by genetic marking of memory T cells in vivo. Nature *399*, 593–597. 10.1038/21208.
11. Chung, H.K., McDonald, B., and Kaech, S.M. (2021). The architectural design of CD8+ T cell responses in acute and chronic infection: Parallel structures with divergent fates. J. Exp. Med. *218*, e20201730. 10.1084/jem.20201730.
12. Merrell, A.J., and Stanger, B.Z. (2016). Adult cell plasticity in vivo: de-differentiation and transdifferentiation are back in style. Nat. Rev. Mol. Cell Biol. *17*, 413–425. 10.1038/nrm.2016.24.
13. Sun, Q., Lee, W., Hu, H., Ogawa, T., De Leon, S., Katehis, I., Lim, C.H., Takeo, M., Cammer, M., Taketo, M.M., et al. (2023). Dedifferentiation maintains melanocyte stem cells in a dynamic niche. Nature *616*, 774–782. 10.1038/s41586-023-05960-6.
14. Zhao, X., Shan, Q., and Xue, H.-H. (2021). TCF1 in T cell immunity: a broadened frontier. Nat. Rev. Immunol. 10.1038/s41577-021-00563-6.
15. Jeannet, G., Boudousquie, C., Gardiol, N., Kang, J., Huelsken, J., and Held, W. (2010). Essential role of the Wnt pathway effector Tcf-1 for the establishment of functional CD8 T cell memory. Proc. Natl. Acad. Sci. *107*, 9777–9782. 10.1073/pnas.0914127107.
16. Harly, C., Kenney, D., Ren, G., Lai, B., Raabe, T., Yang, Q., Cam, M.C., Xue, H.-H., Zhao, K., and Bhandoola, A. (2019). The transcription factor TCF-1 enforces commitment to the innate lymphoid cell lineage. Nat. Immunol. *20*, 1150–1160. 10.1038/s41590-019-0445-7.
17. Mescher, M.F., Curtsinger, J.M., Agarwal, P., Casey, K.A., Gerner, M., Hammerbeck, C.D., Popescu, F., and Xiao, Z. (2006). Signals required for programming effector and memory development by CD8+ T cells. Immunol. Rev. *211*, 81–92. 10.1111/j.0105-2896.2006.00382.x.
18. Rubinstein, M.P., Lind, N.A., Purton, J.F., Filippou, P., Best, J.A., McGhee, P.A., Surh, C.D., and Goldrath, A.W. (2008). IL-7 and IL-15 differentially regulate CD8+ T-cell subsets during contraction of the immune response. Blood *112*, 3704–3712. 10.1182/blood-2008-06-160945.
19. Xiao, Z., Casey, K.A., Jameson, S.C., Curtsinger, J.M., and Mescher, M.F. (2009). Programming for CD8 T Cell Memory Development Requires IL-12 or Type I IFN. J. Immunol. *182*, 2786–2794. 10.4049/jimmunol.0803484.
20. Danilo, M., Chennupati, V., Silva, J.G., Siegert, S., and Held, W. (2018). Suppression of Tcf1 by Inflammatory Cytokines Facilitates Effector CD8 T Cell Differentiation. Cell Rep. *22*, 2107–2117. 10.1016/j.celrep.2018.01.072.
21. Joshi, N.S., Cui, W., Chandele, A., Lee, H.K., Urso, D.R., Hagman, J., Gapin, L., and Kaech, S.M. (2007). Inflammation Directs Memory Precursor and Short-Lived Effector CD8+ T Cell Fates via the Graded Expression of T-bet Transcription Factor. Immunity *27*, 281–295. 10.1016/j.immuni.2007.07.010.

22. Cao, J., Zhou, W., Steemers, F., Trapnell, C., and Shendure, J. (2020). Sci-fate characterizes the dynamics of gene expression in single cells. Nat. Biotechnol. *38*, 980–988. 10.1038/s41587-020-0480-9.
23. Erhard, F., Saliba, A.-E., Lusser, A., Toussaint, C., Hennig, T., Prusty, B.K., Kirschenbaum, D., Abadie, K., Miska, E.A., Friedel, C.C., et al. (2022). Time-resolved single-cell RNA-seq using metabolic RNA labelling. Nat. Rev. Methods Primer *2*, 1–18. 10.1038/s43586-022-00157-z.
24. He, B., Xing, S., Chen, C., Gao, P., Teng, L., Shan, Q., Gullicksrud, J.A., Martin, M.D., Yu, S., Harty, J.T., et al. (2016). CD8 + T Cells Utilize Highly Dynamic Enhancer Repertoires and Regulatory Circuitry in Response to Infections. Immunity *45*, 1341–1354. 10.1016/j.immuni.2016.11.009.
25. Best, J.A., Blair, D.A., Knell, J., Yang, E., Mayya, V., Doedens, A., Dustin, M.L., and Goldrath, A.W. (2013). Transcriptional insights into the CD8+ T cell response to infection and memory T cell formation. Nat. Immunol. *14*, 404–412. 10.1038/ni.2536.
26. Qiu, Q., Hu, P., Qiu, X., Govek, K.W., Cámara, P.G., and Wu, H. (2020). Massively parallel and time-resolved RNA sequencing in single cells with scNT-seq. Nat. Methods. 10.1038/s41592-020-0935-4.
27. Qiu, X., Zhang, Y., Martin-Rufino, J.D., Weng, C., Hosseinzadeh, S., Yang, D., Pogson, A.N., Hein, M.Y., Hoi (Joseph) Min, K., Wang, L., et al. (2022). Mapping transcriptomic vector fields of single cells. Cell *185*, 690-711.e45. 10.1016/j.cell.2021.12.045.
28. Nguyen, P., Chien, S., Dai, J., Jr, R.J.M., Becker, P.S., and Kueh, H.Y. (2021). Unsupervised discovery of dynamic cell phenotypic states from transmitted light movies. PLOS Comput. Biol. *17*, e1009626. 10.1371/journal.pcbi.1009626.
29. Verbist, K.C., Guy, C.S., Milasta, S., Liedmann, S., Kamiński, M.M., Wang, R., and Green, D.R. (2016). Metabolic maintenance of cell asymmetry following division in activated T lymphocytes. Nature *532*, 389–393. 10.1038/nature17442.
30. Buchholz, V.R., Flossdorf, M., Hensel, I., Kretschmer, L., Weissbrich, B., Graf, P., Verschoor, A., Schiemann, M., Hofer, T., and Busch, D.H. (2013). Disparate Individual Fates Compose Robust CD8+ T Cell Immunity. Science *340*, 630–635. 10.1126/science.1235454.
31. Duffy, K.R., Wellard, C.J., Markham, J.F., Zhou, J.H.S., Holmberg, R., Hawkins, E.D., Hasbold, J., Dowling, M.R., and Hodgkin, P.D. (2012). Activation-Induced B Cell Fates Are Selected by Intracellular Stochastic Competition. Science *335*, 338–341. 10.1126/science.1213230.
32. Gerlach, C., Rohr, J.C., Perie, L., van Rooij, N., van Heijst, J.W.J., Velds, A., Urbanus, J., Naik, S.H., Jacobs, H., Beltman, J.B., et al. (2013). Heterogeneous Differentiation Patterns of Individual CD8+ T Cells. Science *340*, 635–639. 10.1126/science.1235487.
33. Horton, M.B., Cheon, H., Duffy, K.R., Brown, D., Naik, S.H., Alvarado, C., Groom, J.R., Heinzel, S., and Hodgkin, P.D. (2022). Lineage tracing reveals B cell antibody class switching is stochastic, cell-autonomous, and tuneable. Immunity *55*, 1843-1855.e6. 10.1016/j.immuni.2022.08.004.
34. Bintu, L., Yong, J., Antebi, Y.E., McCue, K., Kazuki, Y., Uno, N., Oshimura, M., and Elowitz, M.B. (2016). Dynamics of epigenetic regulation at the single-cell level. Science *351*, 720–724. 10.1126/science.aab2956.
35. Pease, N.A., Nguyen, P.H.B., Woodworth, M.A., Ng, K.K.H., Irwin, B., Vaughan, J.C., and Kueh, H.Y. (2021). Tunable, division-independent control of gene activation timing by a polycomb switch. Cell Rep. *34*, 108888. 10.1016/j.celrep.2021.108888.

36. Lövkvist, C., Mikulski, P., Reeck, S., Hartley, M., Dean, C., and Howard, M. (2021). Hybrid protein assembly-histone modification mechanism for PRC2-based epigenetic switching and memory. eLife *10*, e66454. 10.7554/eLife.66454.
37. Gray, S.M., Amezquita, R.A., Guan, T., Kleinstein, S.H., and Kaech, S.M. (2017). Polycomb Repressive Complex 2-Mediated Chromatin Repression Guides Effector CD8 + T Cell Terminal Differentiation and Loss of Multipotency. Immunity *46*, 596–608. 10.1016/j.immuni.2017.03.012.
38. Ladle, B.H., Li, K.-P., Phillips, M.J., Pucsek, A.B., Haile, A., Powell, J.D., Jaffee, E.M., Hildeman, D.A., and Gamper, C.J. (2016). De novo DNA methylation by DNA methyltransferase 3a controls early effector CD8 + T-cell fate decisions following activation. Proc. Natl. Acad. Sci. *113*, 10631–10636. 10.1073/pnas.1524490113.
39. Pais Ferreira, D., Silva, J.G., Wyss, T., Fuertes Marraco, S.A., Scarpellino, L., Charmoy, M., Maas, R., Siddiqui, I., Tang, L., Joyce, J.A., et al. (2020). Central memory CD8+ T cells derive from stem-like Tcf7hi effector cells in the absence of cytotoxic differentiation. Immunity *53*, 1–16. 10.1016/j.immuni.2020.09.005.
40. Silva, J.G., Pais Ferreira, D., Dumez, A., Wyss, T., Veber, R., Danilo, M., Pinschewer, D.D., Charmoy, M., and Held, W. (2023). Emergence and fate of stem cell–like Tcf7+ CD8+ T cells during a primary immune response to viral infection. Sci. Immunol. *8*, eadh3113. 10.1126/sciimmunol.adh3113.
41. Herndler-Brandstetter, D., Ishigame, H., Shinnakasu, R., Plajer, V., Stecher, C., Zhao, J., Lietzenmayer, M., Kroehling, L., Takumi, A., Kometani, K., et al. (2018). KLRG1+ Effector CD8+ T Cells Lose KLRG1, Differentiate into All Memory T Cell Lineages, and Convey Enhanced Protective Immunity. Immunity *48*, 716–729. 10.1016/j.immuni.2018.03.015.
42. Gray, S.M., Amezquita, R.A., Guan, T., Kleinstein, S.H., and Kaech, S.M. (2017). Polycomb Repressive Complex 2-Mediated Chromatin Repression Guides Effector CD8 + T Cell Terminal Differentiation and Loss of Multipotency. Immunity *46*, 596–608. 10.1016/j.immuni.2017.03.012.
43. Hou, S., Hyland, L., Ryan, K.W., Portner, A., and Doherty, P.C. (1994). Virus-specific CD8+ T-cell memory determined by clonal burst size. Nature *369*, 652–654. 10.1038/369652a0.
44. Akondy, R.S., Fitch, M., Edupuganti, S., Yang, S., Kissick, H.T., Li, K.W., Youngblood, B.A., Abdelsamed, H.A., McGuire, D.J., Cohen, K.W., et al. (2017). Origin and differentiation of human memory CD8 T cells after vaccination. Nature *552*, 362–367. 10.1038/nature24633.
45. Plumlee, C.R., Sheridan, B.S., Cicek, B.B., and Lefrançois, L. (2013). Environmental Cues Dictate the Fate of Individual CD8+ T Cells Responding to Infection. Immunity *39*, 347–356. 10.1016/j.immuni.2013.07.014.
46. Abadie, K., Pease, N.A., Wither, M.J., and Kueh, H.Y. (2019). Order by chance: origins and benefits of stochasticity in immune cell fate control. Curr. Opin. Syst. Biol. *18*, 95–103. 10.1016/j.coisb.2019.10.013.
47. Wagner, D.E., and Klein, A.M. (2020). Lineage tracing meets single-cell omics: opportunities and challenges. Nat. Rev. Genet. *21*, 410–427. 10.1038/s41576-020-0223-2.
48. Benjaafar, S., Morin, T.L., and Talavage, J.J. (1995). The strategic value of flexibility in sequential decision making. Eur. J. Oper. Res. *82*, 438–457.
49. Tello-Ramos, M.C., Branch, C.L., Kozlovsky, D.Y., Pitera, A.M., and Pravosudov, V.V. (2019). Spatial memory and cognitive flexibility trade-offs: to be or not to be flexible, that is the question. Anim. Behav. *147*, 129–136.

50. Weinreb, C., and Klein, A.M. (2020). Lineage reconstruction from clonal correlations. Proc. Natl. Acad. Sci. U. S. A. *117*, 17041–17048. 10.1073/pnas.2000238117.
51. Xin, T., Gonzalez, D., Rompolas, P., and Greco, V. (2018). Flexible fate determination ensures robust differentiation in the hair follicle. Nat. Cell Biol. *20*, 1361–1369. 10.1038/s41556-018-0232-y.
52. Manz, M.G., and Boettcher, S. (2014). Emergency granulopoiesis. Nat. Rev. Immunol. *14*, 302–314. 10.1038/nri3660.
53. Cao, J., Spielmann, M., Qiu, X., Huang, X., Ibrahim, D.M., Hill, A.J., Zhang, F., Mundlos, S., Christiansen, L., Steemers, F.J., et al. (2019). The single-cell transcriptional landscape of mammalian organogenesis. Nature *566*, 496–502. 10.1038/s41586-019-0969-x.
54. La Manno, G., Soldatov, R., Zeisel, A., Braun, E., Hochgerner, H., Petukhov, V., Lidschreiber, K., Kastriti, M.E., Lönnerberg, P., Furlan, A., et al. (2018). RNA velocity of single cells. Nature *560*, 494–498. 10.1038/s41586-018-0414-6.
55. Hastie, T., and Stuetzle, W. (1989). Principal Curves. J. Am. Stat. Assoc. *84*, 502–516. 10.1080/01621459.1989.10478797.
56. Jackson, C.H. (2011). Multi-State Models for Panel Data: The **msm** Package for *R*. J. Stat. Softw. *38*. 10.18637/jss.v038.i08.
57. Smith, J.P., Corces, M.R., Xu, J., Reuter, V.P., Chang, H.Y., and Sheffield, N.C. (2021). PEPATAC: an optimized pipeline for ATAC-seq data analysis with serial alignments. NAR Genomics Bioinforma. *3*, lqab101. 10.1093/nargab/lqab101.
58. Langmead, B., and Salzberg, S.L. (2012). Fast gapped-read alignment with Bowtie 2. Nat. Methods *9*, 357–359. 10.1038/nmeth.1923.
59. Heinz, S., Benner, C., Spann, N., Bertolino, E., Lin, Y.C., Laslo, P., Cheng, J.X., Murre, C., Singh, H., and Glass, C.K. (2010). Simple Combinations of Lineage-Determining Transcription Factors Prime cis-Regulatory Elements Required for Macrophage and B Cell Identities. Mol. Cell *38*, 576–589. 10.1016/j.molcel.2010.05.004.
60. Love, M.I., Huber, W., and Anders, S. (2014). Moderated estimation of fold change and dispersion for RNA-seq data with DESeq2. Genome Biol. *15*, 550. 10.1186/s13059-014-0550-8.
61. Korotkevich, G., Sukhov, V., Budin, N., Shpak, B., Artyomov, M.N., and Sergushichev, A. (2021). Fast gene set enrichment analysis. Preprint at bioRxiv, 10.1101/060012 10.1101/060012.
62. Zhu, J., Jankovic, D., Oler, A.J., Wei, G., Sharma, S., Hu, G., Guo, L., Yagi, R., Yamane, H., Punkosdy, G., et al. (2012). The Transcription Factor T-bet Is Induced by Multiple Pathways and Prevents an Endogenous Th2 Cell Program during Th1 Cell Responses. Immunity *37*, 660–673. 10.1016/j.immuni.2012.09.007.
63. Pircher, H., Bürki, K., Lang, R., Hengartner, H., and Zinkernagel, R.M. (1989). Tolerance induction in double specific T-cell receptor transgenic mice varies with antigen. Nature *342*, 559–561. 10.1038/342559a0.
64. Wherry, E.J., Blattman, J.N., Murali-Krishna, K., van der Most, R., and Ahmed, R. (2003). Viral Persistence Alters CD8 T-Cell Immunodominance and Tissue Distribution and Results in Distinct Stages of Functional Impairment. J. Virol. *77*, 4911–4927. 10.1128/JVI.77.8.4911-4927.2003.
65. Cao, J., Packer, J.S., Ramani, V., Cusanovich, D.A., Huynh, C., Daza, R., Qiu, X., Lee, C., Furlan, S.N., Steemers, F.J., et al. (2017). Comprehensive single-cell transcriptional profiling of a multicellular organism. Science *357*, 661–667. 10.1126/science.aam8940.
66. Cao, J., Cusanovich, D.A., Ramani, V., Aghamirzaie, D., Pliner, H.A., Hill, A.J., Daza, R.M., McFaline-Figueroa, J.L., Packer, J.S., Christiansen, L., et al. (2018). Joint profiling of chromatin

accessibility and gene expression in thousands of single cells. Science *361*, 1380–1385. 10.1126/science.aau0730.
67. Arsenio, J., Kakaradov, B., Metz, P.J., Kim, S.H., Yeo, G.W., and Chang, J.T. (2014). Early specification of CD8+ T lymphocyte fates during adaptive immunity revealed by single-cell gene-expression analyses. Nat. Immunol. *15*, 365–372. 10.1038/ni.2842.
68. Kurd, N.S., He, Z., Louis, T.L., Milner, J.J., Omilusik, K.D., Jin, W., Tsai, M.S., Widjaja, C.E., Kanbar, J.N., Olvera, J.G., et al. (2020). Early precursors and molecular determinants of tissue-resident memory CD8 + T lymphocytes revealed by single-cell RNA sequencing. Sci. Immunol. *5*, eaaz6894. 10.1126/sciimmunol.aaz6894.
69. Haghverdi, L., Lun, A.T.L., Morgan, M.D., and Marioni, J.C. (2018). Batch effects in single-cell RNA-sequencing data are corrected by matching mutual nearest neighbors. Nat. Biotechnol. *36*, 421–427. 10.1038/nbt.4091.
70. Rodriguez, A., and Laio, A. (2014). Clustering by fast search and find of density peaks. Science *344*, 1492–1496. 10.1126/science.1242072.
71. Kueh, H.Y., Champhekar, A., Nutt, S.L., Elowitz, M.B., and Rothenberg, E.V. (2013). Positive Feedback Between PU.1 and the Cell Cycle Controls Myeloid Differentiation. Science *341*, 670–673. 10.1126/science.1240831.
72. Kueh, H.Y., Yui, M.A., Ng, K.K.H., Pease, S.S., Zhang, J.A., Damle, S.S., Freedman, G., Siu, S., Bernstein, I.D., Elowitz, M.B., et al. (2016). Asynchronous combinatorial action of four regulatory factors activates Bcl11b for T cell commitment. Nat. Immunol. *17*, 956–965. 10.1038/ni.3514.
73. Polonsky, M., Rimer, J., Kern-Perets, A., Zaretsky, I., Miller, S., Bornstein, C., David, E., Kopelman, N.M., Stelzer, G., Porat, Z., et al. (2018). Induction of CD4 T cell memory by local cellular collectivity. Science *360*, eaaj1853. 10.1126/science.aaj1853.
74. Ng, K.K., Yui, M.A., Mehta, A., Siu, S., Irwin, B., Pease, S., Hirose, S., Elowitz, M.B., Rothenberg, E.V., and Kueh, H.Y. (2018). A stochastic epigenetic switch controls the dynamics of T-cell lineage commitment. eLife *7*, e37851. 10.7554/eLife.37851.
75. Ounkomol, C., Seshamani, S., Maleckar, M.M., Collman, F., and Johnson, G.R. (2018). Label-free prediction of three-dimensional fluorescence images from transmitted-light microscopy. Nat. Methods *15*, 917–920. 10.1038/s41592-018-0111-2.
76. Lian, H., Thompson, W.A., Thurman, R., Stamatoyannopoulos, J.A., Noble, W.S., and Lawrence, C.E. (2008). Automated mapping of large-scale chromatin structure in ENCODE. Bioinformatics *24*, 1911–1916. 10.1093/bioinformatics/btn335.
77. Cohen, J. (1960). A Coefficient of Agreement for Nominal Scales. Educ. Psychol. Meas. *20*, 37–46. 10.1177/001316446002000104.
78. Bray, N.L., Pimentel, H., Melsted, P., and Pachter, L. (2016). Near-optimal probabilistic RNA-seq quantification. Nat. Biotechnol. *34*, 525–527. 10.1038/nbt.3519.
79. Luckey, C.J., Bhattacharya, D., Goldrath, A.W., Weissman, I.L., Benoist, C., and Mathis, D. (2006). Memory T and memory B cells share a transcriptional program of self-renewal with long-term hematopoietic stem cells. Proc. Natl. Acad. Sci. *103*, 3304–3309. 10.1073/pnas.0511137103.
80. Kaech, S.M., Hemby, S., Kersh, E., and Ahmed, R. (2002). Molecular and Functional Profiling of Memory CD8 T Cell Differentiation. Cell *111*, 837–851. 10.1016/S0092-8674(02)01139-X.
81. Saunders, A., Core, L.J., Sutcliffe, C., Lis, J.T., and Ashe, H.L. (2013). Extensive polymerase pausing during Drosophila axis patterning enables high-level and pliable transcription. Genes Dev. *27*, 1146–1158. 10.1101/gad.215459.113.

82. Corces, M.R., Trevino, A.E., Hamilton, E.G., Greenside, P.G., Sinnott-Armstrong, N.A., Vesuna, S., Satpathy, A.T., Rubin, A.J., Montine, K.S., Wu, B., et al. (2017). An improved ATAC-seq protocol reduces background and enables interrogation of frozen tissues. Nat. Methods *14*, 959–962. 10.1038/nmeth.4396.
83. Cusanovich, D.A., Hill, A.J., Aghamirzaie, D., Daza, R.M., Pliner, H.A., Berletch, J.B., Filippova, G.N., Huang, X., Christiansen, L., DeWitt, W.S., et al. (2018). A Single-Cell Atlas of In Vivo Mammalian Chromatin Accessibility. Cell *174*, 1309-1324.e18. 10.1016/j.cell.2018.06.052.

2.7.2 *Figure references*

[1] Hao, Y., Hao, S., Andersen-Nissen, E., Mauck, W.M., Zheng, S., Butler, A., Lee, M.J., Wilk, A.J., Darby, C., Zager, M., et al. (2021). Integrated analysis of multimodal single-cell data. Cell *184*, 3573–3587. 10.1016/j.cell.2021.04.048.
[2] Lian, H., Thompson, W.A., Thurman, R., Stamatoyannopoulos, J.A., Noble, W.S., and Lawrence, C.E. (2008). Automated mapping of large-scale chromatin structure in ENCODE. Bioinformatics *24*, 1911–1916. 10.1093/bioinformatics/btn335.

Chapter 3. EPIGENEITC REGULATION OF THE EXHAUSTED T CELL STATE BY COOPERATIVITY BETWEEN PRC1 AND PRC2

Chapter 3 was adapted with minimal modifications from the following manuscript in preparation at the time of writing:

Joint inhibition of PRC1 and PRC2 during rest reprograms exhausted T cells to a stem-like state. (2024, in preparation). **Elisa Clark***, Kathleen Abadie*, Arjun Kumar*, Oren Barboy, Florence Chardon, Sriram Pendyala, Douglas Fowler, Ido Amit, Shivani Srivastava, Hao Yuan Kueh

*co-first authors

3.1 ABSTRACT

Progressive loss of function, or exhaustion, is greatly limiting for adoptive T cell therapies for cancer. Naive, cytotoxic T cells differentiate first through a precursor exhausted state (T_{PEX}) which is marked by high levels of the transcription factor T cell factor 1 (TCF1), necessary for self-renewal and survival. Differentiation of these $TCF1^+$ cells supplies the tumor with $TCF1^-$ cells that have initial cytotoxic effector function; however, these cells progressively differentiate to a less functional, stably exhausted (T_{EX}) state in the tumor environment. Little is known about what drives the initial formation, maintenance, and differentiation of these $TCF1^+$ self-renewing cells. We have developed a novel *ex vivo* model of chronic antigen stimulation which allows us to precisely control the stimulation environment and differentiation dynamics of individual T cells. Using this model, we observed that cells transition from a $TCF1^+$ state to a plastic, $TCF1^-$ state with the potential to reactivate $TCF1^+$ upon antigen withdrawal. This plasticity is lost with increasing duration of stimulation. We performed a targeted CRISPR-Cas9 screen to determine

the role of transcription factors and epigenetic modifying enzymes on both the initial silencing as well as the stable repression of TCF1. Through both small molecule inhibition and genetic knockout, we determined that the polycomb repressive complexes (PRC) 1 and 2 jointly contribute to stable TCF1 repression in T_{EX} cells. By inhibiting polycomb-mediated repression we demonstrate reversal of the fixed exhausted state, thereby providing a potential therapeutic strategy for increasing $TCF1^{+}$ cells in the tumor environment.

3.2 Introduction

Tumor induced loss of function, or exhaustion, is a critical barrier to T cell responses to cancer. Exhaustion occurs across a wide variety of tumor types and impacts both the endogenous T cell response as well as adoptively transferred cells such as chimeric antigen receptor (CAR)-T cells[1]. Exhaustion differentiation occurs progressively as a result of chronic exposure to antigen, as well as a myriad of other factors in the tumor environment including inflammation and poor nutrient availability[2]. It has been recently established that exhausted T cells (T_{EX}) arise from a stem-like, self-renewing, precursor population (T_{PEX}) with little effector function, that then transition through an intermediate (T_{INT}), cytotoxic state before becoming dysfunctional[3–5]. T_{PEX} are characterized by high expression of the transcription factor TCF1, which is critical for their persistence and ability to differentiate in response to stimulation[3,5–8]. T_{INT} are characterized by high cytotoxic function, loss of TCF1 expression, and lack of exhaustion-associated inhibitory receptors such as T cell immunoglobulin and mucin domain-containing protein 3 (TIM3)[4,9]. T_{EX} cells lack TCF1 expression, and have high expression of TIM3, and other inhibitory receptors such as LAG3, and TIGIT[2,5,10,11].

The transcription factor TOX has been implicated in epigenetic remodeling during exhaustion differentiation, drives expression of inhibitory receptors, and is expressed across T_{PEX}, T_{INT} and T_{EX} states[10,12]. Cells experiencing stimulation in the tumor environment express the inhibitory receptor PD-1, regardless of differentiation state, however all cells experiencing antigen stimulation have elevated levels of PD-1[10,13,14]. Anti-PD-1/PD-L1 checkpoint blockade therapy speeds proliferation and differentiation of T_{PEX} into T_{INT} cells[8,15], and thus patients with increased $TCF1^+$ cells respond better to current therapeutic strategies. Importantly, checkpoint blockade does not alter the epigenetic state of exhausted cells[16] and acts specifically on T_{PEX}. T_{PEX} are thought to transition through an initially plastic state, where exhaustion differentiation can be reversed, but eventually transition to the epigenetically fixed exhausted state[17,18]. There is a therapeutic need to increase the $TCF1^+$ precursor pool to allow for long-lived T cell responses, however it remains unclear whether reversal of the epigenetically fixed exhausted state is possible in the tumor or if these $TCF1^+$ cells must arise from a fresh supply of precursor cells from the lymph node[19,20].

The fixed epigenetic state of exhausted cells in the absence of chronic stimulation could be mediated by mechanisms such as DNA methylation or histone modifications at genomic loci required for self-renewal and effector function[21]. Both DNA methylation[22] and histone modifications imparted by polycomb repressive complexes (PRC) 1[23] and 2[24] have been implicated in regulating terminal effector differentiation during acute infection through repression of pro-memory genes. Similar mechanisms could be regulating the repression of TCF1 and T_{PEX} formation and maintenance. Indeed, rest from T cell receptor (TCR) stimulation

has been implicated in reinvigorating the function of exhausted CAR-T cells and is thought to occur through an Enhancer of zeste homolog 2 (EZH2, PRC2) dependent mechanism[25].

Using a novel *ex vivo* platform for exhaustion differentiation, we sought to identify regulators of the fixed exhausted state with a focus on repression of TCF1 in acute and chronic stimulation. We previously demonstrated silencing of *Tcf7*, the gene encoding for TCF1, occurs epigenetically and stochastically, but is reversible upon stimulation withdrawal and tunable by inflammation (**Chapter 2**). By adapting our *ex vivo* model for chronic stimulation, we observed a transition from a *Tcf7* high T_{PEX} state to an initially plastic, T_{INT} state with *Tcf7* reactivation potential upon rest. With longer periods of stimulation, we observed a transition to a TIM3 high T_{EX} state lacking *Tcf7* reactivation potential. Using a targeted CRISPR-Cas9 screen, we sought to identify factors regulating the initiation of *Tcf7* silencing early after activation and maintenance of *Tcf7* silencing in T_{EX} cells. We identified a role for PRC1 and 2 in cooperatively locking down the epigenetically fixed exhausted state both *ex vivo* and in a solid tumor model. Intriguingly, PRC2 inhibition early after activation inhibited *Tcf7* expression, indicating a context-dependent mechanism for polycomb-mediated regulation of *Tcf7.* This could in part explain challenges associated with using epigenetic targeting drugs for the treatment of T cell exhaustion[21] and provides a basis for the design of therapeutic strategies for reversal of the exhausted state.

3.3 RESULTS

3.3.1 *Cells transition from a precursor to an exhausted state in an* ex vivo *model of chronic stimulation*

Chronic antigen stimulation through the T cell receptor (TCR) and tumor-specific cytokine stimulation have been implicated in driving differentiation of tumor infiltrating T cells[2,10,26,27], however, it is difficult to disentangle the effects of individual stimuli on exhaustion differentiation in a tumor model. To disentangle the mechanisms controlling loss of $TCF1^+$ cells during exhaustion differentiation, we sought to develop an *ex vivo* model to allow for precise control of the stimulation environment and increase ease of manipulation of regulatory mechanisms. To generate this model, we adapted our previous *ex vivo* model system (**Chapter 2**) for chronic stimulation (**Fig. 3.1A**). We stimulated splenic $CD8^+$ cells *ex vivo* over the course of 6 days through the TCR with αCD3 antibodies and added αCD28 co-stimulation for the first 48 hours of the assay to mimic initial priming of the T cells by dendritic cells before migration into the tumor[28]. Similar methods for chronic T cell stimulation have demonstrated exhaustion-associated phenotypes and loss of function *in vitro*[29–31], as well as reduced function after adoptive transfer *in vivo*[29]. Building upon these models, we also added the inflammatory cytokines IL-12 or IFN-α, which we and others have previously demonstrated play important roles in instructing $CD8^+$ T cells toward memory and effector fates[32–34], and importantly drive TCF1 silencing[35] (**Chapter 2**). To assay the regulation of TCF1, we utilized a previously described[36] non perturbing yellow fluorescent protein (YFP) reporter of *Tcf7* activity, the gene encoding for TCF1. We observed that without inflammation, only a fraction of cells transitioned over the 6 day stimulation period to a *Tcf7*$^-$ state, and an even smaller fraction of cells transitioned to a *Tcf7*$^-$$TIM3^+$ state, characteristic of exhausted cells *in vivo*, despite these cells

being chronically stimulated and having high expression of the inhibitory receptor PD-1 (**Fig. 3.1B,C**). However, with inflammation, after 4 days in culture more than half of the cells transition to this T_{EX} state and display even higher levels of PD-1 (**Fig. 3.1B,C**). When the cells are only acutely stimulated, across all inflammatory contexts, the predominant population is *Tcf7*$^{+}$TIM3^{-}, indicating that both chronic stimulation and inflammation are required for the transition to this *Tcf7*$^{-}$TIM3^{+} T_{EX} state. Previous studies have indicated a role for inflammation in driving the exhausted state in tumors and chronic infections, consistent with our findings[37–40].

We additionally observed loss in the production of effector cytokines TNF-α, IFN-γ, and IL-2 over time in chronically stimulated cells (**Fig. 3.1D; Fig. 3.2A**). Intriguingly, we observed chronically stimulated cells had higher production of granzyme B (GZMB) over time (**Fig. 3.1D; Fig. 3.2A**), consistent with reports that the most exhausted differentiated cells in chronic infections have high GZMB production[11]. We also observed upregulation of the exhaustion master regulatory transcription factor TOX over time on stimulation when the cells were treated without inflammation or with IFN-α (**Fig. 3.1D; Fig. 3.2A**). TOX is highly expressed in exhausted cells *in vivo*[10,12,41] and *in vitro*[29] and drives transcription of many exhaustion-associated genes, notably inhibitory receptors[10]. Interestingly, IL-12 decreased TOX protein levels over time, suggesting that IL-12 is driving TCF1 silencing, differentiation, and effector function without TOX-mediated reprogramming, and suggests that TOX is not required for the transition to the *Tcf7*$^{-}$TIM3^{+} state. Indeed, pre-treatment with IL-12 *in vitro* has been previously shown to decrease TOX along with increases in effector function[42].

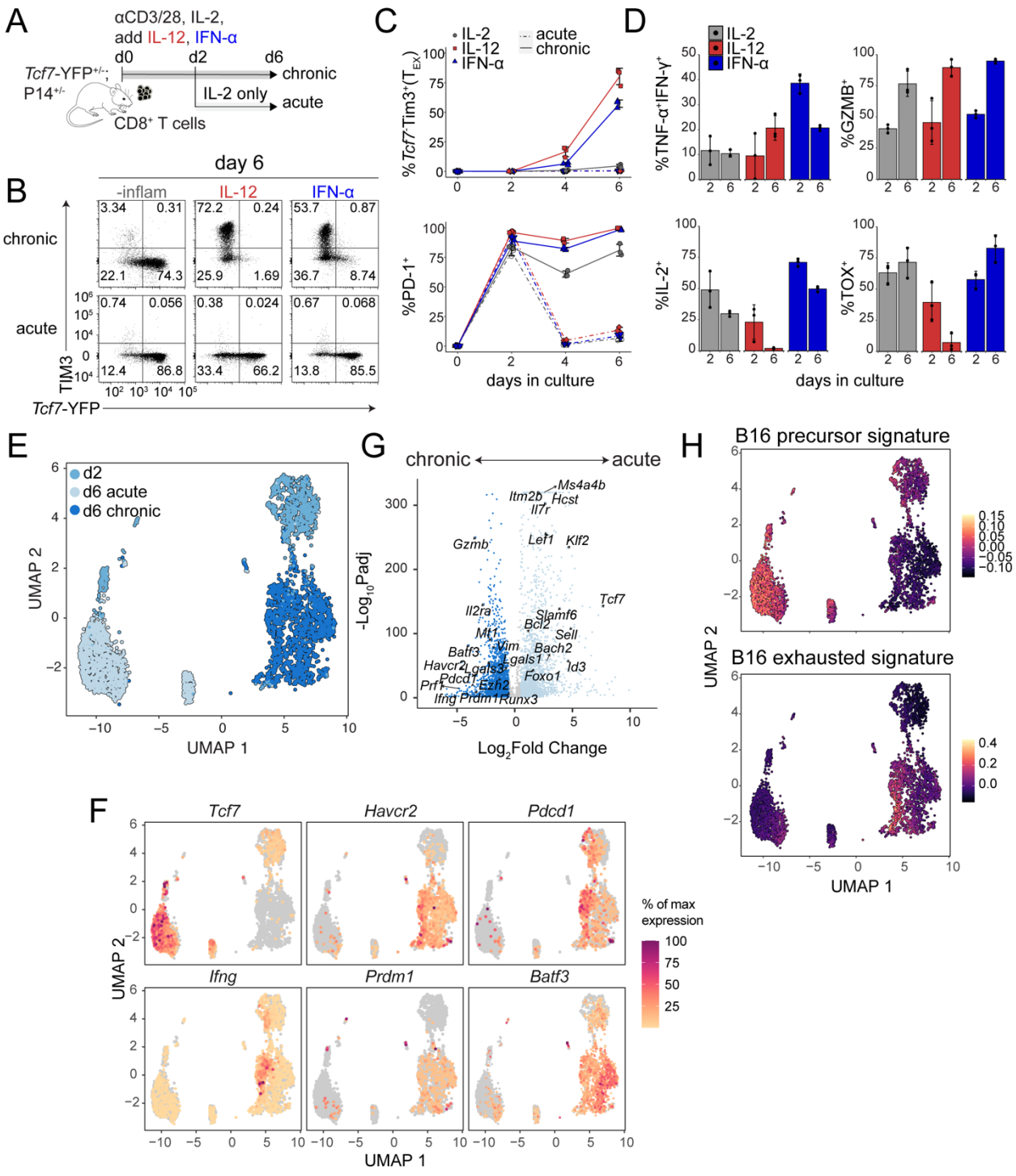

Figure 3.1. *Ex vivo* chronic stimulation recapitulates transition from self-renewing precursor to exhausted state.

(**A**) Overview of chronic stimulation assay. (**B**) Representative day 6 flow cytometry profiles of *Tcf7*-YFPxTIM3 for acute and chronic stimulation for no inflammation (IL-2 only), +IL-12, and +IFN-α. (**C**) Top: Quantification of (B); *Tcf7*-YFP^{-}TIM3^{+} (T_{EX}) cells over time. Bottom: Quantification of PD-1^{+} cells over time. (**D**) Functional cytokine secretion at day 2 and day 6 of chronic stimulation. (**E**) UMAP of IFN-α treated cells from day 2, and day 6 of acute or chronic stimulation. (**F**) UMAPs depicting % of maximum expression in each cell for *Tcf7*, *Havcr2*, *Pdcd1*, *Ifng*, *Prdm1*, and *Batf3*. (**G**) Volcano plot of differentially expressed genes between day 6 chronic (left) and acute

stimulation (right). (**H**) UMAP of enrichment scores for precursor or exhausted gene signatures from day 10 and 20 B16 tumors from Miller *et al.* 2019[5]. [C-D] n=3 biological replicates. Mean±SD.

To better characterize the cell state of cells differentiated *ex vivo*, we performed single cell RNA sequencing (scRNAseq) of cells stimulated for 2 or 6 days in the presence of IFN-α, as well as cells acutely stimulated for 2 days and then rested from stimulation until day 6. After filtering out low quality cells and cells that could not be mapped back to a single condition based on their hashtag antibody label[43], we obtained 4078 cells, with 939 from day 2 of stimulation, 1656 from day 6 of chronic stimulation, and 1483 from day 6 of acute stimulation. Uniform Manifold Approximation and Projection (UMAP) dimensionality reduction[44] (**Fig. 3.1E**) demonstrated distinct transcriptomic signatures between acute and chronic stimulation. The topology of the UMAP indicates a differentiation trajectory from the day 2 cells to the day 6 stimulated cells, while the rested cells cluster further away indicating a larger difference between their transcriptomes. We observed that cells stimulated for 6 days upregulated *Havcr2* (TIM3), while cells stimulated for 2 days and rested until day 6 (acute stimulation) had high expression of *Tcf7* (TCF1), consistent with our flow cytometry data. Stimulated cells expressed *Pdcd1* (PD-1), consistent with the duration of antigen stimulation. We also observed high expression of *Ifng* in the stimulated cells, consistent with our cytokine secretion assay. We uniquely observed *Prdm1* (BLIMP1), and *Batf3* expression only in the day 6 chronically stimulated cells (**Fig 3.1F**). Unsupervised clustering (**Fig 3.2B**) revealed further heterogeneity within and between the culture conditions and generated 7 distinct populations. Looking at the 2 clusters within the day 6 chronically stimulated cells, we noticed differential expression of *Ifng,* which allowed us to subclassify the day 6 chronically stimulated cells into functional and dysfunctional exhausted states. Notably, the transcription factor *Batf3* was also enriched in the dysfunctional cluster (**Fig. 3.1F; Fig. 3.2B**).

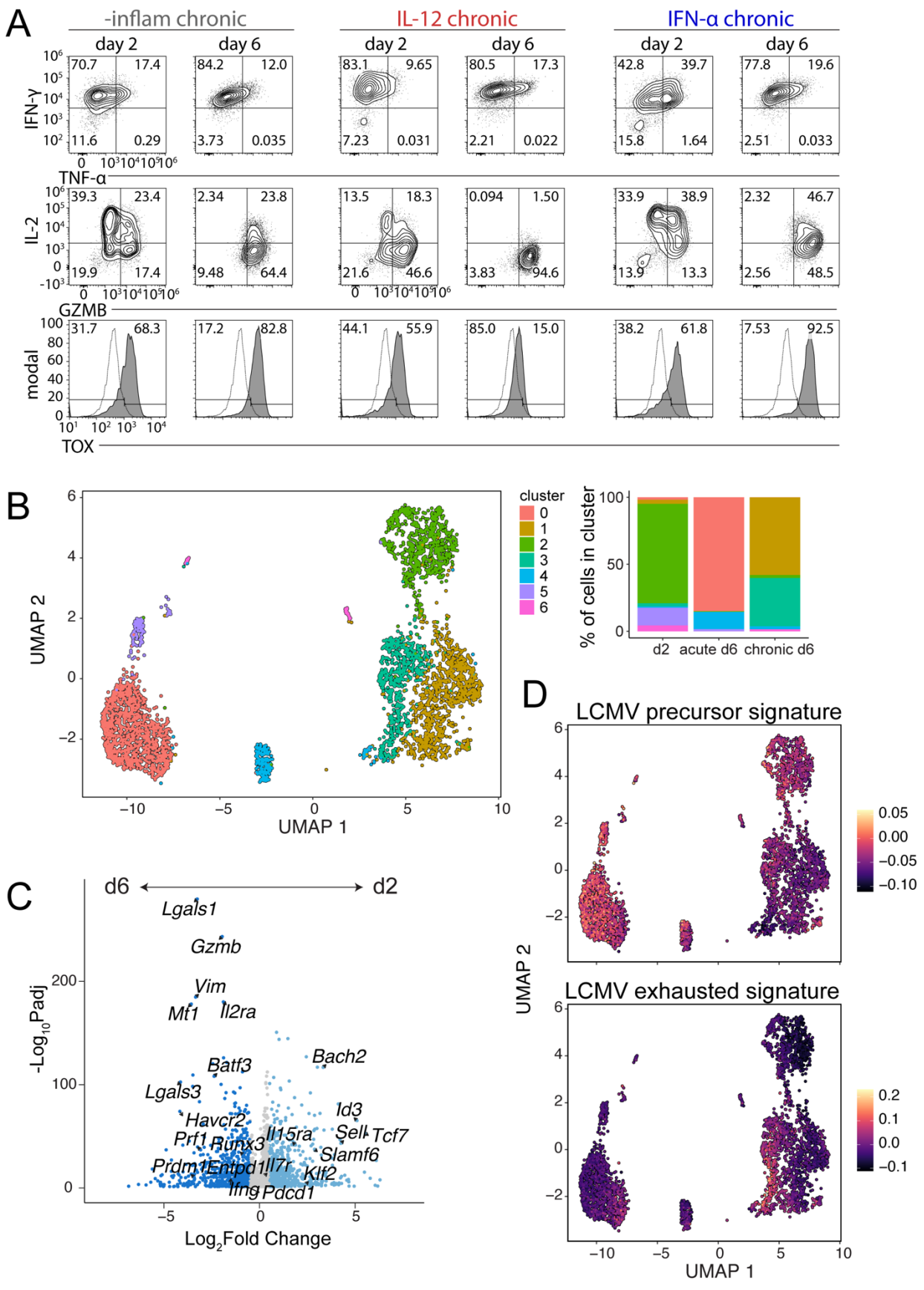
A
-inflam chronic
IL-12 chronic
IFN-α chronic
day 2
day 6
IFN-γ
TNF-α
IL-2
GZMB
modal
TOX
B
UMAP 2
UMAP 1
cluster
% of cells in cluster
d2
acute d6
chronic d6
C
d6
d2
Lgals1
Gzmb
Vim
Mt1
Il2ra
Batf3
Bach2
Lgals3
Id3
Havcr2
Il15ra
Sell
Tcf7
Prf1
Runx3
Slamf6
Prdm1
Entpd1
Il7r
Klf2
Ifng
Pdcd1
-Log10Padj
Log2Fold Change
D
LCMV precursor signature
LCMV exhausted signature
UMAP 2
UMAP 1

Figure 3.2. *Ex vivo* assay recapitulates key hallmarks of exhaustion.
(**A**) Representative day 2 and day 6 flow cytometry profiles of TNF-αxIFN-γ, GZMBxIL-2, and TOX. Open histograms are day 0 unstimulated cells. (**B**) Cluster depiction on UMAP and % of cells from each culture condition in each cluster. (**C**) Volcano plot of differentially expressed genes between day 6 chronic (left) and day 2 of stimulation (right). (**H**) UMAP of enrichment scores for precursor or exhausted gene signatures from day 28 of LCMV infection from Miller *et al.* 2019[5].

We performed differential expression tests between day 2 and day 6 stimulated cells, and between day 6 acute and chronically stimulated cells (**Fig 3.1G; Fig. 3.2C**). We observed that *Tcf7* (TCF1) was significantly upregulated in both the day 2 and day 6 acutely stimulated cells compared to day 6 chronically stimulated cells. Other memory associated genes such as *Sell*[22], *Il7r*[45], and *Id3*[7], and *Bach2*[46] were enriched in the day 2 and day 6 acutely stimulated cells. Cells stimulated for only 2 days had higher *Il2* expression, while cells stimulated for 6 days had higher *Gzmb* and *Ifng* expression, consistent with our functional cytokine secretion results (**Fig. 3.1D**). In addition to *Havcr2*, *Prdm1*, and *Batf3*, day 6 chronically stimulated cells had high expression of *Mt1*, which has been previously identified as a hallmark of dysfunctional tumor infiltrating T cells[47] and the inhibitory receptor *Entpd1* (CD39), which has also been shown to be upregulated in exhausted tumor infiltrating T cells[48]. Chronically stimulated cells also expressed *Runx3*, which is essential for epigenetic remodeling of T cells after activation[49]. Exhaustion differentiation is thought to result from progressive epigenetic remodeling[17,21], and consistent with this hypothesis, we also observed increased expression of *Ezh2* (EZH2) in chronically stimulated cells (**Fig. 3.1G**).

We lastly sought to compare the transcriptomes of chronically stimulated cells from our *ex vivo* assay to exhausted cells from solid tumors and from chronic Lymphocytic Choriomeningitis Virus (LCMV) infection. We compared our dataset to previously published progenitor and terminally exhausted cells from day 10 and day 20 B16 melanoma tumors, and from day 28 of

LCMV infection from Miller *et al.* 2019[5]. We found enrichment from both *in vivo* contexts for the precursor exhausted signature in our acutely stimulated cells, and for the terminally exhausted signature in our day 6 chronically stimulated cells (**Fig 3.1H; Fig. 3.2D**). Intriguingly, some acutely stimulated cells were enriched for the exhausted gene signature, suggesting stability of the exhaustion gene program in some acutely stimulated cells, consistent with reports that the exhaustion epigenetic signature is still present even after antigen withdrawal[50]. Taken together, our phenotypic, functional, and transcriptomic data suggest that our minimal *ex vivo* model of chronic stimulation recapitulates key characteristics of *in vivo* exhausted cells and can be used as a screening tool to identify novel regulators of the exhausted state.

3.3.2 *The exhausted state is epigenetically stable*

Previously we demonstrated that *Tcf7*$^{-}$ cells can reactivate *Tcf7* expression upon stimulation withdrawal both *ex vivo* and *in vivo,* but this flexibility to reactivate *Tcf7*/TCF1 diminishes over time on stimulation in the presence of IL-12 (**Chapter 2; Fig. 2.8**). To determine if this loss of plasticity is also present when cells are activated in the presence of IFN-α, we stimulated cells for 2, 4, or 6 days in the presence of IFN-α, rested the cells without inflammation for 1 day, sorted *Tcf7*-YFP^{-} cells and recultured them without stimulation or inflammation for an additional 7 days (8 days of rest total) (**Fig 3.3A**). We observed, as observed previously with IL-12 (**Chapter 2; Fig. 2.8B**), a decrease in *Tcf7* reactivation potential that was driven by increased duration of stimulation (**Fig. 3.3B-C**).

Next, we sought to determine if this loss in *Tcf7* reactivation potential was dependent on the transition to the *Tcf7*$^{-}$TIM3^{+} T_{EX} state. To do this we chronically stimulated cells for 6 days in the presence of either IL-12 or IFN-α and sorted the *Tcf7*$^{-}$TIM3^{+} T_{EX} cells, along with the *Tcf7*$^{-}$

TIM3$^-$ T_{INT} cells. We observed a significant decrease in *Tcf7* reactivation potential in the T_{EX} cells compared to the T_{INT} cells across both inflammatory contexts (**Fig. 3.3D-E; Fig. 3.4A**), suggesting that the loss of reactivation potential observed over time on stimulation is correlated with the TIM3$^+$ state. This loss in reactivation potential was also preserved over time in the absence of stimulation, suggesting epigenetic stability of the *Tcf7*$^-$ state.

Exhausted cells from tumors and chronic infections are also epigenetically stable, such that treatment with checkpoint blockade does not alter the fixed chromatin state[16]. Rest from TCR stimulation has been suggested to reverse this epigenetic stability in CAR-T cells[25], however the epigenetic stability of the TCF1$^-$ state in tumors has not been explored. To determine if tumor T_{EX} cells are also locked into the TCF1$^-$ state, we adoptively transferred activated *Tcf7*-YFP$^{+/-}$;OT-I$^{+/-}$;CD45.1/.2$^{+/-}$ cells into a transplantable B16-Ova solid tumor model (**Fig. 3.3F**). After 8 days in the tumor environment, we observed distinct *Tcf7*$^-$TIM3$^-$ T_{INT} and *Tcf7*$^-$TIM3$^+$ T_{EX} populations (**Fig. 3.3F; Fig. 3.4B**) in the tumor, and a distinct T_{EX} population in the draining lymph node despite the absence of antigen indicated by lack of PD-1 expression (**Fig. 3.4B**). We sorted the live, CD8$^+$, CD45.1/2$^+$ T_{INT} and T_{EX} cell populations from the tumor and recultured them *ex vivo* in the presence of IL-15, which has been previously demonstrated to promote proliferation and effector function in tumor cells *ex vivo*[17,51]. Similarly to *ex vivo* stimulated cells, we observed a significant reduction in the TCF1 reactivation potential in the tumor T_{EX} cells compared to T_{INT} cells and stability of the *Tcf7*$^-$ state over longer time on rest (**Fig. 3.3G-H**). This indicates a conserved mechanism for stable repression of *Tcf7*/TCF1 in T_{EX} cells differentiated both *in vivo* and *ex vivo.*

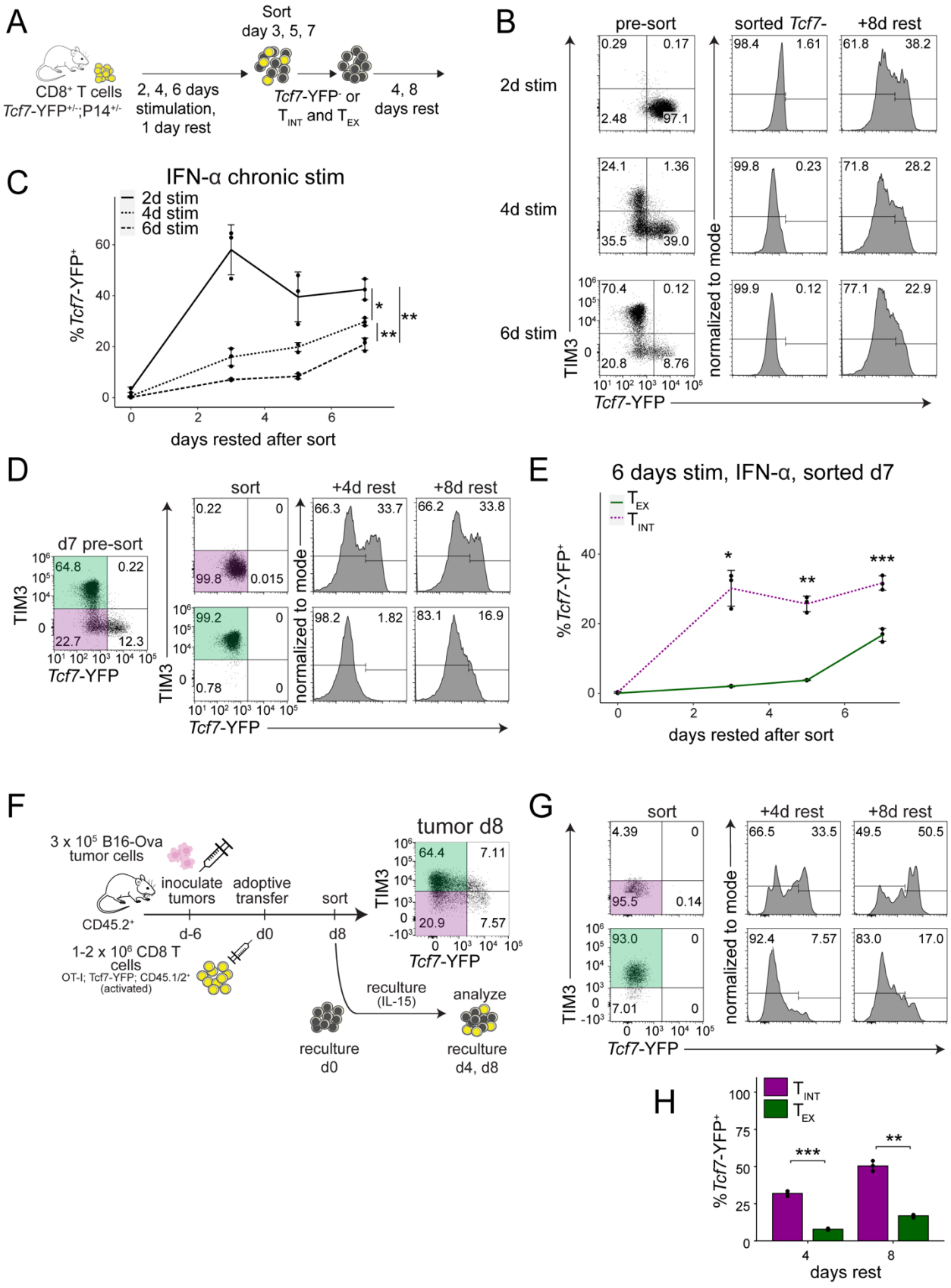
A
Sort
day 3, 5, 7
CD8⁺ T cells
Tcf7-YFP+/-;P14+/-
2, 4, 6 days
stimulation,
1 day rest
Tcf7-YFP- or
T INT and T EX
4, 8
days rest
B
pre-sort
sorted Tcf7-
+8d rest
2d stim
4d stim
6d stim
0.29
0.17
2.48
97.1
98.4
1.61
61.8
38.2
24.1
1.36
35.5
39.0
99.8
0.23
71.8
28.2
70.4
0.12
20.8
8.76
99.9
0.12
77.1
22.9
TIM3
Tcf7-YFP
normalized to mode
C
IFN-α chronic stim
2d stim
4d stim
6d stim
% Tcf7-YFP+
days rested after sort
D
d7 pre-sort
sort
+4d rest
+8d rest
64.8
0.22
22.7
12.3
0.22
0
99.8
0.015
66.3
33.7
66.2
33.8
99.2
0
0.78
0
98.2
1.82
83.1
16.9
TIM3
Tcf7-YFP
normalized to mode
E
6 days stim, IFN-α, sorted d7
T EX
T INT
% Tcf7-YFP+
days rested after sort
F
3 x 10⁵ B16-Ova
tumor cells
CD45.2+
inoculate
tumors
adoptive
transfer
sort
d-6
d0
d8
1-2 x 10⁶ CD8 T
cells
OT-I; Tcf7-YFP; CD45.1/2+
(activated)
tumor d8
64.4
7.11
20.9
7.57
TIM3
Tcf7-YFP
reculture
(IL-15)
analyze
reculture
d0
reculture
d4, d8
G
sort
+4d rest
+8d rest
4.39
0
95.5
0.14
66.5
33.5
49.5
50.5
93.0
0
7.01
0
92.4
7.57
83.0
17.0
TIM3
Tcf7-YFP
normalized to mode
H
T INT
T EX
% Tcf7-YFP+
days rest

Figure 3.3. The exhausted state is epigenetically stable.
(**A**) Schematic for stimulation followed by rest assay. CD8$^+$ T cells were stimulated for 2, 4, or 6 days *ex vivo* in IFN-α rested for 1 day, and then sorted for either total *Tcf7*-YFP$^-$ or Tcf7-YFP$^-$TIM3$^-$ (T_{INT}) or *Tcf7*-YFP$^-$TIM3$^+$ (T_{EX}), and then rested an additional 3 or 7 days (4 and 8 days total rest). (**B**) Representative flow cytometry of *Tcf7*-YFPxTIM3 at each timepoint pre-sort, and *Tcf7*-YFP post sort, and after 8 days of total rest. (**C**) Quantification of *Tcf7*-YFP reactivation over time from (B). (**D**) Representative flow cytometry of *Tcf7*-YFPxTIM3 at day 7 pre-sort and post-sort, and after 4 and 8 days of total rest. (**E**) Quantification of *Tcf7*-YFP reactivation over time from (D). (**F**) Schematic for B16 experiment. CD8$^+$ T cells were activated and adoptively transferred into tumor bearing mice, then harvested and sorted at day 8 post-transfer, then rested in IL-15 for 4 or 8 days. Pre-sort flow profile from day 8 post transfer. (**G**) Representative flow cytometry of *Tcf7*-YFPxTIM3 post sort, and *Tcf7*-YFP histograms at 4 and 8 days of rest. (**H**) Quantification of *Tcf7*-YFP from (G). [B-E] n=3 biological replicates. [C] Mean±SD.T-test performed between sort groups at day 6. [E] Mean±SD. T-test performed between T_{INT} and T_{EX} at each timepoint. [H] n=3 technical replicates from pooled tumors. Mean±SD. T-test performed between T_{INT} and T_{EX} at each timepoint. [C,E,H] *p <0.05, **p<0.01, ***p<0.001, ****p <0.0001.

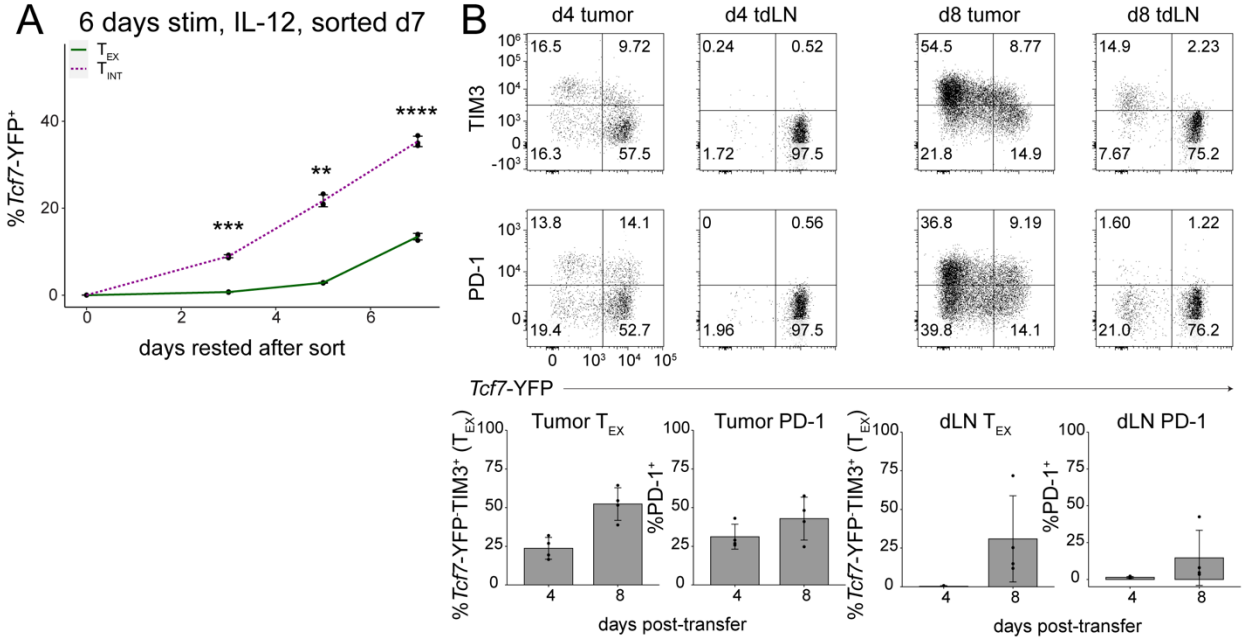

Figure 3.4. The exhausted state is epigenetically stable across stimulation contexts.
(**A**) CD8$^+$ T cells were stimulated 6 days *ex vivo* in IL-12 rested for 1 day, and then sorted for either *Tcf7*-YFP$^-$ TIM3$^-$ (T_{INT}) or *Tcf7*-YFP$^-$TIM3$^+$ (T_{EX}), and then rested an additional 3 or 7 days (4 and 8 days total rest). Corresponds to Fig. 3.2E. (**B**) Top: Representative flow cytometry profiles of day 4 and day 8 post-adoptive transfer tumor and inguinal tumor draining lymph nodes (dLN). (**C**) Quantification of *Tcf7*-YFP$^-$TIM3$^+$ T_{EX} cells and PD-1+ cells from tumors and dLN. [A] n=3 biological replicates. Mean±SD. T-test performed between T_{INT} and T_{EX} at each timepoint. *p <0.05, **p<0.01, ***p<0.001, ****p <0.0001. [B] n=4 biological replicates. Mean±SD.

3.3.3 *CRISPR screen reveals regulators controlling initiation and maintenance of* Tcf7 *silencing*

To investigate how *Tcf7* is regulated initially after T cell activation and how it is stably repressed during exhaustion differentiation, we designed a targeted CRISPR-Cas9 knockout screen and

applied this screen across 7 stimulation contexts (**Fig 3.5A**) using a library of 118 unique genes (**Supplemental Table 5**), consisting of transcription factors associated with $CD8^+$ T cell activation and differentiation as well as epigenetic DNA and histone modifying enzymes. This allowed us to screen both trans– and cis– acting mechanisms for their role in *Tcf7* regulation. We assayed the regulation of initial silencing (S) of *Tcf7* by isolating and activating $CD8^+$ T cells from *Tcf7*$^{+/-}$; P14$^{+/-}$; Cas9$^{+/-}$ mice and transducing in the sgRNA library 1 day after activation and sorting for *Tcf7*-YFP expression at 3 or 4 days of activation. (**Fig. 3.5A**). To determine regulation of maintenance (M) of the *Tcf7* silent state, we transduced in the sgRNA library at day 3 after activation in the IL-12 context, and day 6 of chronic stimulation in both IL-12 and IFN-α contexts. At both maintenance timepoints, we sorted both T_{INT} and T_{EX} cells prior to library transduction and then rested the cells for 6 or 7 days before sorting for *Tcf7*-YFP expression (**Fig. 3.5A**).

Across all 7 screen contexts we observed the expected positive control result that *Tcf7* targeting sgRNAs were enriched in the *Tcf7* low sort bins (**Fig. 3.5B-D**). We additionally observed consistent enrichment across all 7 screens of *Foxo1* and *Myb* in the *Tcf7* low population (**Fig. 3.5B-D**). This is unsurprising given the role both transcription factors play in commitment to the memory fate and counteracting the effector program[52–56]. Consistent with these results, *Foxo1* overexpression is currently under investigation to enhance the memory and self-renewal potential of CAR-T cells[57]. We also observed in all 7 contexts that *Prdm1* (BLIMP1) and *Tbx21* (T-bet) knockout consistently enriched *Tcf7* high cells, indicating that these transcription factors suppress *Tcf7* expression regardless of differentiation stage (**Fig 3.5B-D**). Both of these transcription factors are known to drive effector T cell differentiation and suppression of the

memory program[58–60], and *Prdm1*/BLIMP1 is hypothesized to play a role in exhaustion differentiation[61]. *Prdm1* KO in CAR-T cells has also been shown to promote their persistence[62], consistent with its role in suppressing *Tcf7* expression in our screens. We further validated the role of *Prdm1* KO in increasing *Tcf7* expression using Cas9 RNPs with the top two sgRNA (**Supplemental Table 5**) from the screen both in the initial silencing and maintenance phase (**Fig 3.6A**).

When looking specifically at the initial silencing state across both inflammatory contexts, we observed the involvement of more trans– regulators than cis– regulators. This is perhaps unsurprising as these trans– factors are expressed downstream of T cell activation and would therefore be highly expressed at this stage in our screen. Aside from knockout of *Prdm1* and *Tbx21*, which increased *Tcf7* expression across all screen contexts, we observed that knockout of transcription factor *Runx3* increased *Tcf7* expression only in the initial silencing phase (**Fig. 3.5 B-D**). *Runx3* has been demonstrated to play a significant role in epigenetic remodeling of $CD8^+$ T cells early after activation and promote both memory and effector differentiation[49,63], and its overexpression has been shown to suppress *Tcf7*[49], consistent with our findings. In the IL-12 screen, we saw that *Stat4* KO increased *Tcf7* expression, consistent with the role of IL-12 in promoting *Tcf7* silencing as we and others have previously demonstrated[35] (**Fig. 3.5B, D; Chapter 2**). In the IFN-α screen, we observed the IFN-α receptor, *Infar1,* knockout promoted *Tcf7* expression, indicating that type I IFN inflammation is also playing a direct role in the suppression of *Tcf7*, which we and others have previously demonstrated with IFN-β[35] (**Fig. 3.5B, D; Chapter 2**). Surprisingly, in the initial silencing screen, we did not see that DNA methylation, via *Dnmt1* or *Dnmt3a/b,* was playing a significant role in suppression of *Tcf7*. This

contrasts with the previously demonstrated role for DNMT3a in suppressing memory genes such as *Sell* (CD62L)[22] and previous reports that the *Tcf7* locus is methylated after chronic peptide stimulation *in vitro*[64] and that DNMT inhibition by Decitabine promotes *Tcf7* expression[35]. The lack of a major role for DNA methylation could be a product of our *ex vivo* screening conditions and does not necessarily rule out the possibility of a role for DNA methylation in *Tcf7* suppression early after activation *in vivo.* We also did not see a role for polycomb-mediated suppression of *Tcf7* early after activation but did observe *Hdac1* knockout promoted *Tcf7* expression across both inflammatory contexts (**Fig. 3.5B**). Our results suggest that *Hdac1* expression early after activation may promote the effector program and suppress the memory/self-renewing program, however the role of *Hdac1* in effector $CD8^+$ differentiation has been largely unexplored, with one study demonstrating the necessity for *Hdac1* for the $CD8^+$ T cell effector response to Lymphocytic Choriomeningitis Virus (LCMV)[65].

When we looked specifically at the maintenance of *Tcf7* silencing after 3 (early) and 6 days of stimulation, we saw some specific hits that upregulated *Tcf7* but were either not present in the initial silencing phase, or decreased *Tcf7* expression in the initial phase. Such hits were knockout of the transcription factors *Batf3* and *Foxp1*, which we saw decreased *Tcf7* in the initial silencing phase but increased in all maintenance phase screens (**Fig. 3.5C**). *Batf3* was upregulated in our scRNAseq from the day 6 chronically stimulated exhausted cells, which may explain why it is acting only in the maintenance phase (**Fig. 3.1F-G; Fig. 3.2C**). Additionally, *Batf3* has been shown to be required early after activation for memory formation[66,67], consistent with its role here in suppressing *Tcf7* when knocked out in the initiation phase. *Batf3* overexpression in CAR-T cells countered the exhaustion program *in vitro* and *in vivo* when administered early after

activation[68], consistent with its pro-memory effects, however the role of *Batf3* after exhaustion differentiation has already occurred, and upon rest, is not understood. *Foxp1* has also been demonstrated to have these context-dependent effects; we saw that *Foxp1* knockout early after activation promoted *Tcf7* silencing, consistent with reports that *Foxp1* knockout causes naive cells to differentiate into effector cells without the need for TCR stimulation[69]. The role of *Foxp1* in exhausted cells may be opposite to naive cells, where *Foxp1* knockout has been shown to enhance tumor control[70]. Taken together, our results indicate *Batf3* and *Foxp1* may be promising targets for reversing the epigenetically fixed exhausted state, but only if the intervention occurs after the cells have already become exhausted and not during the initial activation phase.

We found that compared to the initial silencing context, the maintenance screens had enrichment of *Tcf7* expression with knockout of cis– acting factors, in particular components of PRC1, *Ring1* and *Cbx4*, and components of PRC2, *Ezh2* and *Rbbp4*[71] (**Fig. 3.5D; Fig. 3.7A**). Conversely, many BAF complex components had the opposite effect as PRC1 and 2 components, and decreased *Tcf7* in the maintenance phase, and many in the initiation phase as well (**Fig. 3.7A**). It has been speculated that BAF and PRC1/2 have opposing effects[72,73], which is consistent with our observations across screen contexts. However, these results were surprising given a recent study that demonstrated that deletion of BAF complex subunits, particularly *Arid1a*, counteract the epigenetic program of exhaustion and improve T cell persistence[30]. Taken together, our results are consistent with stimulation and differentiation contexts playing a large role in gene regulation and necessitate the validation of genetic targets across multiple phases of exhaustion for use therapeutically.

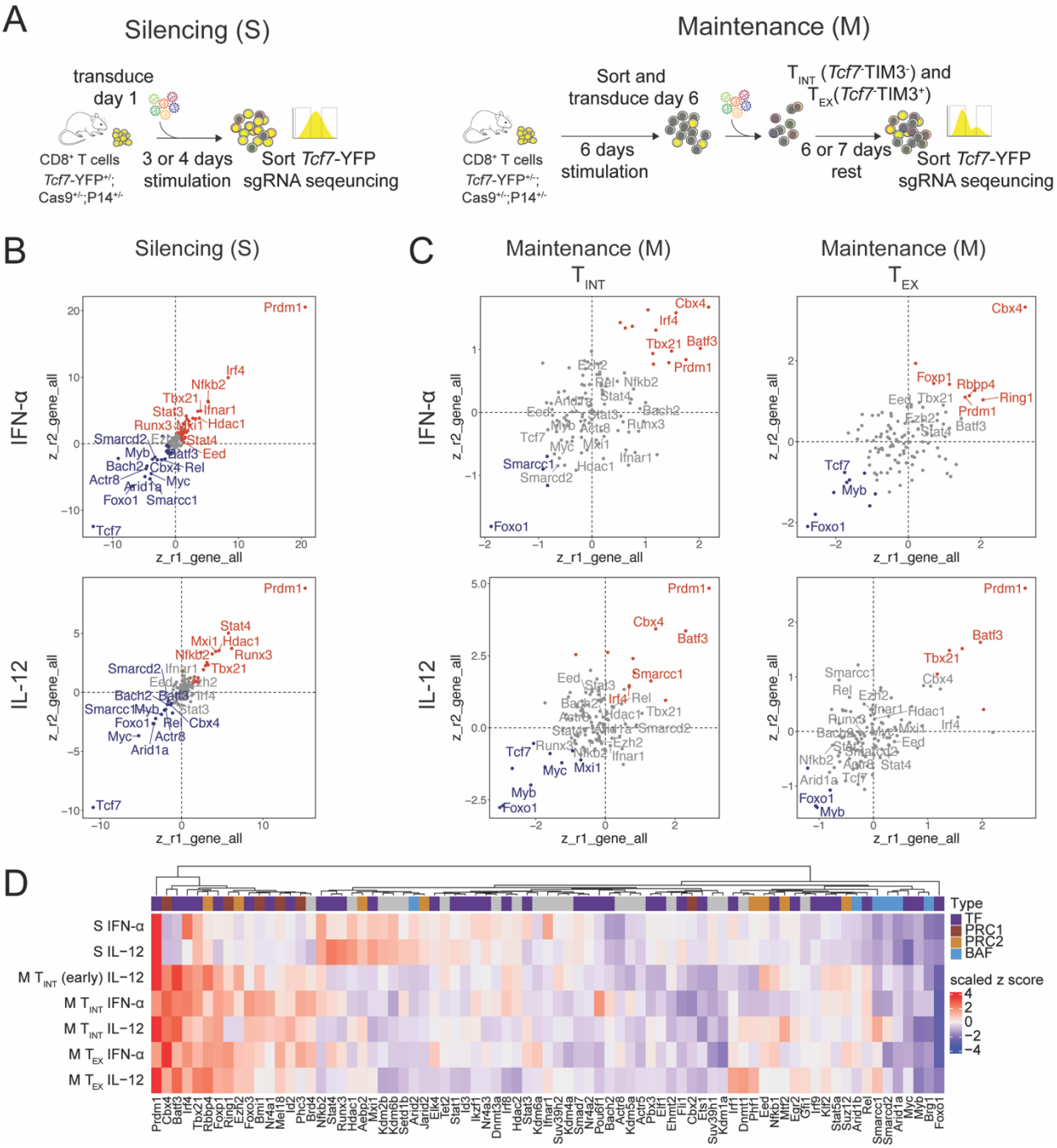

Figure 3.5. CRISPR screen reveals regulation of initiation and maintenance of *Tcf7* silencing.
(**A**) Schematic for silencing and maintenance screens. CD8$^+$ T cells from *Tcf7*-YFP;Cas9;P14 mice were activated *ex vivo* and transduced with sgRNA library at 1 day after activation for silencing (S) screen, kept in stimulation and inflammation, and sorted for *Tcf7*-YFP and sequenced at 3 days after activation for IL-12 or 4 days after activation for IFN-α. For the maintenance (M) screen, T cells were chronically stimulated and then sorted as *Tcf7*$^-$TIM3$^-$ (T_{INT}) or Tcf7$^-$TIM3$^+$ (T_{EX}) and then transduced with sgRNA library and cultured in the absence of stimulation or inflammation for an addition 5 or 6 days, then sorted for *Tcf7*-YFP and sequenced. (**B**) Z-scored log2 fold change (LFC) between replicates for initial silencing screen for IFN-α and IL-12. (**C**) Z-scored log2 fold change (LFC)

between replicates for day 6 maintenance screen for IFN-α and IL-12 T_{INT} and T_{EX}. (**D**) Scaled gene z-scores from all screens colored by sgRNA target type, transcription factor (TF), PRC1, PRC2, and BAF complex.

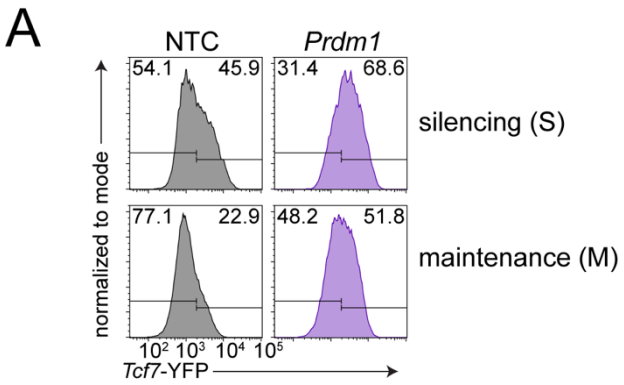

Figure 3.6. *Prdm1* represses *Tcf7* across stimulation contexts.
(**A**) Cells were stimulated with IFN-α as in **Fig 3.5A** and nucleofected with either non-targeting control (NTC) Cas9 RNP or *Prdm1* targeting Cas9 RNP. Cells were stimulated for 1 day before RNP nucleofection for the silencing phase and analyzed at day 6, or 6 days prior to RNP nucleofection for the maintenance phase, rested and analyzed at day 13.

3.3.4 *Polycomb repressive complexes 1 and 2 cooperate to lock down the exhausted state*

From our CRISPR screen we observed enrichment in the maintenance phase for PRC1 and 2, while the early silencing of TCF1 was largely controlled by transcription factors. We compared the hits from the initial silencing phase against the maintenance of the day 6 T_{EX} phase for both IFN-α (**Fig. 3.7A**) and IL-12 (**Fig. 3.8A**). We observed that the PRC1 and PRC2 subunits (displayed in **Fig. 3.7A**) had both concordant (upper right quadrant) and discordant behavior (upper left quadrant) between the two screens. We hypothesized that PRC1 and 2 may be cooperating to lock down the exhausted state after chronic stimulation, while early after stimulation PRC1 and 2 may be repressing the naive and memory program in favor of effector differentiation, as has been previously demonstrated[23,24]. In support of this hypothesis, we observed increased *Ezh2* expression in our scRNAseq with 6 days of chronic stimulation compared to acutely stimulated, rested cells (**Fig. 3.1G**).

To validate the effect of PRC1 and 2 knockout on maintenance of *Tcf7* repression in *Tcf7*$^{-}$ cells after chronic stimulation, we stimulated cells for 6 days in the presence of IFN-α and sorted out total *Tcf7*$^{-}$ (comprised of both T_{INT} and T_{EX} cells) and nucleofected them with Cas9 RNPs, prepared with 2 sgRNA each from the CRISPR screen (**Supplemental Table 5**), targeted toward the PRC2 subunits: *Ezh2* and *Rbbp4* and the PRC1 subunits *Ring1* and *Cbx4*, or 2 validated non-targeting control (NTC) guides from IDT, and rested them for 7 days in the absence of stimulation and inflammation (**Fig. 3.7B**). Consistent with the screen results, all tested PRC1 and 2 knockouts increased TCF1 expression compared to the NTC, while also decreasing TIM3 (**Fig. 3.7B**). This is consistent with the previously described role of PRC2 in restraining TCF1 expression and other pro-memory genes during terminal effector differentiation[24]. *Cbx4* KO had the greatest effect on TCF1 reactivation, consistent with its significant effects in our CRISPR screen (**Fig. 3.5**). CBX4 (Chromobox homolog 4) has been implicated in the terminal differentiation of effector cells during acute infection and restraining of memory cell formation[23]. Additionally, CBX4 is linked to both PRC1 and PRC2, as it is hypothesized that CBX4 can enhance EZH2 methyltransferase activity and increase H3K27me3 deposition[74]. It remains unknown whether PRC1 or PRC2 initiates repression at specific loci, however it is suggested that there may be cooperativity between both polycomb repressive complexes in maintenance of histone modifications across cell divisions[75].

To explore the relationship between PRC1 and PRC2 in T_{EX} cells after 6 days of stimulation in the presence of IFN-α or IL-12, we utilized single and combinatorial small molecule inhibition of EZH2 (1 μM Tazemetostat), RING1 (10 μM PRT4165), and CBX4 (10 μM UNC3866) against a

carrier control (DMSO). We observed that EZH2 inhibition alone increased the *Tcf7*$^{+}$ population upon rest, and the *Tcf7* reactivation potential of T_{EX} cells was further increased with the combination of both PRC1 and PRC2 inhibition (**Fig 3.7 C-D; Fig. 3.8B**). This indicates cooperativity between PRC1 and PRC2 in maintaining the stable *Tcf7* repression seen in T_{EX} cells over long periods of rest regardless of inflammatory context, indicating a conserved mechanism for *Tcf7* repression.

From our CRISPR screen we observed that knockout of PRC1/2 components such as *Cbx4* had opposite effects on *Tcf7* reactivation when the knockout occurred during the initial silencing as opposed to the maintenance phase (**Fig. 3.7A; Fig. 3.8A**). To validate these results, we utilized the same small molecule inhibition of EZH2 but applied the inhibitors 1 day after activation and observed the effects on silencing of *Tcf7* in the presence of IFN-α or IL-12 (**Fig. 3.7E; Fig. 3.8C**). We observed EZH2 inhibition repressed *Tcf7* in both inflammatory contexts compared to the DMSO carrier control. This early repression of *Tcf7* when PRC1/2 are inhibited could be a result of repression of the effector program in naive cells and early after activation by PRC1/2. Transcription factors such as *Prdm1*/BLIMP1, and *Tbx21*/T-bet blocked *Tcf7* expression in the early silencing screen (**Fig. 3.5; Fig. 3.6**) and may be among the effector genes repressed early by PRC1/2. Such models for repression of memory genes by PRC2[24] and DNA methylation[22] have been previously proposed, and early repression of effector genes by PRC1 is currently under investigation[76] and will be a promising avenue for future study.

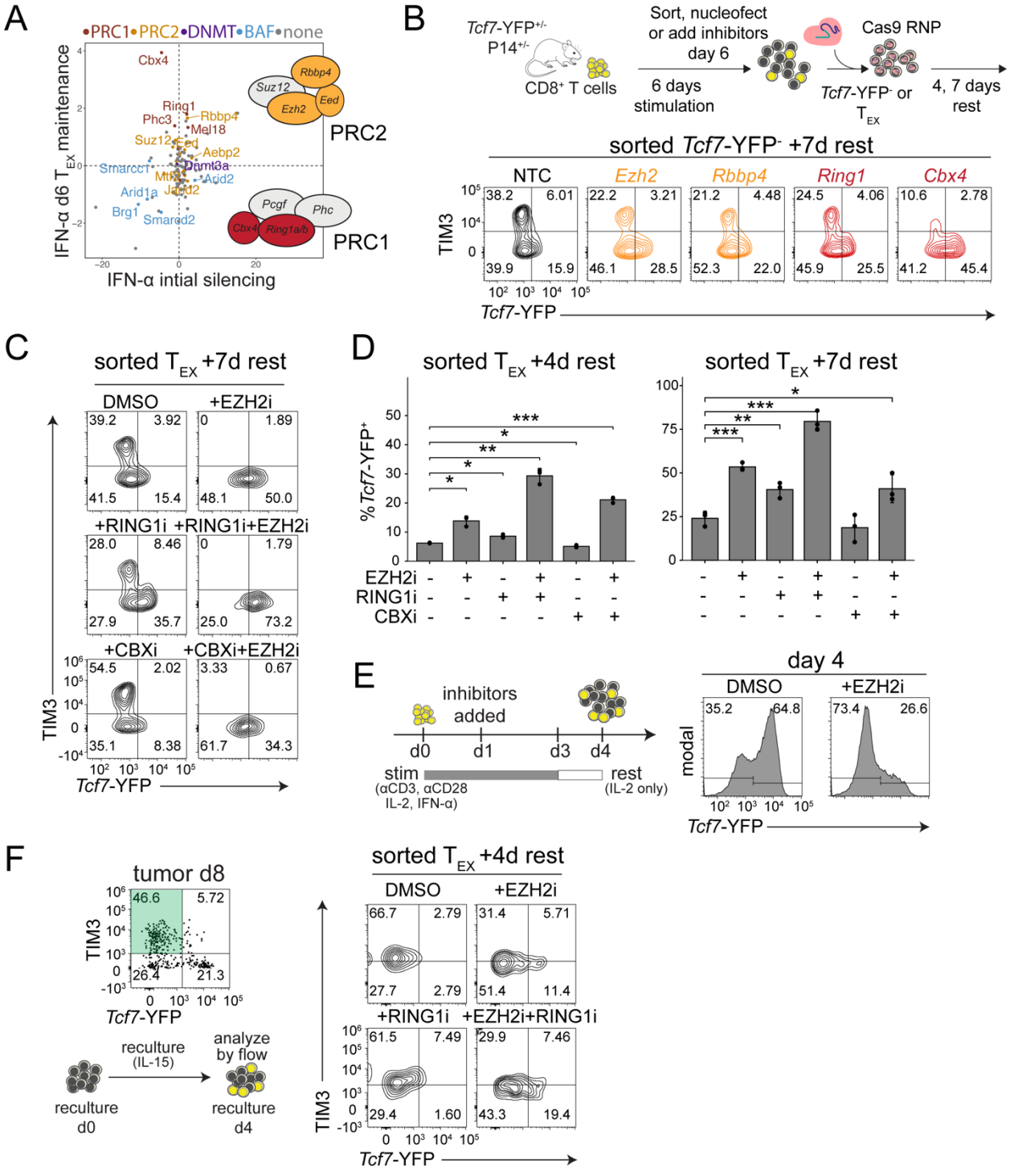

Figure 3.7 PRC1/2 cooperate to lock down the exhausted state ex vivo and in tumors.
(**A**) CRISPR screen identifies PRC1/2 components having context-dependent effects in maintenance and initiation of T_{EX} state in IFN-α screens. (**B**) (top) Timeline for ex vivo validation of PRC1/2 hits in maintenance of T_{EX} using Cas9 RNPs and small molecule inhibitors. Cells were initially stimulated with IFN-α. (bottom) Cas9 KO of select PRC1/2 components increase *Tcf7*-YFP and decrease TIM3. (**C**) Representative flow cytometry plots showing effect of small molecule inhibition of EZH2 (1 μM Tazemetostat), RING1 (10 μM PRT4615), and CBX (10 μM UNC3866) on T_{EX} cells sorted at day 6 after stimulation with IFN-α. (**D**) Quantification of (C) for n=3 technical

replicates. Mean±SD. *p<0.05, **p<0.01, ***p<0.001 for t-test comparison of each group to DMSO control. (**E**) PRC2 inhibition decreases *Tcf7*-YFP during initiation of silencing, (EZH2i = 1 μM Tazemetostat). (**F**) B16 adoptive transfer was performed as in Fig. 3.3. Sorted T_{EX} cells 8 days post-transfer were recultured in IL-15 with the same concentrations of small molecule inhibitors in (C).

Lastly, to determine if PRC1/2 were also contributing to stable repression of TCF1 *in vivo* in solid tumors, we again sorted T_{EX} cells from day 8 post-transfer (as in **Fig. 3.3F-H**) and recultured them in the presence of IL-15 as well as EZH2, RING1 and combination inhibition against a carrier control. Again, we observed stability of *Tcf7* silencing in sorted T_{EX} cells after 4 days of rest, and similarly to our *ex vivo* results, EZH2 inhibition increased the *Tcf7*$^{+}$ population, while RING1 inhibition had no effect on *Tcf7* reactivation. The combination of EZH2 and RING1 inhibition had the greatest effect on *Tcf7* reactivation, consistent with the cooperation of PRC1 and 2 in locking down the exhausted state in tumors (**Fig. 3.7F**).

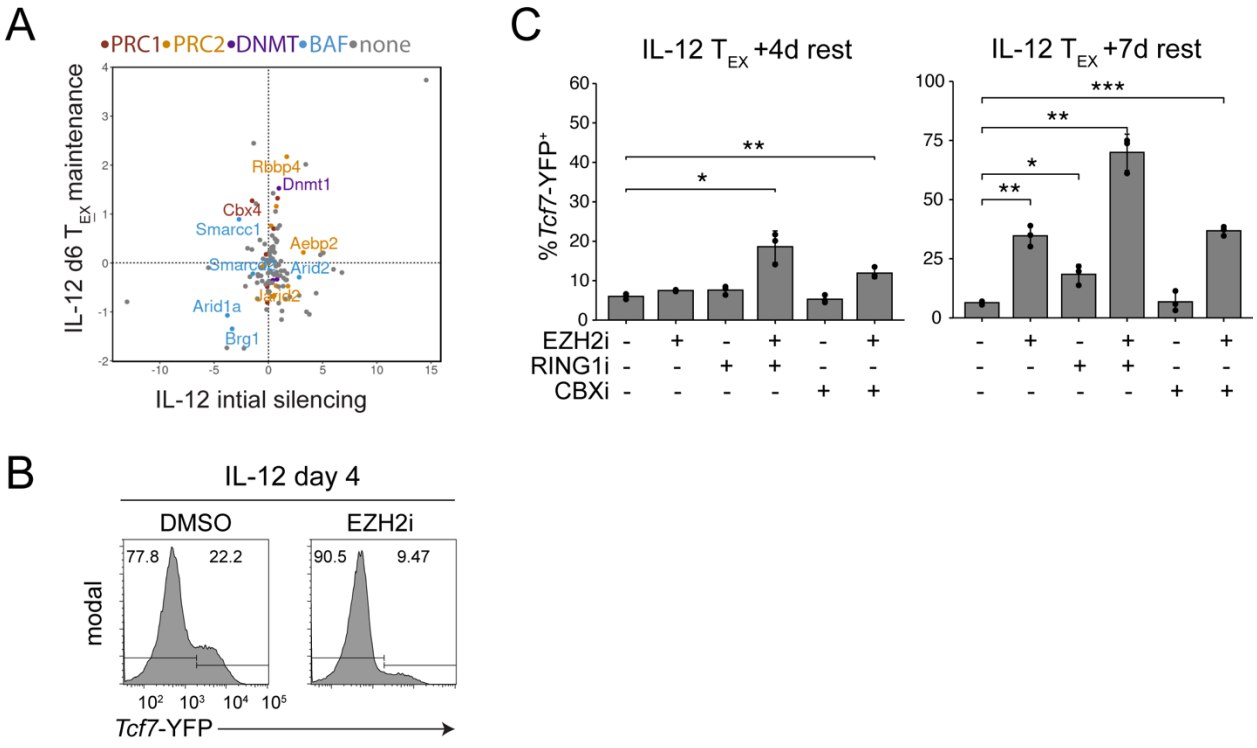

Figure 3.8. PRC1/2 cooperatively lock down exhausted T cells across signaling contexts.
(**A**) Context-dependent effects in maintenance and initiation of T_{EX} state in IL-12 screen. (**B**) Experiment was performed as in Fig. 3.7C-D, in the presence of IL-12 in initial stimulation instead of IFN-α. (**C**) Experiment was performed as in Fig. 3.7E in the presence of IL-12 in initial stimulation instead of IFN-α. [A] n=3 technical replicates. Mean±SD. *p<0.05, **p<0.01, ***p<0.001 for t-test comparison of each group to DMSO control.

3.4 DISCUSSION

In this study, we sought to develop an *ex vivo* screening platform for identifying key regulators of the transition from precursor to exhausted T cells. Our *ex vivo* chronic stimulation assay recapitulated key hallmarks of the exhausted state, including the transition from a $TCF1^+$ precursor state to a $TCF1^-TIM3^+$ exhausted state, and these exhausted cells were epigenetically stable upon stimulation withdrawal, consistent with exhausted cells from tumors[17] and chronic infection[50]. This system allowed us to precisely link the duration of antigen stimulation and inflammatory cytokine signaling with this transition to the exhausted state, which would not have been feasible with *in vivo* systems such as chronic infections or tumor models. This system also allowed us to perform multiple CRISPR-Cas9 screens in parallel to probe the same genetic perturbations in early activated cells, cells that have silenced *Tcf7* but still have self-renewal potential, and cells that have stably entered the exhausted state.

By conducting our screens across all these contexts, we were able to generate a network of transcription factors downstream of TCR signaling that control silencing initiation. We observed some transcription factors such as *Prdm1* and *Tbx21* stably repress *Tcf7* across all screen contexts, though most act only during silencing initiation while TCR stimulation is still present. The transcription factors *Batf3* and *Foxp1*, however, repressed *Tcf7* only in the maintenance screen, and had the opposite effect during silencing initiation. These context dependent results may reconcile opposing studies of these and other transcription factors in T cell differentiation and highlight the importance of conducting screens across multiple signaling contexts, and the necessity of minimal *ex vivo* model systems to aid in such approaches.

Intriguingly, we observed that polycomb repressive complexes act predominantly to stably repress *Tcf7* only after longer durations of stimulation. This is consistent with the proposed paradigm of PRC2 stably repressing pro-memory genes in the process of terminal effector differentiation[24]. Knockout of the PRC1 component *Cbx4* had the greatest effect in our maintenance screen and Cas9 RNP validation, indicating the importance of PRC1 in stable repression of *Tcf7*, consistent with *Cbx4* controlling terminal effector differentiation[23]. However, the cooperative effect we observed between PRC1 and 2 in repressing *Tcf7* has implications for stable repression of genes in other cell types. Indeed, there is evidence of cooperation between PRC1 and 2 in repressing lineage specifying genes and maintaining stemness in mouse embryonic stem (ES) cells[77]. Our findings suggest that for stable repression in the absence of stimulus and across cell divisions, both PRC1 and PRC2 may be necessary. In future studies, it will be exciting to determine the mechanism of interaction between the complexes. Such studies have been performed in *D. Melanogaster* but to our knowledge not in mammalian $CD8^+$ T cells[78].

Increasing $TCF1^+$ cells in the tumor environment is critical for increasing patient responses to immunotherapy and for adoptive cell therapies. The context-dependence of transcription factor hits and PRC2 inhibition, and the necessity of rest for *Tcf7* reactivation indicates that therapeutic targeting of PRC1/2 will require inducible systems for timed intervention to generate $TCF1^+$ cells and combination with either blocking TCR signaling through use of kinase inhibitors, or rest of engineered T cells through inducible TCRs or CARs[25]. Our results lay the groundwork for engineering of such systems and will aid in the design of therapeutic T cells with improved stemness and persistence.

3.5 METHODS

Mice

All mice were used following the guidelines of the University of Washington Institutional Animal Care and Use Committee (approved protocol #4397-01). C57Bl/6J mice (Strain #000664), Cas9 mice (Strain #028239[79]), and P14 mice (Strain #004694[80]) were purchased from the Jackson laboratory. *Tcf7*-YFP mice were donated by Avinash Bhandoola, NIH[36]. OT-I mice were gifted from Michael Gerner UW Immunology.

$CD8^+$ T cell isolation

Spleens were harvested and a single cell suspension of splenocytes was generated by manual dissociation between rough microscope slides and filtered over 50 µm nylon mesh. Red blood cells (RBC) were lysed for 3-5 minutes at room temperature using in house RBC lysis buffer (1 mM EDTA, 10 mM NaHCO3, 150 mM NH4Cl) and quenched with HBH flow buffer (HBSS + 0.5% BSA). Cells were resuspended in Fc blocking buffer (2.4G2 supernatant in HBH) and incubated on ice for 15-30 minutes. $CD8^+$ T cells were isolated by magnetic separation following the manufacturer's instructions with the CD8a+ T cell isolation kit (Miltenyi #130-104-075).

Ex vivo $CD8^+$ T cell differentiation

One day prior to T cell activation, cell culture plates were coated with 1 µg/mL αCD3 (Cytek Clone: 145-2C11) and 0.5 µg/mL αCD28 (Cytek Clone: Clone: 37.51) in PBS and incubated overnight at 4℃. $CD8^+$ T cells were plated in 24 well plates with 0.1-2.5 E6 cells/mL in T cell medium (TCM, RPMI 1640 + L-Glutamine (Gibco), 10% heat inactivated FBS (VWR), 1% Non essential amino acids (Gibco), 1% Sodium Pyruvate (Gibco), 2% 1M HEPES (Gibco), 1% Pen-

Strep-Glutamine (Life Technologies) and 50 μM 2-Mercaptoethanol (BME, Sigma Aldrich)). TCM was supplemented with 100 U/mL recombinant human IL-2 (Peprotech #200-02), and where applicable 1 μg/mL murine IL-12 (Peprotech #210-12), or 1000 U/mL murine IFN-α (Biolegend #752804). On days 2, and 4 of culture, 50% of the cells were harvested for flow cytometry analysis and the remaining 50% was plated into fresh stimulation plates. Cells were incubated at 37°C, 5% CO_2. For resting assays, cells were transferred to non-coated plates and cultured in 100 U/mL IL-2 only unless otherwise noted in the figure caption. Where applicable, cells were stained following the manufacturer's instructions with 5 μm CellTrace Violet (ThermoFisher #C34557).

Flow cytometry, sorting, and intracellular cytokine secretion (ICS)

Cells were incubated in Fc blocking buffer for 10-15 minutes on ice, then stained with extracellular antibodies for 20 minutes on ice and resuspended in HBH buffer. Cells were analyzed on an Attune NxT (Thermofisher), or sorted on a FACS Aria II (BD, UW Genome Sciences) or FACS Aria III (BD, UW Pathology). Data analysis was performed with FlowJo (BD). For ICS, cells were transferred to round bottom 96 well plates and resuspended in TCM containing 1x Cell stimulation cocktail (Thermo/eBioscience #00-4970-93). Cells were incubated at 37°C, 5% CO2 for 1 hour, and then 500x Protein Transport Inhibitor (Thermo/eBioscience #00-4980-93) was added to a final concentration of 1x. Cells were incubated at 37°C, 5% CO2 for an additional 4 hours. Cells were centrifuged at 300g for 5 minutes and resuspended in Fc blocking buffer and incubated for 10-15 minutes on ice, then fixed in 4% paraformaldehyde (Electron Microscopy Sciences) in PBS for 15 minutes on ice. Cells were rinsed 2x and stored in HBH 4°C before processing. Cells were subsequently

permeabilized for 15 minutes in 1x Perm/Wash buffer (BD #554714) on ice. Cells were washed 2x in 1x Perm/Wash buffer, then resuspended in the following antibodies at 1:100 dilution in Perm/Wash buffer: anti-Granzyme B (Pacific Blue, Biolegend #515407), anti-IFN-γ (APC-Cy7, Biolegend #505850), anti-TNF-α (BV711, Biolegend #100759), anti-IL-2 (PE/Dazzle-594, Biolegend #503840), and anti-TOX (PE, Miltenyi #130-120-716).

Small molecule inhibition of PRC1/2

Where applicable, cells were cultured in 1 μM EZH2i Tazemetostat (Selleckchem #S7128), 10 μM RING1i PRT4165 (MedChemExpress #HY-19817), 10 μM CBXi UNC3866 (Selleckchem #S8359), or 0.1% DMSO.

scRNAseq sample preparation

Cells were activated following *ex vivo* differentiation, described above, with the modification of 2 μg/mL αCD3, and 1μg/mL αCD28 co-stimulation (2x). 1E6 cells from each culture condition were resuspended in Fc blocking buffer and stained with 1 uL of hashtag oligo (HTO) antibody or CITE-seq antibody (Biolegend, TotalSeq™B Mouse Hashtag 1-4 #:#:155831, 155833, 155835, 155837, Biolegend TotalSeq™-A0003 anti-mouse CD366 (TIM3) #119729) for 15-30 minutes on ice. Prior to sorting, cells were resuspended in 1:1000 diluted Propodium Iodide (Alfa Aesar Cat #J66584). Cells were counted, then 5,700 cells from each condition were loaded and run through the 10X Genomics platform following the manufacturer's instructions (CG000206 Rev D Chromium Next GEM Single Cell 3′ Reagent Kits v3.1 with Feature Barcoding technology for Cell Surface Protein). Cells were loaded into a single 10X reaction following the hashtag oligo overloading protocol[43]. RNA and HTO Libraries were diluted to 2

nM and loaded onto a NextSeq 550 High Output Kit v2.5 (75 Cycles) (Illumina), using Read 1: 28 cycles, Read 2: 8 cycles, Read 3: 56 cycles. CellRanger (10X Genomics, v6.0.1) was used for transcriptome and HTO reads, cell demultiplexing, and aligning to the GRCm38/mm10 reference genome. We note that a subset of cells that were sequenced were treated with an additional culture condition outside the scope of this study and subsetted out of the analysis.

scRNAseq analysis

scRNAseq analysis was performed using Seurat (v5.0.0) and transferred to Monocle3 (v1.3.4) using SeuratWrappers (v0.3.2). Hashtag demultiplexing was performed following the Demultiplexing with hashtag oligos (HTOs) vignette from Seurat. After assigning conditions, doublets and cells with >20% mitochondrial reads were removed. Clusters were assigned using Seurat FindClusters. Differential expression testing was performed using monocle fit_models. Precursor and exhausted signatures were calculated by downloading Table S3 from Miller *et al.*[5]. Genes with p values > 0.05 and abs(log2 fold change <1.5) were excluded from the analysis. Enrichment scores for gene signatures were calculated using Seurat AddModuleScore.

B16 tumor model

One day prior to tumor transplant, the right flanks of recipient mice ($CD45.2^+$) were shaved for ease of injection. B16-Ova cells were supplied by Ido Amit. 3E5 cells were injected subcutaneously into the right flank of recipient mice subcutaneously. $CD8^+$ T cells were harvested from *Tcf7*-$YFP^{+/-}$;$OT\text{-}I^{+/-}$ ($CD45.1^{+/-}CD45.2^{+/-}$) donor mice and activated with 1 µg/mL αCD3 and 0.5 µg/mL αCD28 and 100 U/mL IL-2 for 24 hours as described above for *ex vivo* T cell differentiation. After 24 hours, cells were transferred to non coated stimulation free plates,

and cultured in 100 U/mL for an additional 48 hours prior to adoptive transfer. 6 days after tumor transplantation, 1-2E6 $CD8^+$ T cells were adoptively transferred via retro-orbital injection to recipient mice. For the experiment in Fig. 3.3 tumor-bearing mice were additionally treated with 150 mg/kg cyclophosphamide (Cytoxan) ~24 hours prior to T cell adoptive transfer. Tumors were harvested, manually dissociated using a razor blade, and digested for 30 minutes in 1 mg/mL type 4 collagenase (Worthington, #LS004188) and 12.5 µg/mL DNase I (Roche #11284932001) in RPMI 1640 (Gibco). Every 10 minutes during the 30-minute digestion, cells were manually dissociated by repeatedly plunging through 1 mL syringes with 18-20g needles. Cells were filtered through 100 µm strainers, centrifuged at 350g for 6 minutes, and resuspended in 3 mL of RBC lysis buffer for 3-5 minutes at room temperature. Cells were quenched with 6 mL of HBH, centrifuged at 350g for 6 minutes and washed with 1x PBS, then stained with 1:1000 of Zombie Aqua (Biolegend #423117) for 15 minutes at room temperature. Cells were Fc blocked for 10-15 minutes on ice, then $CD8^+$ T cells were enriched using the CD8 TIL MicroBeads, mouse kit (Miltenyi #130-116-478) following the manufacturer's instructions. Cells were then stained with anti-CD8a (APC-eFluor780, 1:600, Invitrogen/ThermoFisher #47-0621-82), anti-CD45.1 (PE, 1:400, Biolegend #110707), anti-CD45.2 (BV421, 1:200 Biolegend #109832), and anti-TIM3 (APC, 1:100, Biolegend #119706) for 20 minutes on ice. Tumor T_{INT} and T_{EX} cells were sorted as Live, $CD8^+$, CD45.1/.2 double positive and *Tcf7*-YFP^-TIM3^- (T_{INT}) and *Tcf7*-YFP^-TIM3^+ (T_{EX}). Sorted cells were recultured in 50 ng/mL murine IL-15 (Peprotech #210-15). Where applicable, inguinal lymph nodes from the right side were harvested, manually dissociated over a 100 µm cell strainer, and resuspended for flow cytometry analysis as described above.

sgRNA library design and cloning

The 500 sgRNAs were ordered as a Twist oligo pool with the following design: the 20 nucleotide spacer sequence was flanked on the 5' and 3' ends by gibson overhang sequences for cloning into lentiGuide-puro (Addgene #52963). Additional PCR handles were included for subcloning two separate libraries from the pool, one handle set for all of the sgRNA targeting transcription factors, and one for all of the sgRNA targeting chromatin modifiers. Each sublibrary was PCR amplified using 10 ng input and 12 cycles. Each amplified sublibrary was then further amplified for 6 cycles and cloned into lentiGuide-puro digested with BsmBI using NEBuilder HiFi DNA Assembly (NEB, Cat. 657 No. E2621S). For each sublibrary, a 433 base pair segment from the U6 promoter to the gRNA scaffold was then amplified from the lentiGuide-puro backbone and inserted to a MSCV backbone with an mRuby3 constitutive reporter. For all CRISPR screen experiments, equimolar amounts of the transcription factor and chromatin modifier sublibraries were mixed prior to HEK293T transfections for viral particle generation. All amplifications for cloning were performed using KAPA HiFi polymerase (Roche, #KK2601).

Retrovirus production and transduction

Retroviral particles were produced in 293T cells with the MSCV library and pCL-Eco plasmids using Lipofectamine 3000, with transfection of 293Ts at roughly 90% confluence in 10 cm dishes. Viral supernatant was harvested at 48 hours post-transfection, filtered through a 0.45 μm syringe filter, flash frozen in 1 mL aliquots, and stored at -80°C until use. Titration experiments were performed for transduction of T cells at different stages of differentiation, targeting 10-30% transduction efficiency at each stage. Immediately prior to transduction, supernatant was thawed at 37°C and mixed with TCM for the appropriately titrated supernatant concentration, as well as

polybrene and IL-2 for 6 ug/mL and 100 U/mL respectively in the final mixture of cells and viral particles. The viral supernatant was then added to wells already containing T cells and spun at 2000 g for 60 minutes at 32°C. The media was switched back to TCM between 4 and 24 hours after transduction.

sgRNA library gDNA extraction, amplification, and sequencing

Genomic DNA was extracted from sorted cell pellets by lysis in 50 µL per 100,000 cells of lysis buffer (20 mM Tris, 10 mM EDTA, 0.4 mg/mL Proteinase K), and then cleaned with a 1x ratio of KAPA Pure Beads (Roche, #KK8000). Extracted gDNA was the PCR amplified in two steps using KAPA HiFi polymerase (Roche, #KK2601) to prepare for sequencing. The first PCR added parts of Nextera Read 1 and Truseq Read 2, with one 50 µL PCR reaction performed for DNA from every 100,000 sorted cells. The first PCR reaction was cleaned with a 1.5x bead ratio, and reactions from the same starting sample were pooled before the second PCR, unless intentionally kept separate to assess PCR technical replication. The second PCR completed Nextera Read 1 and Truseq Read 2 and added i5 and i7 indices and P5 and P7 adapters. All PCRs were stopped at low cycle number in the logarithmic phase of amplification to prevent overamplification, which was roughly 21 cycles for the first PCR and 5 cycles for the second PCR. The plasmid library was amplified in the same manner, with the first PCR requiring roughly 12 cycles. After a 1x bead clean following the second PCR, amplicons from all samples were pooled and sequenced on a NextSeq 2000 P1 100 cycle kit with at least 45 cycles on Read 1 and 10 cycles on each index.

sgRNA screening data analysis

Reads for each sgRNA in each sample were counted using a Python script adapted from Joung *et al.*[81] (Joung et al., 2017). Only perfect matches were included in downstream analysis. All subsequent processing was performed in R. For each separate screen, the log2 fold change z-scores between sorted *Tcf7*-YFP high and low bins were calculated as follows. For each sgRNA, the number of reads for that sgRNA was divided by the total sample read count, then multiplied by 1,000,000, and a pseudocount of 1 was added. The log2 was taken to generate a log2 fold change (LFC). To generate z-scores, the mean LFC of the non-targeting control (NTC) sgRNA was subtracted from the sgRNA LFC, and that was then divided by the standard deviation of the NTC LFC. Gene level z-score were calculated as the average of all sgRNA for each gene.

Cas9 RNP preparation and nucleofection

Cas9 RNP preparation and nucleofection protocol was performed as previously described[82]. Briefly, crRNA and tracrRNA were purchased from IDT and resuspended to 100 µM in duplex buffer (IDT). crRNA and tracrRNA were duplexed by mixing equal volumes and incubating at 95°C for 5 minutes. The duplex was allowed to cool to room temperature before preparing RNP. Extra duplex was stored at -20°C for reuse. Cas9 was purchased from ThermoFisher (#A36499) and was mixed with sgRNA duplex at 1.2 µL Cas9: 1.8 µL of sgRNA duplex and was incubated at room temperature for 10-30 minutes. T cells were harvested and centrifuged at 300g for 7 minutes. 0.5E6 $CD8^+$ T cells were used per electroporation reaction and were resuspended in 20 µL of complete P3 Primary Cell buffer prepared as described by the manufacturer's instructions (Lonza #V4XP-3032). 3 µL of each RNP was added to the solution (2 RNPs were used per KO conditions) and transferred to each lane of the Nucleocuvette™. Cells were electroporated using the 4D-Nucleofector™ X (Lonza) using pulse code DN100. After nucleofection, 100 µL of

prewarmed complete TCM was added to each well of the cuvette. The entire volume was then transferred to 24 well culture plates either with or without continued TCR stimulation and inflammation as indicated in the figure caption for each context. crRNA sequences used are listed in **Supplemental Table 5**.

3.6 REFERENCES

1. Gumber, D., and Wang, L.D. (2022). Improving CAR-T immunotherapy: Overcoming the challenges of T cell exhaustion. eBioMedicine *77*. 10.1016/j.ebiom.2022.103941.
2. McLane, L.M., Abdel-Hakeem, M.S., and Wherry, E.J. (2019). CD8 T Cell Exhaustion During Chronic Viral Infection and Cancer. Annual Review of Immunology *37*, 457–495. 10.1146/annurev-immunol-041015-055318.
3. Zehn, D., Thimme, R., Lugli, E., de Almeida, G.P., and Oxenius, A. (2022). 'Stem-like' precursors are the fount to sustain persistent CD8+ T cell responses. Nat Immunol, 1–12. 10.1038/s41590-022-01219-w.
4. Hudson, W.H., Gensheimer, J., Hashimoto, M., Wieland, A., Valanparambil, R.M., Li, P., Lin, J.-X., Konieczny, B.T., Im, S.J., Freeman, G.J., et al. (2019). Proliferating Transitory T Cells with an Effector-like Transcriptional Signature Emerge from PD-1+ Stem-like CD8+ T Cells during Chronic Infection. Immunity *51*, 1043-1058.e4. 10.1016/j.immuni.2019.11.002.
5. Miller, B.C., Sen, D.R., Al Abosy, R., Bi, K., Virkud, Y.V., LaFleur, M.W., Yates, K.B., Lako, A., Felt, K., Naik, G.S., et al. (2019). Subsets of exhausted CD8+ T cells differentially mediate tumor control and respond to checkpoint blockade. Nat Immunol *20*, 326–336. 10.1038/s41590-019-0312-6.
6. Kallies, A., Zehn, D., and Utzschneider, D.T. (2020). Precursor exhausted T cells: key to successful immunotherapy? Nature Reviews Immunology *20*, 128–136. 10.1038/s41577-019-0223-7.
7. Utzschneider, D.T., Gabriel, S.S., Chisanga, D., Gloury, R., Gubser, P.M., Vasanthakumar, A., Shi, W., and Kallies, A. (2020). Early precursor T cells establish and propagate T cell exhaustion in chronic infection. Nat Immunol. 10.1038/s41590-020-0760-z.
8. Im, S.J., Hashimoto, M., Gerner, M.Y., Lee, J., Kissick, H.T., Burger, M.C., Shan, Q., Hale, J.S., Lee, J., Nasti, T.H., et al. (2016). Defining CD8+ T cells that provide the proliferative burst after PD-1 therapy. Nature *537*, 417–421. 10.1038/nature19330.
9. Franco, F., Jaccard, A., Romero, P., Yu, Y.-R., and Ho, P.-C. (2020). Metabolic and epigenetic regulation of T-cell exhaustion. Nat Metab *2*, 1001–1012. 10.1038/s42255-020-00280-9.
10. Scott, A.C., Dündar, F., Zumbo, P., Chandran, S.S., Klebanoff, C.A., Shakiba, M., Trivedi, P., Menocal, L., Appleby, H., Camara, S., et al. (2019). TOX is a critical regulator of tumour-specific T cell differentiation. Nature *571*, 270–274. 10.1038/s41586-019-1324-y.
11. Beltra, J.-C., Manne, S., Abdel-Hakeem, M.S., Kurachi, M., Giles, J.R., Chen, Z., Casella, V., Ngiow, S.F., Khan, O., Huang, Y.J., et al. (2020). Developmental Relationships of Four Exhausted CD8+ T Cell Subsets Reveals Underlying Transcriptional and Epigenetic Landscape Control Mechanisms. Immunity *52*, 825-841.e8. 10.1016/j.immuni.2020.04.014.

12. Khan, O., Giles, J.R., McDonald, S., Manne, S., Ngiow, S.F., Patel, K.P., Werner, M.T., Huang, A.C., Alexander, K.A., Wu, J.E., et al. (2019). TOX transcriptionally and epigenetically programs CD8 + T cell exhaustion. Nature *571*, 211–218. 10.1038/s41586-019-1325-x.
13. Blackburn, S.D., Shin, H., Haining, W.N., Zou, T., Workman, C.J., Polley, A., Betts, M.R., Freeman, G.J., Vignali, D.A.A., and Wherry, E.J. (2009). Coregulation of CD8+ T cell exhaustion by multiple inhibitory receptors during chronic viral infection. Nat Immunol *10*, 29–37. 10.1038/ni.1679.
14. Jubel, J.M., Barbati, Z.R., Burger, C., Wirtz, D.C., and Schildberg, F.A. (2020). The Role of PD-1 in Acute and Chronic Infection. Frontiers in Immunology *11*.
15. Sade-Feldman, M., Yizhak, K., Bjorgaard, S.L., Ray, J.P., de Boer, C.G., Jenkins, R.W., Lieb, D.J., Chen, J.H., Frederick, D.T., Barzily-Rokni, M., et al. (2018). Defining T Cell States Associated with Response to Checkpoint Immunotherapy in Melanoma. Cell *175*, 998-1013.e20. 10.1016/j.cell.2018.10.038.
16. Pauken, K.E., Sammons, M.A., Odorizzi, P.M., Manne, S., Godec, J., Khan, O., Drake, A.M., Chen, Z., Sen, D.R., Kurachi, M., et al. (2016). Epigenetic stability of exhausted T cells limits durability of reinvigoration by PD-1 blockade. Science *354*, 1160–1165. 10.1126/science.aaf2807.
17. Philip, M., Fairchild, L., Sun, L., Horste, E.L., Camara, S., Shakiba, M., Scott, A.C., Viale, A., Lauer, P., Merghoub, T., et al. (2017). Chromatin states define tumor-specific T cell dysfunction and reprogramming. Nature *545*, 452–456. 10.1038/nature22367.
18. Ford, B.R., Vignali, P.D.A., Rittenhouse, N.L., Scharping, N.E., Peralta, R., Lontos, K., Frisch, A.T., Delgoffe, G.M., and Poholek, A.C. (2022). Tumor microenvironmental signals reshape chromatin landscapes to limit the functional potential of exhausted T cells. Science Immunology *7*, eabj9123. 10.1126/sciimmunol.abj9123.
19. Connolly, K.A., Kuchroo, M., Venkat, A., Khatun, A., Wang, J., William, I., Hornick, N.I., Fitzgerald, B.L., Damo, M., Kasmani, M.Y., et al. (2021). A reservoir of stem-like CD8+ T cells in the tumor-draining lymph node preserves the ongoing antitumor immune response. Science Immunology *6*, eabg7836. 10.1126/sciimmunol.abg7836.
20. Li, Z., Tuong, Z.K., Dean, I., Willis, C., Gaspal, F., Fiancette, R., Idris, S., Kennedy, B., Ferdinand, J.R., Peñalver, A., et al. (2022). In vivo labeling reveals continuous trafficking of TCF-1+ T cells between tumor and lymphoid tissue. J Exp Med *219*, e20210749. 10.1084/jem.20210749.
21. Belk, J.A., Daniel, B., and Satpathy, A.T. (2022). Epigenetic regulation of T cell exhaustion. Nat Immunol *23*, 848–860. 10.1038/s41590-022-01224-z.
22. Youngblood, B., Hale, J.S., Kissick, H.T., Ahn, E., Xu, X., Wieland, A., Araki, K., West, E.E., Ghoneim, H.E., Fan, Y., et al. (2017). Effector CD8 T cells dedifferentiate into long-lived memory cells. Nature *552*, 404–409. 10.1038/nature25144.
23. Melo, G.A., Xu, T., Calôba, C., Schutte, A., Passos, T.O., Neto, M.A.N., Brum, G., Oliveira-Vieira, B., Higa, L., Monteiro, F.L.L., et al. (2023). Cutting Edge: Polycomb Repressive Complex 1 Subunit Cbx4 Positively Regulates Effector Responses in CD8 T Cells. The Journal of Immunology, ji2200757. 10.4049/jimmunol.2200757.
24. Gray, S.M., Amezquita, R.A., Guan, T., Kleinstein, S.H., and Kaech, S.M. (2017). Polycomb Repressive Complex 2-Mediated Chromatin Repression Guides Effector CD8+ T Cell Terminal Differentiation and Loss of Multipotency. Immunity *46*, 596–608. 10.1016/j.immuni.2017.03.012.

25. Weber, E.W., Parker, K.R., Sotillo, E., Lynn, R.C., Anbunathan, H., Lattin, J., Good, Z., Belk, J.A., Daniel, B., Klysz, D., et al. (2021). Transient rest restores functionality in exhausted CAR-T cells through epigenetic remodeling. Science *372*. 10.1126/science.aba1786.
26. Angelosanto, J.M., Blackburn, S.D., Crawford, A., and Wherry, E.J. (2012). Progressive Loss of Memory T Cell Potential and Commitment to Exhaustion during Chronic Viral Infection. J Virol *86*, 8161–8170. 10.1128/JVI.00889-12.
27. Richter, K., Brocker, T., and Oxenius, A. (2012). Antigen amount dictates CD8+ T-cell exhaustion during chronic viral infection irrespective of the type of antigen presenting cell. European Journal of Immunology *42*, 2290–2304. 10.1002/eji.201142275.
28. Prokhnevska, N., Cardenas, M.A., Valanparambil, R.M., Sobierajska, E., Barwick, B.G., Jansen, C., Moon, A.R., Gregorova, P., delBalzo, L., Greenwald, R., et al. (2023). CD8+ T cell activation in cancer comprises an initial activation phase in lymph nodes followed by effector differentiation within the tumor. Immunity *56*, 107-124.e5. 10.1016/j.immuni.2022.12.002.
29. Vardhana, S.A., Hwee, M.A., Berisa, M., Wells, D.K., Yost, K.E., King, B., Smith, M., Herrera, P.S., Chang, H.Y., Satpathy, A.T., et al. (2020). Impaired mitochondrial oxidative phosphorylation limits the self-renewal of T cells exposed to persistent antigen. Nat Immunol *21*, 1022–1033. 10.1038/s41590-020-0725-2.
30. Belk, J.A., Yao, W., Ly, N., Freitas, K.A., Chen, Y.-T., Shi, Q., Valencia, A.M., Shifrut, E., Kale, N., Yost, K.E., et al. (2022). Genome-wide CRISPR screens of T cell exhaustion identify chromatin remodeling factors that limit T cell persistence. Cancer Cell *40*, 768-786.e7. 10.1016/j.ccell.2022.06.001.
31. Scharping, N.E., Rivadeneira, D.B., Menk, A.V., Vignali, P.D.A., Ford, B.R., Rittenhouse, N.L., Peralta, R., Wang, Y., Wang, Y., DePeaux, K., et al. (2021). Mitochondrial stress induced by continuous stimulation under hypoxia rapidly drives T cell exhaustion. Nat Immunol *22*, 205–215. 10.1038/s41590-020-00834-9.
32. Curtsinger, J.M., Johnson, C.M., and Mescher, M.F. (2003). CD8 T Cell Clonal Expansion and Development of Effector Function Require Prolonged Exposure to Antigen, Costimulation, and Signal 3 Cytokine. The Journal of Immunology *171*, 5165–5171. 10.4049/jimmunol.171.10.5165.
33. Curtsinger, J.M., and Mescher, M.F. (2010). Inflammatory cytokines as a third signal for T cell activation. Curr Opin Immunol *22*, 333–340. 10.1016/j.coi.2010.02.013.
34. Curtsinger, J.M., Valenzuela, J.O., Agarwal, P., Lins, D., and Mescher, M.F. (2005). Cutting Edge: Type I IFNs Provide a Third Signal to CD8 T Cells to Stimulate Clonal Expansion and Differentiation. The Journal of Immunology *174*, 4465–4469. 10.4049/jimmunol.174.8.4465.
35. Danilo, M., Chennupati, V., Silva, J.G., Siegert, S., and Held, W. (2018). Suppression of Tcf1 by Inflammatory Cytokines Facilitates Effector CD8 T Cell Differentiation. Cell Reports *22*, 2107–2117. 10.1016/j.celrep.2018.01.072.
36. Harly, C., Kenney, D., Ren, G., Lai, B., Raabe, T., Yang, Q., Cam, M.C., Xue, H.-H., Zhao, K., and Bhandoola, A. (2019). The transcription factor TCF-1 enforces commitment to the innate lymphoid cell lineage. Nat Immunol *20*, 1150–1160. 10.1038/s41590-019-0445-7.
37. Wu, T., Ji, Y., Moseman, E.A., Xu, H.C., Manglani, M., Kirby, M., Anderson, S.M., Handon, R., Kenyon, E., Elkahloun, A., et al. (2016). The TCF1-Bcl6 axis counteracts type I interferon to repress exhaustion and maintain T cell stemness. Science Immunology *1*, eaai8593. 10.1126/sciimmunol.aai8593.

38. Gong, W., Donnelly, C.R., Heath, B.R., Bellile, E., Donnelly, L.A., Taner, H.F., Broses, L., Brenner, J.C., Chinn, S.B., Ji, R.-R., et al. (2021). Cancer-specific type-I interferon receptor signaling promotes cancer stemness and effector CD8+ T-cell exhaustion. Oncoimmunology *10*, 1997385. 10.1080/2162402X.2021.1997385.
39. Lukhele, S., Rabbo, D.A., Guo, M., Shen, J., Elsaesser, H.J., Quevedo, R., Carew, M., Gadalla, R., Snell, L.M., Mahesh, L., et al. (2022). The transcription factor IRF2 drives interferon-mediated CD8+ T cell exhaustion to restrict anti-tumor immunity. Immunity *55*, 2369-2385.e10. 10.1016/j.immuni.2022.10.020.
40. Kasmani, M.Y., Zander, R., Chung, H.K., Chen, Y., Khatun, A., Damo, M., Topchyan, P., Johnson, K.E., Levashova, D., Burns, R., et al. (2022). Clonal lineage tracing reveals mechanisms skewing CD8+ T cell fate decisions in chronic infection. Journal of Experimental Medicine *220*, e20220679. 10.1084/jem.20220679.
41. Yao, C., Sun, H.-W., Lacey, N.E., Ji, Y., Moseman, E.A., Shih, H.-Y., Heuston, E.F., Kirby, M., Anderson, S., Cheng, J., et al. (2019). Single-cell RNA-seq reveals TOX as a key regulator of CD8+ T cell persistence in chronic infection. Nat Immunol *20*, 890–901. 10.1038/s41590-019-0403-4.
42. Tucker, C.G., Mitchell, J.S., Martinov, T., Burbach, B.J., Beura, L.K., Wilson, J.C., Dwyer, A.J., Singh, L.M., Mescher, M.F., and Fife, B.T. (2020). Adoptive T-cell therapy with IL-12 pre-conditioned low avidity T-cells prevents exhaustion and results in enhanced T-cell activation, tumor clearance, and decreased risk for autoimmunity. J Immunol *205*, 1449–1460. 10.4049/jimmunol.2000007.
43. Stoeckius, M., Zheng, S., Houck-Loomis, B., Hao, S., Yeung, B.Z., Mauck, W.M., Smibert, P., and Satija, R. (2018). Cell Hashing with barcoded antibodies enables multiplexing and doublet detection for single cell genomics. Genome Biology *19*, 224. 10.1186/s13059-018-1603-1.
44. Hao, Y., Hao, S., Andersen-Nissen, E., Mauck, W.M., Zheng, S., Butler, A., Lee, M.J., Wilk, A.J., Darby, C., Zager, M., et al. (2021). Integrated analysis of multimodal single-cell data. Cell *184*, 3573-3587.e29. 10.1016/j.cell.2021.04.048.
45. Huster, K.M., Busch, V., Schiemann, M., Linkemann, K., Kerksiek, K.M., Wagner, H., and Busch, D.H. (2004). Selective expression of IL-7 receptor on memory T cells identifies early CD40L-dependent generation of distinct CD8+ memory T cell subsets. Proc Natl Acad Sci U S A *101*, 5610–5615. 10.1073/pnas.0308054101.
46. Roychoudhuri, R., Clever, D., Li, P., Wakabayashi, Y., Quinn, K.M., Klebanoff, C.A., Ji, Y., Sukumar, M., Eil, R.L., Yu, Z., et al. (2016). BACH2 regulates CD8+ T cell differentiation by controlling access of AP-1 factors to enhancers. Nat Immunol *17*, 851–860. 10.1038/ni.3441.
47. Singer, M., Wang, C., Cong, L., Marjanovic, N.D., Kowalczyk, M.S., Zhang, H., Nyman, J., Sakuishi, K., Kurtulus, S., Gennert, D., et al. (2016). A distinct gene module for dysfunction uncoupled from activation in tumor-infiltrating T cells. Cell *166*, 1500-1511.e9. 10.1016/j.cell.2016.08.052.
48. Duhen, T., Duhen, R., Montler, R., Moses, J., Moudgil, T., de Miranda, N.F., Goodall, C.P., Blair, T.C., Fox, B.A., McDermott, J.E., et al. (2018). Co-expression of CD39 and CD103 identifies tumor-reactive CD8 T cells in human solid tumors. Nat Commun *9*, 2724. 10.1038/s41467-018-05072-0.
49. Wang, D., Diao, H., Getzler, A.J., Rogal, W., Frederick, M.A., Milner, J., Yu, B., Crotty, S., Goldrath, A.W., and Pipkin, M.E. (2018). The Transcription Factor Runx3 Establishes

Chromatin Accessibility of cis-Regulatory Landscapes that Drive Memory Cytotoxic T Lymphocyte Formation. Immunity *48*, 659-674.e6. 10.1016/j.immuni.2018.03.028.
50. Abdel-Hakeem, M.S., Manne, S., Beltra, J.-C., Stelekati, E., Chen, Z., Nzingha, K., Ali, M.-A., Johnson, J.L., Giles, J.R., Mathew, D., et al. (2021). Epigenetic scarring of exhausted T cells hinders memory differentiation upon eliminating chronic antigenic stimulation. Nat Immunol *22*, 1008–1019. 10.1038/s41590-021-00975-5.
51. Teague, R.M., Sather, B.D., Sacks, J.A., Huang, M.Z., Dossett, M.L., Morimoto, J., Tan, X., Sutton, S.E., Cooke, M.P., Öhlén, C., et al. (2006). Interleukin-15 rescues tolerant CD8+ T cells for use in adoptive immunotherapy of established tumors. Nat Med *12*, 335–341. 10.1038/nm1359.
52. Gautam, S., Fioravanti, J., Zhu, W., Le Gall, J.B., Brohawn, P., Lacey, N.E., Hu, J., Hocker, J.D., Hawk, N.V., Kapoor, V., et al. (2019). The transcription factor c-Myb regulates CD8+ T cell stemness and antitumor immunity. Nat Immunol *20*, 337–349. 10.1038/s41590-018-0311-z.
53. Tsui, C., Kretschmer, L., Rapelius, S., Gabriel, S.S., Chisanga, D., Knöpper, K., Utzschneider, D.T., Nüssing, S., Liao, Y., Mason, T., et al. (2022). MYB orchestrates T cell exhaustion and response to checkpoint inhibition. Nature, 1–7. 10.1038/s41586-022-05105-1.
54. Delpoux, A., Lai, C.-Y., Hedrick, S.M., and Doedens, A.L. (2017). FOXO1 opposition of CD8+ T cell effector programming confers early memory properties and phenotypic diversity. Proceedings of the National Academy of Sciences *114*, E8865–E8874. 10.1073/pnas.1618916114.
55. Delpoux, A., Marcel, N., Hess Michelini, R., Katayama, C.D., Allison, K.A., Glass, C.K., Quiñones-Parra, S.M., Murre, C., Loh, L., Kedzierska, K., et al. (2021). FOXO1 constrains activation and regulates senescence in CD8 T cells. Cell Reports *34*, 108674. 10.1016/j.celrep.2020.108674.
56. Hess Michelini, R., Doedens, A.L., Goldrath, A.W., and Hedrick, S.M. (2013). Differentiation of CD8 memory T cells depends on Foxo1. J Exp Med *210*, 1189–1200. 10.1084/jem.20130392.
57. Doan, A.E., Mueller, K.P., Chen, A., Rouin, G., Daniel, B., Lattin, J., Chen, Y., Mozarsky, B., Markovska, M., Arias-Umana, J., et al. (2023). 247 FOXO1 is a master regulator of CAR T memory programming. In Regular and Young Investigator Award Abstracts (BMJ Publishing Group Ltd), pp. A286–A286. 10.1136/jitc-2023-SITC2023.0247.
58. Rutishauser, R.L., Martins, G.A., Kalachikov, S., Chandele, A., Parish, I.A., Meffre, E., Jacob, J., Calame, K., and Kaech, S.M. (2009). Transcriptional Repressor Blimp-1 Promotes CD8+ T Cell Terminal Differentiation and Represses the Acquisition of Central Memory T Cell Properties. Immunity *31*, 296–308. 10.1016/j.immuni.2009.05.014.
59. Dominguez, C.X., Amezquita, R.A., Guan, T., Marshall, H.D., Joshi, N.S., Kleinstein, S.H., and Kaech, S.M. (2015). The transcription factors ZEB2 and T-bet cooperate to program cytotoxic T cell terminal differentiation in response to LCMV viral infection. Journal of Experimental Medicine *212*, 2041–2056. 10.1084/jem.20150186.
60. Intlekofer, A.M., Takemoto, N., Wherry, E.J., Longworth, S.A., Northrup, J.T., Palanivel, V.R., Mullen, A.C., Gasink, C.R., Kaech, S.M., Miller, J.D., et al. (2005). Effector and memory CD8+ T cell fate coupled by T-bet and eomesodermin. Nat Immunol *6*, 1236–1244. 10.1038/ni1268.

61. Shin, H., Blackburn, S.D., Intlekofer, A.M., Kao, C., Angelosanto, J.M., Reiner, S.L., and Wherry, E.J. (2009). A role for the transcriptional repressor Blimp-1 in CD8(+) T cell exhaustion during chronic viral infection. Immunity *31*, 309–320. 10.1016/j.immuni.2009.06.019.
62. Yoshikawa, T., Wu, Z., Inoue, S., Kasuya, H., Matsushita, H., Takahashi, Y., Kuroda, H., Hosoda, W., Suzuki, S., and Kagoya, Y. (2022). Genetic ablation of PRDM1 in antitumor T cells enhances therapeutic efficacy of adoptive immunotherapy. Blood *139*, 2156–2172. 10.1182/blood.2021012714.
63. Shan, Q., Zeng, Z., Xing, S., Li, F., Hartwig, S.M., Gullicksrud, J.A., Kurup, S.P., Van Braeckel-Budimir, N., Su, Y., Martin, M.D., et al. (2017). Runx3 guards cytotoxic CD8+ effector T cells against deviation towards TFH cell lineage. Nat Immunol *18*, 931–939. 10.1038/ni.3773.
64. Zhao, M., Kiernan, C.H., Stairiker, C.J., Hope, J.L., Leon, L.G., Meurs, M. van, Brouwers-Haspels, I., Boers, R., Boers, J., Gribnau, J., et al. (2020). Rapid in vitro generation of bona fide exhausted CD8+ T cells is accompanied by Tcf7 promotor methylation. PLOS Pathogens *16*, e1008555. 10.1371/journal.ppat.1008555.
65. Pieniawska, M., and Iżykowska, K. (2022). Role of Histone Deacetylases in T-Cell Development and Function. Int J Mol Sci *23*, 7828. 10.3390/ijms23147828.
66. Qiu, Z., Khairallah, C., Romanov, G., and Sheridan, B.S. (2020). Batf3 expression by CD8 T cells critically regulates the development of memory populations. J Immunol *205*, 901–906. 10.4049/jimmunol.2000228.
67. Ataide, M.A., Komander, K., Knöpper, K., Peters, A.E., Wu, H., Eickhoff, S., Gogishvili, T., Weber, J., Grafen, A., Kallies, A., et al. (2020). BATF3 programs CD8+ T cell memory. Nat Immunol *21*, 1397–1407. 10.1038/s41590-020-0786-2.
68. McCutcheon, S.R., Swartz, A.M., Brown, M.C., Barrera, A., McRoberts Amador, C., Siklenka, K., Humayun, L., ter Weele, M.A., Isaacs, J.M., Reddy, T.E., et al. (2023). Transcriptional and epigenetic regulators of human CD8+ T cell function identified through orthogonal CRISPR screens. Nat Genet, 1–13. 10.1038/s41588-023-01554-0.
69. Feng, X., Wang, H., Takata, H., Day, T.J., Willen, J., and Hu, H. (2011). Transcription factor Foxp1 exerts essential cell-intrinsic regulation of the quiescence of naive T cells. Nat Immunol *12*, 544–550. 10.1038/ni.2034.
70. Stephen, T.L., Rutkowski, M.R., Allegrezza, M.J., Perales-Puchalt, A., Tesone, A.J., Svoronos, N., Nguyen, J.M., Sarmin, F., Borowsky, M.E., Tchou, J., et al. (2014). TRANSFORMING GROWTH FACTOR-BETA MEDIATED SUPPRESSION OF ANTI-TUMOR T CELLS REQUIRES FOXP1 TRANSCRIPTION FACTOR EXPRESSION. Immunity *41*, 427–439. 10.1016/j.immuni.2014.08.012.
71. Blackledge, N.P., and Klose, R.J. (2021). The molecular principles of gene regulation by Polycomb repressive complexes. Nat Rev Mol Cell Biol *22*, 815–833. 10.1038/s41580-021-00398-y.
72. Alfert, A., Moreno, N., and Kerl, K. (2019). The BAF complex in development and disease. Epigenetics & Chromatin *12*, 19. 10.1186/s13072-019-0264-y.
73. Ho, L., Miller, E.L., Ronan, J.L., Ho, W.Q., Jothi, R., and Crabtree, G.R. (2011). esBAF facilitates pluripotency by conditioning the genome for LIF/STAT3 signalling and by regulating polycomb function. Nat Cell Biol *13*, 903–913. 10.1038/ncb2285.

74. Wu, L., Pan, T., Zhou, M., Chen, T., Wu, S., Lv, X., Liu, J., Yu, F., Guan, Y., Liu, B., et al. (2022). CBX4 contributes to HIV-1 latency by forming phase-separated nuclear bodies and SUMOylating EZH2. EMBO Rep *23*, e53855. 10.15252/embr.202153855.
75. Flury, V., Reverón-Gómez, N., Alcaraz, N., Stewart-Morgan, K.R., Wenger, A., Klose, R.J., and Groth, A. (2023). Recycling of modified H2A-H2B provides short-term memory of chromatin states. Cell *186*, 1050-1065.e19. 10.1016/j.cell.2023.01.007.
76. Turner, S.J., Udupa, V., Bruer, T., Sng, X., O'Hara, J., Barugahare, A., Bennett, T., Zhang, Z., Degli-Esposti, M., and Russ, B. (2023). BMI-1 repression of the CD8 +T cell effector program is essential for memory formation. The Journal of Immunology *210*, 83.03. 10.4049/jimmunol.210.Supp.83.03.
77. Zepeda-Martinez, J.A., Pribitzer, C., Wang, J., Bsteh, D., Golumbeanu, S., Zhao, Q., Burkard, T.R., Reichholf, B., Rhie, S.K., Jude, J., et al. (2020). Parallel PRC2/cPRC1 and vPRC1 pathways silence lineage-specific genes and maintain self-renewal in mouse embryonic stem cells. Sci Adv *6*, eaax5692. 10.1126/sciadv.aax5692.
78. Kahn, T.G., Dorafshan, E., Schultheis, D., Zare, A., Stenberg, P., Reim, I., Pirrotta, V., and Schwartz, Y.B. (2016). Interdependence of PRC1 and PRC2 for recruitment to Polycomb Response Elements. Nucleic Acids Res *44*, 10132–10149. 10.1093/nar/gkw701.
79. Chiou, S.-H., Winters, I.P., Wang, J., Naranjo, S., Dudgeon, C., Tamburini, F.B., Brady, J.J., Yang, D., Grüner, B.M., Chuang, C.-H., et al. (2015). Pancreatic cancer modeling using retrograde viral vector delivery and in vivo CRISPR/Cas9-mediated somatic genome editing. Genes Dev *29*, 1576–1585. 10.1101/gad.264861.115.
80. Pircher, H., Bürki, K., Lang, R., Hengartner, H., and Zinkernagel, R.M. (1989). Tolerance induction in double specific T-cell receptor transgenic mice varies with antigen. Nature *342*, 559–561. 10.1038/342559a0.
81. Joung, J., Konermann, S., Gootenberg, J.S., Abudayyeh, O.O., Platt, R.J., Brigham, M.D., Sanjana, N.E., and Zhang, F. (2017). Genome-scale CRISPR-Cas9 Knockout and Transcriptional Activation Screening. Nat Protoc *12*, 828–863. 10.1038/nprot.2017.016.
82. Pfenninger, P., Yerly, L., and Abe, J. (2022). Naïve Primary Mouse CD8+ T Cells Retain In Vivo Immune Responsiveness After Electroporation-Based CRISPR/Cas9 Genetic Engineering. Frontiers in Immunology *13*.

Chapter 4. DEVELOPING TOOLS FOR MULTIPLEXED SCREENING OF CYTOKINE EFFECTS ON CD8$^+$ T CELL DIFFERENTIATION

Chapter 4 was adapted with modifications from the following manuscript in preparation at the time of writing:

A multimodal atlas of cytokine effects derived from multiplexed cell barcoding reveals principles of T cell programming. (2024, in preparation). Sriram Pendyala*, **Elisa Clark***, Matthew J. Wither, Kathleen Abadie, Arjun Kumar, Mitchell Kluesner, Shivani Srivastava, Hao Yuan Kueh#, Douglas M. Fowler#

*co-first authors, #co-corresponding authors

4.1 ABSTRACT

Living cells must sense diverse environmental signals and translate them to cell state changes and functional responses. A key challenge in linking extracellular signals to responses is disentangling the complexity of signaling environments *in vivo*. Reductionist, *ex vivo* systems have allowed for controlled profiling of functional and transcriptomic effects of individual stimuli, however these models lack the ability to profile the full range of environmental signals in a high throughput manner. Immune cells face unique signaling challenges due to their ability to patrol through multiple organ systems and persist over long timescales of immune challenges and beyond as memory cells. Cytokines are the main mode of communication between immune cells and are among the key signals that drive their differentiation and function. In this study, we investigated the effects of cytokine signals on T cell transcriptional and functional responses across a variety of T cell signaling contexts. To do so, we developed a cell barcoding workflow, we call CellCode, to genetically tag live CD8$^+$ T cell clones during the course of *ex vivo* activation in order to record signaling environments and perturbations in a massively-paralleled

format. Following expansion, we pooled T cells from the multiplexed conditions, sequenced their transcriptomes, and subjected these pools to functional assays. Using CellCode, we profiled T cell transcriptional responses to 28 cytokines across a range of concentrations and evaluated the functional implications of their transcriptional effects on long term survival in *in vitro* functional assays.

4.2 INTRODUCTION

Cells divide and change their function in response to external cues. Immune cells must coordinate action in a large range of environments, against a diverse range of threats, and over timescales of response to pathogens ranging from days to years. Immune cells respond to cell-surface signals and soluble signals called cytokines secreted by other cells. The variability of these signals over space and time serves to organize the immune response by generating large populations of cells with heterogeneous functions. $CD8^+$ T cells are a component of the adaptive response to infections and tumors that receive activation signals through their T cell receptor (TCR, signal 1), co-stimulatory or inhibitory receptors (signal 2), and cytokine receptors (signal 3)[1]. As a response to these three classes of signals, they undergo expansion and diversification in transcriptional state and function.

In conjunction with stimulation context, cytokines drive $CD8^+$ fate choice and are necessary for functional responses. For example, high levels of interleukin (IL)-2 and presence of inflammatory cytokines like IL-12 produced by bacterial infection and type I interferon (IFN-I) produced by viral infection are necessary for priming effector T cells[2–4]. However, the role of specific individual cytokines on $CD8^+$ T cells, in conjunction with signals 1 and 2, is difficult to disentangle *in vivo* due to the complexity of the signaling environment. As a result, many

cytokines have been reported to have opposing effects on T cell differentiation depending on signaling context. For example, the common γ-chain (γc) cytokine IL-21[5] has been demonstrated to both promote long-lived memory cells *in vivo*[6] and naive-like stem cell memory cells (T_{SCM}) *ex vivo*[7–9], but also to increase effector differentiation *in vivo*[10,11].

Such context dependent effects necessitate comprehensive mapping between signaling environments, transcriptomic state, and functional outcomes for $CD8^+$ T cells. *In vivo* experiments provide snapshot characterizations of T cells at various stages of the immune response but do not connect state or function to external signals. Much of the known effects of cytokines on T cells are derived from mouse knockouts of receptor components or ligands, or *in vivo* administration of cytokines, however such techniques are low throughput. A recent study probed the transcriptomic effects of cytokines *in vivo* in a high throughput manner[12], however their study still cannot disentangle stimulation context, combinatorial effects of signals, or distinguish between signals that act directly on a cell type of interest and signals that act through an intermediate cell type. Higher throughput screening technologies, such as Perturb-seq[13] can increase throughput of *in vivo* receptor knockout studies and can be utilized directly for $CD8^+$ T cells by adoptive transfer, however they still lack the ability to link cytokine function to combinatorial external stimuli such as Signal 1 and 2, or convey information about the dose of the cytokine. *Ex vivo* systems provide a solution by enabling the reduction of transcriptomic state and cellular function to the direct influence of cell-extrinsic signals and have been demonstrated to recapitulate transcriptomic, epigenetic, functional and phenotypic properties of *in vivo* generated T cells[14–17], however we are still lacking the necessary technology to link particular combinations of signals to transcriptomes and function at a clonal level.

In this study we developed CellCode, a novel method that tags individual T cell clones prior to culturing in highly multiplexed signaling environments, followed by pooling and subjecting cells to common functional *ex vivo* secondary challenges. We applied this method to generate an atlas of $CD8^+$ T cell transcriptional states resulting from 28 cytokines across different stimulation and co-stimulation environments, and linked transcriptomic data to functional outcomes, including growth and persistence in secondary challenge, and regulation of the gene *Tcf7*, encoding for T cell factor 1 (TCF1), a marker of memory potential. Our atlas can provide insight for opposing effects of cytokines dependent on stimulation context and provides a reference of $CD8^+$ T cell states that may inform rational therapeutic design.

4.3 RESULTS

4.3.1 *CellCode: a novel barcoding strategy for recording perturbations in live cells*

To track the effects of external perturbations in live cells, we needed to develop a method, which we call CellCode, for labeling cells with a unique DNA barcode that can be sequenced in both separate and pooled assays. To generate our CellCode barcode library, we used Golden-Gate cloning to insert a 25-nucleotide barcode downstream of a minimal U6 promoter in a gamma retroviral MSCV backbone. A nuclear localized mRuby3 fluorescent protein allows for detection of the barcode library after transduction. We additionally added the 10X Genomics capture sequence 1 (CS1) downstream of the minimal U6 to enable barcode in RNA when performing single cell RNA sequencing (scRNAseq) with the 10X Genomics platform (**Fig. 4.1A**). We generated the full CellCode library by combining 12 separate plasmid sublibraries for a total of more than 10^8 unique barcodes.

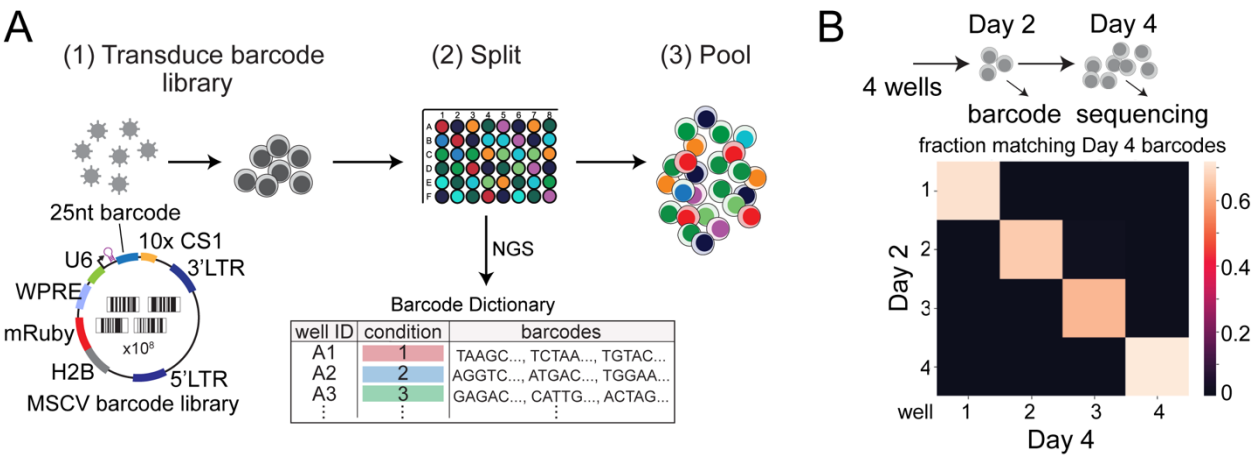

Figure 4.1. CellCode: a novel viral barcoding method for tracking external perturbations in live cells. (**A**) CellCode workflow: cells are transduced with barcode library and split into different culture conditions, and then then be pooled for downstream assays. (**B**) Validation of CellCode in P2C2 cells demonstrates >70% mapping of cells on day 4 back to their original well on day 2.

We tested the ability of CellCode to label cells in different cell culture wells (and thereby different culture conditions/perturbations), by infecting a murine lymphocyte cell line (P2C2) with the barcode library and splitting the cells into 4 wells. After 2 days of culture, we sampled 75% and froze the samples for sequencing, and then sampled the remainder of the cells 2 days later (day 4 of culture) and sequenced the barcodes from both time points using next generation sequencing (**Fig. 4.1B**). We were able map more than 70% of the barcodes sequenced on day 4 to the same well as day 2, with barcode misassignment rates under 2% (**Fig. 4.1B**). This indicates that CellCode can be used to map a large portion of cells back to the correct culture wells with a low error rate, validating its use for screening *ex vivo* cell culture conditions and their effects on downstream transcriptomic state and function.

4.3.2 *Transcriptomic changes downstream of cytokines are dependent on stimulation context*

After validating the efficacy of CellCode for tracking cells in different culture conditions, we wanted to expand its use to probe the effects of cytokines on $CD8^+$ T cell differentiation states. T

cells sense cytokine signals and translate them to changes in cell state through secondary messengers that phosphorylate transcription factors and drive changes in gene expression. We therefore sought to comprehensively profile the transcriptomes of $CD8^+$ T cells responding to cytokines. An advantage of using CellCode *ex vivo* is not only the ability to control cytokine dosage, which would not be possible with cytokine receptor knockout studies, but also the ability to control the combination of signal 1, 2, and 3.

We first needed to determine which cytokines could be sensed by early activated T cells *ex vivo*. We compiled the gene expression data from Immgen Skyline for $CD8^+$ T cells responding to Listeria Monocytogenes and Lymphocytic choriomeningitis (LCMV) at early time points (**Fig. 4.2**). From these receptor expression profiles, we selected 28 cytokines (**Table 4.1**) to test in combination with IL-2 (null condition) which is necessary for *ex vivo* T cell assays. For 10 of the 28 cytokines, we selected 3 doses ranging from 0.1-100 ng/mL, and for all other cytokines we tested a single dose of either 10 or 100 ng/mL (**Table 4.1**). We tested each cytokine against 4 combinations of signals, 1, 2, and 3, which we call base conditions: no TCR stimulation or co-stimulation (Rest), TCR stimulation only (αCD3), TCR stimulation+co-stimulation (αCD3/28), and TCR stimulation+co-stimulation+IL-12 inflammation (αCD3/28+IL-12 (1 ng/mL IL-12)). We chose these base conditions to mimic the type of priming a $CD8^+$ T cell may receive *in vivo* after initial activation. After selection of cytokines and base conditions, we performed the final transcriptomic screen across 192 base condition x cytokine combinations in duplicate or triplicate.

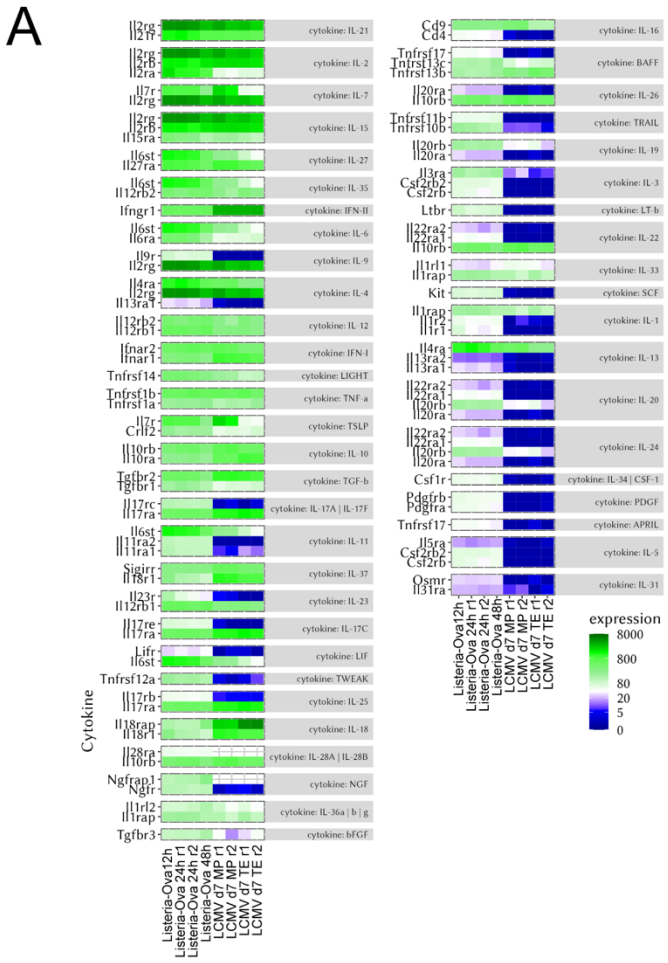

Figure 4.2. Cytokine receptor expression in CD8$^+$ T cells responding to acute infections.
(**A**) Heatmap of cytokine receptor expression in CD8$^+$ T cells from ImmGen Skyline for acute infections with Listeria (12-48 hours post infection, spleen) and LCMV (d7 memory precursor (MP) and effector (TE) states, spleen).

To transduce in the CellCode library, we activated CD8$^+$ T cells from donor mice heterozygous for a YFP reporter for *Tcf7*[18] (see **Chapters 2 and 3**) for ~22 hours in IL-2 (see **4.5 Methods**) and then infected them with the CellCode library and split them into primary perturbations consisting of combinations of cytokine and base conditions. We chose this timeline because with these activation conditions the cells will make their first division by around 30 hours[19] (**Chapter 2, Fig. 2.5**), and it is essential that the cells have not divided prior to labeling with the barcode library such that each clone is labeled with a unique barcode to pass on to its progeny. The

donors used were also heterozygous for the P14 transgenic TCR to ensure a monoclonal starting population. We sampled 50% of the cells at day 2.5 of culture and sequenced the barcodes to generate a barcode-condition map for referencing in pooled assays and continued the culture until day 4. On day 4, we counted the cells from one replicate of each condition, pooled the cells based on count, then sorted live, mRuby^{+} (barcoded cells) and performed scRNAseq with the 10X Genomics platform (**Fig. 4.3A**).

After filtering out low quality cells and aligning over reactions, we plotted the transcriptomes of 67,292 cells in uniform manifold approximation and projection (UMAP) space. We plotted all the cells in the UMAP, not just those that could be assigned back to an initial condition based on their barcode, to determine the overall transcriptomic states in different regions of the UMAP and to see how cytokines pushed cells to various cell states (**Fig. 4.3B**). Cells broadly separated in UMAP space by base condition, the exception being the overlap of cells treated with and without co-stimulation, which clustered together. Rested cells formed their own subcluster but were more closely related to cells stimulated without inflammation (**Fig. 4.3B**, left side) than those treated with inflammation (**Fig. 4.3B**, right side). There were 2 areas of the UMAP that had large overlap between base conditions (**Fig. 4.3**, bottom left hand side, adjacent to rest, and top right hand side, forming a small cluster).

We then sought to determine the cell states represented by these regions of the UMAP. To do this, we utilized community detection based[20] unbiased clustering in Monocle3[21–23] to generate 27 clusters (**Fig. 4.3C**). We next determined the top marker genes for each cluster and used these to define cell states in various regions of the UMAP. By plotting the expression of some of these

key marker genes, we were able to categorize the UMAP regions into broad T cell states. The clusters on the left hand side of the UMAP displayed hallmarks of various memory T cell states, including expression of *Sell*[24,25] (CD62L), *Eomes*[26,27], *Klf2*[28], *Id3*[29], *Bach2*[30], and *Ccr7*[31] (**Fig. 4.3D**). These memory markers were spread across different areas of the UMAP, suggestive of heterogeneity within these memory-like states. Within this memory-like region, cluster 23, which was a combination of all 4 base conditions (**Fig. 4.3D**) had a resident memory-like phenotype, with expression of the cell surface receptor *Itgae*[32] (CD103) and the transcription factor *Runx3*[33].

On the right hand side of the UMAP, which was primarily the IL-12-treated base condition, we observed expression patterns consistent with effector $CD8^+$ T cell states, including expression of the transcription factors *Tbx21*[34] (T-bet), *Zeb2*[34], *Runx3*[35], *Prdm1*[36] (BLIMP1), and the IL-2 receptor alpha, *Il2ra*, which is also more highly expressed in effector-like cells[37] (**Fig. 4.3D**). We also observed increased markers of effector and cytotoxic function in the top portion of the UMAP in the IL-12 treated base, in the same region where effector transcription factors (TFs) were enriched, including *Tnf*, *Ifng*, and *Gzmb*. In the bottom right hand side of the UMAP, we observed higher expression of markers of T cell dysfunction, including *Batf3* (**Chapter 3**), *Mt1*[38], and *Tox*[39–41]. We also observed anticorrelation between *Tbx21* and *Tox*, consistent with the recent finding that the effector and exhausted lineages are controlled by these TFs in a mutually exclusive manner[42]. Lastly, we observed a small cluster at the top, right hand side of the UMAP (cluster 16) that was separated from the other cells, and had high expression of *Gata3*, consistent with a type 2 effector (Tc2) state[43–45].

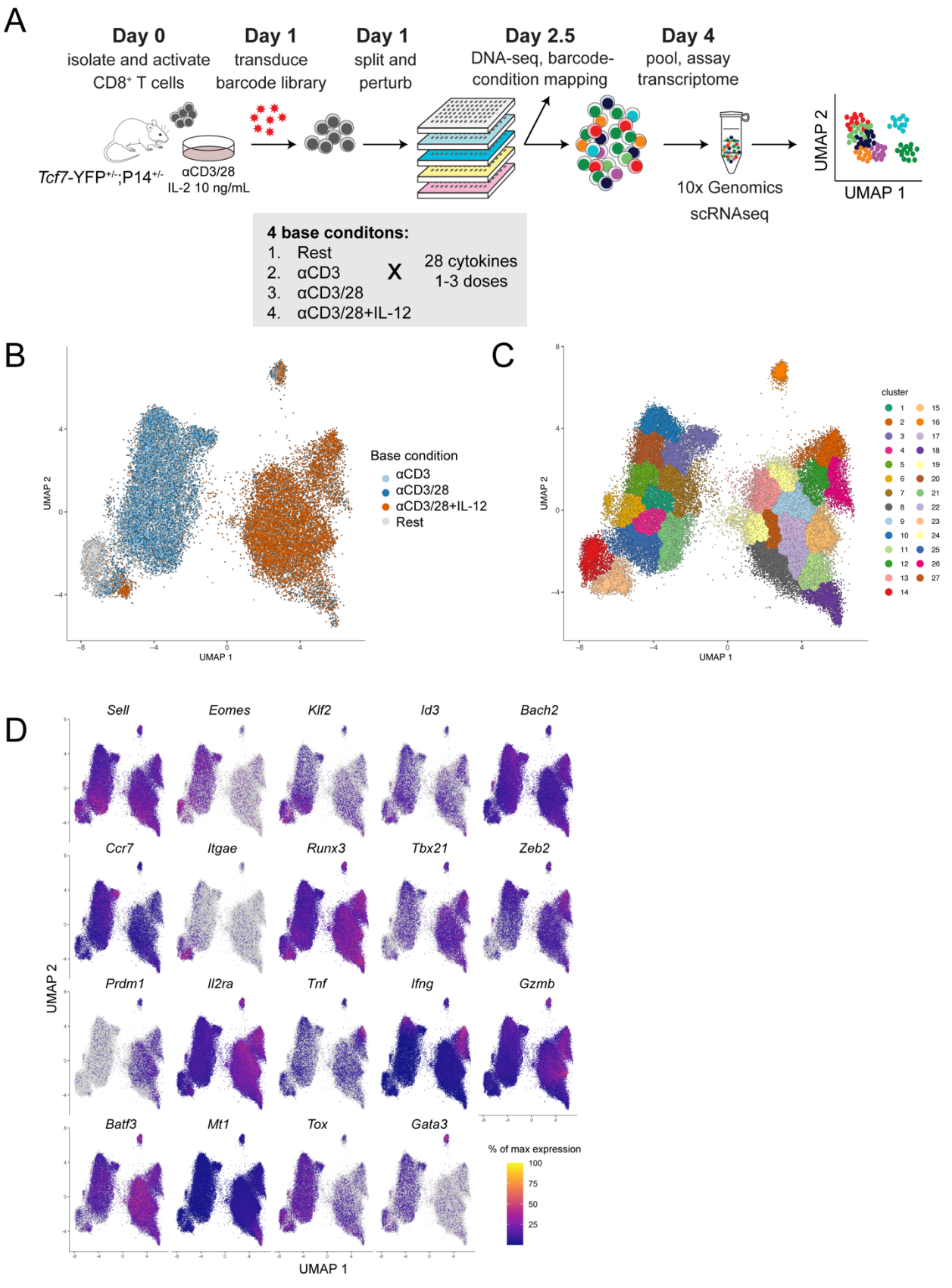
A
Day 0
isolate and activate CD8+ T cells
Day 1
transduce barcode library
Day 1
split and perturb
Day 2.5
DNA-seq, barcode-condition mapping
Day 4
pool, assay transcriptome
Tcf7-YFP+/-;P14+/-
αCD3/28
IL-2 10 ng/mL
10x Genomics
scRNAseq
UMAP 2
UMAP 1
4 base conditons:
1. Rest
2. αCD3
3. αCD3/28
4. αCD3/28+IL-12
X
28 cytokines
1-3 doses
B
Base condition
αCD3
αCD3/28
αCD3/28+IL-12
Rest
C
cluster
D
Sell
Eomes
Klf2
Id3
Bach2
Ccr7
Itgae
Runx3
Tbx21
Zeb2
Prdm1
Il2ra
Tnf
Ifng
Gzmb
Batf3
Mt1
Tox
Gata3
% of max expression
100
75
50
25

Figure 4.3. Cytokines drive transcriptomic state changes dependent on TCR signaling context.
(**A**) Overview of $CD8^+$ T cell activation and transduction with CellCode library prior to 10X scRNAseq. (**B**) UMAP of all cells colored by base condition. (**C**) UMAP of cells colored by clusters generated by Monocle3. (**D**) Expression of memory, effector, and dysfunctional states on UMAP. Color scale indicates percentage of maximum expression.

We assigned all the cell states above without defining which cytokines these cells were treated with, and we therefore wanted to ask which cytokines pushed cells toward which clusters/areas of the UMAP. We plotted the percentage of cells from each cytokine x base condition treatment in each cluster of the UMAP (**Fig. 4.4A**). From this we observed that a few cytokines pushed cells to unique clusters regardless of base condition: TGF-β enriched cluster 23, and IL-4 enriched cluster 16, in every base except for the rest base condition. Some cytokines enriched specific clusters only in certain base condition signaling contexts: IFN-α promoted cluster 25 in the rest base condition, cluster 6 with stimulation, and cluster 8 in the αCD3/28+IL-12 base, while IL-18 pushed cells to clusters 3 and 7 with stimulation, and to cluster 8 in the αCD3/28+IL-12 base. IL-12 pushed cells to clusters 11 and 18 in both the αCD3 and αCD3/28 contexts, which could indicate that the presence of chronic inflammation pushes cells toward dysfunctional states. Most cytokines had the same effects that became more pronounced at higher concentrations, however IL-21 had unique effects at the highest dose compared to the lower concentrations. This difference in the effect of IL-21 could be due to competition with IL-2 for the shared γc receptor at lower concentrations.

We observed that many of the other cytokines had convergent or subtle effects on the transcriptome, and that transcriptomic state is largely driven by the base condition. This could be due to lack of cytokine signaling due to downregulation of the receptors over time in culture, or due to lack of saturation at the tested concentrations, or the combination of each cytokine with IL-2 as mentioned for IL-21. A key feature and technological advance of CellCode that differs

from traditional high throughput genomic methods like hashing[46] or combinatorial indexing[47] is the ability to label live cells in culture instead of at the endpoint, which enables tracking over time in culture or functional assays in pooled format. To disentangle whether these cytokines with small effects on the transcriptome were having effects on the function of the cells, we sought to perform pooled, secondary assays in combination with our transcriptomic atlas.

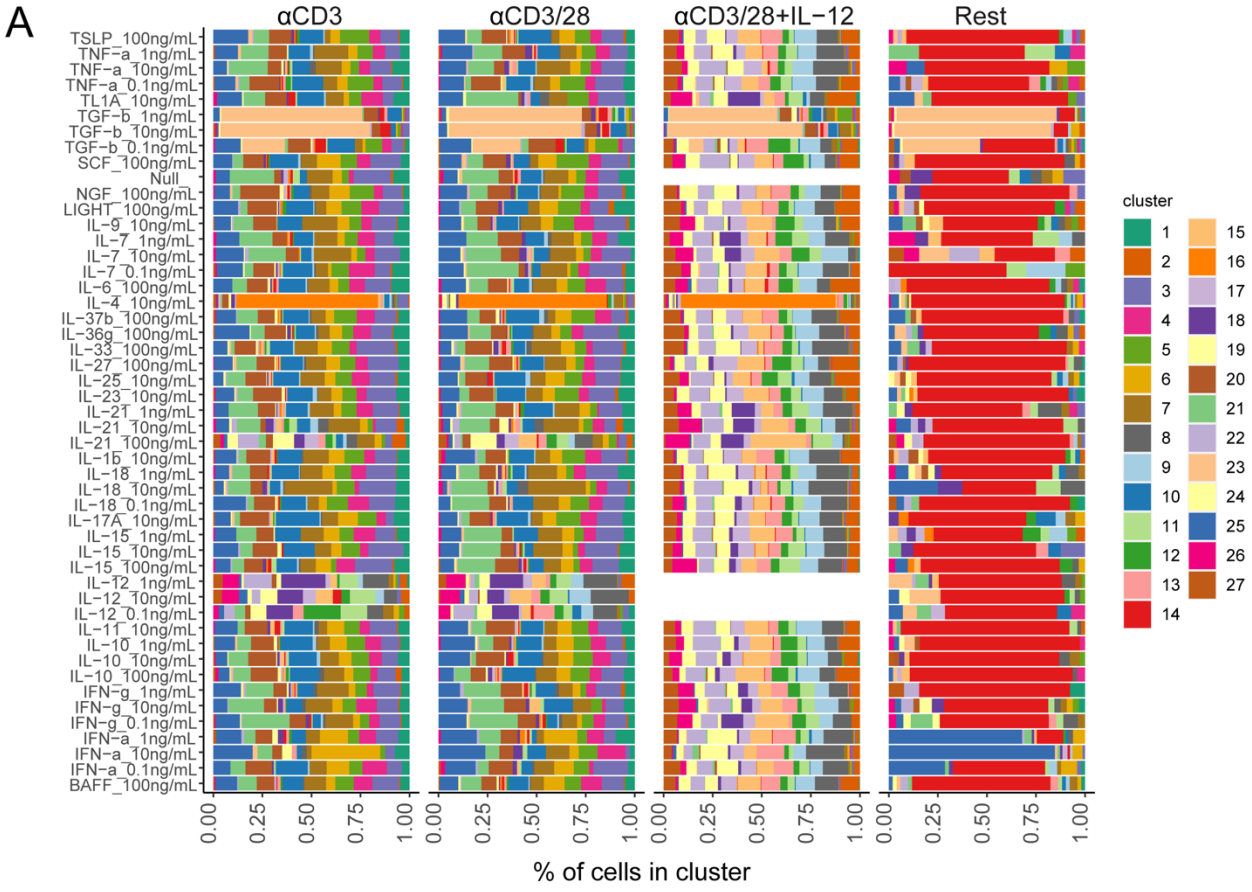

Figure 4.4. Cytokine treatments push cells to specific clusters.
(**A**) Percentage of cells from each condition that are found in each cluster of the UMAP, separated by base condition. Null for αCD3/28+IL-12 base is the 1 ng/mL IL-12 in the αCD3/28 base.

4.3.3 *CellCode uncovers context-dependent cytokine regulation of* Tcf7

To validate the use of CellCode for such pooled phenotyping assays, and to gain insight into the functional state of the T cells, we performed Sort-seq on the expression of the *Tcf7*-YFP

reporter[48]. *Tcf7* encodes for the transcription factor TCF1, which is expressed in naive, memory, and precursor exhausted cells, and is essential for their persistence and stem-like function[49]. We binned cells into quartiles based on *Tcf7* expression and sequenced the barcodes enriched in each quartile (**Fig. 4.5A**). This allowed us to calculate the fraction of cells from a given condition in each quartile expression bin, and a weighted average of the *Tcf7*-YFP expression for each condition[48].

IL-12 and other inflammatory cytokines such as IFN-β are known to silence *Tcf7* in conjunction with TCR stimulation[50], however the effects of other cytokines directly *Tcf7*/TCF1 have been largely unexplored. We first looked at the impact of cytokines on *Tcf7* expression separately by base condition (**Fig. 4.5B**). First, looking only at αCD3 stimulation vs αCD28 co-stimulation, we can see that cytokines largely have the same effects across these two base conditions. This suggests that the addition of co-stimulation is not having strong effects on *Tcf7* compared to stimulation alone, consistent with what we observed in the transcriptomics. This does not rule out the possibility that co-stimulation can have a large effect on T cell state. The lack of differences here on *Tcf7* could be in part because all cells were initially primed with co-stimulation for 1 day prior to CellCode library transduction, or that the stimulation to co-stimulation ratio used was 2:1.

We observed as expected that IFN-α and IL-12 silenced *Tcf7* and did so in a dose-dependent manner. We observed surprisingly that IL-4 had strong silencing effects similar in magnitude to IL-12, and that TGF-β also had moderate suppression of *Tcf7*. The common γc cytokines IL-7 and IL-15 had small effects on silencing *Tcf7* at high doses, while most other cytokines had little

to no effect on *Tcf7* at the doses that we tested in this study. Conversely, we observed IL-18 and IL-21 increased average expression of *Tcf7* in a dose-dependent manner. The effect of IL-21 on increasing *Tcf7* expression was surprising given that IL-21 is known to promote effector differentiation[10], and that IL-21 treated cells had shared transcriptomic profiles with those treated with IL-12, which would coincide with silencing of *Tcf7.* However, when we looked specifically at enrichment of cells in each quartile (**Fig. 4.5C**), we observed that IL-21 was causing a strong polarization to either quartile 1 (lowest *Tcf7*), or quartile 4 (highest *Tcf7*). Intriguingly, IL-21 was the only cytokine tested to have this strong bimodal effect on *Tcf7*, and this could in part explain its seemingly opposite effects on memory and effector differentiation in different studies[5]. The effect of IL-18 on increasing *Tcf7* was also surprising given that IL-18 has been classified as a proinflammatory cytokine[51]. A recent study demonstrated that IL-18 receptor knockout decreases exhaustion phenotypes in $CD8^+$ T cells[52]. While exhausted cells do not express *Tcf7*, they are derived from *Tcf7* high progenitor cells and differentiate in a TCF1-dependent manner[53], which could, in part, explain this finding.

We have recently demonstrated that rest from TCR stimulation promotes high levels of *Tcf7* through survival of starting *Tcf7* high cells as well as reactivation of *Tcf7* low cells (**Chapter 2**). Consistent with this hypothesis, we observed an increase in the weighted average *Tcf7* expression for the null distribution upon rest (**Fig. 4.5B**). Similarly to with TCR stimulation and co-stimulation, IL-12, IFN-α, IL-4 and TGF-β decreased *Tcf7* in the resting base condition, while IL-18 and IL-21 increased average *Tcf7*. IL-7 displayed dose-dependent moderate silencing of *Tcf7* with stimulation and stimulation+co-stimulation, however it increased *Tcf7* in a dose-dependent manner upon rest. This may be expected due to the increased IL-7 receptor alpha

(CD127) expression in memory T cells[54], which may allow for outcompeting of IL-7 for the common γc in these cells compared to stimulated cells. We saw that IL-15 at the highest dose, 100 ng/mL, reduced *Tcf7*. IL-15 contributes to the longevity and maintenance of homeostatic proliferation of TCF1^{+} memory cells, therefore we expected that it would increase *Tcf7* upon rest in a similar manner to IL-7. However, this decrease in *Tcf7* could be consistent with the necessity of IL-15 for the proliferation and rapid effector differentiation of memory cells to effector cells[55,56].

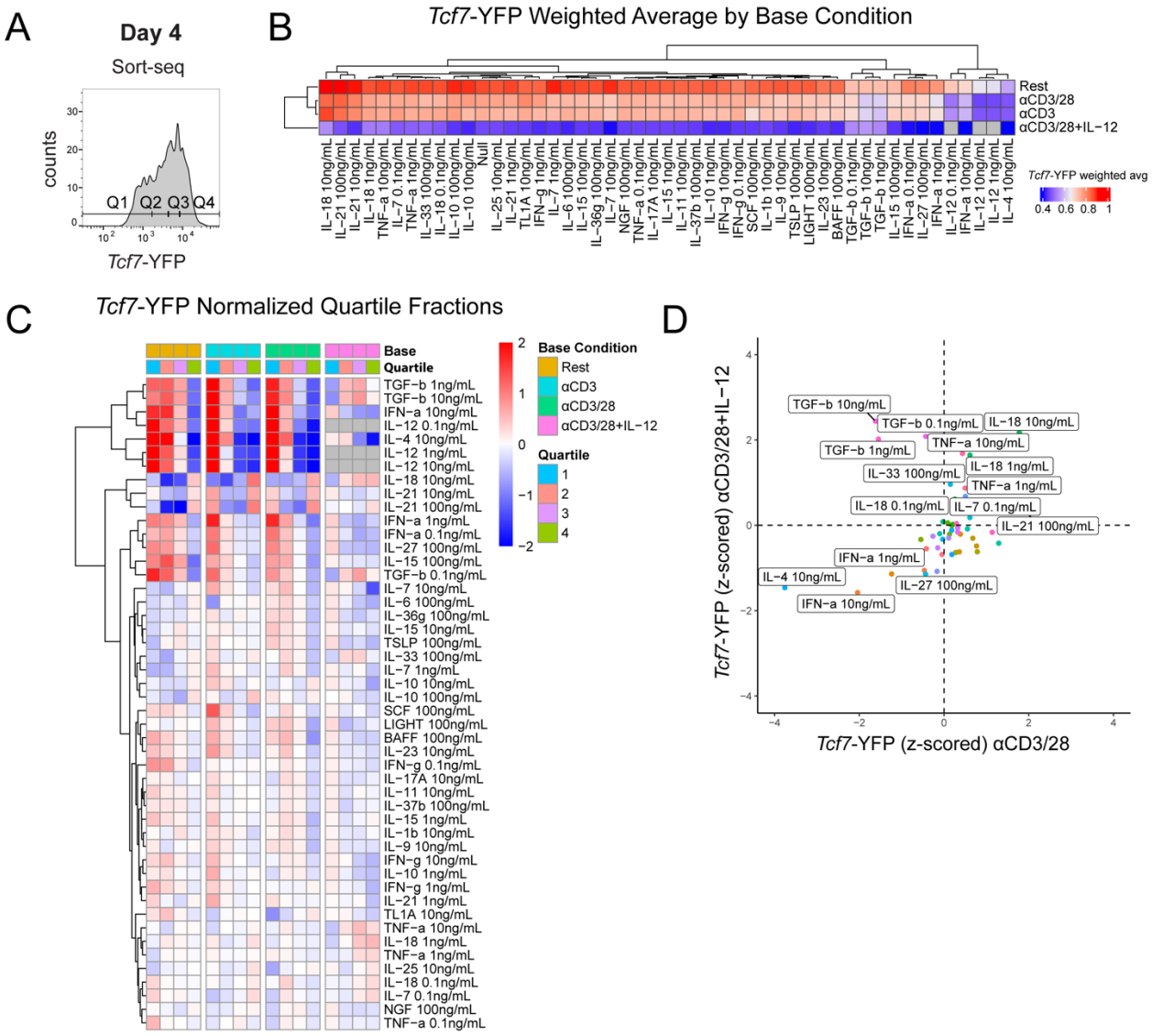

Figure 4.5. Cytokines differentially regulate *Tcf7* expression in a context-dependent manner.
(**A**) Overview for experiment. Cells from the pool at day 4 (see Fig. 4.3A) were sorted into quartile bins based on *Tcf7*-YFP expression. (**B**) Heatmap of weighted average of *Tcf7*-YFP for every cytokine x base condition treatment. (**C**) Fractions of cells from each cytokine x base condition in each quartile bin were calculated, normalized to the null condition from the base condition, and log2 transformed. (**D**) 2D plot of z-scored weighted averages for the *Tcf7*-YFP levels for each cytokine treatment in the αCD3/28 (x axis) and αCD3/28+IL-12 base conditions.

Lastly, we looked at the effects of cytokines in the inflammatory base condition with IL-12 (**Fig. 4.5B**). As expected, based on the effects of IL-12 alone, the average *Tcf7* expression for all cytokine conditions was reduced with IL-12. Combining IFN-α and IL-4 further reduced *Tcf7*, which was unsurprising given their strong silencing effects across the other base conditions. IL-18 also increased *Tcf7* in this context and was the only cytokine that uniformly increased *Tcf7* compared to null across all base conditions. While IL-21 increased average *Tcf7* expression on stimulation without inflammation, it did not strongly increase *Tcf7* when combined with inflammation, even at the highest dose. Surprisingly, TGF-β yielded the highest *Tcf7* levels aside from IL-18 in combination with inflammation, despite its effects on reducing *Tcf7* in the 3 other signaling contexts. TGF-β has been shown to have similar context dependent effects on $TCF1^+$ in chronic LCMV infection: it can increase the proportion of $TCF1^+$ precursor cells, but also decreases the function and speeds exhaustion differentiation in cells that have already silenced TCF1[57,58]. The direct effects of TGF-β on counteracting inflammation in $CD8^+$ T cells have not been demonstrated to our knowledge. TNF-α also showed a moderate increase on *Tcf7* in conjunction with inflammation, though its effects were less pronounced than TGF-β and not opposite the other stimulation contexts. By visualizing in 2 dimensions the mean, z-scored, weighted average of each treatment for both the IL-12 and stimulation+co-stimulation contexts, we can clearly see this context-dependent effect of TGF-β at all 3 doses (**Fig. 4.5D**). We also observed that IL-33 was pushing off of the diagonal toward the upper left hand quadrant, suggesting that IL-33 may increase *Tcf7* more with inflammation than without, and indeed IL-33

has been recently demonstrated to counteract IFN-driven inflammation in chronic infection and promote the formation of TCF1$^+$ cells[59].

4.3.4 *Cytokines have distinct, context-dependent effects on cell proliferation and survival in secondary challenge*

In both CD4$^+$ and CD8$^+$ T cells, expression of *Tcf7* is often correlated with persistence[49], however we sought to utilize the advantage that CellCode can track live cells in pooled culture to uncover the effects of cytokines on growth and persistence of CD8$^+$ T cells in response to *ex vivo* secondary challenges. We designed 3 secondary challenge contexts: (1) no TCR stimulation, with low (10 U/mL) IL-2 and additional IL-7 (5 ng/mL) and IL-15 (50 ng/mL), (2) continued TCR stimulation (αCD3 only), and (3) continued TCR stimulation with αCD28 co-stimulation and IL-12 (1 ng/mL). These *ex vivo* culture conditions were designed to minimally mimic various *in vivo* signaling environments that the cell could experience, for example condition (1) was designed to mimic clearance of an acute threat, (2) to mimic persistent antigen such as in the tumor environment and (3) to mimic ongoing bacterial infection. To assay growth and persistence in these secondary challenges, we pooled the cells at day 4 after the primary cytokine x base condition perturbations, plated them into each secondary challenge condition, and sequenced 50% of the cells, representative of the surviving barcodes (clones) at day 6, 9, 13, and 17 of culture (**Fig. 4.6A**).

From the barcode sequencing data, we were able to ask the following question: how did initial stimulation conditions, priming by both cytokines and base condition, impact cell growth (clonal expansion) in each secondary rechallenge environment (1-3)? We defined growth as the log2 fold change of total reads that mapped to a particular condition at each timepoint. First, we

looked at the growth of cells separately in each primary base condition x secondary challenge combination (**Fig. 4.6B**). Looking just in secondary condition (1) (**Fig. 4.6B**, top row), we observed that initial cytokine priming without stimulation (rest base) did not lead to proliferation or survival of cells. On the other hand, priming with stimulation improved growth with some conditions: the pro-inflammatory cytokines IL-12, IL-18, IL-21, IL-33, and IL-4, but impaired growth with TGF-β, which is typically immunosuppressive. Consistent with this observation, most cytokines performed better in the αCD3/28+IL-12 base, except for IFN-α. Intriguingly, when combined with inflammation, IL-18 and IL-33 were the best performing cytokines, and TGF-β also performed well despite cell death in the other conditions without inflammation. This could be due to the increases in *Tcf7* for these 3 cytokines in combination with IL-12 (**Fig. 4.6B**), and the previously known roles of IL-33[59] and TGF-β[57,58] in promoting persistence in chronic infection. It has been previously established that signal 3 inflammatory cytokines such as IL-12 and IFN-α/β are required to prime the function and survival of both effector and memory cells[2], and that IL-21 has similar signal 3 capabilities[10,60]. However, to our knowledge the ability for IL-18, IL-33, and IL-4 to prime $CD8^+$ T cells for memory-like survival in the absence of TCR stimulation has not been established.

In condition (2) (**Fig. 4.6B**, middle row), we observed overall improved performance of cells from the rest base condition, except for rest with IL-12, IL-21 and IFN-α, which all caused an early decline, in contrast to their improved performance in secondary culture condition (1). This is in line with reports that naive-like or stem-like chimeric antigen receptor (CAR)-T cells persist longer in the tumor environment than more differentiated cells[61]. TGF-β, IL-21, and IL-33 treated cells were the exceptions to this trend of improved performance in the rested base

condition. TGF-β improved performance in all base conditions, consistent with its recently published role in enhancing persistence of CAR-T cells in solid tumors[62]. IL-21, however, improved performance only with stimulation (both αCD3 and αCD3/28 bases) and not with stimulation+inflammation (αCD3/28+IL-12 base), consistent with its proposed role in priming cells for survival in tumors after adoptive transfer[8]. Similarly to in secondary culture condition (1), IL-33 also promoted growth also when primed with inflammation. IL-4 decreased performance in all base conditions except for the resting condition, suggesting that cells primed with IL-4 are not long-lived in chronic stimulation conditions, but are primed instead for survival in the absence of stimulation (**Fig. 4.6B**, condition (1), top). IL-15 also promoted growth only in the resting condition. IL-15 has been demonstrated to prime CAR-T cells for persistence in tumors[63], but our results indicate that this priming effect occurs only in the absence of stimulation. Intriguingly, despite IL-12 having detrimental effects on growth when combined with rest, priming with stimulation and IL-12 increased growth compared to priming without stimulation and IL-12 (see **Fig. 4.6B** black line null condition), suggesting again that signal 3 inflammation in combination with stimulation enhances the overall T cell response.

Lastly, we looked at growth in secondary stimulation condition (3), with continued inflammation. Here, we observed similar growth as in condition (2), with one exception: cells primed with the combination of rest and IL-21 initially declined, but then grew significantly after day 6. This suggests that cells primed with rest and IL-21 can differentiate to both memory-like, long-lived cells which can respond to the secondary challenge, and also to effector-like cells. Consistent with this hypothesis, we observed the previously mentioned bifurcation in expression

of *Tcf7*-YFP: that treatment with IL-21 pushed cells to either high or low expression of *Tcf7*-YFP, unlike other cytokines.

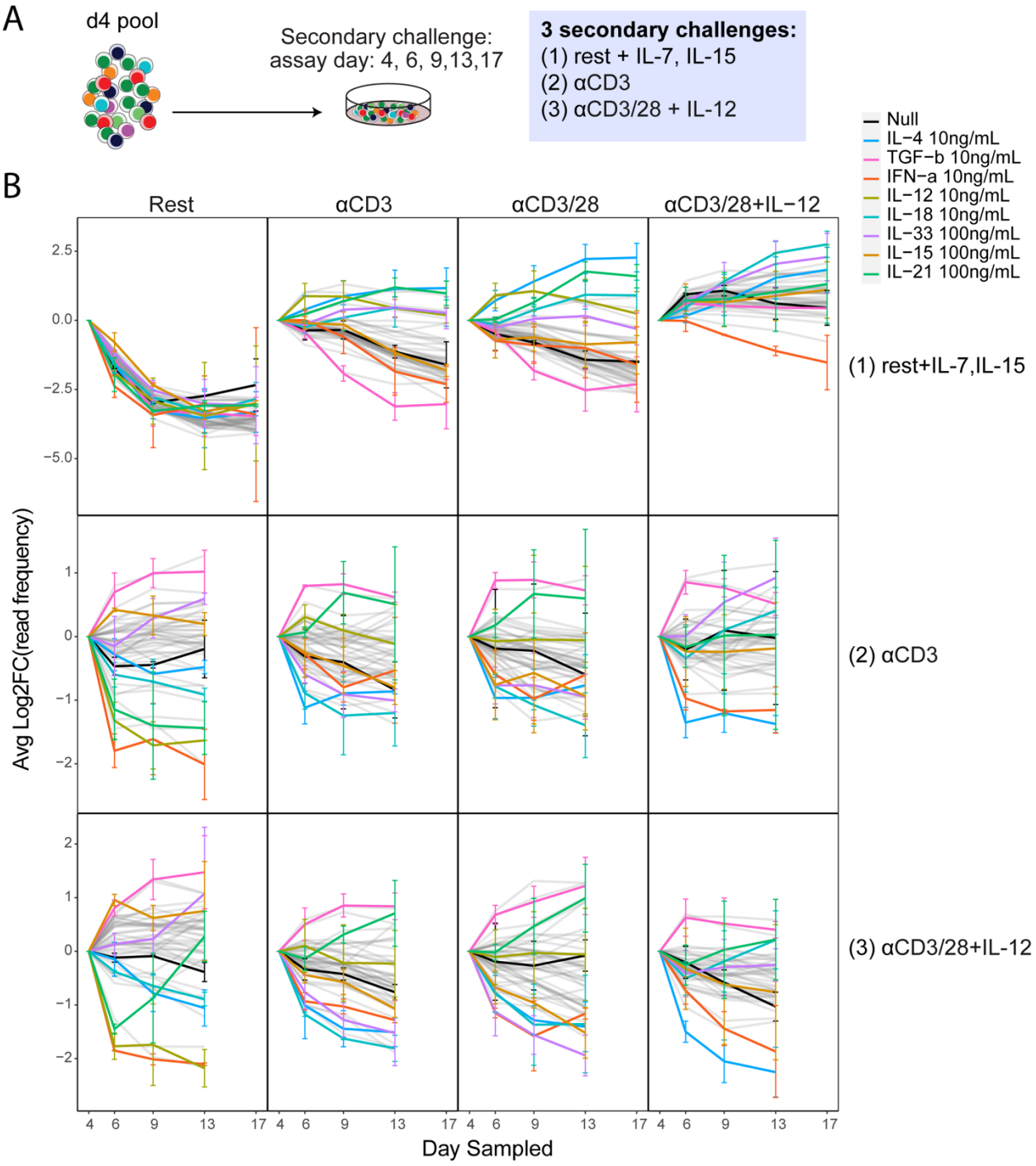

Figure 4.6. Cytokines differentially prime cells for growth and survival in secondary challenges.
(**A**) Overview of secondary *ex vivo* challenges. (**B**) Growth (average log2 fold change of read frequency) for barcodes mapping back to a particular cytokine condition. Colored lines represent cytokines with key differences in performance, highlighted in legend. Gray lines represent all other treatment conditions.

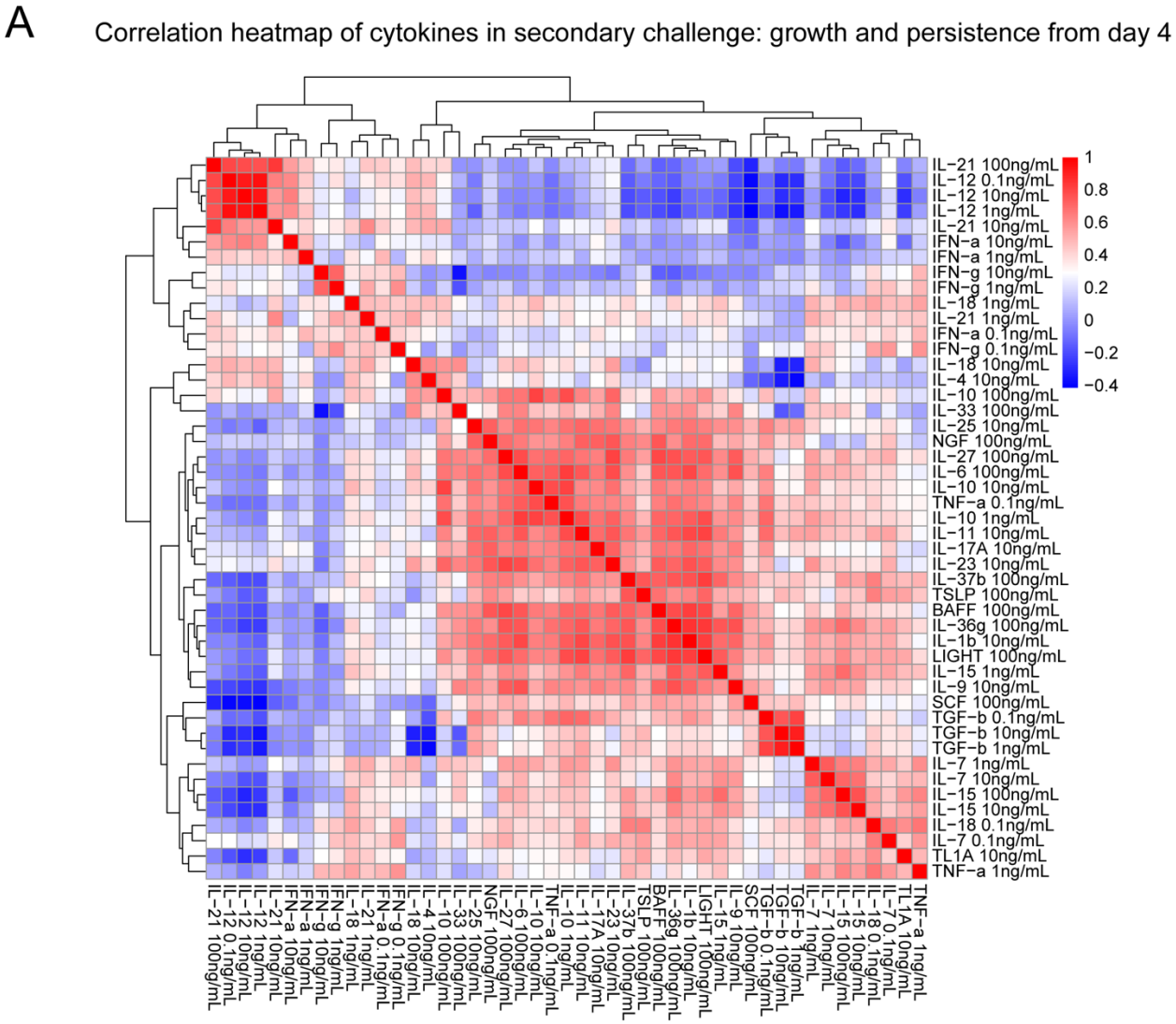

Figure 4.7. Cytokines cluster based on growth and persistence independent of base condition.
(**A**) PCA correlation of growth and day 4 persistence for all cytokine x base condition treatments.

Similarly to the transcriptomic and *Tcf7*-YFP results, we observed most cytokines were not having strong effects on growth when compared to the null condition. To better compare these cytokines to the null and to each other, we performed principal component analysis (PCA) for all cytokine x base condition treatments at all timepoints for growth, and for persistence, which we defined as the barcodes that were present at a particular time point that were also present in the

pool at day 4. Each value for growth and persistence was normalized to the null for the base condition from that treatment. When we visualize the correlation plot of cytokine treatments, we can see patterns of cytokines that are clustered together (**Fig. 4.7A**). We see, like the transcriptomic effects, that IL-12 and the higher doses of IL-21 cluster together, and these are closely related to the other inflammatory cytokines IFN-α/γ, IL-18, IL-4, IL-33 and low-dose IL-21. We see a large cluster of cytokines in the middle of the heatmap that have shared effects, similar to what we observed in the transcriptome. All 3 doses of TGF-β are clustered uniquely together, and closely with SCF as well, but on the opposite end of the heatmap as the inflammatory cytokines, and closer to the cytokines that have traditionally been thought of as memory-promoting or homeostatic: IL-7 and IL-15[64], which intriguingly also clustered with TL1A and TNF-α. TNF-α also clustered with cytokines that increased *Tcf7*-YFP (**Fig. 4.5**), suggesting a shared pro-memory and pro-survival program. By clustering the cytokines in this way, we eliminated patterns elicited solely by base conditions and focused on the shared effects of the cytokines themselves.

4.4 DISCUSSION

In this study, we developed and validated CellCode as a method for recording transcriptomic and functional responses to hundreds of soluble perturbations in live, primary cells. We utilized $CD8^+$ T cells and cytokines for this study, however the utility of CellCode is that it can be applied to any cell type that can be readily virally transduced, and to any external perturbation during the culture process: small molecules, metabolites, growth factors, or any other cell culture media additives. We hope that CellCode can be utilized to uncover the effects of signals in other cell types, and also used to screen the infusion product of cells used in adoptive transfer therapies.

Our goal for this project was to develop a comprehensive atlas of transcriptomic and functional responses of $CD8^+$ T cells to combinations of signal 1, 2, and 3 with the hopes of understanding the scope of possible $CD8^+$ T cell states and responses *in vivo.* We comprehensively tested 28 cytokines, with dose responses, across 4 different stimulation contexts and uncovered that the effects of cytokines on transcriptome and function are highly context-dependent. While some cytokines like IL-4 and TGF-β had strong, largely context-independent effects on the transcriptome of $CD8^+$ T cells, many cytokines had opposing effects dependent on whether the cells were concurrently primed with signals 1, 2, and 3. Our atlas can be used as a reference of $CD8^+$ T cell states for benchmarking transcriptomic data, and also for potentially linking the signaling environment that led to a particular cell state *in vitro* or *in vivo*.

Beyond the use of CellCode for screening therapeutic candidates, we believe our atlas of functional assay data could be utilized therapeutically. T cell growth and performance in secondary challenge condition (1) could have implications for vaccine design, while growth and performance in conditions (2) and (3) could have implications for adoptive cell therapies, such as CAR-T cells. Cytokines can be readily implemented as vaccine adjuvants[65] and are already being explored in CAR-T manufacturing[66]. Our atlas could be used as a reference in the design of both types of therapeutics moving forward.

4.5 BRIEF METHODS

Mice

All animal use was in accordance with the Institutional Care and Use Committee at the University of Washington, approved protocol #4397-01. P14 mice were purchased from Jackson

labs, *Tcf7*-YFP mice were previously described[18]. All mice were 8-16 weeks of age, both male and female mice were utilized for experiments.

$CD8^+$ T cell isolation

Spleens were extracted from *Tcf7*-YFPxP14 mice and smashed between rough glass slides to generate a single cell suspension, which was filtered over 50 μm nylon mesh. Cells were centrifuged at 300g for 5 minutes and resuspended in red blood cell (RBC) lysis buffer (1 mM EDTA, 10 mM $NaHCO_3$, 150 mM NH_4Cl) for 3-5 minutes at room temperature and quenched with HBH (Hank's Balanced Salt Solution (HBSS, Gibco), 0.5% Bovine Serum Albumin (BSA, VWR), 10 mM HEPES, pH 7.4). Cells were subsequently centrifuged at 300g for 5 minutes and resuspended in Fc blocking buffer (2.4G2 supernatant in HBH) for 15-30 minutes on ice. $CD8^+$ T cells were isolated from splenocytes using the CD8a+ T cell isolation kit (Miltenyi #130-104-075) following the manufacturer's instructions.

Barcode sublibrary cloning and virus preparation

Unless otherwise indicated, all PCR reactions were carried out using Q5 polymerase (NEB #M0491) in a 50μL reaction and all Gibson assemblies were carried out using NEBuilder HiFi DNA Assembly MasterMix (NEB #E2621) in a 10μL reaction. All primers and gblocks were ordered from IDT. The plasmid backbone carrying the MSCV viral sequences was a gift from Ellen Rothenberg. To prepare MSCV_H2B-mRuby, this plasmid was cut with MfeI (NEB #R3589) and MluI-HF (NEB #R3189) and the resultant fragment was Gibson-assembled with a H2B-mRuby gblock ordered from IDT to generate MSCV_H2B-mRuby. The resultant plasmid was PCR amplified and the corresponding fragment was Gibson-assembled with a WPRE

fragment PCR amplified from LentiGuide-Puro (Addgene #52963) to generate MSCV_H2B-mRuby-WPRE. This plasmid was cut with EcoRI-HF (NEB #R3101) and BamHI-HF (NEB #R3136) and Gibson-assembled with the ultramer MSCV_GoldenGateSites_v2 to generate MSCV_H2B-mRuby-WPRE-GGsites_v2, which has the BbsI sites used for GoldenGate assembly of the barcode library v2.4 in the correct orientation.

For the construction of library v2.4, the ultramer MSCV_GGv2_Template_v4 (Table PX) was PCR amplified for 6 cycles to generate a high-complexity barcoded fragment with BbsI sites in the complementary orientation for assembly. 50ng of this PCR fragment was mixed with 500ng of plasmid MSCV_H2B-mRuby-WPRE-GGsites_v2 in the presence of T4 ligase (NEB #M0202T) and BbsI-HF (NEB #R3539) in eight 25µL reactions each and cycled between 5 minutes at 37C and 16C thirty times in GoldenGate assembly before pooling and concentrating into 15µL. 1µL of that assembled ligation was transformed into 12-14 cuvettes of 25µL NEB 10-beta electrocompetent *E coli* (NEB #C3020K) each. After pooling, transformed cells were plated onto three large 25cm-square LB-agar plates with 100ug/mL carbenecillin and grown at 30C overnight. Each plate was scraped and maxiprepped (Zymo #D4203) to generate one library portion. This procedure was repeated four times to generate twelve portions (sublibraries) of the MSCV_GGv2.4_BC_Library.

Each sublibrary was transfected into a separate 10 cm dish of HEK293T cells with pCL-Eco plasmids. Viral supernatant was harvested ~60 hours after transfection and filtered through 0.45 µm syringe filters and used immediately for T cell transduction (see below).

$CD8^+$ T cell activation and transduction

One day prior to activation (day -1), plates were coated with anti-CD3e (Cytek #40-0031-U500) and anti-CD28 in PBS (Cytek #40-0281-U100) at 1 µg/mL and 0.5 µg/mL respectively. On the day of stimulation (day 0), coated 24-well plates were rinsed 2x with PBS and $CD8^+$ T cells were plated at 1M cells/mL in 500 µL of T cell medium (TCM) (RPMI 1640 + L-Glutamine (Gibco), 10% heat inactivated FBS (VWR), 1% Non essential amino acids (Gibco), 1% Sodium Pyruvate (Gibco), 2% HEPES, 1% Pen-Strep-Glutamine, and 50 µM 2-Mercaptoethanol (BME)). Cells were centrifuged onto the coated plates at 50g for 1 minute to allow for adhesion.

Cells were incubated for 22 hours at 37°C, 5% CO_2 prior to transduction. Barcode sublibraries were mixed in equal amounts to generate a supermix, along with 2x the final desired concentration of polybrene, IL-2, and BME. 500 µL of virus was added to each well of the 24 well plate for a final concentration of 1x polybrene (4 µg/mL), IL-2 (10 ng/mL) and BME (50 µM). Cells were spinfected at 30°C, 2000g (no acceleration, no brake) for 60 minutes, then incubated at 37°C, 5% CO_2 for 4 hours.

Large scale *ex vivo* screen

Cells were pooled, centrifuged at 300g for 7 minutes, and washed twice with TCM containing no BME or cytokines. Cells were resuspended in TCM at 0.3E6/mL and 100 µL (0.03E6 cells) were seeded into 96 well plates already containing 2x cytokine and BME, for a final concentration of 1x. Individual cytokine media were prepared at 4x in TCM, and mixed 50/50 with 4x base medium containing 4x BME and 4x IL-2 or IL-2+IL/12. Cytokine manufacturers and product numbers are listed in **Table 4.1**. Where applicable, plates were coated with anti-CD3e only or

anti-CD3 and anti-CD28 as described above and rinsed 2x prior to cell seeding. Cells not requiring continued stimulation were seeded into uncoated tissue culture treated 96 well plates. 2.5 days after initial activation (1.5 days after spinfection) 75% of the cells were sampled for barcode sequencing and centrifuged at 700g for 5 minutes, rinsed 1x with HBH, centrifuged again at 700g for 5 minutes and flash frozen in liquid nitrogen prior to storage at -80°C. The remaining cells were topped off with fresh TCM containing the appropriate cytokines and base medium and cultured until day 4 at 37°C, 5% CO_2. On day 4, 25 µL of culture from one replicate of each condition was sampled and counted using an Attune NxT flow cytometer (Thermo). Cells from each replicate were subsequently pooled by plate for single cell RNA sequencing (scRNAseq, see below), ranging from 2-12.5k cells per condition being pooled. The remaining cells were pooled separately by replicate (without normalization by cell number). 25% of the pool was sampled for barcode sequencing, 33% of the pool was used for sorting on *Tcf7*-YFP the remaining cells were used for pooled follow-up perturbations.

Extracellular staining, FACS, and flow cytometry

Sorting was performed on a FACSAria III (BD, UW Pathology Flow Core). Analyses were performed in Flowjo (BD). Each pool for scRNAseq was resuspended in Fc blocking buffer and stained with 1 µL of hashtag antibody (Biolegend, TotalSeq B Mouse Hashtag 1-6 #s:155831, 155833, 155835, 155837, 155839, 155841) for 15-30 minutes on ice. Prior to sorting, cells were resuspended in 100 ng/mL Dapi in HBH. Live, barcoded cells were sorted as $Dapi^{-}mRuby^{+}$ and taken immediately for processing for 10x sequencing (see below). For *Tcf7*-YFP sorting, each replicate was resuspended in HBH and sorted based on live (FSC/SSC gated), $mRuby^{+}$ into quartiles based on YFP expression.

Pooled *ex vivo* assays

Replicates were pooled separately as described and split into 3 follow-up perturbations: (1) no TCR stimulation with low IL-2 (1 ng/mL), IL-7 (5 ng/mL) and IL-15 (50 ng/mL). (2) + TCR stimulation (anti-CD3 (1 µg/mL) coating only) + IL-2 (10 ng/mL) and +TCR stimulation + Costimulation (anti-CD3 (1 µg/mL) and anti-CD28 (0.5 µg/mL) coating). Plates were coated as described in $CD8^+$ T cell activation and where applicable, cells were transferred to freshly coated plates on day 4, day 6, and day 9. At day 4, day 6, day 9, and day 13 cells were counted and sampled for DNA sequencing, then resuspended in fresh 1x cytokine medium and transferred to a new culture plate. On day 13, all cells in conditions 2 and 3 were saved for DNA sequencing. Cells in condition 1 only were cultured until day 17.

Single cell sequencing library preparation and analysis

Sorted cells were resuspended in PBS+1% BSA and loaded into 8 separate 10x Next GEM Single Cell 3' HT v3.1 reactions following the manufacturer's instructions. A small portion of the unfragmented cDNA from supernatant and bead fractions was used for amplification of RNA barcodes via a three-step PCR. Transcriptome and barcode libraries were sequenced using a 28 (read 1) - 8 (index 1) - 8 (index 2) - 94 (read 2) configuration on an Illumina P3 100 cycle kit (Illumina #20040559) on the NextSeq 2000 (Illumina).

Barcode amplification

Cell pellets were stored at -80℃ prior to implications. Pellets were thawed on ice, and then resuspended in 50 µL of lysis buffer (30 mM Tris, 10 mM EDTA, 0.4 mg/mL proteinase K) per

1E5 cells. Cells were lysed to prepare gDNA by incubating for 1 hour at 56℃ on a thermomixer set to 1250 rpm and then proteinase K was inactivated at 94℃ with no mixing for 20 minutes. gDNA was placed immediately on ice, then cleaned with 1:1 AMPure XP beads (Beckman Coulter) and amplified for 5 cycles with primers flanking the barcode with the following condition. Amplified gDNA was cleaned using 1:1 AMPure XP beads, then a second, indexing PCR was performed for an additional 16 cycles. Final PCR products were cleaned using 0.8:1 AMPure XP beads and then sequenced using a 27 (read 1) - 8 (index 1) - 8 (index 2) - 27 (read 2) configuration on an P3 50 cycle kit (Illumina #20046810) on a NextSeq 2000 (Illumina).

Cytokines

* multiple doses tested, otherwise a single dose was tested
** 10 ng/mL used in perturbation phase of *ex vivo* testing, 1 or 10 ng/mL used in *ex vivo* pooled follow-up perturbations

Table 4.1. Cytokines used for *ex vivo* assays

Cytokine	Concentrations	Manufacturer	Product Number
IL-2**	1, 5, 10 ng/mL	Peprotech	200-02
IL-12*	0.1, 1, 10 ng/mL	Peprotech	210-12
IL-21*	1, 10, 100 ng/mL	Peprotech	210-21
IFN-γ*	0.1, 1, 10 ng/mL	Peprotech	315-05
IL-7*	0.1, 1, 10 ng/mL	Peprotech	200-07
IL-15*	1, 10, 100 ng/mL	Peprotech	210-15
IL-18*	0.1, 1, 10 ng/mL	Biolegend	767002
IFN-α*	0.1, 1, 10 ng/mL	Biolegend	752804
TNF-α*	0.1, 1, 10 ng/mL	Peprotech	315-01A
TGF-β*	0.1, 1, 10 ng/mL	Biolegend	763102
IL-10*	1, 10, 100 ng/mL	Peprotech	210-10
IL-6	100 ng/mL	Peprotech	216-16
SCF	100 ng/mL	Peprotech	250-03
IL-27	100 ng/mL	Peprotech	200-38
IL-9	10 ng/mL	Peprotech	219-19
IL-25/IL-17E	10 ng/mL	Peprotech	210-17E
IL-17A	10 ng/mL	Peprotech	210-17
IL-23	10 ng/mL	Peprotech	200-23

IL-11	10 ng/mL	Peprotech	220-11
IL-1β	10 ng//mL	Peprotech	211-11B
IL-33	100 ng/mL	Peprotech	210-33
IL-36γ	100 ng/mL	Peprotech	200-36G
IL-37b	100 ng/mL	Peprotech	200-39
IL-4	10 ng/mL	Peprotech	214-14
TSLP	100 ng/mL	Peprotech	300-62
LIGHT	100 ng/mL	Peprotech	315-12
BAFF	100 ng/mL	Peprotech	310-13
NGF	100 ng/mL	Peprotech	450-34
TL1A	10 ng/mL	Peprotech	310-23

4.6 REFERENCES

1. Curtsinger, J. M., Lins, D. C. & Mescher, M. F. Signal 3 Determines Tolerance versus Full Activation of Naive CD8 T Cells : Dissociating Proliferation and Development of Effector Function. *J. Exp. Med.* **197**, 1141–1151 (2003).
2. Curtsinger, J. M. & Mescher, M. F. Inflammatory cytokines as a third signal for T cell activation. *Curr. Opin. Immunol.* **22**, 333–340 (2010).
3. Curtsinger, J. M., Valenzuela, J. O., Agarwal, P., Lins, D. & Mescher, M. F. Cutting Edge: Type I IFNs Provide a Third Signal to CD8 T Cells to Stimulate Clonal Expansion and Differentiation. *J. Immunol.* **174**, 4465–4469 (2005).
4. Curtsinger, J. M., Johnson, C. M. & Mescher, M. F. CD8 T Cell Clonal Expansion and Development of Effector Function Require Prolonged Exposure to Antigen, Costimulation, and Signal 3 Cytokine. *J. Immunol.* **171**, 5165–5171 (2003).
5. Tian, Y. & Zajac, A. J. IL-21 and T cell differentiation: consider the context. *Trends Immunol.* **37**, 557–568 (2016).
6. Barker, B. R., Gladstone, M. N., Gillard, G. O., Panas, M. W. & Letvin, N. L. Critical role for IL-21 in both primary and memory anti-viral CD8+ T-cell responses. *Eur. J. Immunol.* **40**, 3085–3096 (2010).
7. Alvarez-Fernández, C., Escribà-Garcia, L., Vidal, S., Sierra, J. & Briones, J. A short CD3/CD28 costimulation combined with IL-21 enhance the generation of human memory stem T cells for adoptive immunotherapy. *J. Transl. Med.* **14**, 214 (2016).
8. Hinrichs, C. S. *et al.* IL-2 and IL-21 confer opposing differentiation programs to CD8+ T cells for adoptive immunotherapy. *Blood* **111**, 5326–5333 (2008).
9. Deng, S. *et al.* Targeting tumors with IL-21 reshapes the tumor microenvironment by proliferating PD-1intTim-3–CD8+ T cells. *JCI Insight* **5**, e132000.
10. Casey, K. A. & Mescher, M. F. IL-21 Promotes Differentiation of Naive CD8 T Cells to a Unique Effector Phenotype1. *J. Immunol.* **178**, 7640–7648 (2007).
11. Zander, R. *et al.* Tfh-cell-derived interleukin 21 sustains effector CD8+ T cell responses during chronic viral infection. *Immunity* **55**, 475-493.e5 (2022).

12. Cui, A. *et al.* Dictionary of immune responses to cytokines at single-cell resolution. *Nature* 1–8 (2023) doi:10.1038/s41586-023-06816-9.
13. Dixit, A. *et al.* Perturb-seq: Dissecting molecular circuits with scalable single cell RNA profiling of pooled genetic screens. *Cell* **167**, 1853-1866.e17 (2016).
14. Vardhana, S. A. *et al.* Impaired mitochondrial oxidative phosphorylation limits the self-renewal of T cells exposed to persistent antigen. *Nat. Immunol.* **21**, 1022–1033 (2020).
15. Scharping, N. E. *et al.* Mitochondrial stress induced by continuous stimulation under hypoxia rapidly drives T cell exhaustion. *Nat. Immunol.* **22**, 205–215 (2021).
16. Belk, J. A. *et al.* Genome-wide CRISPR screens of T cell exhaustion identify chromatin remodeling factors that limit T cell persistence. *Cancer Cell* **40**, 768-786.e7 (2022).
17. Zhao, M. *et al.* Rapid in vitro generation of bona fide exhausted CD8+ T cells is accompanied by Tcf7 promotor methylation. *PLOS Pathog.* **16**, e1008555 (2020).
18. Harly, C. *et al.* The transcription factor TCF-1 enforces commitment to the innate lymphoid cell lineage. *Nat. Immunol.* **20**, 1150–1160 (2019).
19. Wither, M. J. *et al.* Antigen perception in T cells by long-term Erk and NFAT signaling dynamics. *Proc. Natl. Acad. Sci.* **120**, e2308366120 (2023).
20. Levine, J. H. *et al.* Data-driven phenotypic dissection of AML reveals progenitor-like cells that correlate with prognosis. *Cell* **162**, 184–197 (2015).
21. Trapnell, C. *et al.* The dynamics and regulators of cell fate decisions are revealed by pseudotemporal ordering of single cells. *Nat. Biotechnol.* **32**, 381–386 (2014).
22. Qiu, X. *et al.* Reversed graph embedding resolves complex single-cell trajectories. *Nat. Methods* **14**, 979–982 (2017).
23. Cao, J. *et al.* The single-cell transcriptional landscape of mammalian organogenesis. *Nature* **566**, 496–502 (2019).
24. Kaech, S. M., Hemby, S., Kersh, E. & Ahmed, R. Molecular and Functional Profiling of Memory CD8 T Cell Differentiation. *Cell* **111**, 837–851 (2002).
25. Kaech, S. M. & Ahmed, R. Memory CD8+ T cell differentiation: initial antigen encounter triggers a developmental program in naïve cells. *Nat. Immunol.* **2**, 415–422 (2001).
26. Banerjee, A. *et al.* The Transcription Factor Eomesodermin Enables CD8+ T Cells to Compete for the Memory Cell Niche. *J. Immunol. Baltim. Md 1950* **185**, 4988–4992 (2010).
27. Intlekofer, A. M. *et al.* Effector and memory CD8+ T cell fate coupled by T-bet and eomesodermin. *Nat. Immunol.* **6**, 1236–1244 (2005).
28. Takada, K. *et al.* KLF2 is required for trafficking but not quiescence in post-activated T cells. *J. Immunol. Baltim. Md 1950* **186**, 775–783 (2011).
29. Yang, C. Y. *et al.* The transcriptional regulators Id2 and Id3 control the formation of distinct memory CD8+ T cell subsets. *Nat. Immunol.* **12**, 1221–1229 (2011).
30. Roychoudhuri, R. *et al.* BACH2 regulates CD8+ T cell differentiation by controlling access of AP-1 factors to enhancers. *Nat. Immunol.* **17**, 851–860 (2016).
31. Sallusto, F., Lenig, D., Förster, R., Lipp, M. & Lanzavecchia, A. Two subsets of memory T lymphocytes with distinct homing potentials and effector functions. *Nature* **401**, 708–712 (1999).
32. Reilly, E. C. *et al.* TRM integrins CD103 and CD49a differentially support adherence and motility after resolution of influenza virus infection. *Proc. Natl. Acad. Sci.* **117**, 12306–12314 (2020).
33. Milner, J. J. *et al.* Runx3 programs CD8+ T cell residency in non-lymphoid tissues and tumours. *Nature* **552**, 253–257 (2017).

34. Dominguez, C. X. *et al.* The transcription factors ZEB2 and T-bet cooperate to program cytotoxic T cell terminal differentiation in response to LCMV viral infection. *J. Exp. Med.* **212**, 2041–2056 (2015).
35. Shan, Q. *et al.* Runx3 guards cytotoxic CD8+ effector T cells against deviation towards TFH cell lineage. *Nat. Immunol.* **18**, 931–939 (2017).
36. Rutishauser, R. L. *et al.* Transcriptional Repressor Blimp-1 Promotes CD8+ T Cell Terminal Differentiation and Represses the Acquisition of Central Memory T Cell Properties. *Immunity* **31**, 296–308 (2009).
37. Kalia, V. *et al.* Prolonged Interleukin-2Rα Expression on Virus-Specific CD8+ T Cells Favors Terminal-Effector Differentiation In Vivo. *Immunity* **32**, 91–103 (2010).
38. Singer, M. *et al.* A distinct gene module for dysfunction uncoupled from activation in tumor-infiltrating T cells. *Cell* **166**, 1500-1511.e9 (2016).
39. Khan, O. *et al.* TOX transcriptionally and epigenetically programs CD8 + T cell exhaustion. *Nature* **571**, 211–218 (2019).
40. Scott, A. C. *et al.* TOX is a critical regulator of tumour-specific T cell differentiation. *Nature* **571**, 270–274 (2019).
41. Seo, H. *et al.* TOX and TOX2 transcription factors cooperate with NR4A transcription factors to impose CD8+ T cell exhaustion. *Proc. Natl. Acad. Sci.* **116**, 12410–12415 (2019).
42. Beltra, J.-C. *et al.* Stat5 opposes the transcription factor Tox and rewires exhausted CD8+ T cells toward durable effector-like states during chronic antigen exposure. *Immunity* **56**, 2699-2718.e11 (2023).
43. Koh, C.-H., Lee, S., Kwak, M., Kim, B.-S. & Chung, Y. CD8 T-cell subsets: heterogeneity, functions, and therapeutic potential. *Exp. Mol. Med.* **55**, 2287–2299 (2023).
44. Tai, T.-S., Pai, S.-Y. & Ho, I.-C. GATA-3 regulates the homeostasis and activation of CD8+ T cells. *J. Immunol. Baltim. Md 1950* **190**, 428–437 (2013).
45. van der Ploeg, E. K. *et al.* Type-2 CD8+ T-cell formation relies on interleukin-33 and is linked to asthma exacerbations. *Nat. Commun.* **14**, 5137 (2023).
46. Stoeckius, M. *et al.* Cell Hashing with barcoded antibodies enables multiplexing and doublet detection for single cell genomics. *Genome Biol.* **19**, 224 (2018).
47. Cao, J. *et al.* Comprehensive single cell transcriptional profiling of a multicellular organism. *Science* **357**, 661–667 (2017).
48. Matreyek, K. A. *et al.* Multiplex Assessment of Protein Variant Abundance by Massively Parallel Sequencing. *Nat. Genet.* **50**, 874–882 (2018).
49. Escobar, G., Mangani, D. & Anderson, A. C. T cell factor 1 (Tcf1): a master regulator of the T cell response in disease. *Sci. Immunol.* **5**, eabb9726 (2020).
50. Danilo, M., Chennupati, V., Silva, J. G., Siegert, S. & Held, W. Suppression of Tcf1 by Inflammatory Cytokines Facilitates Effector CD8 T Cell Differentiation. *Cell Rep.* **22**, 2107–2117 (2018).
51. Dinarello, C. A. Overview of the IL-1 family in innate inflammation and acquired immunity. *Immunol. Rev.* **281**, 8–27 (2018).
52. Lutz, V. *et al.* IL18 Receptor Signaling Regulates Tumor-Reactive CD8+ T-cell Exhaustion via Activation of the IL2/STAT5/mTOR Pathway in a Pancreatic Cancer Model. *Cancer Immunol. Res.* **11**, 421–434 (2023).
53. Chen, Z. *et al.* TCF-1-Centered Transcriptional Network Drives an Effector versus Exhausted CD8 T Cell-Fate Decision. *Immunity* **51**, 840-855.e5 (2019).

54. Huster, K. M. *et al.* Selective expression of IL-7 receptor on memory T cells identifies early CD40L-dependent generation of distinct CD8+ memory T cell subsets. *Proc. Natl. Acad. Sci. U. S. A.* **101**, 5610–5615 (2004).
55. Richer, M. J. *et al.* Inflammatory IL-15 is required for optimal memory T cell responses. *J. Clin. Invest.* **125**, 3477–3490 (2015).
56. Becker, T. C. *et al.* Interleukin 15 is required for proliferative renewal of virus-specific memory CD8 T cells. *J. Exp. Med.* **195**, 1541–1548 (2002).
57. Gabriel, S. S. *et al.* Transforming growth factor-β-regulated mTOR activity preserves cellular metabolism to maintain long-term T cell responses in chronic infection. *Immunity* **0**, (2021).
58. Hu, Y. *et al.* TGF-β regulates the stem-like state of PD-1+ TCF-1+ virus-specific CD8 T cells during chronic infection. *J. Exp. Med.* **219**, e20211574 (2022).
59. Marx, A.-F. *et al.* The alarmin interleukin-33 promotes the expansion and preserves the stemness of Tcf-1+ CD8+ T cells in chronic viral infection. *Immunity* **56**, 813-828.e10 (2023).
60. Moroz, A. *et al.* IL-21 enhances and sustains CD8+ T cell responses to achieve durable tumor immunity: comparative evaluation of IL-2, IL-15, and IL-21. *J. Immunol. Baltim. Md 1950* **173**, 900–909 (2004).
61. TSTEM-like CAR-T cells exhibit improved persistence and tumor control compared with conventional CAR-T cells in preclinical models. *Sci. Transl. Med.*
62. Jung, I.-Y. *et al.* Tissue-resident memory CAR T cells with stem-like characteristics display enhanced efficacy against solid and liquid tumors. *Cell Rep. Med.* **4**, 101053 (2023).
63. Alizadeh, D. *et al.* IL15 Enhances CAR-T Cell Antitumor Activity by Reducing mTORC1 Activity and Preserving Their Stem Cell Memory Phenotype. *Cancer Immunol. Res.* **7**, 759–772 (2019).
64. Yang, L., Yu, Y., Kalwani, M., Tseng, T.-W. J. & Baltimore, D. Homeostatic cytokines orchestrate the segregation of CD4 and CD8 memory T-cell reservoirs in mice. *Blood* **118**, 3039–3050 (2011).
65. Tovey, M. G. & Lallemand, C. Adjuvant Activity of Cytokines. in *Vaccine Adjuvants: Methods and Protocols* (ed. Davies, G.) 287–309 (Humana Press, 2010). doi:10.1007/978-1-60761-585-9_19.
66. Dwyer, C. J. *et al.* Fueling Cancer Immunotherapy With Common Gamma Chain Cytokines. *Front. Immunol.* **10**, (2019).

Chapter 5. CONCLUSIONS AND FUTURE DIRECTIONS

Chapter 5 includes data collected in collaboration with Sarah Garrison and Shivani Srivastava and is representative of their work and ideas as well as mine.

5.1 SUMMARY

In **Chapters 2 and 3** of this dissertation, I focused primarily on the regulation of *Tcf7*/TCF1 in $CD8^+$ T cells responding to acute, and chronic threats. As outlined in **Chapter 1**, $TCF1^+$ cells are necessary for long term immune responses and are therefore of great therapeutic interest. The insights from our studies in **Chapter 2** could have value for the design of vaccines, while the insights from our studies in **Chapter 3** are of particular interest for adoptive cell therapies for cancer. Optimizing a particular phenotype in a cell therapy product presents unique challenges, one of which is the ability to test changes to the cell activation and expansion process in high throughput. In **Chapter 4**, we developed CellCode, a method which allows for multiplexed recording of the effects of signal perturbations on transcriptome and function in live cells. We used CellCode to investigate the impact of cytokines on *Tcf7*/TCF1, however this technology could be used to optimize any phenotype of interest in any cell type to be used as an adoptive cell therapy. In this chapter, I will focus on some of the challenges still facing CAR-T cell therapy in solid tumors, and how CellCode, as well as the insights gained in this thesis on *Tcf7* regulation could be used to address these unmet needs.

5.2 FUTURE DIRECTIONS

CAR-T therapies have shown great efficacy and have been approved for treatment of hematologic malignancies such as leukemia and lymphoma. However, translating this clinical

success to solid tumor indications has proven difficult. This is due to a combination of factors, including limited infiltration of CAR-T cells into solid tumors, lack of persistence of the cells in the tumor environment, and differentiation to the exhausted state[1]. Programming CAR-T cells to have a more stem-like, $TCF1^+$, phenotype, either through use of cytokines in the preculture[2], or through genetic modifications[3,4], have demonstrated increased persistence and efficacy in mouse solid tumor models. However, there are other phenotypes aside from stemness that may be beneficial to optimize in the infusion product to increase the engraftment of the cells in solid tumors. It has been demonstrated that patients with increased "resident-memory" like $CD8^+$ T (tumor T_{RM}) cells have better prognoses, and therefore strategies to improve the residency phenotype in CAR-T cells have been proposed specifically for the treatment of solid tumors[5,6]. These tumor T_{RM} are characterized by high expression of the surface receptors CD69, and CD103, which together have the engraftment functions of reducing egress to the lymph nodes[7], and binding to the epithelial protein E-cadherin[8], respectively[9].

As we described in **Chapter 4**, cytokines can be used to program $CD8^+$ T cell states and have been used to optimize phenotypes in CAR-T cells. For example, pre-treatment with IL-15 has been demonstrated to increase persistence of transplanted CAR-T cells[2], while pre-treatment with IL-12 increases effector function[10,11]. TGF-β has been implicated in directing naive $CD8^+$ T cells toward a resident memory phenotype and has been explored alone[12] or in combination with hypoxia[13] in CAR-T cells to reprogram them for stemness and residency in solid tumors. However, TGF-β is known to suppress the cytotoxic function of $CD8^+$ T cells, and therefore may not present the optimal strategy for generating a functional CAR-T infusion product. We hypothesized that combining TGF-β with a pro-inflammatory cytokine could produce a CAR-T

cell with the optimal combination of stemness, effector function, and residency capabilities for solid tumors.

We tested first the effects of combining TGF-β with either IFN-α or IL-12, or each cytokine alone, in non-CAR-expressing $CD8^+$ T cells and looked at its effects on *Tcf7,* effector function (Granzyme B production), and tumor residency potential by expression of CD69 and CD103 (**Fig. 5.1A-B**). Similarly to what we observed in **Chapter 4** in our larger CellCode screen, TGF-β increased the T_{PEX} population in combination with inflammatory cytokines. However, TGF-β significantly decreased effector function (reduced granzyme B), but this effect was somewhat rescued with the combination of inflammation. Strikingly, the combination of IFN-α and TGF-β led to the strongest residency potential ($CD69^+CD103^+$), and therefore we decided to move forward with testing either IFN-α alone, TGF-β alone, or the combination of the two in an *in vivo* transplantable non-small cell lung cancer (NSCLC) model, against a control CAR expansion condition of IL-2 and IL-15[14] (**Fig. 5.2A**).

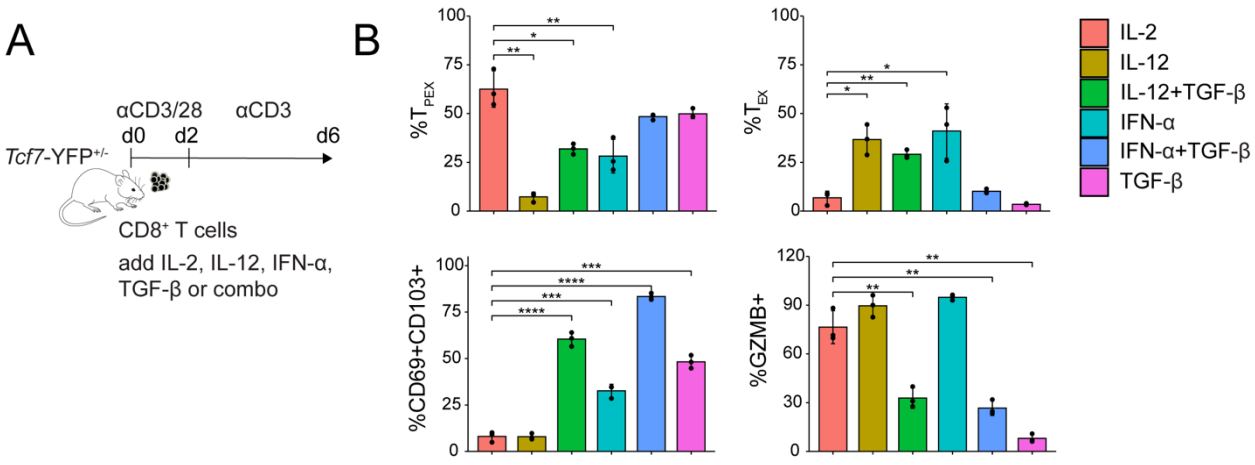

Figure 5.1. Generation of RM-like $CD8^+$ T cells ex vivo using cytokines.
(**A**) Schematic of cell expansion process. (**B**) Flow cytometry phenotyping of cells at day 6 of culture, for T_{PEX} (*Tcf7*-YFP^+TIM3^-), T_{EX} (*Tcf7*-YFP^-TIM3^+), RM-like cells ($CD69^+CD103^+$), and granzyme B^+ cells. [B] n=3

biological replicates from a single experiment. Mean±SD. *p<0.05, **p<0.01, ***p<0.001, ****p<0.0001, for t-test comparison of each cytokine treatment to IL-2 only control.

We harvested tumors at day 4 and day 17 after transfer, and analyzed their engraftment, T_{PEX} and T_{EX} phenotypes by differential expression of TCF1 and TIM3, the amount of interaction with antigen by PD-1, and the residency phenotype by CD69 and CD103 expression, and lack of the lymph node homing marker, CD62L (**Fig. 5.2B**). We also looked at the proliferative capability of the cells by Ki67 staining. Intriguingly, we saw engraftment was the highest at day 4 in the IFN-α treated group, consistent with the hypothesis that effector-like CAR-T cells, secreting IFN-γ can remodel the tumor early to enhance engraftment[15–17]. At day 4, the combination treatment had the greatest CD103 expression, indicating better residency potential, however this phenotype was lost by day 17, and the control condition had the greatest engraftment at this time point. Intriguingly, the combination condition did not increase the stem-like $TCF1^+$ T_{PEX} population as it had *ex vivo* and this could be potentially due to increased interaction with the tumor as evidenced by higher PD-1 in this condition. We therefore concluded that the combination treatment did not improve engraftment or stemness, had low impact on residency potential, and all of these phenotypes led to no significant improvement in tumor control (data not shown).

These *in vivo* experiments are intensive, require large animal numbers, and have a high degree of biological replicate variability, as evidenced in the error bars in **Fig. 5.2**. We believe that the CellCode platform that we developed in **Chapter 4** provides a solution to both the throughput and variability challenges. In a single experiment for CellCode, we were able to screen 192 unique culture conditions in triplicate, which would massively increase the throughput for a CAR-T cell screening effort. Importantly, with CellCode, we can pool cells from different treatment conditions and adoptively transfer the pool individually to biological replicates, and in

doing so compete CAR-T cell preculture conditions directly within the same animal. In support of this goal, we have generated a retrovirus containing both the CellCode library and a ROR1 CAR and have validated the CAR expression and ability to capture barcodes (data not shown).

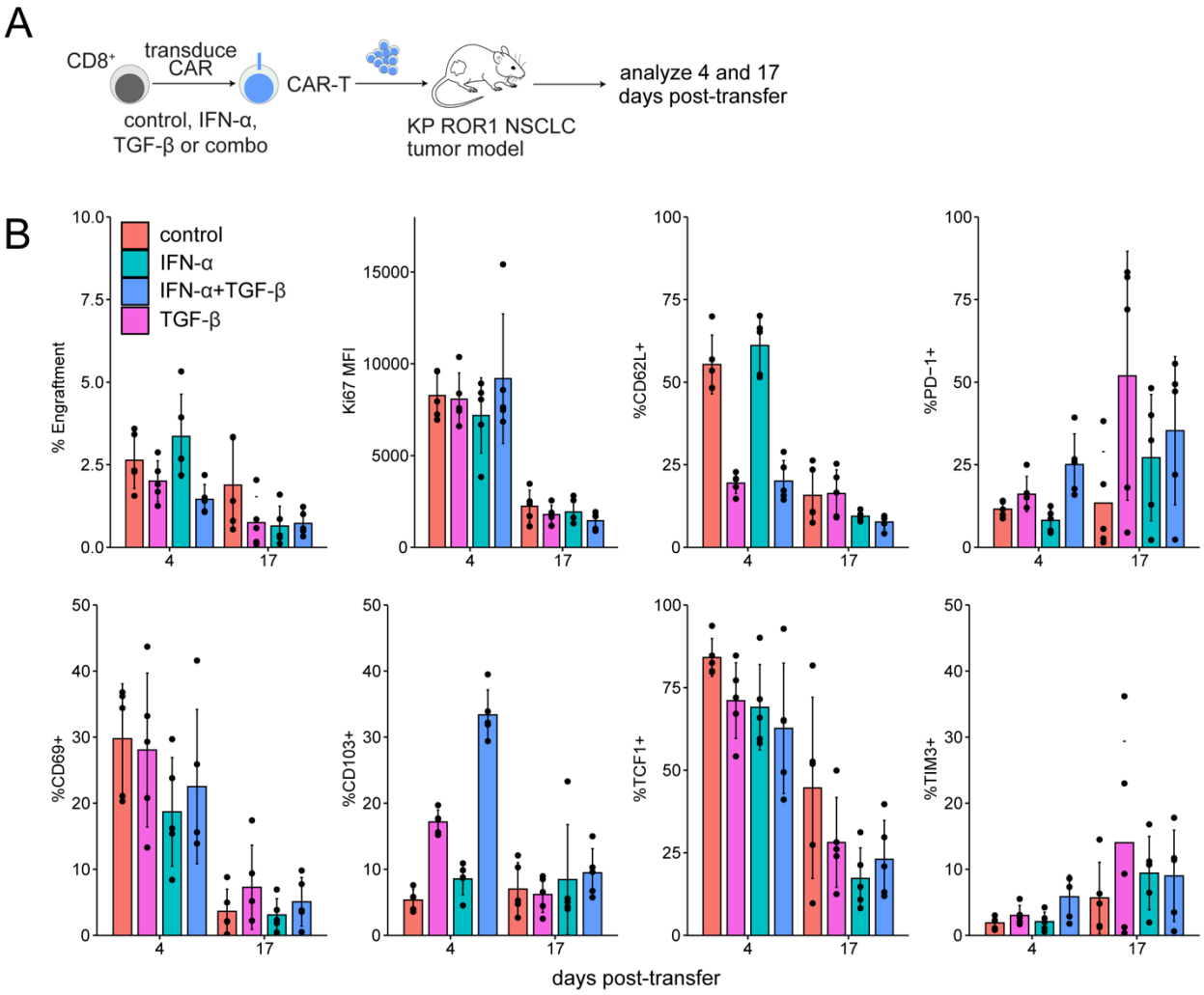

Figure 5.2. TRM promoting conditions do not show improved performance in a NSCLC model.
(**A**) Schematic of CAR-T expansion and tumor model. (**B**) Flow cytometry phenotyping of cells at day 4 and day 17 post-adoptive transfer for % Engraftment (% CAR^+ cells/total live cells recovered), mean fluorescence intensity (MFI) of Ki67, % $CD62L^+$, % $PD\text{-}1^+$, % $CD69^+$, % $CD103^+$, % $TCF1^+$, % $TIM3^+$. [B] n=5 biological replicates per treatment group.

While our original experiments with combination of IFN-α and TGF-β did not yield the expected results, we are optimistic that by screening more cytokines and cytokine combinations, we will find a preculture regimen that can improve the CAR-T infusion product for solid tumors.

These efforts, combined with our insights into regulation of *Tcf7* in the tumor environment will hopefully have an impact on next-generation immunotherapy strategies with optimization of both preculture conditions and genetic engineering.

5.3 REFERENCES

1. Srivastava, S. & Riddell, S. R. CAR T Cell Therapy: Challenges to Bench-to-Bedside Efficacy. *J. Immunol. Baltim. Md 1950* **200**, 459–468 (2018).
2. Alizadeh, D. *et al.* IL15 Enhances CAR-T Cell Antitumor Activity by Reducing mTORC1 Activity and Preserving Their Stem Cell Memory Phenotype. *Cancer Immunol. Res.* **7**, 759–772 (2019).
3. Yoshikawa, T. *et al.* Genetic ablation of PRDM1 in antitumor T cells enhances therapeutic efficacy of adoptive immunotherapy. *Blood* **139**, 2156–2172 (2022).
4. Lynn, R. C. *et al.* c-Jun overexpression in CAR T cells induces exhaustion resistance. *Nature* **576**, 293–300 (2019).
5. Anadon, C. M. *et al.* Ovarian cancer immunogenicity is governed by a narrow subset of progenitor tissue-resident memory T cells. *Cancer Cell* **40**, 545-557.e13 (2022).
6. Corgnac, S., Boutet, M., Kfoury, M., Naltet, C. & Mami-Chouaib, F. The Emerging Role of CD8+ Tissue Resident Memory T (TRM) Cells in Antitumor Immunity: A Unique Functional Contribution of the CD103 Integrin. *Front. Immunol.* **9**, 1904 (2018).
7. Mackay, L. K. *et al.* Cutting Edge: CD69 Interference with Sphingosine-1-Phosphate Receptor Function Regulates Peripheral T Cell Retention. *J. Immunol.* **194**, 2059–2063 (2015).
8. Hardenberg, J.-H. B., Braun, A. & Schön, M. P. A Yin and Yang in Epithelial Immunology: The Roles of the αE(CD103)β7 Integrin in T Cells. *J. Invest. Dermatol.* **138**, 23–31 (2018).
9. Duhen, T. *et al.* Co-expression of CD39 and CD103 identifies tumor-reactive CD8 T cells in human solid tumors. *Nat. Commun.* **9**, 2724 (2018).
10. Tucker, C. G. *et al.* Adoptive T-cell therapy with IL-12 pre-conditioned low avidity T-cells prevents exhaustion and results in enhanced T-cell activation, tumor clearance, and decreased risk for autoimmunity. *J. Immunol. Baltim. Md 1950* **205**, 1449–1460 (2020).
11. Agliardi, G. *et al.* Intratumoral IL-12 delivery empowers CAR-T cell immunotherapy in a pre-clinical model of glioblastoma. *Nat. Commun.* **12**, 444 (2021).
12. Jung, I.-Y. *et al.* Tissue-resident memory CAR T cells with stem-like characteristics display enhanced efficacy against solid and liquid tumors. *Cell Rep. Med.* **4**, 101053 (2023).
13. Hasan, F., Chiu, Y., Shaw, R. M., Wang, J. & Yee, C. Hypoxia acts as an environmental cue for the human tissue-resident memory T cell differentiation program. https://insight.jci.org/articles/view/138970/pdf (2021) doi:10.1172/jci.insight.138970.
14. Srivastava, S. *et al.* Immunogenic Chemotherapy Enhances Recruitment of CAR-T Cells to Lung Tumors and Improves Antitumor Efficacy when Combined with Checkpoint Blockade. *Cancer Cell* **39**, 193-208.e10 (2021).
15. Boulch, M. *et al.* A cross-talk between CAR T cell subsets and the tumor microenvironment is essential for sustained cytotoxic activity. *Sci. Immunol.* **6**, eabd4344 (2021).

16. Larson, R. C. *et al.* CAR T cell killing requires the IFNγR pathway in solid but not liquid tumours. *Nature* **604**, 563–570 (2022).
17. Alizadeh, D. *et al.* IFNγ Is Critical for CAR T Cell-Mediated Myeloid Activation and Induction of Endogenous Immunity. *Cancer Discov.* **11**, 2248–2265 (2021).

MATHEMATICAL APPENDIX

We consider a series of mathematical models that describe these T cell memory decision making strategies in response to an acute infection: (1) memory decisions are made in a flexible manner, occurring either early or late; (2) memory decision arise early, as a result of irreversibility in the decision to become short-lived effector cells ("Early decision model") (Chang et al., 2007; Lin et al., 2016; Kakaradov et al., 2017); and (3) memory decision occur late in effector cells, as a result of a direct conversion of naive cells to effector cells following antigen encounter ("Late decision model") (Jacob and Baltimore, 1999; Bannard et al., 2009; Youngblood et al., 2017). In all models, we account for replication of pathogen, its removal by effector T cells, as well as the differentiation of naive cells into effector and memory cells following different decision-making strategies described above. Additionally, our model explicitly accounts for activity of the innate immune system, which acts both as a first-line responder and as an executor of T cell-directed effector activity. By comparing the performance of these different models using modeling, we aim to gain insight as to why certain decision-making strategies may have been functionally beneficial for pathogen defense by the immune system and hence, selected for during evolution.

Flexible decision model

Here, we describe the reversible model for T cell memory decision making (Fig. 7). In this model, naive cells first transition into memory cell precursors in the presence of pathogens. These memory precursors then transition into effector cells with a probability that increases with increasing pathogen load. Both memory precursors and effector cells proliferate with a similar rate that increases with antigen level, as previously observed (Plambeck et al., 2022); however, only effector cells undergo apoptosis as a result of activation-induced cell death, a reflection of their short-lived nature. In addition to T cells, we also consider the innate immune system in both its inactive and active states, and collectively model the innate immune response in these two states using two variables. T cells and innate cells then mediate pathogen killing, both independently from each other and in a cooperative manner. This model is described by the following system of equations:

naive T cell: $\frac{dT_n}{dt} = -\alpha_n v T_n$

memory T cell: $\frac{dT_m}{dt} = \alpha_n v T_n + \left(\frac{v}{v+K_m}\right) \gamma_m T_m - \left(\frac{v}{v+K_{m,e}}\right) \alpha_{m,e} T_m + \left(\frac{K_{e,m}}{v+K_{e,m}}\right) \beta_{e,m} T_e$

effector T cell: $\frac{dT_e}{dt} = \left(\frac{v}{v+K_e}\right) \gamma_e T_e + \left(\frac{v}{v+K_{m,e}}\right) \alpha_{m,e} T_m - \left(\frac{K_{e,m}}{v+K_{e,m}}\right) \beta_{e,m} T_e - \delta_e T_e$

pathogen: $\frac{dv}{dt} = \left(\frac{v}{\epsilon+v}\right)^N \gamma_v v - (\delta_{v1} T_e + \delta_{v2} z^* + \delta_{v3} z^* T_e) v$

inactive innate cell: $\frac{dz}{dt} = -\alpha_z v z$

active innate cell: $\frac{dz^*}{dt} = \alpha_z v z + \left(\frac{v}{v+K_{z^*}}\right)\gamma_{z^*} z^* - \delta_{z^*} z^*$

(1)

Here, the subscripts *n*, *m*, and *e* denote naive, memory, and effector types, respectively, *v* denotes the pathogen population, and *z* and z^* denote the inactive and active innate immune cells, respectively. The rates $\alpha_{x,y}$ denote differentiation rates from the *x* to the *y* cell type (for *x, y* $\in \{n, m, e\}$), $\beta_{e,m}$ denotes the de-differentiation rate from effector to memory (i.e., the only reversed differentiation in the model), γ_x denotes proliferation rate of cell type *x*, and δ_x denotes the death rate of cell type *x*. The parameters $K_{(.)}$denote the pathogen load for half maximal rate of a process indicated in the subscript.

A detailed description of the model variables, parameters and initial conditions are given in the two tables below. Parameters have been chosen based on the immune compartment sizes as measured in mice, as well as T cell biological parameters that we and others have measured. The initial conditions have been chosen to reflect the initial onset of an infection by a pathogen for which no prior immunological memory has been developed; specifically, antigen-specific naive cells are present at low amounts, effector and memory cells are absent and the initiating pathogen is introduced at a low initial level:

	Variable description	Initial value
T_n	naive T cell	0.02 cells/μL
T_m	memory T cell	0 cells/μL
T_e	effector T cell	0 cells/μL
v	pathogen load	10^{-3} units/μL
z	inactive innate cell	1 cell/μL
z^*	activated innate cell	0 cells/μL

We point out that this system is fundamentally a Lotka-Volterra model where immune cells are predators and pathogens are prey. However, we have modified this framework to describe the immune response in the following ways: first, we have incorporated saturation terms in the rates of pathogen-induced T cell and innate cell division (K_m, K_e), as well as T cell effector to memory differentiation ($K_{m,e}$) and de-differentiation ($K_{e,m}$)). The values for these saturation terms are further chosen to reflect the biological upper-bounds for these cellular processes. Second, we incorporate a threshold pathogen load, ϵ, below which the pathogen replication rate drops to zero, reflecting extinction of the pathogen. This pathogen extinction threshold ensures that this deterministic system of equations, when simulated, has a well-defined behavior and is not subject to numerical integration errors at very low pathogen loads (Fowler, 2021). However, we note that the dynamics of simulated response does not generally depend on the exact value of the extinction coefficient chosen.

From numerical simulations, we see that the flexible decision model reproduces the canonical dynamics of the adaptive immune response (Fig. 7B, Fig. S7A-B). Upon introduction to the system, pathogens increase exponentially in number, giving rise to a subsequent expansion of the T cell numbers from their initial low levels in the naive cell population. This expansion occurs concomitantly with pathogen clearance, and is followed by a decline in T cell numbers to a stable

elevated baseline, reflecting the generation of long-lived memory cells that can survive following pathogen clearance. During the course of the immune response, the numbers of activated innate immune cells increases rapidly and decreases steadily for the reminder of simulation (Fig. S7A-B). This heightened innate immune activity is critical for ensuring that pathogens clear after T cell contraction and do not rebound in number.

	Parameter description	Value
α_n	naive cell activation rate constant	5/(units/μL)/hr
γ_m	maximal memory cell proliferation rate constant	0.25/hr
K_m	pathogen load for half maximal memory cell proliferation	0.1 units/μL
$\alpha_{m,e}$	maximal effector differentiation rate constant	0.25/hr
$K_{m,e}$	pathogen load for half maximal effector differentiation	0.1 units/μL
γ_e	maximal effector cell proliferation rate constant	0.25/hr
K_e	pathogen load for half maximal effector proliferation	0.1 units/μL
$\beta_{e,m}$	maximal rate of effector de-differentiation	$8\text{x}10^{-4}$/hr
$K_{e,m}$	pathogen load for half maximal effector de-differentiation	$2.5\text{x}10^{-3}$ units/μL
δ_e	rate constant for effector cell death	0.016/hr
γ_v	rate of pathogen replication	0.003-0.45/hr
ϵ	pathogen load for extinction	10^{-4}/μL
N	sharpness of extinction effect for pathogen	100
δ_{v_1}	rate constant for T cell pathogen killing	$4.5\text{x}10^{-3}$/(cells/μL)/hr
δ_{v_2}	rate constant for innate cell pathogen killing	$1.5\text{x}10^{-3}$/(cells/μL)/hr
δ_{v_3}	rate constant for T-cell assisted innate cell pathogen killing	$1.5\text{x}10^{-3}$/(cells/μL)$^{-2}$/hr
α_z	innate cell activation rate constant	2.5/(units/μL)/hr
γ_z*	maximal activated innate cell proliferation rate	0.02/hr
K_z*	pathogen load for half maximal innate cell proliferation	0.01 units/μL
δ_z*	turnover rate for activated innate cell	$2\text{x}10^{-4}$/hr

How does the size of the generated memory population depend on the severity of infection in the reversible switching model? In particular, we wish to ascertain whether this system can produce memory cells in numbers that scale linearly with the peak T cell numbers during an infection, as observed experimentally (Murali-Krishna et al., 1998). To ask this question, we performed simulations of the system with different values of pathogen replication rate, γ_v, as a means to vary pathogen virulence. We found that pathogens with different replication rates gave rise to different degrees of T cell expansion and contraction, with faster-replicating pathogens generating a stronger T cell response, as expected (Fig. 7B).

However, the fraction f_{T_m} of memory cells to the total number of T cells present at the expansion peak becomes a fixed number (Fig. 7B, 7C: shaded area). Specifically, in the regime where there is substantial T cell expansion (> 10^2 fold relative to naive cell numbers), the memory fraction f_{T_m} remains constant for a broad range of viral replication rates γ_v, spanning an order of magnitude (Fig. 7C, top, shaded area). On the other hand, for slowly growing pathogens (small γ_v), the memory fraction f_{T_m} increases, with a non- linear inverse dependence on the virulence

and the average viral load accumulated during the infection (Fig. 7C); in this regime, the number of memory cells depends strongly on the initial number of naive cells present. In summary, these results show that a flexible switching strategy for T cell memory generation allows for the amount of the generated T cell memory to scale with the size of the T cell response, in a way that depends on the severity of the infection. Our analytical results in the following section well recapitulates the behavior of this memory fraction, as indicated in Fig. 7.

Analytical results for the flexible decision model

Consider the dynamics of memory T_m and effector T_e populations, given by eq. 1. We begin by identifying the dominant processes in different regimes of accumulated viral load v. Specifically, we compare the viral load with the half maximal loads ($K_{(.)}$'s in eq. 1), necessary for different processes. Below the terms that are relevant for the dynamics of memory and effector populations in the high viral load ($v \gg K_e, K_{m,e}$) and the low viral load ($v \ll K_{e,m}$) regimes are indicated:

$$\text{memory T cell: } \frac{dT_m}{dt} = \underbrace{\alpha_n v T_n + \left(\frac{v}{v+K_m}\right)\cdot \gamma_m T_m - \left(\frac{v}{v+K_{m,e}}\right)\cdot \alpha_{m,e} T_m}_{v \gg K_m, K_{m,e}} + \underbrace{\left(\frac{K_{e,m}}{v+K_{e,m}}\right)\cdot \beta_{e,m} T_e}_{v \ll K_{e,m}} \tag{2}$$

$$\text{effector T cell: } \frac{dT_e}{dt} = \underbrace{\left(\frac{v}{v+K_e}\right)\cdot \gamma_e T_e + \left(\frac{v}{v+K_{m,e}}\right)\cdot \alpha_{m,e} T_m}_{v \gg K_e, K_{m,e}} - \underbrace{\left(\frac{K_{e,m}}{v+K_{e,m}}\right)\cdot \beta_{e,m} T_e - \delta_e T_e}_{v \ll K_{e,m}} \tag{3}$$

We can formally integrate over the dynamical equation in eq. 2 to find a formal solution for the number of memory cells $T_m(t)$ at time t post infection,

$$\begin{aligned} T_m(t) = T_m(0)\exp\left[\int_0^t \gamma_m - \alpha_{m,e} - \frac{\gamma_m K_m}{v(s)+K_m} + \frac{\alpha_m K_{m,e}}{v(s)+K_{m,e}}\,\mathrm{d}s\right] \\ + \left[\int_0^t \exp\left[\int_s^t \gamma_m - \alpha_{m,e} - \frac{\gamma_m K_m}{v(s)+K_m} + \frac{\alpha_m K_{m,e}}{v(s)+K_{m,e}}\,\mathrm{d}s\right] \right. \\ \left. \times \left(\alpha_n v(s) T_n(s) + \frac{K_{e,m}}{v(s)+K_{e,m}}\beta_{e,m} T_e(s)\right)\mathrm{d}s\right] \end{aligned} \tag{4}$$

$$\begin{aligned} \approx T_m(0)\exp\left[\left(\gamma_m - \alpha_{m,e}\right)\min(t, \tau_{v\approx 0})\right] \\ + \int_0^{\min(t,\tau_{v\approx 0})} \exp\left[\left(\gamma_m - \alpha_{m,e}\right)(\min(t,\tau_{v\approx 0}) - s)\right]\alpha_n\, v(s) T_n(s)\mathrm{d}s \\ + H(t-\tau_{v\approx 0})\int_{\tau_{v\approx 0}}^t \beta_{e,m} T_e\,(s)\mathrm{d}s \end{aligned} \tag{5}$$

where $\tau_{v\approx 0}$ is the time to effectively clear the infection, and $H(t-\tau_{v\approx 0})$ is a Heaviside step function that takes value 1 for $t > \tau_{v\approx 0}$, and 0, otherwise. In arriving at eq. 5, we assumed that the typical viral load over the course of the infection is much higher than the differentiation thresholds K_m, $K_{m,e}$, K_e, and $K_{e,m}$, and thus, we approximated these processes by their maximal rates in eq. 4.

The following terms are important in determining the size of the memory pool:

1. $T_m(0)$: the initial memory size;
2. $\gamma_m - \alpha_{m,e}$: the effective growth rate of the memory pool;
3. $\tau_{v\approx 0}$: time to effectively clear the infection;
4. $\beta_{e,m}$ the transition rate from effector to memory.

Here, we are interested in an immune response to a primary infection, and therefore, we can assume that $T_m(0) = 0$. Moreover, given parameters used for the model, we can neglect the effective growth of the memory pool, i.e., $\gamma_m - \alpha_{m,e} \approx 0$. With these assumptions, the size of the memory pool from eq. 5 follows,

$$T_m(t) \approx \int_0^{\min(t,\tau_{v\approx 0})} \alpha_n v(s) T_n(s) \mathrm{d}s + H(t-\tau_{v\approx 0}) \int_{\tau_{v\approx 0}}^{t} \beta_{e,m} T_e(s) \mathrm{d}s$$

Our goal is to estimate the asymptotic (long-term) fraction of memory to the total number of T cells (primarily effector cells) present at the expansion peak $f_{T_m} = T_m(\infty)/{T_e}^{\max}$. The asymptotic amount of memory follows,

$$T_m(t\to\infty) \approx \int_0^{\tau_{v\approx 0}} \alpha_n v(s) T_n(s) \mathrm{d}s + \int_{\tau_{v\approx 0}}^{\infty} \beta_{e,m} T_e(s) \mathrm{d}s$$

then assuming $\tau_{v\approx 0} \approx {T_e}^{\max}$,

$$\begin{aligned} T_m(\infty) &\approx \int_0^{{\tau_e}^{\max}} \alpha_n v(s) T_n(s) \mathrm{d}s + \int_{{\tau_e}^{\max}}^{\infty} \beta_{e,m} T_e(s) \mathrm{d}s \\ &\approx \int_0^{{\tau_e}^{\max}} \alpha_n v(s) T_n(s) \mathrm{d}s + \int_{{\tau_e}^{\max}}^{\infty} \beta_{e,m} {T_e}^{\max} e^{-(\beta_{e,m}+\delta_e)s} \,\mathrm{d}s \\ &\approx \int_0^{{\tau_e}^{\max}} \alpha_n v(s) \mathrm{d}s + \beta_{e,m} \frac{{\tau_e}^{\max}}{\beta_{e,m}+\delta_e} \end{aligned} \tag{6}$$

where we used the relation $T_e(t > {\tau_e}^{\max}) = T_e e^{-(\beta_{e,m}+\delta_e)s}$, indicating an exponential decay of effector cells after the peak of the response ($v \ll K_{e,m}$), from eq. 3.

From eq. 1, we can also formally express the size of the naive pool as,

$$T_n(t) = T_n(0)\exp\left[-\alpha_n \int_0^t v(s)\mathrm{d}s\right]$$

Therefore, the first term in the solution of eq. 6 follows,

$$\alpha_n \int_0^{{\tau_e}^{\max}} v(s)T_n(s)\mathrm{d}s = T_n(0)\left[1 - e^{-\alpha_n \tilde{V}}\right], \text{ with } \tilde{V} = \int_0^{{\tau_e}^{\max}} v(r)\mathrm{d}r$$

Here, $\tilde{V}$ reflects the total amount of pathogens accumulated during the infection. Putting it all together, we find

$$T_m(\infty) \approx T_n(0)\left[1 - e^{-\alpha_n \tilde{V}}\right] + \beta_{e,m}\frac{{T_e}^{\max}}{\beta_{e,m} + \delta_e} \tag{7}$$

resulting the following memory fraction,

$$f_{T_m} = \frac{T_m(\infty)}{{T_e}^{\max}} \approx \frac{x(0)}{{T_e}^{\max}}\left[1 - e^{-\alpha_n \tilde{V}}\right] + \beta_{e,m}\frac{{T_e}^{\max}}{\beta_{e,m} + \delta_e} \tag{8}$$

When ${T_e}^{\max} \gg T_n(0)$, we recover the constant memory fraction $f_{T_m} \approx \frac{\beta_{e,m}}{\beta_{e,m}+\delta_e}$.

So far we have assumed that $\gamma_m - \alpha_{m,e} \approx 0$. When this assumption does not hold, the first term in our expression for f_{T_m} becomes,

$$\begin{aligned} C_0 &= \frac{1}{{T_e}^{\max}} \int_0^{{\tau_e}^{\max}} \exp\left[\left(\gamma_m - \alpha_{m,e}\right)\left({\tau_e}^{\max} - s\right)\right] \alpha_n v(s)T_n(s)\mathrm{d}s \\ &= \frac{\alpha_n T_n(0)}{{T_e}^{\max}} \int_0^{{\tau_e}^{\max}} \exp\left[\left(\gamma_m - \alpha_{m,e}\right)\left({\tau_e}^{\max} - s\right) - \alpha_n \int_0^s v(r)\mathrm{d}r\right] v(s)\mathrm{d}s \\ &\leq \frac{\alpha_n T_n(0)}{{T_e}^{\max}} \int_0^{{\tau_e}^{\max}} \exp\left[\left(\gamma_m - \alpha_{m,e}\right)\left({\tau_e}^{\max} - s\right)\right] v(s)\mathrm{d}s \end{aligned} \tag{9}$$

with a strong dependence on $\gamma_m - \alpha_{m,e}$.

Note that the innate immune dynamics does not explicitly determine the memory fraction f_{T_m}, however, it influences the magnitude of $\tilde{V}$ and so it is expected to be important in the low viral replication γ_v regime.

Early decision model

From experimental studies, it has been proposed that memory cells originate primarily from cells that have undergone little or no effector differentiation, and that memory precursors, upon silencing the memory regulator TCF1 and differentiating, are committed to becoming short-lived effectors (Lin et al., 2016; Pais Ferreira et al., 2020). Using the mathematical modeling framework developed above, we evaluate whether this irreversible effector decision strategy could also enable the asymptotic (long-term) memory T cell numbers $T_m(\infty)$ to scale linearly with the peak T cell number (primary effector cells) ${T_e}^{\max}$. To do so, we performed simulations of the above model, rendering effector differentiation irreversible by setting the rate of effector de-differentiation $\beta_{e,m}$ to zero.

From our simulations, we found that the number of memory T cells emerging depends on the balance between effector differentiation and memory precursor proliferation, as determined by the rate constants $\alpha_{m,e}$ and γ_m respectively. When these two rate constants are equal, the number of generated memory cells cannot exceed the initial number of naive cells (Fig. S7C-F). This is because the memory cell population, upon emerging from the naive cell pool, cannot further change in number as proliferation is balanced exactly by differentiation. We note that this regime captures the dynamics of obligate asymmetric division, where the division of each memory precursor necessarily gives rise to a precursor and a differentiated progeny. When the rate of effector differentiation $\alpha_{m,e}$ is smaller than that of memory precursor proliferation γ_m, the number of memory cells can exceed the initial naive cell number, due to a net proliferation of this population; in this regime, the size of the memory pool grows with increasing γ_v.

To perform a mathematically comparable comparison of the flexible and irreversible switching models (Alves and Savageau, 2000), we chose a rate of effector differentiation for the latter model to be $\alpha_{m,e}$ = 0.12/hr, such that the fraction of memory cells generated under conditions of moderate pathogen virulence (γ_m = 0.04/hr) were equivalent for the two models with f_{T_m} = 0.05. All other parameters were kept constant. These simulations show that the irreversible switching model is unable to generate a constant fraction of memory cells amid changes in pathogen replication rates (Fig. 7C middle). The memory fraction was upheld at a similar value f_{T_m} = 0.05 at moderate pathogen replication rates γ_v = 0.04/hr; however, this fraction decreased steadily with increasing γ_v, eventually approaching less than 0.01 at high pathogen replication rates (Fig. 7C, middle; Fig. S7C-F). Indeed, from an approximate analytical solution of this system, we found that the memory cell fraction has an inherently inverse dependence on the peak T cell population size, as follows:

$$f_{T_m} \approx \frac{T_n(0)}{T_e max} \tag{10}$$

This dependence cannot be offset when the fraction is much smaller than unity, which typically holds in the regime where the majority of cells generated at the height of an acute infection are those with effector function. Thus, from these results, we conclude that the T cell decision making strategy, where the memory precursors switch irreversibly into becoming short-lived effectors, cannot produce memory T cell numbers that scale proportionally with the peak T cell population sizes.

Late decision model (obligate reversible decision model)

An alternate strategy for memory differentiation is that, upon activation, all naive cells must first pass through an effector stage prior to the decision as whether to differentiate into memory (Fig. 7, bottom). This view is supported by the evidence that cells with a history of effector gene expression can become memory cells (Bannard et al., 2009), and that cells on the road to forming memory retain chromatin signatures of the effector state, while harboring the ability to reactivate memory genes that are silenced during effector differentiation (Youngblood et al., 2017); this model can be thought as an obligate reversible decision model.

To evaluate such a decision making strategy, we alter our model above, such that naive cells, upon activation, directly transition to an effector state instead of a memory precursor state (Fig. 7, bottom, Fig. S7G-H). Following the model in eq. 1, the ordinary differential equations describing the T cell populations in the late decision model are modified as follows:

naive T cell: $\frac{dT_n}{dt} = -\alpha_n v T_n$

memory T cell: $\frac{dT_m}{dt} = \left(\frac{v}{v+K_m}\right) \cdot \gamma_m T_m - \left(\frac{v}{v+K_{m,e}}\right) \cdot \alpha_{m,e} T_m + \left(\frac{K_e}{v+K_e}\right) \cdot \beta_{e,m} T_e$

effector T cell: $\frac{dT_e}{dt} = \alpha_n v T_n + \left(\frac{v}{v+K_e}\right) \cdot \gamma_e T_e + \left(\frac{v}{v+K_{m,e}}\right) \cdot \alpha_{m,e} T_m - \left(\frac{K_{e,m}}{v+K_{e,m}}\right) \cdot \beta_{e,m} T_e - \delta_e T_e$

For direct comparison of this decision-making strategy to the model with flexible switching, we keep all the parameters unchanged. From simulations, we find this obligate reversible switching strategy can generate constant fractions of memory cells over a range of pathogen proliferation rates, but fails to generate any substantial memory when pathogens replicate slowly (small γ_v) and the ensuing immune responses are mild. When pathogens replicate rapidly and give rise to a substantial T cell expansion, memory cells form robustly at defined fraction and number, similar to the flexible switching model (Fig. 7C, bottom, Fig. S7G-H, center, right); however, when pathogens proliferate very slowly, such that there is minimal amount of T cell expansion, the number of formed memory cells constitutes only a small fraction of the starting naive cells. Consequently, in this regime, the ability of the immune system to respond to a secondary challenge is no longer heightened, and is likely compromised.

Analysis of late decision model

Following the analytical analyses for the flexible switching model, we can again identify the dominant terms in different regimes of viral load. By assuming that the viral load triggered by the infection is much larger than the cellular differentiation thresholds K_m, $K_{m,e}$, K_e, and $K_{e,m}$ we arrive at the following approximate expression for the size of the memory pool $T_m(t)$ at time t in the late decision model.

$$T_m(t) \approx T_m(0)\exp\left[\left(\gamma_m - \alpha_{m,e}\right)\min(t, \tau_{v\approx 0})\right] + H(t - \tau_{v\approx 0}) \int_{\tau_{v\approx 0}}^{t} \beta_{e,m} T_e\,(s)\mathrm{d}s$$

Then for primary immune response ($T_m(0) = 0$) we have,

$$f_{T_m} = \frac{T_m(\infty)}{T_e max} \approx \frac{\beta_{e,m}}{\beta_{e,m} + \delta_e} \tag{11}$$

We note that this expression does not hold in the regime of slow/inefficient virus dynamics, consistent with results from simulations (Fig. 7).

VITA

Elisa Clark was born and raised in Massachusetts. She completed a Bachelor of Science in Bioengineering from Rice University in 2015 and then worked in Cell Line and Upstream Process Engineering at ImmunoGen, Inc. in Waltham, MA. She started her doctoral studies at the University of Washington in 2017.